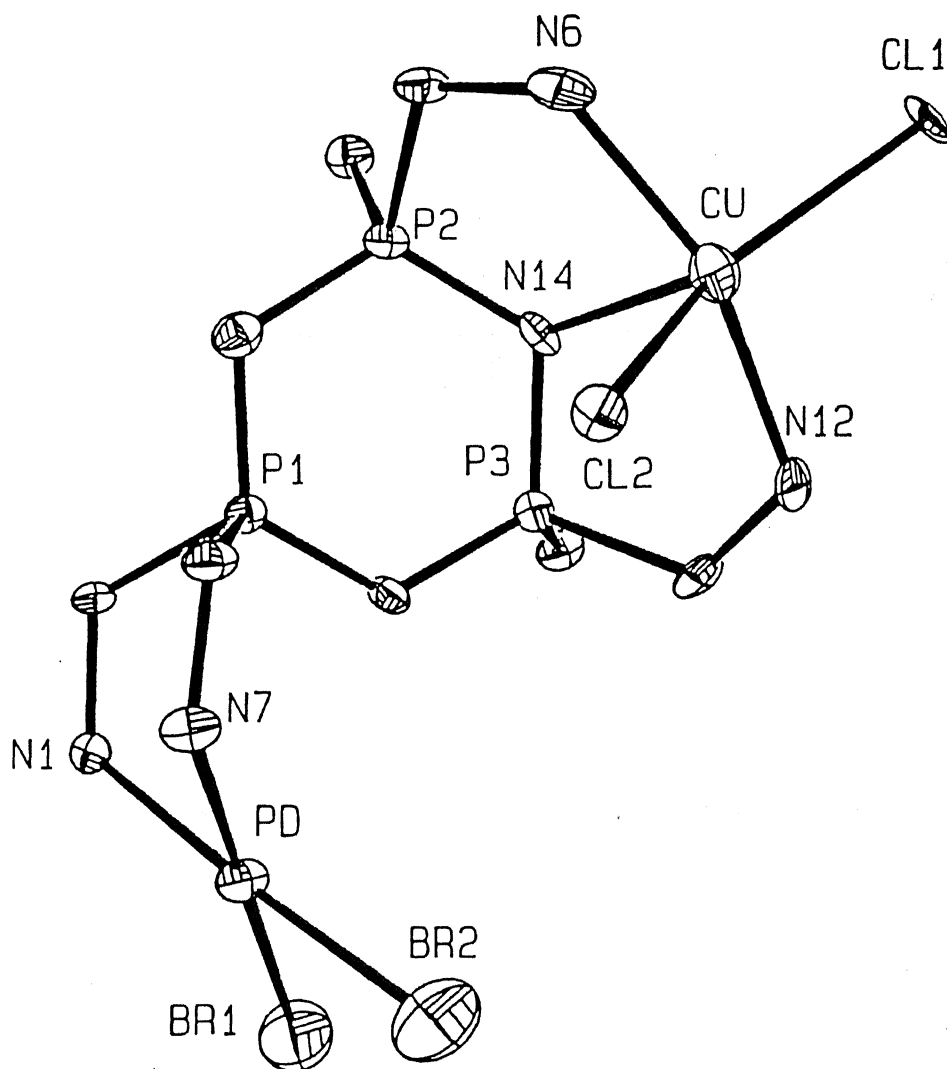


✓ **Cyclophosphazenes as Transition Metal Carriers: Synthesis and Characterization of Cu(II), Ni(II) and Co(II) Complexes of Pyrazolylcyclotriphosphazenes**

Cyclophosphazenes as Transition Metal Carriers: Synthesis and Characterization of Cu(II), Ni(II) and Co(II) Complexes of Pyrazolylcyclotriphosphazenes



K.R. Justin Thomas

**CYCLOPHOSPHAZENES AS TRANSITION METAL
CARRIERS: SYNTHESIS AND CHARACTERIZATION OF
Cu(II), Ni(II) AND Co(II) COMPLEXES OF
PYRAZOLYLCYCLOTRIPHOSPHAZENES**

A Thesis Submitted

In Partial Fulfilment of the Requirements

for the Degree of

DOCTOR OF PHILOSOPHY

by

K.R. JUSTIN THOMAS

to the

**DEPARTMENT OF CHEMISTRY
INDIAN INSTITUTE OF TECHNOLOGY KANPUR**

DECEMBER, 1993

All mankind are like grass,
and all their glory is like wild flowers.
The grass withers and the flowers fall.

—1 Peter 1:24

Wavering between the profit and the loss
In this brief transit where the dreams cross
The dream crossed twilight between birth and dying

—T.S. Eliot

To **AKR and SM**

my defenders

my philosophers

my tranquillizers

my joy

my parents

with all my heart

and love

k.r.j.t.

STATEMENT

I hereby declare that the matter embodied in this thesis, "Cyclophosphazenes as Transition Metal Carriers: Synthesis and Characterization of Cu(II), Ni(II) and Co(II) Complexes of Pyrazolylcyclotriphosphazenes", is the result of investigations carried out by me in the Department of Chemistry, Indian Institute of Technology, Kanpur, India under the supervision of Dr. V. Chandrasekhar.

In keeping with the general practice of reporting scientific observations, due acknowledgement has been made wherever the work described is based on the findings of other investigators.

Kanpur
December, 1993

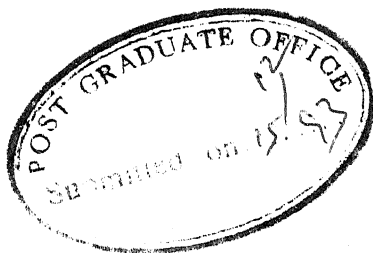


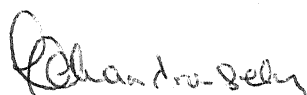
(K.R. Justin Thomas)

CERTIFICATE

It is certified that the work contained in the thesis entitled, "Cyclophosphazenes as Transition Metal Carriers: Synthesis and Characterization of Cu(II), Ni(II) and Co(II) Complexes of Pyrazolylcyclotriphosphazenes", by K.R. JUSTIN THOMAS, has been carried out under my supervision and same has not been submitted elsewhere for a degree.

Kanpur
December 1993




(V. Chandrasekhar)
Thesis Supervisor
Department of Chemistry
Indian Institute of Technology
Kanpur-208 016, India

DEPARTMENT OF CHEMISTRY
INDIAN INSTITUTE OF TECHNOLOGY KANPUR, INDIA

CERTIFICATE OF COURSE WORK

This is to certify that **K.R. JUSTIN THOMAS** has satisfactorily completed all the courses required for the Ph.D degree. The courses include:

CHM 605	Principles of Organic Chemistry
CHM 625	Principles of Physical Chemistry
CHM 645	Principles of Inorganic Chemistry
CHM 664	Modern Physical Methods in Chemistry
CHM 641	Advanced Inorganic Chemistry I
CHM 661	Application of Modern Instrumental Techniques for Structure Elucidation
CHM 800	General Seminar
CHM 801	Special Seminar
CHM 900	Post-graduate Research

K.R. Justin Thomas was admitted to the candidacy of the Ph.D degree in September 1991 after he successfully completed the written and oral qualifying examinations.

N. Sathyanarayana
for **(P.K. Ghosh)**
Head
Department of Chemistry
I.I.T. Kanpur

N. Sathyanarayana
for **(J. Iqbal)**
Convenor, DPGC
Department of Chemistry
I.I.T. Kanpur

Acknowledgements

I would like to thank *Jesus*, my savior and god for giving me life and wisdom to carry out this research. [Jesus answered him, "I am the way, the truth, and the life ..." – John 14:6]

I wish to pay tribute to my parents who sacrificed their worldly interests to promote the interests of me. Indeed they are quite ignorant about the research I have been pursuing these days. However, I should admit that they have been instrumental, beginning from my childhood, in enriching me with knowledges on subjects varying from mathematics to medical sciences. I have dedicated this thesis to them.

Most of all, however, I sincerely express my indebtedness to Prof. V. Chandrasekhar, I.I.T., Kanpur, for his inimitable style of guidance and inspiring help to carry out this research in a peaceful manner. I owe special gratitude to him for introducing me to phosphazene chemistry and encouraging me to do whatever studies I wished to conduct.

I wish to express my gratitude to collaborators Profs. A.W. Cordes, Department of Chemistry, University of Arkansas, Fayetteville, USA and E.R.T. Tiekink, Department of Inorganic and Physical chemistry, University of Adelaide, Adelaide, South Australia 5005, Australia. Whose skilled and dedicated X-ray crystallographic work provided much needed structural evidence for the work described in this thesis.

Enthusiastic interest and collaboration in the electrochemical studies of heterobimetallic compounds described in this thesis by Prof. P. Zanello, Italy had helped the author to understand the roots of the electrochemical processes of them.

I am very much grateful to Prof. G. Balducci, Italy for providing me the cyclic voltammetric simulation program and literating me with computational techniques. I also like to record that he has patiently endured endless questioning on details of his own work and of that in the literature, to enable me to modify the programs suitable

for the situations. Unfortunately results in this direction are yet in infancy and could not be included in this thesis at all.

It is my pleasure to acknowledge Professors T.K. Chandrasekhar, S.K. Dogra, B.D. Gupta, S. Sarkar, N.S. Gajbhiye and Dr. P.K. Chaudhury for their kindness and very helpful suggestions.

I am very much delighted by the love and affection of my brother (Jawahar) and sisters (Mary and Lizy).

Acknowledgments are also due to Mr. N. Ahmed and Mr. D.K. Kannaujia for their assistance in recording IR and EPR spectra respectively.

The support of my labmates (Dr. P. Tharmaraj, Mr. I.I. Selvaraj and Mr. K. Vivekanandan) and friends (Mr. E. Samuel and Mr. G. Venkatasubramaniyan) was very much viable in times of demand. I also thank Dr. D. Reddy, Dr. R.P. Pandian and Dr. M. Ravikanth for their help and association.

Had I missed any one, he is also thanked.

k.r.j.t.

The aim of the research described in this thesis is to explore the coordination chemistry of the pyrazolylcyclotriphosphazene ligands (Chapter 1). These ligands have multiple donor sites and therefore can be utilized either to obtain complex ligands which possess vacant sites for the uptake of a second metal or to achieve directly polynuclear complexes of catalytic interest.

The thesis is divided into seven chapters. The thesis starts with a brief description about the cyclophosphazene ligands and their interaction with the transition metals (Chapter 2). Three types of interaction have been realized: (a) where the skeletal ring nitrogen alone coordinates to the transition metal or the cyclophosphazene merely forms a counter cation to the transition metal anionic species (b) where the exocyclic donor atom participates in coordination to the metal exclusively or sometimes along with the ring nitrogen atom (c) where the skeletal phosphorus directly interacts with the metal. It has been observed that the ring nitrogen atoms engage in coordination only when the substituents on phosphorus are appreciably electron releasing thus increasing the basicity of the ring nitrogen. This fact has to be taken into account while designing a cyclophosphazene ligand.

Of the three possible modes of interaction of cyclophosphazenes with transition metals method (b) is most versatile as it offers the opportunity of varying the number and nature of the exocyclic donor group. We have examined the coordination behavior of six pyrazolylcyclotriphosphazenes (Fig. 1) which contain pyrazolyl substituents in the phosphorus atoms of the cyclophosphazene. The ligands have been chosen in such a way, that the influence of small changes in either pyrazolyl substituent or cyclophosphazene ring could be studied. The ligand, hexakis(3,5-dimethylpyrazolyl)cyclotriphosphazene (hdpctp) forms both mononuclear and dinuclear copper complexes. The mononuclear complexes are further converted into heterobimetallics by treating

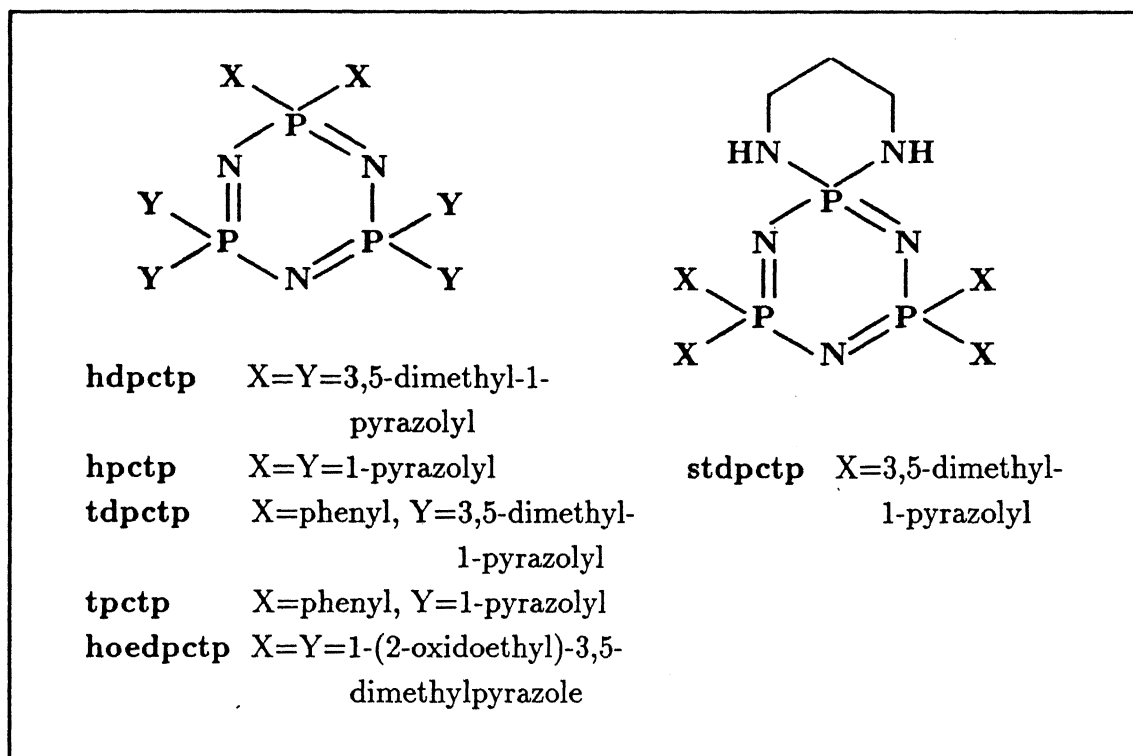


Figure 1: Structures of the ligands

them with platinum or palladium halides. However, with cobalt only a dinuclear complex has been isolated. The full experimental details are embodied in chapter 3. The ligands, 2,2-diphenyl-4,4,6,6-tetrakis(3,5-dimethylpyrazolyl)cyclotriphosphazene (tdpctp) and 2,2-spiro-(1,3-diaminopropane)-4,4,6,6-tetrakis(3,5-dimethylpyrazolyl)cyclotriphosphazene (stdpctp) which contain two pyrazolyl groups less than that in hdpctp, lead to a selective assembly of mononuclear copper, cobalt and nickel complexes. In most of the hdpctp, tdpctp and stdpctp complexes investigated the metal exists in a distorted trigonal bipyramidal environment with an exception being the copper perchlorate adducts. The copper in tdpctp·Cu(ClO₄)₂·2H₂O and tdpctp·Cu(ClO₄)₂·2Im assumes distorted octahedral and square pyramidal geometries respectively. The ligating properties of these three ligands derived from 3,5-dimethylpyrazole are described in the chapter 4. To study the influence of the bridge between the phosphorus and the pyrazolyl nitrogen a new ligand, hexakis(1-(2-oxidoethyl)-

3,5-dimethylpyrazolyl)cyclotriphosphazene (hoedpctp) has been prepared (Chapter 6). This forms dinuclear copper, cobalt, platinum and zinc complexes thus indicating the flexibility of the ligand.

The ligands discussed so far all contain two methyl groups at the pyrazole ring. To delineate the influence of the methyl group on the coordination behavior of the ligands, the ligands hexakis(1-pyrazolyl)cyclotriphosphazene (hpctp) and 2,2-diphenyl-4,4,6,6-tetrakis(1-pyrazolyl)cyclotriphosphazene (tpctp) have been subjected to coordination (Chapter 5). In contrast to hdpctp no mononuclear complexes could be obtained with hpctp. Mainly intermolecularly linked insoluble complexes are formed. However, tpctp forms mononuclear complexes analogous to that of tdpctp. The cobalt metal in tpctp·CoCl₂ is in a distorted trigonal bipyramidal geometry with the axial

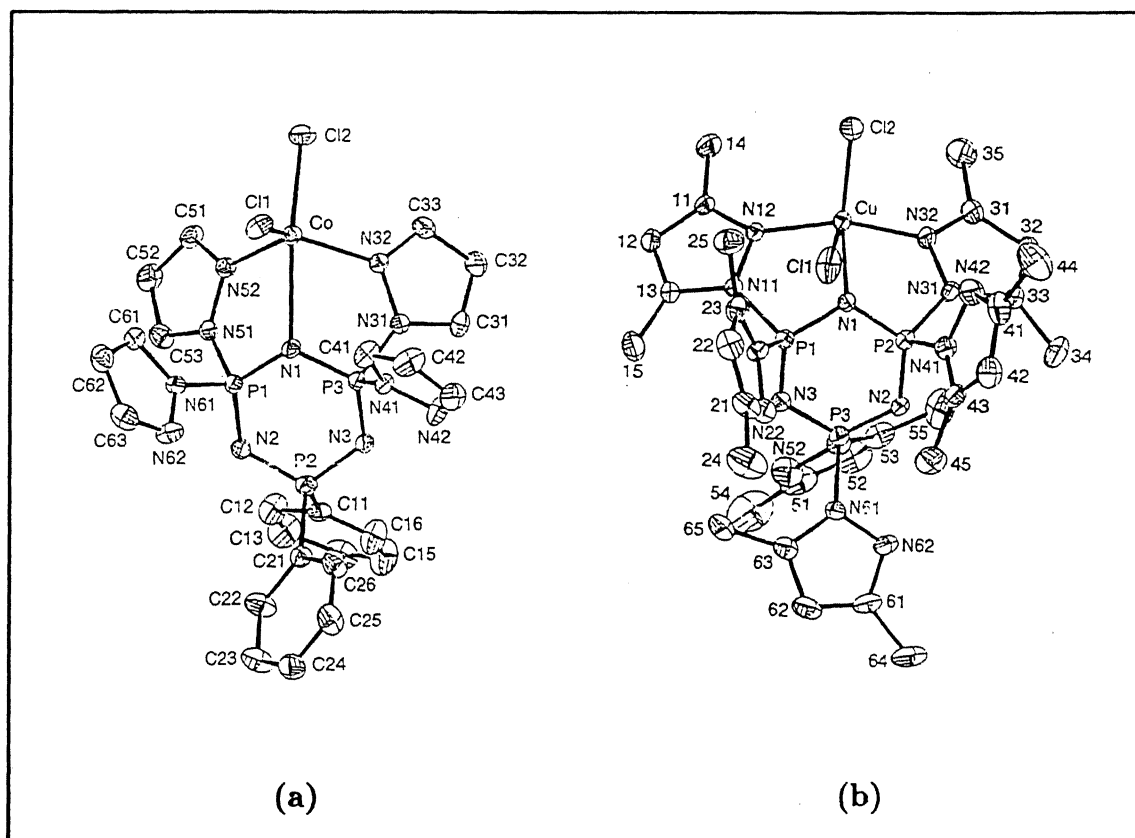


Figure 2: ORTEP diagrams of tpctp·CoCl₂ (a) and hdpctp·CuCl₂ (b)

positions being occupied by the cyclophosphazene ring nitrogen and a chloride ion

(Fig. 2). This is in contrast to the general observation with the methylated ligands (viz., hdptcp, tdpctp.) where the axial positions are being always comprised of pyrazolyl ring nitrogens. This difference may originate from the steric hindrance of the methyl groups in the pyrazolyl rings.

In general, the five-coordinate complexes prepared from copper(II) halides show EPR spectra suggestive of distorted trigonal bipyramidal geometry with $d_{x^2-y^2}$ ground state (axial, $g_{\parallel} > g_{\perp} > 2.0$). The six- or five-coordinate complexes obtained by the interaction of the ligands with copper(II) perchlorate and additional nitrogenous bases exhibit EPR spectra which reveal a tetrahedrally distorted tetragonal geometry for them (axial, $g_{\parallel} > g_{\perp} > 2.0$, $A_{\parallel} = 110-200$ G). The electronic spectra are supportive of this conclusions. The redox behavior of the copper complexes has been studied. The mononuclear complexes exhibit a quasi reversible or an irreversible Cu(II)–Cu(I) redox change. In the dinuclear complexes the presence of second metal centre, further increases the stereochemical rigidity of the molecular backbone, hinders any redox flexibility. The chapter 7 summarizes the results of these investigations. A brief account on the comparison of x-ray structures of the complexes with the related N_3 donor ligand complexes is given.

List of Abbreviations

Az	Aziridinyl
bipy	2,2'-Bipyridine
Bu	Butyl
BZA	Benzylidene acetone
Cp	Cyclopentadienyl anion
CTP	Cyclotriphosphazene
DMF	Dimethyl formamide
dmIm	1,2-Dimethyl imidazole
DMSO	Dimethyl sulfoxide
dpph	Diphenyl picryl hydrazyl
EPR	Electron paramagnetic spin resonance
Et	Ethyl
exo	Exocyclic
hdpctp	Hexakis(3,5-dimethyl-1-pyrazolyl)cyclotriphosphazene
hep	1-(2-Hydroxyethyl)-3,5-dimethylpyrazole
hoedpctp	Hexakis(1-(2-oxidomethyl)-3,5-dimethylpyrazole)cyclotriphosphazene
hpctp	Hexakis(1-pyrazolyl)cyclotriphosphazene
ImH	Imidazole
Ino	Inosine
IR	Infra-red
LCAO	Linear Combination of Atomic Orbitals
l.m.c.t.	Ligand to metal charge transfer
LNT	Liquid nitrogen temperature
Me	Methyl
MO	Molecular Orbital
NMR	Nuclear magnetic resonance
oep	1-(2-Oxidoethyl)-3,5-dimethylpyrazole
omp	1-(oxidomethyl)-3,5-dimethylpyrazole
Ph	Phenyl
phen	1,10-Phenanthroline
Pr	Propyl
py	Pyridine
Pz	3,5-Dimethyl-1-pyrazolyl
pz	1-Pyrazolyl
SCE	Saturated calomel electrode

stdpctp	Spiro(1,3-diaminopropane)-4,4,6,6-tetrakis(3,5-dimethyl-1-pyrazolyl) cyclotriphosphazene
stcctp	Spiro(1,3-diaminopropane)-4,4,6,6-tetrachloro cyclotriphosphazene
stpctp	Spiro(1,3-diaminopropane)-4,4,6,6-tetrakis(1-pyrazolyl)cyclotri- phosphazene
terpy	Terpyridine
tdpctp	2,2-Diphenyl-4,4,6,6-tetrakis(3,5-dimethyl-1-pyrazolyl)cyclotri- phosphazene
tpctp	2,2-Diphenyl-4,4,6,6-tetrakis(1-pyrazolyl)cyclotriphosphazene

Table of Contents

	Acknowledgements	vi
	Synopsis	viii
	List of Abbreviations	xii
Chapter 1	Coordination chemistry of pyrazolylcyclotriphosphazene: scope and some additional information	1
	References	5
Chapter 2	Cyclophosphazenes as transition metal carriers: synthetic strategies and structural perspectives	7
2.1	Introduction	7
2.2	Skeletal nitrogen coordination	11
2.3	Ionic, salt-type species	13
2.4	Effect of metal coordination or protonation to ring nitrogen on the structure of cyclotriphosphazenes	14
2.5	Ring phosphorus interactions with metals	15
2.6	Effect of skeletal phosphorus interaction with metals on the structure of cyclotriphosphazenes	21
2.7	Exocyclic group participation in coordination	23
2.8	Concluding remarks	28
	References	31
Chapter 3	Synthesis of the ligands and of the coordination compounds; physical methods	36
3.1	Introduction	36
3.2	Starting materials	37
3.3	Physical and chemical measurements	38
3.4	Synthesis of pyrazolylcyclotriphosphazenes	41
3.5	Synthesis of the coordination compounds	46
3.6	Concluding remarks	61
	References	61
Chapter 4	Varying the number of pyrazolyl substituents in cyclotriphosphazene skeleton to control the degree of nuclearity	63
4.1	Introduction	63
4.2	Synthesis and characterization of the ligands	64
4.3	Coordination compounds of the ligand hexakis(3,5-dimethyl-1-pyrazolyl)cyclotriphosphazene, hdpctp	70

4.4	Coordination compounds of the ligand 2,2-diphenyl-4,4,6,6-tetrakis(3,5-dimethyl-1-pyrazolyl)cyclotriphosphazene, tdpctp	105
4.5	Ligating properties of the ligand 2,2-spiro(1,3-diaminopropane)-4,4,6,6-tetrakis(3,5-dimethyl-1-pyrazolyl)cyclotriphosphazene, stdpctp	136
4.6	Conclusions	140
	References	141
Chapter 5	Substituents at the pyrazole ring: electronic or steric influence on coordination behavior?	146
5.1	Introduction	146
5.2	Synthesis of the ligands	149
5.3	Coordination compounds of hpctp and tpctp	152
5.4	Conclusion	169
	References	170
Chapter 6	Increasing the spacer length between the pyrazolyl group and cyclotriphosphazene ring to maximixe flexibility	172
6.1	Introduction	172
6.2	Synthesis of the ligand	174
6.3	Coordination compounds of hoedpctp and their spectroscopic features	177
6.4	Concluding remarks	182
	References	183
Chapter 7	Coordination chemistry of pyrazolylcyclotriphosphazene: summary and future prospects	185
7.1	Introduction	185
7.2	The number and nature of exocyclic donor groups	186
7.3	Electronic versus steric effects	188
7.4	Spacer effects	190
7.5	Concluding remarks	190
	References	191

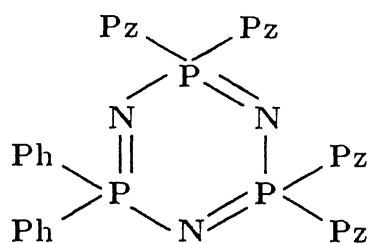
Coordination Chemistry of Pyrazolylcyclotriphosphazenes: Scope and Some Additional Information

"I have yet to see any problem, however complicated, which, when you look at it in the right way, did not become still more complicated"

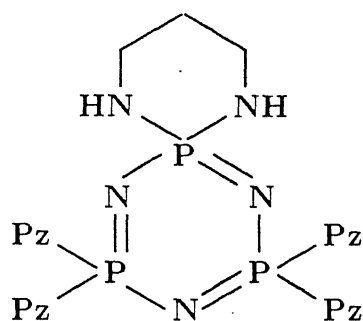
-Paul Anderson

The synthesis of chelating cyclophosphazene ligands and their coordination compounds provides an opportunity to transform this idea latter to the linear phosphazene polymers, which may for instance lead to immobilized catalysts and to ion-exchange resins with improved selectivity. Pyrazolylcyclophosphazenes were introduced by Paddock and coworkers into coordination chemistry for the first time [1,2]. These contain exocyclic pyrazolyl substituents on the phosphorus atoms of the inorganic heterocyclic P-N ring (Figure 1). They provide two modes of coordination possibilities, i.e., exclusive coordination *via* pyrazolyl pyridinic nitrogen atoms or through both pyrazolyl and cyclotriphosphazene skeletal nitrogen atoms. While the former mode has been achieved by Paddock and coworkers [1, 2], results from our laboratory as well as from those of Krishnamurthy [3, 4] has shown the possibility of latter mode of coordination (Figure 2).

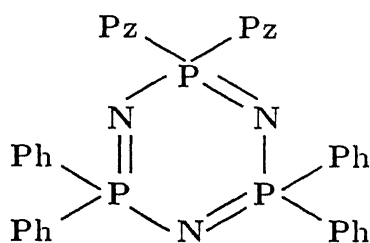
We have undertaken a detailed investigation on these ligands particularly with the paramagnetic metal copper. We have chosen copper as there is a flurry of interest



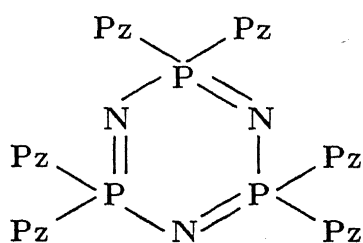
tdpctp



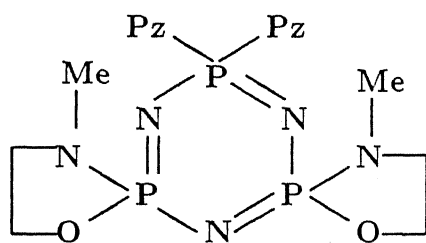
stdpctp



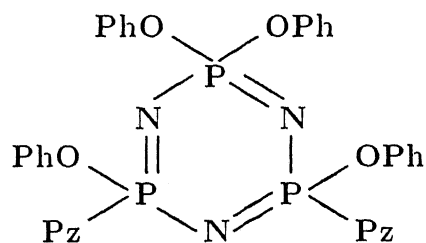
L3



hdpctp



L1



L2

Figure 1: Structures of some pyrazolylcyclotriphosphazene ligands

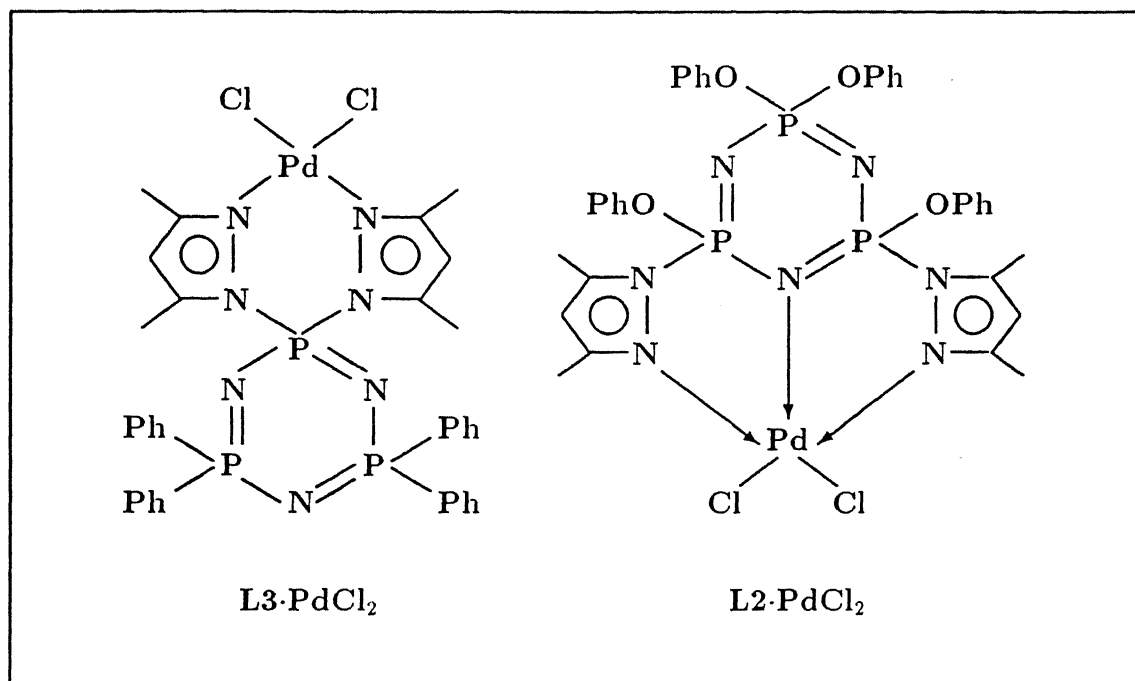


Figure 2: Structures of the palladium complexes of L3 and L2

in the coordination chemistry of copper with relevance to biology [5-7]. It is also important to investigate the ligating properties of the ligands in a wider sense, with respect to other transition metals like zinc, cobalt, nickel etc. For instance: some spectroscopic techniques offer more characterization possibilities with other metal ions than with Cu(II), like NMR (zinc), and electronic spectroscopy (nickel, cobalt). This so-called substitution technique has also been applied in metal-substituted proteins [8]. Furthermore, the coordination chemistry of the other transition metals (Ni, Co, etc.) with this special ligand system may also be of interest in itself because of the greater preference for a certain coordination geometry of especially Co(II) and Ni(II), whereas Cu(II) is flexible or shows plasticity often resulting in isomers or temperature dependent structures [9, 10].

This thesis describes the synthesis of pyrazolylcyclotriphosphazene ligands and the formation and characterization of coordination compounds with these ligands. Other cyclophosphazene ligands will also be described in chapter 2. The terms '*geminal coordination*' and '*nongeminal coordination*' alternating with the analogous terms

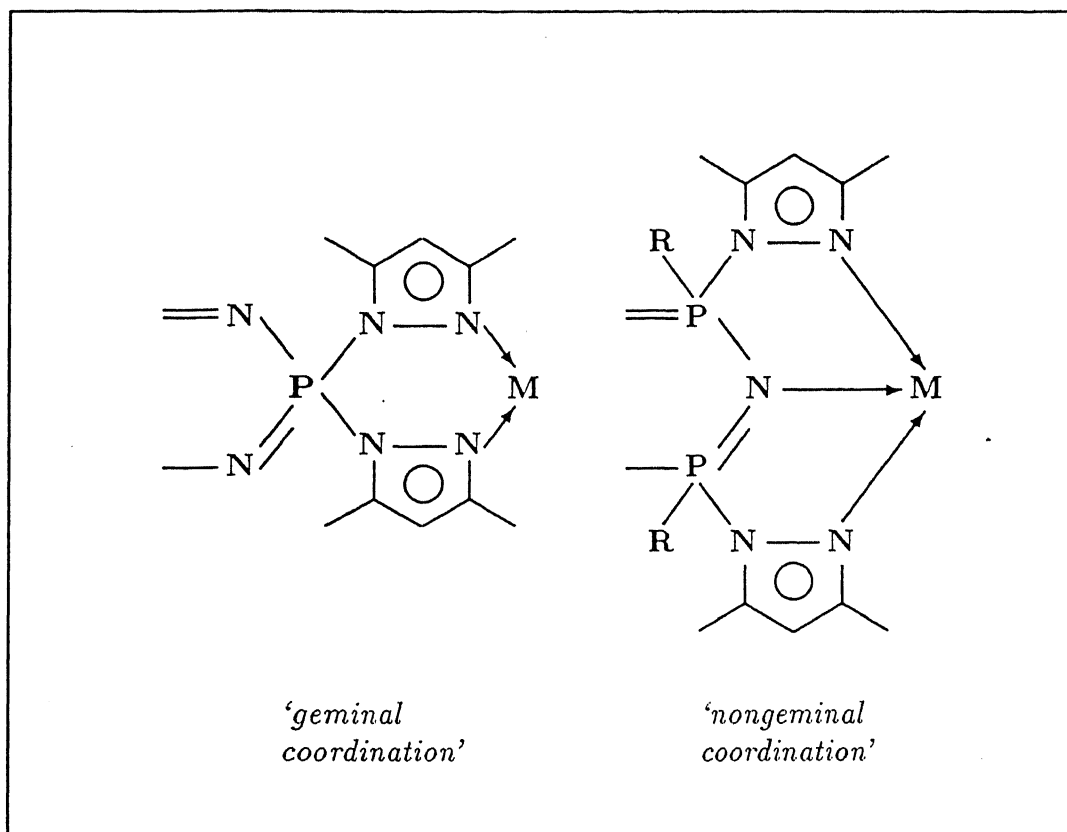


Figure 3: A six-membered and a five membered chelate rings

'six-membered chelate ring' and *'five-membered chelate ring'* will be used throughout this thesis. These terms are visualized in Figure 3.

In chapter 2 a review on the coordination chemistry of cyclophosphazene based ligands is presented. The scope of this review is limited to the cyclophosphazene ligands which interact with the transition metals through the ring donor atom or the exocyclic donor group. Both the skeletal nitrogen and phosphorus atoms are found to interact with transition metals. The interaction of skeletal nitrogen atom is purely coordinate while with the phosphorus both covalent and coordinate interactions are envisaged [11]. In chapter 3 a summary of all experimental data is provided. In the other chapters no further experimental details are given, unless necessary for the discussion.

Chapters 4-6 give the detailed description on the crystal structures and the spectroscopic aspects of the coordination compounds. Also the cyclic voltammetric behavior of the coordination compounds is discussed at the end of each chapter in an appropriate length. In chapter 4 the methylated pyrazolylcyclotriphosphazene ligands are described. In chapter 5 the steric influence of the methyl group is highlighted by a discussion of the ligating behavior of the unsubstituted pyrazolylcyclotriphosphazene ligands. In chapter 6 a more flexible ligand resulting in eight-membered chelate rings is discussed. The differences and similarities of the tridentate N_3 ligands with different ligand bites are compared.

Crystal structures of six copper complexes and one each in nickel and cobalt have been solved during this research. The full details of the work discussed in this thesis have already been published [12-15] or have recently been submitted for publication.

References

- [1] Gallicano, K.D., Paddock, N.L., Rettig, S.J. and Trotter, J. *Inorg. Nucl. Chem. Letts.*, **1979**, *15*, 417.
- [2] Gallicano, K.D. and Paddock, N.L. *Can. J. Chem.*, **1982**, *60*, 521.
- [3] Krishnamurthy, S.S., Reddy, V.S., Chandrasekharan, A. and Nethaji, M. *Phosphorus Sulfur and Silicon*, **1992**, *64*, 99.
- [4] Chandrasekharan, A., Krishnamurthy, S.S. and Nethaji, M. *Curr. Sci.*, **1991**, *60*, 700.
- [5] Spiro, T.G. (Ed.) *Copper Proteins*, Wiley, New York, **1981**.
- [6] Karlin, K.D. and Zubieta, J. (Eds.) *Biological and Inorganic Copper Chemistry*, Guilderland, Adenine Press, **1986**.
- [7] Bouwman, E., Driessen, W.L. and Reedijk, J. *Coord. Chem. Rev.*, **1990**, *104*, 143.
- [8] Vasak, M. *J. Am. Chem. Soc.*, **1980**, *102*, 3953.
- [9] Hathaway, B.J. *Struct. Bonding (Berlin)*, **1984**, *57*, 55.

- [10] Gazo, J., Bersuker, I.B., Garaj, L., Kebesova, M., Kohout, J., Langfelderova, H. Melnik, M., Serator, M. and Valach, F. *Coord. Chem. Rev.*, **1976**, *19*, 253.
- [11] Allcock, H.R., Desorcie, J.L. and Riding, G.A. *Polyhedron*, **1987**, *6*, 119.
- [12] Justin Thomas, K.R., Chandrasekhar, V., Pal, P., Scott, S.R., Hallford, R., Cordes, A.W. *Inorg. Chem.*, **1993**, *32*, 606.
- [13] Chandrasekhar, V. and Justin Thomas, K.R. *Appl. Organomet. Chem.*, **1993**, *7*, 1.
- [14] Justin Thomas, K.R., Chandrasekhar, V., Scott, S.R., Hallford, R., Cordes, A.W. *J. Chem. Soc. Dalton Trans.*, **1993**, 2589.
- [15] Chandrasekhar, V. and Justin Thomas, K.R. *Struct. Bonding (Berlin)*, **1993**, *81*, 41.

Cyclophosphazenes as Transition Metal Carriers: Synthetic Strategies and Structural Perspectives

“Much of life can be understood in rational terms if expressed in the language of chemistry. It is an international language, a language for all time, and a language that explains where we came from, what we are, and where the physical world will allow us to go. Chemical language has great esthetic beauty”

–Arthur Kornberg in *Biochemistry*, 1987, 26, 6888.

2.1 Introduction

Since the first isolation of inorganic heterocyclic compounds $N_3P_3Cl_6$ (1) and $N_4P_4Cl_8$ (2), from the reaction of PCl_5 with ammonia or ammonium chloride the study on these heterocyclic compounds has progressed for two main reasons:

- Interesting and simple chemical properties
- Capability to serve as carriers for active side groups which are extremely adaptable for biomedical [1-3] and industrial applications [4].

So it is not a surprising fact, that cyclophosphazenes occupy a prominent place among the inorganic heterocyclic compounds [5, 6].

In cyclophosphazenes the ring system is made up of alternating phosphorus and nitrogen atoms. Phosphorus is pentavalent and tetracoordinate while nitrogen is trivalent and dicoordinate. Two exocyclic substituents are present on phosphorus while none are on nitrogen. Although the ring size can vary from four to a maximum isolated ring size of thirty four the most widely studied examples are the six-membered and eight-membered rings. An important facet of cyclophosphazene chemistry is its built in relationship to the high polymer chemistry [7]. The ring opening polymerization of **1** leads to a hydrolytically unstable linear polymer (**3**) of high molecular weight (Figure 1) [8]. This reactive polymer (**3**) can be reacted with several nucleophiles, thereby affording a route to structurally diverse macromolecules. Small rings are excellent models for exploratory reactions that can be applied subsequently at the high polymer level. Conventional research on cyclophosphazenes has mainly centred on the following themes [9-13]:

- (a) Substitution reactions involving the P-Cl bond in $\text{N}_3\text{P}_3\text{Cl}_6$ (**1**) and $\text{N}_4\text{P}_4\text{Cl}_8$ (**2**) by various types of nucleophiles including amines, alcohols, phenols, thiols, main group and transition-metal organometallic reagents etc. (Figures 1 and 2).
- (b) Interaction of transition metals with cyclophosphazene derivatives. This area of research has been receiving immense attention in recent years.

The flexible reactivity of halogenocyclophosphazenes promises the possibility of incorporating several functional groups in cyclophosphazenes, thus giving rise to novel tailored ligands. The mode of interaction of transition-metals to cyclophosphazenes can be conveniently divided into three categories. (1) Attachment of skeletal atoms (nitrogen or phosphorus) of phosphazenes to transition-metals. (2) Coordination of the metal to an organic donor that is itself connected as a substituent to a skeletal phosphorus atom. (3) Ionic or salt-type linkages.

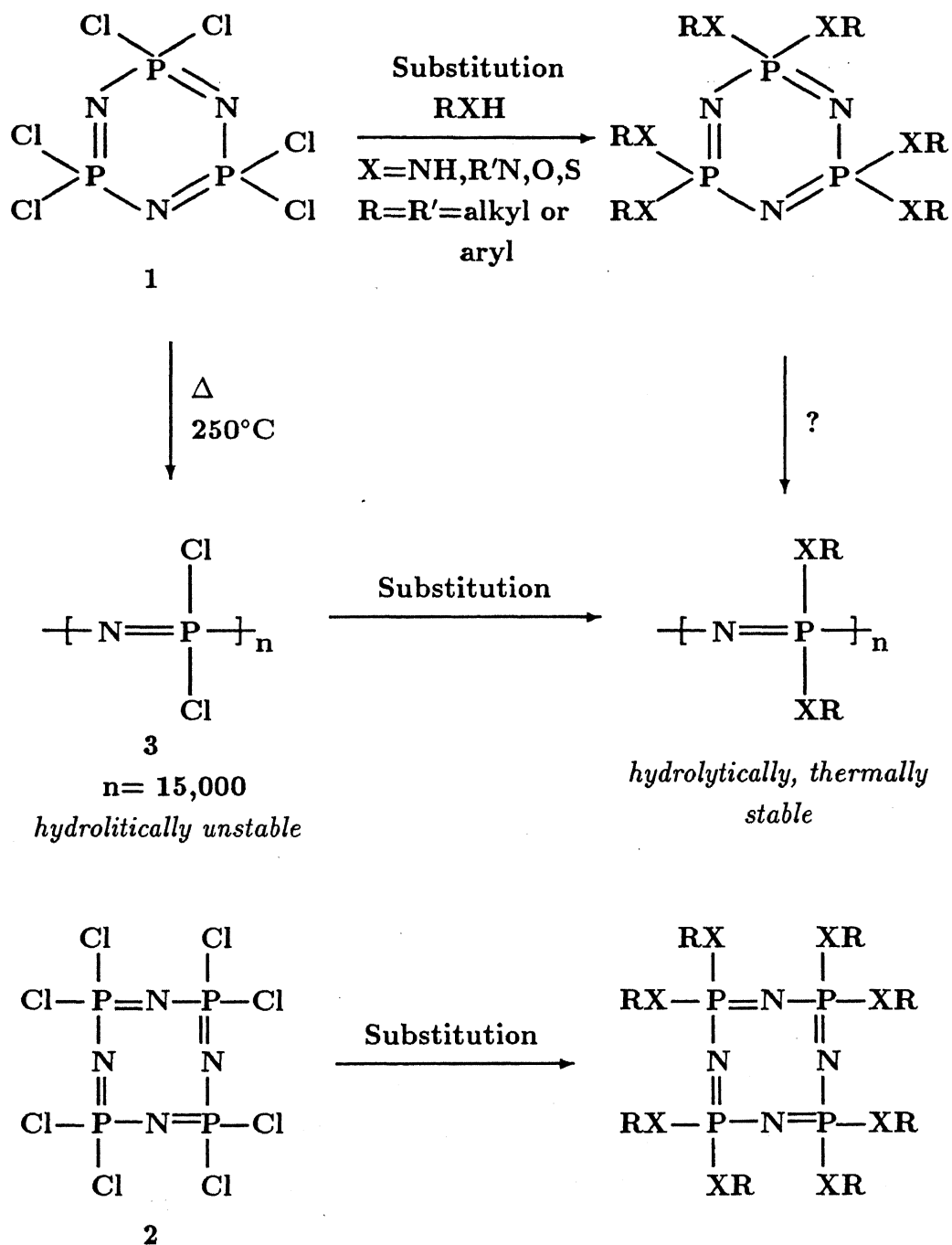


Figure 1: Summary of chemistry of cyclophosphazenes

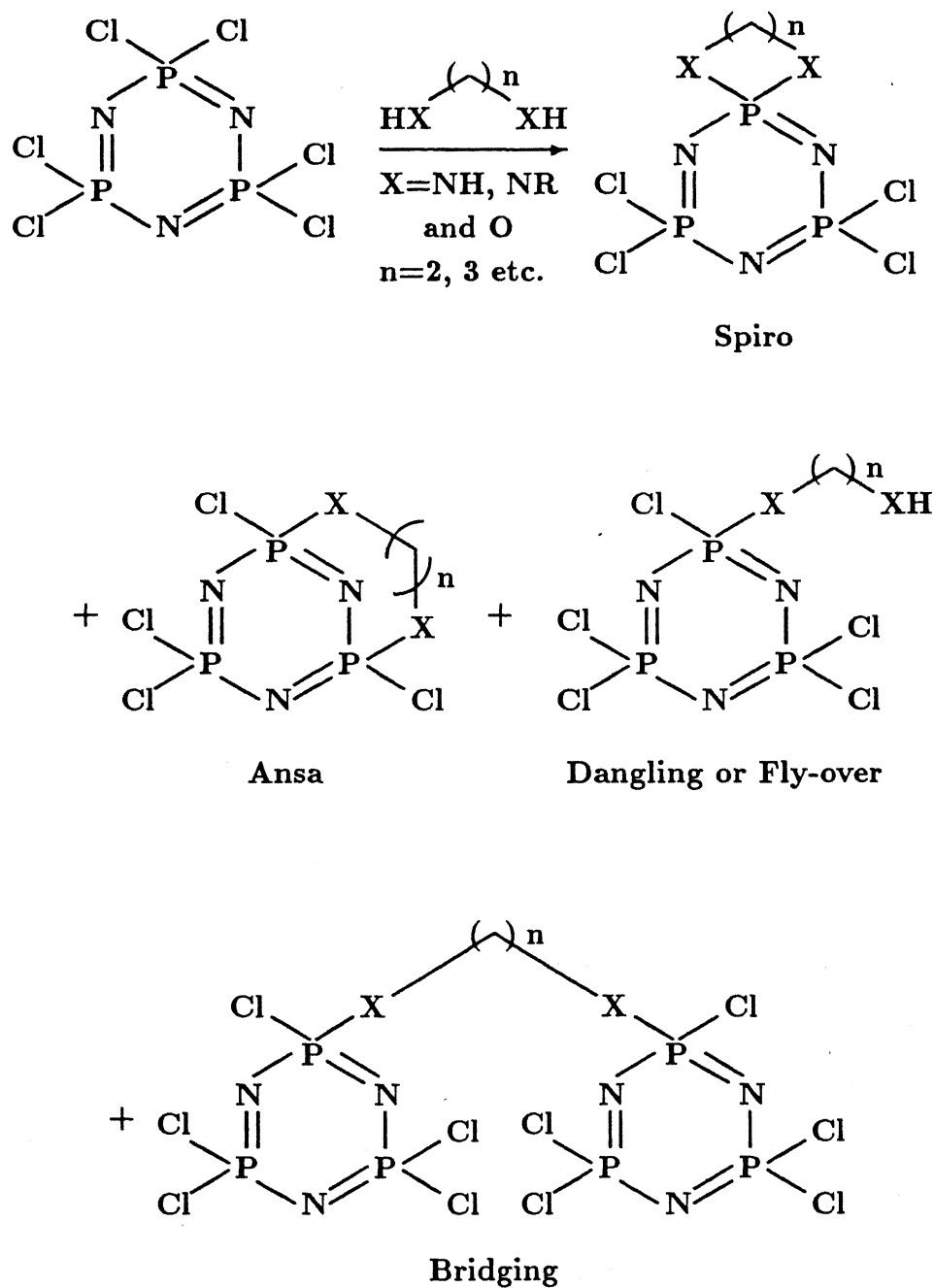


Figure 2: Reactions of difunctional reagents with halogenocyclotriphosphazenes

2.2 Skeletal Nitrogen Coordination

Each skeletal nitrogen atom of a phosphazene bears a lone pair of electrons and therefore, phosphazenes can be used as classical ligands. However, the availability of lone pair of electrons for donation to metals depends on the substituents on phosphorus. Electron-withdrawing side groups, such as fluorine or trifluoroethoxy, reduce the basicity of skeletal nitrogen but, at the same time, strengthen the skeletal bonds. Conversely, electron-releasing substituents such as alkylamino, alkyl etc., enhance the basicity of the skeletal nitrogen atoms. An additional feature that governs the ligating behavior of cyclophosphazenes is the ring size. Thus, larger sized rings which are puckered can easily accomodate the metals in their preferential coordination geometries.

Although cyclotriphosphazenes possess three nitrogen donors, no case has been reported in which two or three nitrogens engage simultaneously in coordination. Thus, $N_3P_3(CH_3)_6$ interacts with titanium tetrachloride in an unidentate fashion [14]. Aminophosphazenes such as $N_3P_3(NHPr^n)_6$ and $N_3P_3(NHBu^n)_6$ were reported to form complexes with cobalt, copper and nickel halides [15]. However, the structures of these have not been established as no crystal structures are available.

Cyclotetraphosphazenes behave both as monodentate and bidentate ligands in the favorable circumstances i.e., depending upon the nature of the metal. Thus, $N_4P_4(CH_3)_8$ reacts with anhydrous cupric chloride in methyl ethyl ketone, to result in a complex in which the copper is bonded to a ring nitrogen; in this complex cyclotetraphosphazene functions as an unidentate ligand [16] (Figure 3). An antipodal nitrogen is found protonated in this complex. But an analogous reaction of $N_4P_4(CH_3)_8$ with $PtCl_2$ results in a square planar complex, with the two opposite ring nitrogen atoms coordinated to platinum in a cis-manner (Figure 3) [17]. A complex of similar structure has been isolated in the reaction of $N_4P_4(NHMe)_8$ with K_2PtCl_4 in the presence of 18-Crown-6 [18]. In these complexes the cyclotetraphosphazenes

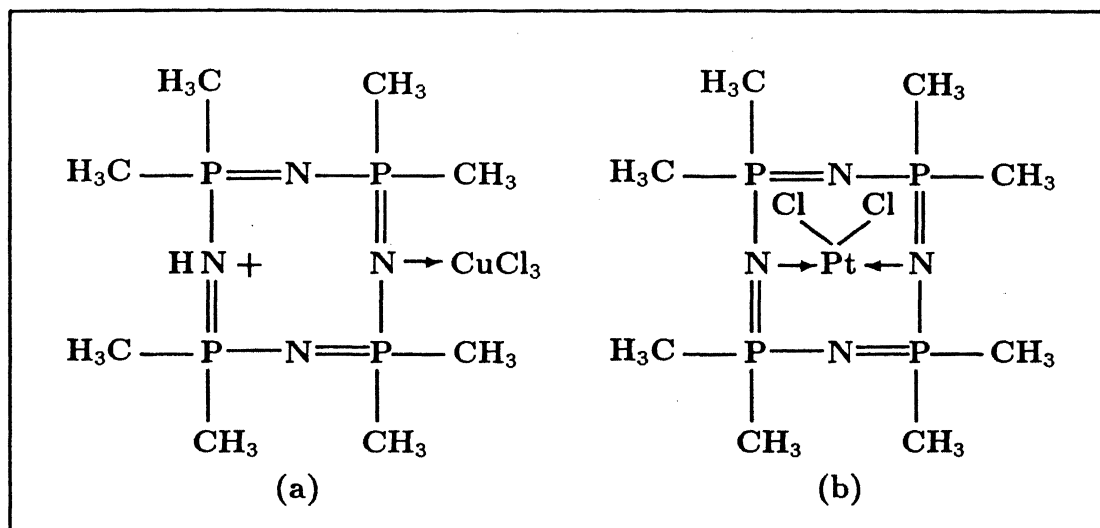


Figure 3: Examples of ring nitrogen coordination of cyclotetraphosphazenes

function in a bidentate manner.

With higher membered ring systems such as $N_6P_6(NMe_2)_{12}$, $N_6P_6(CH_3)_{12}$ and $N_8P_8(CH_3)_{16}$ coordination of two or four skeletal nitrogen atoms is observed [19-24]. The twelve-membered ring compound $N_6P_6(CH_3)_{12}$ forms 1:1 complexes with $PdCl_2$ and $PtCl_2$. Two ring nitrogen atoms coordinate to the metal and occupy cis positions in the square planar complex [23]. This type of complexation results in six- and ten-membered chelate rings (Figure 4). $N_6P_6(NMe_2)_{12}$ forms 1:2 complexes of the general formula $[N_6P_6(NMe_2)_{12}] \cdot 2 MCl_2$ ($M = Mn, Fe, Co, Cu, Zn$) [19]. The crystal structures of cobalt and copper complexes show that the basal site of a distorted square pyramid is occupied by four skeletal nitrogen atoms and a chlorine atom at the apical position [20-22]. The structure is unique in that it contains two six-membered and two four-membered chelate rings (Figure 4). The nitrate analogs $[N_6P_6(NMe_2)_{12}] \cdot M(NO_3)_2$ ($M = Co, Ni, Cu, Mn$) are also believed to have similar structures [25]. $N_8P_8(CH_3)_{16}$ forms a complex with cobalt nitrate, $[N_8P_8(CH_3)_{16}] \cdot Co(NO_3)](NO_3)$ in which the cobalt exists in a trigonal prismatic geometry [24]. The metal environment consists of two oxygens from a nitrato group and four skeletal nitrogen atoms of the cyclophosphazene ring.

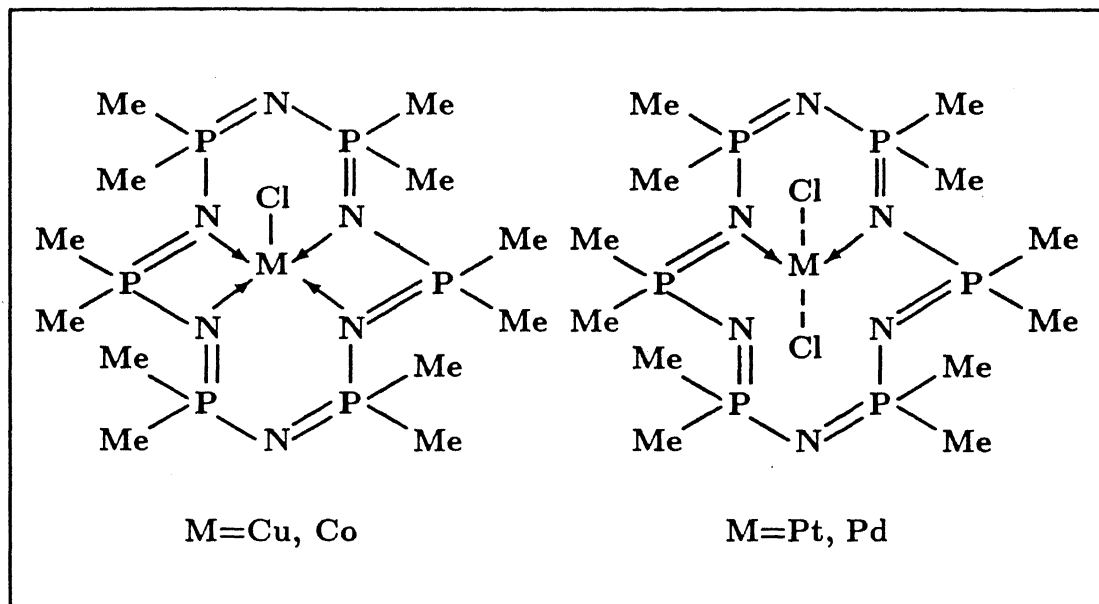


Figure 4: Different coordination modes of cyclohexaphosphazenes

2.3 Ionic, Salt-type Species

In the aminophosphazenes the amino substituents being electron-donating groups, increase the basicity of the skeletal nitrogen atom. This basic nitrogen can acquire a proton or alkyl cation to generate onium-type sites that function as counterions for metallo anionic units. Thus, $\text{N}_3\text{P}_3(\text{NMe}_2)_6$ and $\text{N}_4\text{P}_4(\text{CH}_3)_8$ react with CoCl_2 to give ring protonated species $[\text{N}_3\text{P}_3(\text{NMe}_2)_6\text{H}^+]_2[\text{CoCl}_4^{2-}]$ and $[\text{N}_4\text{P}_4(\text{CH}_3)_8\text{H}^+]_2[\text{CoCl}_4^{2-}]$ respectively [26-28]. Similarly $\text{N}_4\text{P}_4(\text{NHMe})_8$ reacts with K_2PtCl_4 in the presence of HCl to afford $[\text{N}_4\text{P}_4(\text{NHMe})_8\text{H}_2^{2+}][\text{PtCl}_4^{2-}]$ [17]. A hexamolybdate salt of formula $[\text{N}_3\text{P}_3(\text{NMe}_2)_6\text{H}^+]_2[\text{Mo}_6\text{O}_{19}^{2-}]$ was formed when $\text{N}_3\text{P}_3(\text{NMe}_2)_6$ reacted with MoO_3 in water [29]. The methyl iodide quarternary salt of $\text{N}_4\text{P}_4(\text{CH}_3)_8$, $[\text{N}_4\text{P}_4(\text{CH}_3)_9]^+\text{I}^-$ reacts with chromium or molybdenum hexacarbonyl to generate the species $[\text{N}_4\text{P}_4(\text{CH}_3)_9]^+[\text{M}(\text{CO})_5\text{I}^-]$ ($\text{M}=\text{Cr}$ or Mo) [30, 31]. $\text{N}_5\text{P}_5(\text{CH}_3)_{10}$ on interaction with CuCl_2 forms a diprotonated salt $[\text{N}_5\text{P}_5(\text{CH}_3)_{10}\text{H}_2^{2+}][\text{CuCl}_4^{2-}]$ [32].

2.4 Effect of Metal Coordination or Protonation to Ring Nitrogen on the Structure of Cyclophosphazenes

The basic σ -frame work of the cyclophosphazene is constituted from the sp^3 hybrid orbitals of phosphorus and approximately sp^2 hybrid orbitals of nitrogen. Two sp^2 orbitals of nitrogen are involved in bonding to phosphorus while the third which is *in-plane* with the P-N-P segment is occupied by a lone pair. The remaining non-sigma bonding electrons, one from phosphorus and one from nitrogen are believed to participate in a $d_{\pi}-p_{\pi}$ bond that makes use of a nitrogen $2p_z$ orbital and one of several phosphorus 3d orbitals [33]. The delocalization of these π -electrons occurs over three skeletal atoms only in a way that permits an equalization of bond lengths around a ring [34]. This π -bonding can be supplemented by an *in-plane* dative π -bonding between the nitrogen lone pair electrons and a suitable phosphorus 3d-orbital. Thus, in homogenously persubstituted cyclophosphazenes $N_3P_3(R)_6$, $N_4P_4(R)_8$ etc., the P-N bond lengths are virtually equal within a molecule and are shorter (1.51–1.60 Å) than 'normal' P-N single bonds (1.77 Å). Also, the ring P-N bond distances decrease with increasing electronegativity of the exocyclic substituents on phosphorus [9]. Such electron-withdrawing groups on phosphorus strengthen the skeletal bonds probably by causing a contraction of the phosphorus d-orbitals and improving their overlap efficiency or accentuating the π_s bonding. The electron donating substituents weaken the skeletal bonds, but would enhance π -bonding between phosphorus and the exocyclic substituent and localize the lone pair of electrons on skeletal nitrogen atoms. The effects of metal coordination or protonation to ring nitrogen are easily understood in the background of the above theories.

The principal effect of protonation or coordination is the variations in the P-N bond lengths within a molecule. The P-N bond lengths involving the coordinated or protonated nitrogen atom (in P-NM-P segment, M=metal or proton) are longer than

in the free ligand. Protonation is more effective; thus in $[\text{N}_3\text{P}_3(\text{NMe}_2)_6\text{H}^+]_2 [\text{Mo}_6\text{O}_{19}^{2-}]$ the P–N bond lengths adjacent to the protonated nitrogen atom increase to 1.67\AA [29] while in the free ligand $\text{N}_3\text{P}_3(\text{NMe}_2)_6$ it is only 1.59\AA [35]. This lengthening is understood by considering that the lone pair of electrons on skeletal nitrogen is now not available for *in-plane* π -bonding. The ring bond angles and conformation are not affected to the same extent. However, in some cases deviations in bond angles and nonplanar conformations of the cyclophosphazene rings are observed which originate from the geometrical requirements of the metal environment. This aspect is substantiated in the latter part of this thesis.

2.5 Ring Phosphorus Interactions with Metals

Two types of phosphorus interactions with transition metals are observed: (1) covalent (2) coordinate. Cyclophosphazene derivatives which contain direct metal-phosphorus covalent bond are obtained by employing either of the methods enumerated below [36]:

- (1) Nucleophilic substitution reactions of transition metal carbonyl anions with halogenocyclophosphazenes.
- (2) Reactions of phosphazene anions with metal carbonyl halides.

The first technique is complex and halogen abstraction and skeletal cleavage side reactions occur concurrently.

Allcock and co-workers have found that the reaction of $\text{N}_3\text{P}_3\text{F}_6$ with $\text{NaFeCp}(\text{CO})_2$ affords the geminally substituted derivative, $\text{N}_3\text{P}_3\text{F}_4[\text{FeCp}(\text{CO})_2]_2$ [37-39]. This on photolysis gives a three membered spirocyclic product containing a Fe–Fe bond and a bridging carbonyl group (Figure 5) [37]. The reaction of $\text{N}_3\text{P}_3\text{Cl}_6$ with disodium octacarbonyldiferrate yields a spiro diiron octacarbonyl bonded phosphazene, 2,2- $\text{N}_3\text{P}_3\text{Cl}_4\text{Fe}_2(\text{CO})_8$ and a triiron decacarbonyl bonded phosphazene $\text{N}_3\text{P}_3\text{Cl}_4\text{Fe}_3(\text{CO})_{10}$

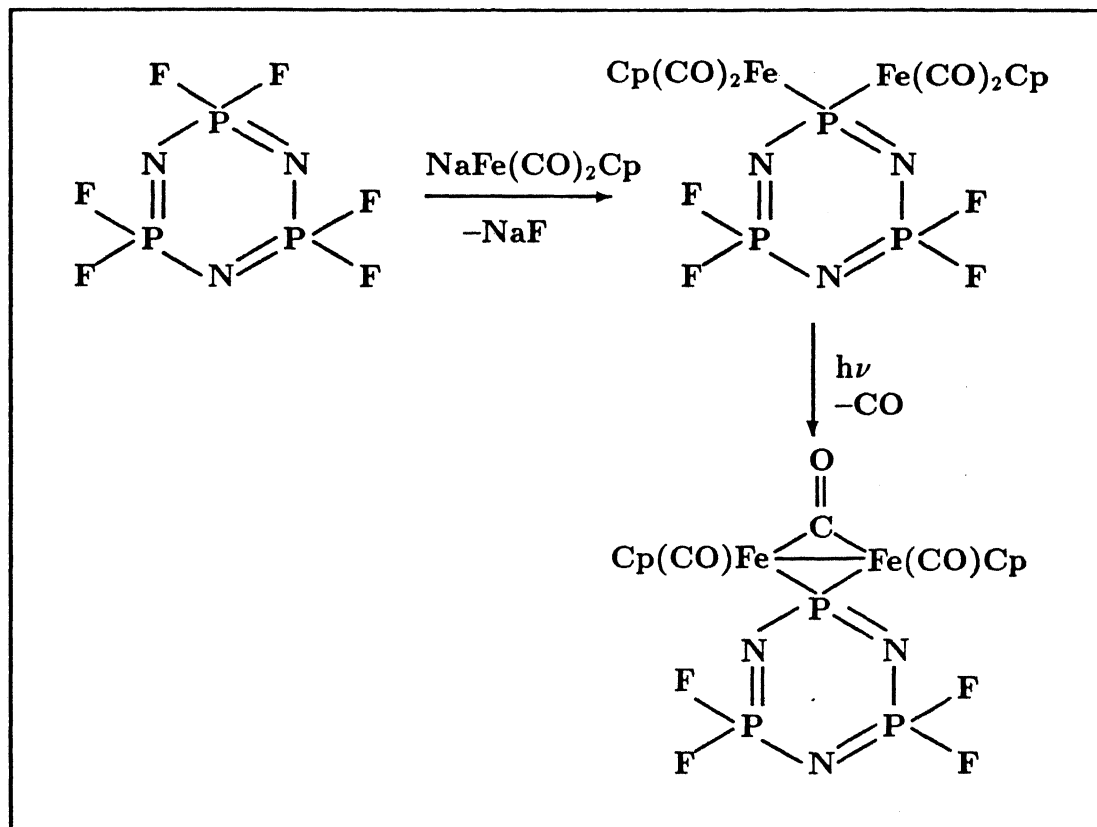


Figure 5: Reaction of $\text{N}_3\text{P}_3\text{F}_6$ with NaFeCp(CO)_2

(Figure 6) [40,41]. The latter metalloccluster contains both covalent phosphorus-metal and nitrogen-metal coordination bonds, demonstrating both the covalent and coordinative capacities of the cyclophosphazene ring. The diiron derivative acts as a template for the construction of similar dimetal derivatives and clusters with other metals (Figure 6) [41, 42].

In an another reaction, chloride substitution of $\text{N}_3\text{P}_3\text{Cl}_6$ with $[\text{M(CO)}_3\text{Cp}^-] [\text{n-Bu}_4\text{N}^+]$ ($\text{M} = \text{Cr}, \text{Mo}, \text{W}$) gives rise to a series of phosphorus-metal covalently linked derivatives (Equation 1) [43]. With molybdenum and tungsten carbonyl anions an additional chloride displacement also occurs; in the resulting derivative, phosphorus is also linked to a cyclopentadienyl group (Equation 1).

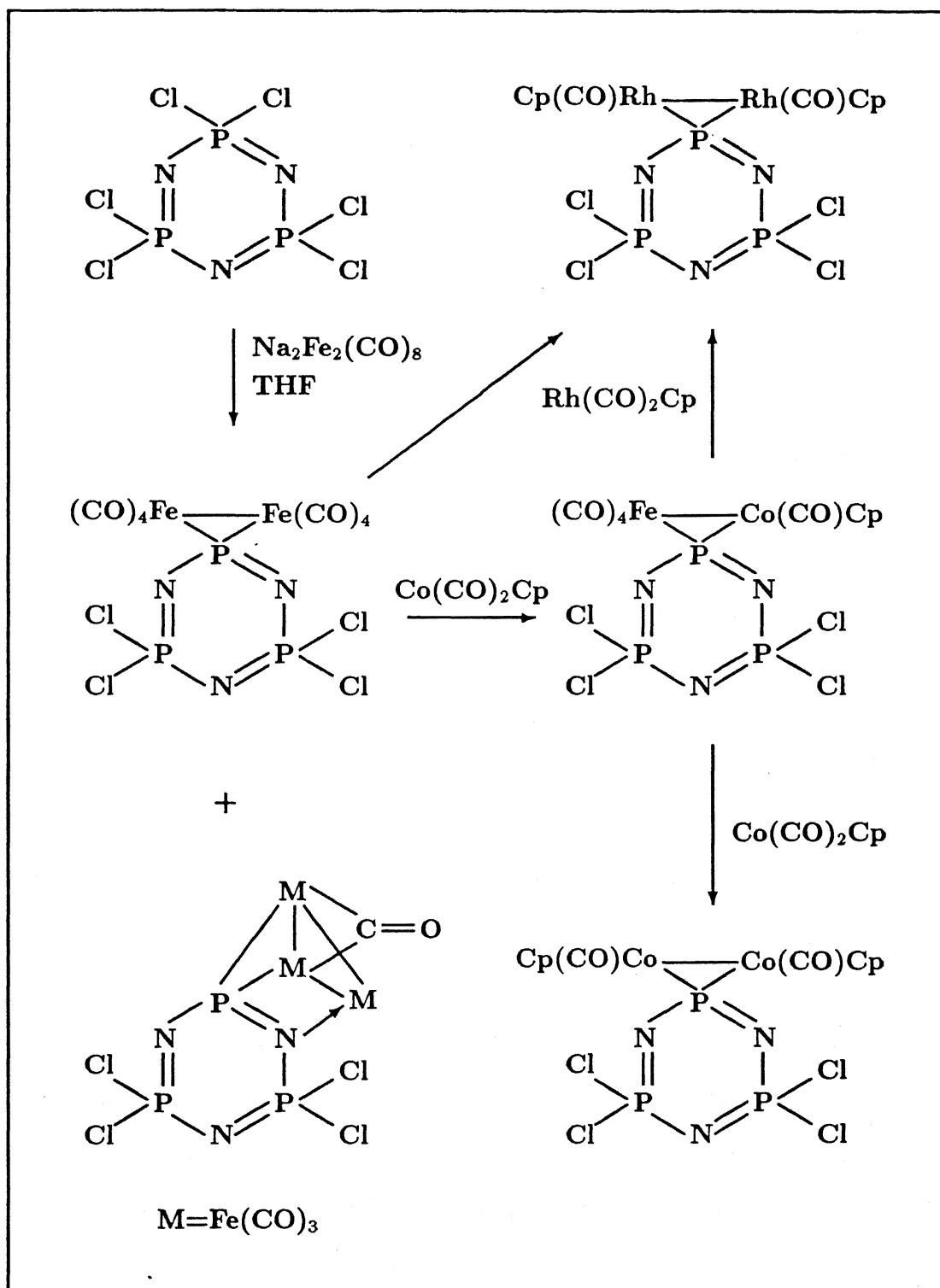
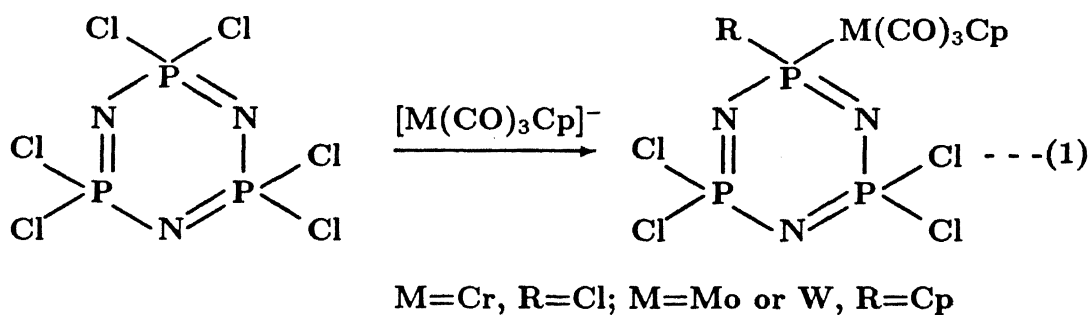


Figure 6: Reaction of $\text{N}_3\text{P}_3\text{Cl}_6$ with $\text{Na}_2\text{Fe}_2(\text{CO})_8$ and related reagents



Atleast three procedures are used to synthesize the phosphazene anions. (a) Hydrido phosphazenes on treatment with alkyl lithium reagents generate the phosphazene anion intermediates [44,45]. (b) LiBEt_3H reacts with halogenocyclophosphazenes to produce the same [46]. (c) Phosphorus-phosphorus bridged bicyclic phosphazenes are cleaved by LiBEt_3H to result in phosphazene anions [44]. These phosphazene anions on treatment with a metal carbonyl halide, $\text{FeCp}(\text{CO})_2\text{I}$ gives the desired phosphorus-metal covalently linked derivative (Figure 7) [44-46].

Coordination to metal *via* cyclophosphazene phosphorus is not possible as it is pentavalent and has no lone pair of electrons for donation. However, hydridophosphazenes containing a P-H bond exist in two resonance forms (Figure 8). One of these structures (II) contains a trivalent phosphine-like phosphorus which can interact with transition metals. This possibility has been utilized to link the phosphorus atom of the cyclophosphazene ring directly to a metal [47,48]. Thus, $\text{N}_3\text{P}_3\text{Ph}_4(\text{CH}_3)\text{H}$ forms complexes of the type $\text{L}\cdot\text{M}$ with $\text{Au}(\text{CO})\text{Cl}$ and $[(\text{CH}_3)_2\text{AuCl}]_2$ [47]. But with palladium and platinum halides $\text{L}_2\cdot\text{M}$ type complexes are obtained (Figure 9) [48].

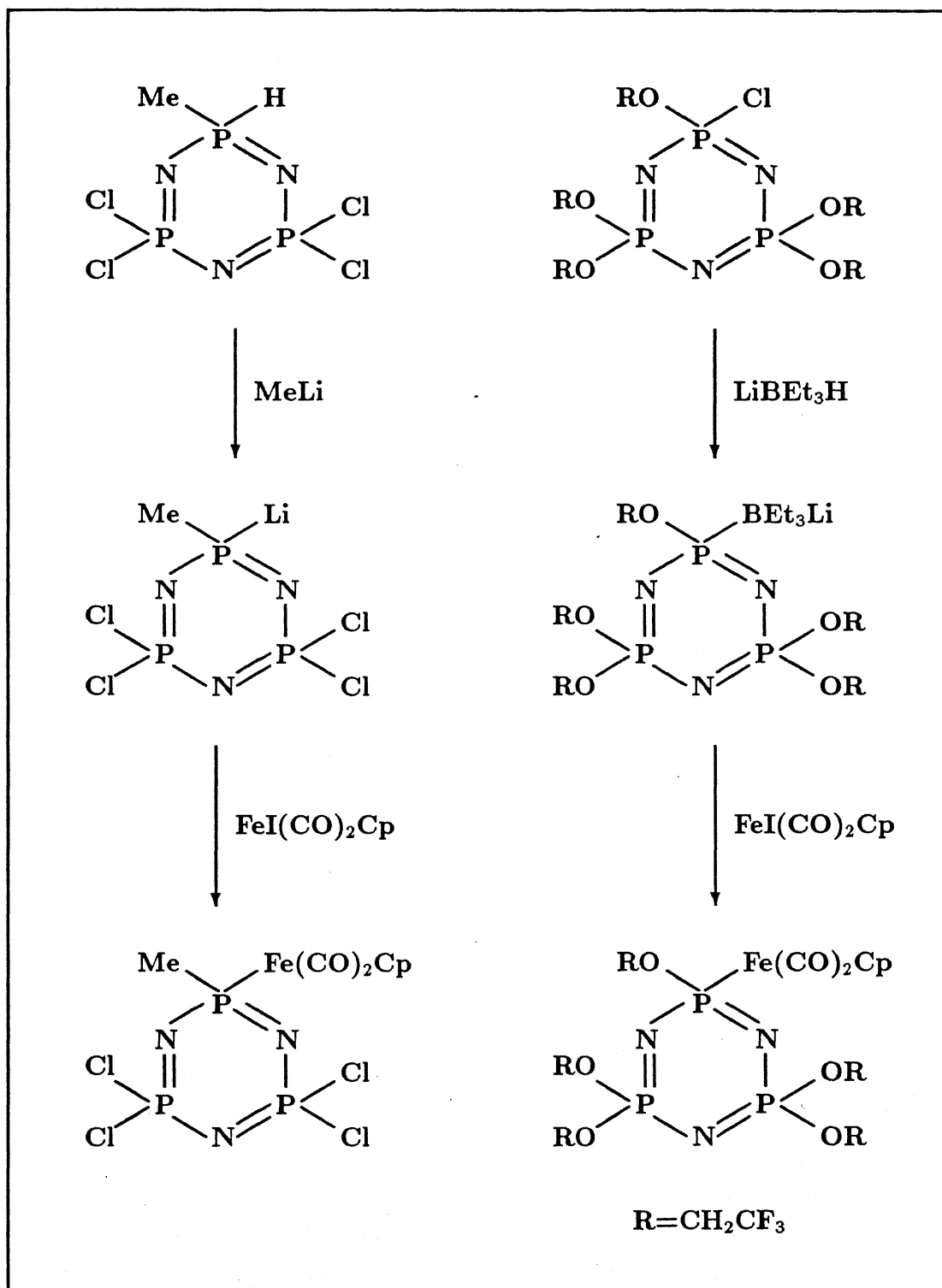


Figure 7: Synthesis of phosphazene anions and their reaction with FeCp(CO)_2

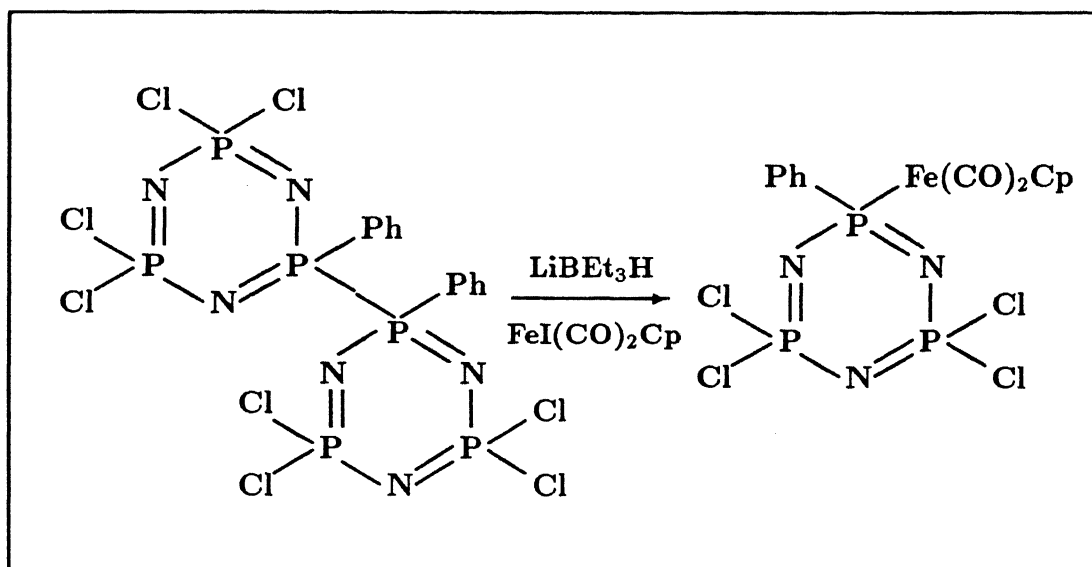


Figure 7: continued

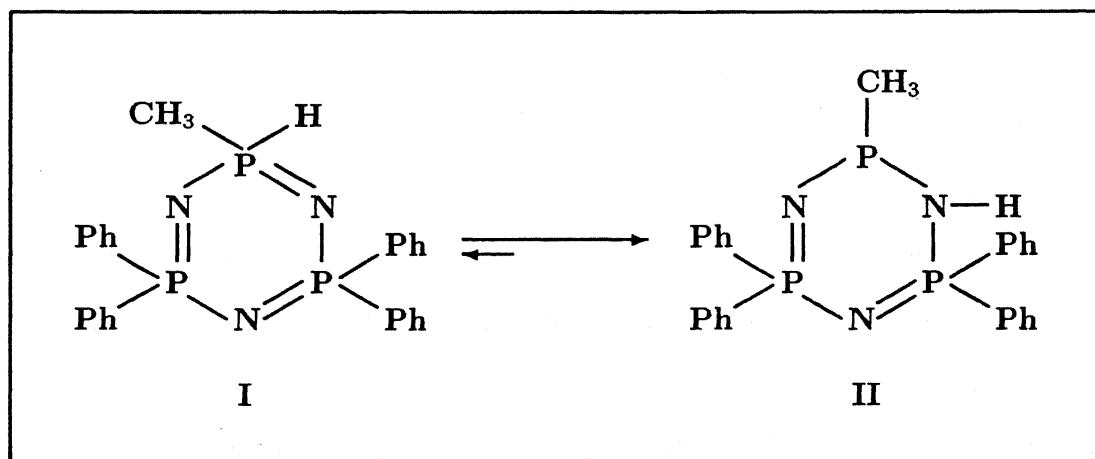


Figure 8: Tautomers of hydridophosphazenes

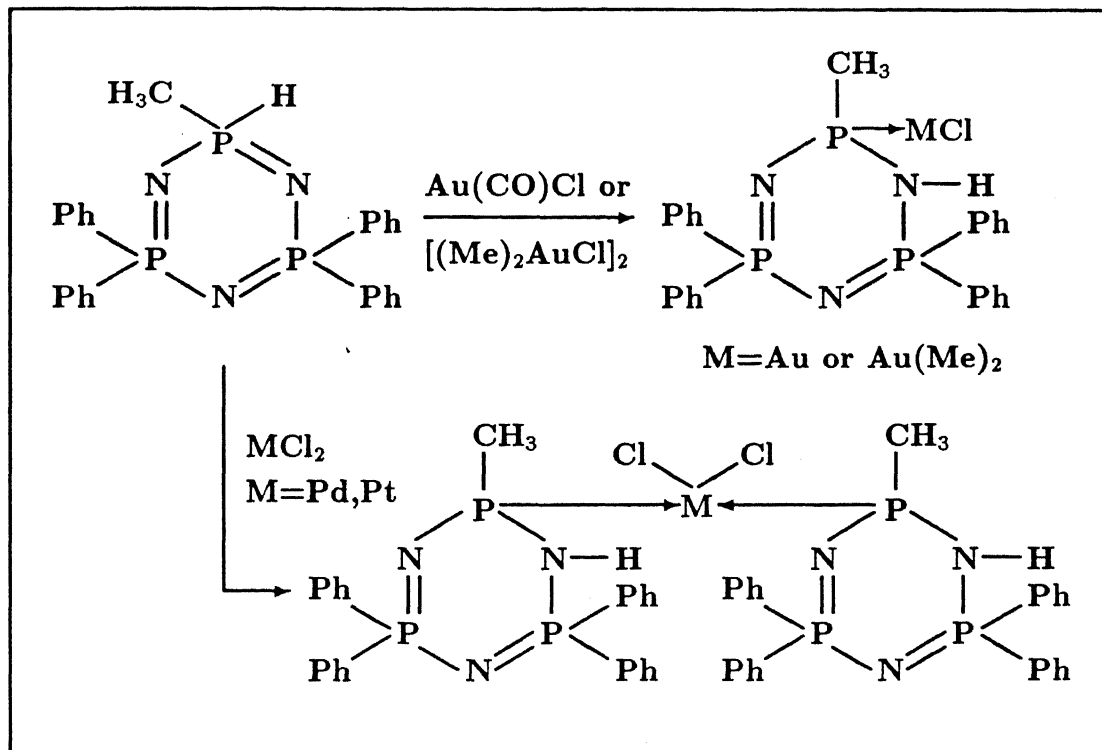


Figure 9: Interactions of hydridophosphazene with metal halides

2.6 Effect of Skeletal Phosphorus Interaction with Metals on the Structure of Cyclophosphazenes

Crystal Structures of as many as fifteen compounds having direct metal-phosphorus bond have been solved so far, allowing a good rationalization on the structural effects prevalent on the cyclophosphazene unit because of the presence of the new exocyclic phosphorus-metal bond. As earlier noted the ring nitrogen coordination to the metal mainly hampers the skeletal π_s bonding, which really gives a superficial appearance of aromaticity to the free base cyclophosphazenes, and affects the uniformity of the skeletal bond distances. Such an effect is more severe with the phosphorus-metal interactions. The general trends observable are illustrated in Figure 10. The following features are noteworthy:

- (i) The two P-N bonds (denoted as 'a' in Figure 10(a)) proximal to the metal atoms are the longest, the adjacent pair of P-N bonds ('b' in Figure 10(a)) are

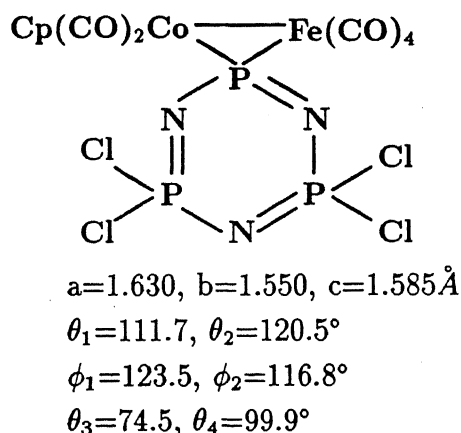
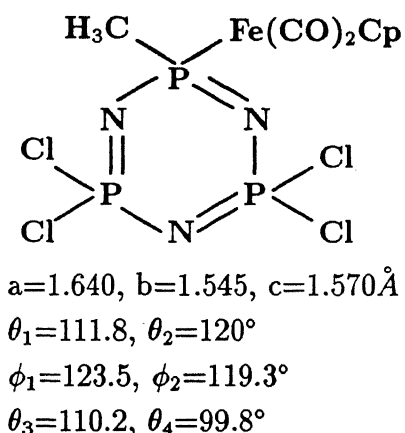
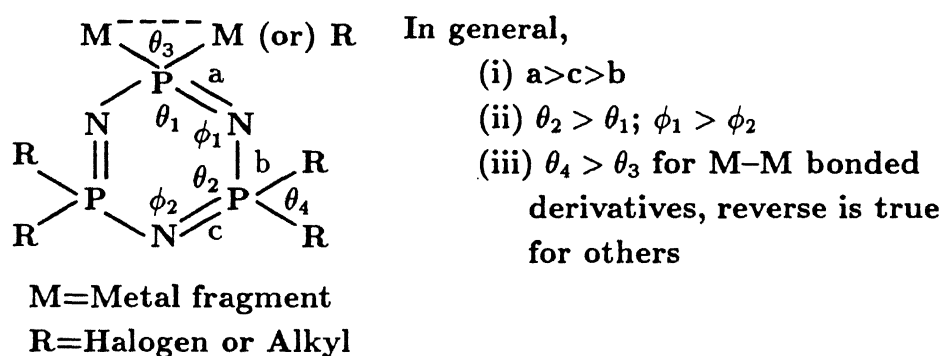


Figure 10: Trends in the bonding parameters of cyclotriphosphazenes with direct P-Metal covalent bond

the shortest and those farthest from the metal fragment of intermediate length (close to the normal cyclophosphazene P-N bond length ('c' in Figure 10(a)).

- (ii) The skeletal phosphorus atoms in cyclophosphazenes usually adopt a distorted tetrahedral geometry with an endocyclic ring angle near 120° and an exocyclic substituents angle around 100° . In contrast, in these compounds the exocyclic angle at the metallated phosphorus is constricted, while the exocyclic angle at phosphorus is either narrowed (M-M bonded spiro derivatives) or widened (see for examples Figure 10).
- (iii) The bond angles at the nitrogen adjacent to the phosphorus bearing metal are normal while, that at the distal nitrogen are contracted.

Electron releasing or less electronegative organic substituents do exert similar bond length and bond angle variations by filling the d-orbitals at the phosphorus and making them less available for π -bonding with ring nitrogens [9]. For the skeletal nitrogen coordination the structural effects are mainly in the vicinity of that nitrogen. But it is spread over the cyclophosphazene ring in the case of phosphorus-metal linkage.

2.7 Exocyclic Group Participation in Coordination

Several complexes have been reported in which the substituents on phosphorus of cyclophosphazene involve in coordination to the metal. In general, two synthetic methodologies are practiced (Figure 11). (a) A suitable donor group such as alkynes, arenes, schiff bases etc. is incorporated in cyclophosphazene by the usual substitution technique and then treated with metal precursors. (b) In the second synthetic approach, a complex containing a reactive functional group on the ligand is subjected to halide displacement reaction with halogenocyclophosphazenes.

For convenience these cyclophosphazene ligands are divided into two categories in keeping with the general practice.

(1) π -acid ligands and π -complexes

(2) classical ligands

2.7.1 Π -acid ligands and Π -complexes

Cyclophosphazene ligands containing exocyclic substituents such as, phosphines, alkynes, arenes, cyclopentadienyl group etc. are considered for discussion in this section. Two types of phosphine ligands have been prepared and these are given in Figure 12 [49, 50]. L6 in which a phosphino group is directly bound to the cyclophosphazene skeleton by a P-P bond reacts with $\text{Cr}(\text{CO})_5(\text{THF})$ or $\text{Fe}_2(\text{CO})_9$ to afford the

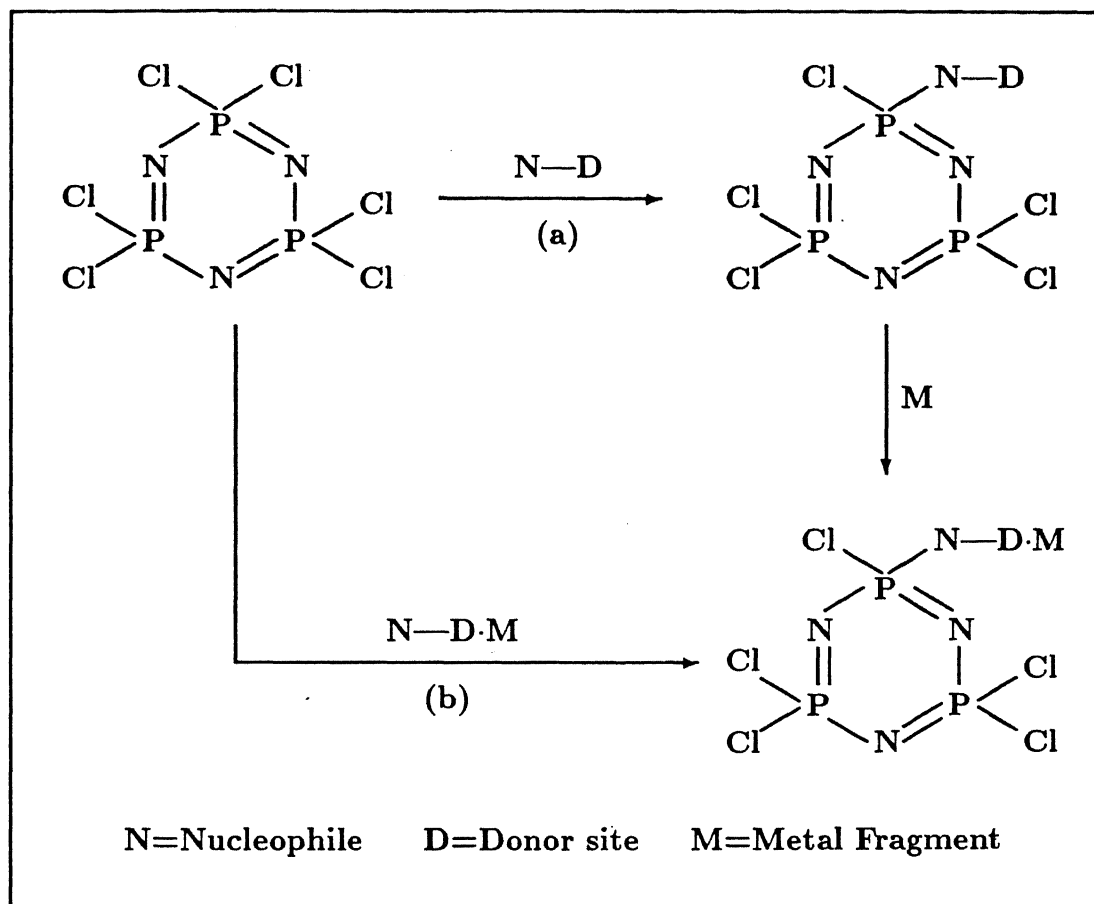


Figure 11: Synthetic strategies of exocyclic group coordinated cyclophosphazenes

mononuclear complexes $\text{L6} \cdot \text{Cr}(\text{CO})_5$ or $\text{L6} \cdot \text{Fe}(\text{CO})_4$ [50]. L6 behaves as a monodentate ligand *via* the phosphino group. A triruthenium cluster $\text{L6} \cdot \text{Ru}_3(\text{CO})_{11}$ in which the phosphino group is bonded to a ruthenium atom is also obtained from the reaction of L6 with $\text{Ru}_3(\text{CO})_{12}$. The ligating behavior of L4 and L5 is complex in which the phosphino group is tied with the cyclophosphazene through a spacer unit [49]. Thus, with $[\text{RhCl}(\text{CO})_2]_2$ and $\text{Fe}(\text{CO})_3\text{BZA}$, L4 forms complexes of ligand-metal ratio 2:1, $(\text{L4})_2 \cdot \text{M}$ ($\text{M}=\text{RhCl}(\text{CO})$ and $\text{Fe}(\text{CO})_3$) while with AuCl , $\text{H}_3\text{Os}_3(\text{CO})_{10}$ and $\text{Mn}(\text{CO})_2\text{Cp}(\text{THF})$ it forms complexes of the type $\text{L4} \cdot \text{M}$ ($\text{M}=\text{AuCl}$, $\text{H}_2\text{Os}_3(\text{CO})_{10}$ and $\text{Mn}(\text{CO})_2\text{Cp}$). L5, a potential hexadentate ligand, coordinates in a monodentate or bidentate fashion towards a metal, leading to a series of polynuclear coordination compounds [49]. The osmium derivatives of L4 and L5 function as catalysts for the

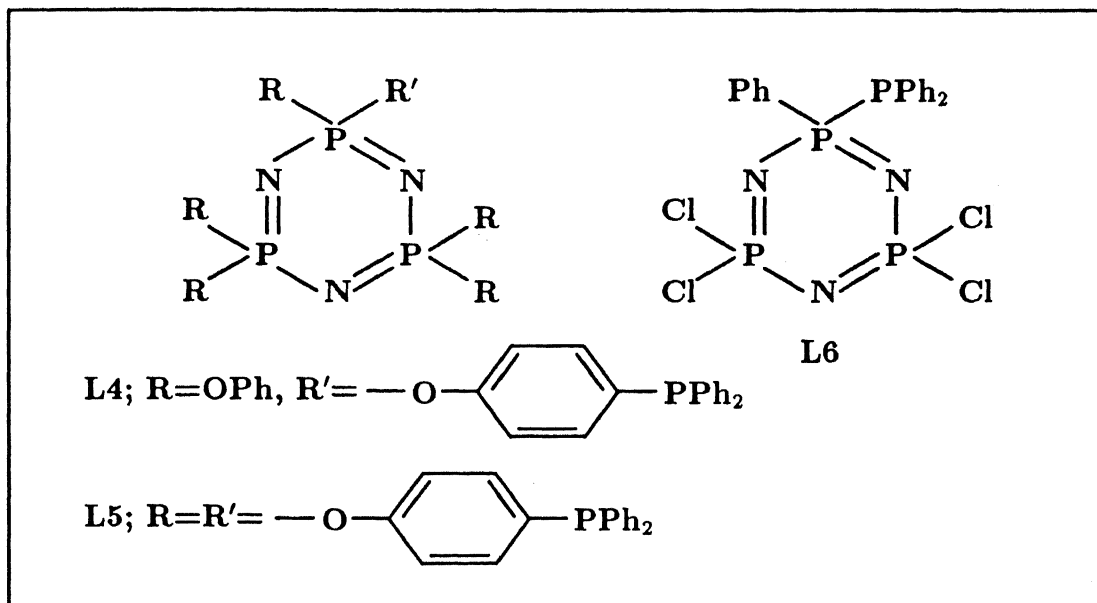


Figure 12: Structures of cyclotriphosphazenes containing pendant phosphino group(s) isomerization of 1-hexene to 2-hexene [49].

A large number of alkynyl phosphazene bridging dicobalt complexes of the general formula $\text{N}_3\text{P}_3\text{X}_5\text{C}\equiv\text{CR}\cdot\text{Co}_2(\text{CO})_6$ have been synthesized starting from alkynyl phosphazenes, $\text{N}_3\text{P}_3\text{X}_5\text{C}\equiv\text{CR}$ ($R=\text{SiMe}_3$, $n\text{-C}_4\text{H}_9$, Ph and $\text{X}=\text{F}$) and $\text{Co}_2(\text{CO})_8$ [51, 52]. A novel tetracobalt cluster, $2,2\text{-N}_3\text{P}_3\text{F}_4(\text{C}\equiv\text{CPh}\cdot\text{Co}_2(\text{CO})_6)_2$ has been obtained from the reaction of the alkynyl phosphazene, $2,2\text{-N}_3\text{P}_3\text{F}_4(\text{C}\equiv\text{CPh})_2$ with $\text{Co}_2(\text{CO})_8$ [51]. Allcock and coworkers have reported the formation of two series of π -complexes from the alkynyl phosphazenes, with the general formula $\text{gem-N}_3\text{P}_3\text{Cl}_4(\text{R})(\text{CH}_2\text{C}\equiv\text{CH})\cdot\text{Co}_2(\text{CO})_6$ and $\text{N}_3\text{P}_3\text{Cl}_4(\text{R})(\text{C}\equiv\text{C-CH}_3)\cdot\text{Co}_2(\text{CO})_6$ where R = methyl, ethyl, n -propyl, i -propyl, n -butyl, t -butyl and allyl groups (Figure 13) [53]. In all these complexes only the alkynyl unit interacts with the cobalt carbonyl fragment and no interference is noticed from the skeletal nitrogen atoms (Figure 13). Interestingly some of these complexes are identified as promising catalysts for the cyclotrimerization of alkynes [53].

Aryl phosphazenes form phosphazene- $(\eta^6\text{-arene})\text{Cr}(\text{CO})_3$ complexes on treatment with $\text{Cr}(\text{CO})_6$ [54]. Alternatively they are obtained by reacting the sodium salt of

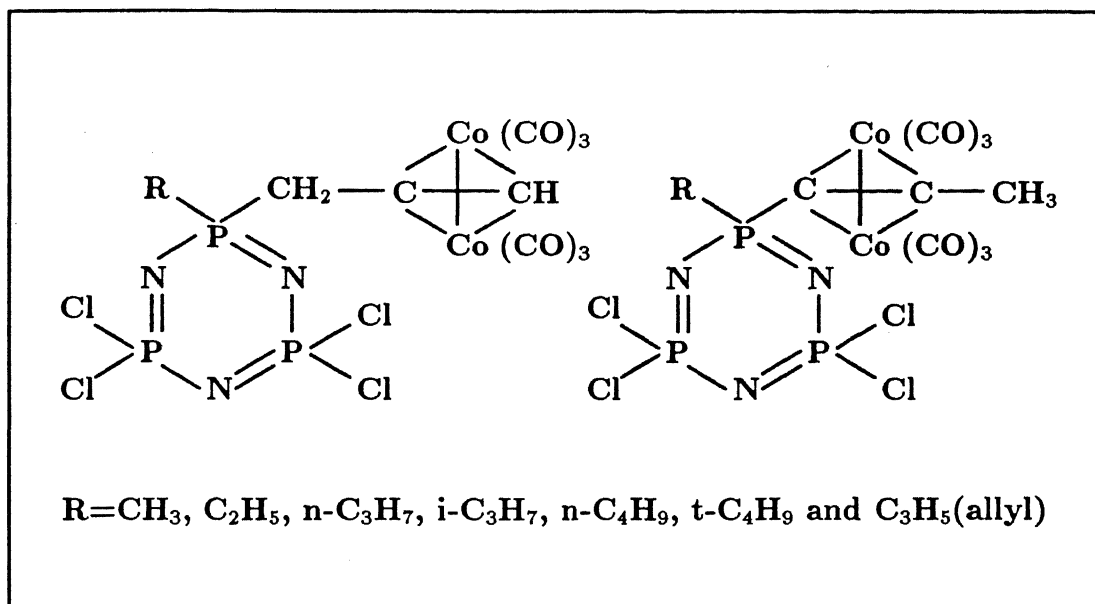
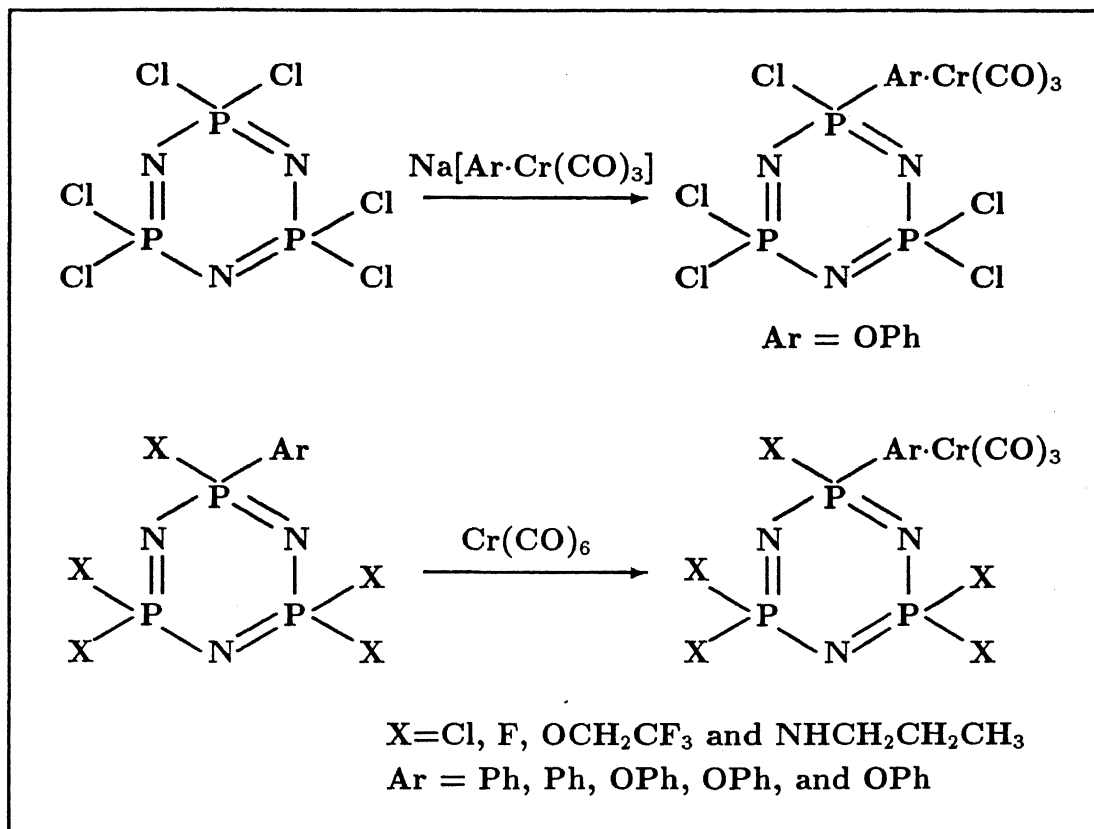


Figure 13: π -complexes of alkynylcyclophosphazenes

an alcoholic or phenolic chromium tricarbonyl complex with $\text{N}_3\text{P}_3\text{Cl}_6$. Figure 14 summarizes these reactions [54].

Allcock and coworkers have prepared ferrocenyl or ruthenocenyl linked cyclophosphazenes by treating a lithioferrocene or ruthenocene with the halogenocyclophosphazenes [55-60]. Both the trimeric and tetrameric derivatives have been obtained. Depending on the mode of attachment of the metallocene to the cyclophosphazene ring they fall into two groups i.e., pendant (I) and transannular (II) linked derivatives (*cf.* Figure 15). Apart from this, with cyclotetraphosphazenes an antipodally linked metallocene derivative is also isolated [60]. Crystal structure of one such compound, $\text{N}_4\text{P}_4\text{F}_4[(\eta\text{-C}_5\text{H}_4)_2\text{Ru}]_2$ is presented in Figure 16. Cyclic voltammetric studies of these compounds indicate that phosphazenes are highly electron withdrawing units, and give rise to marked positive shift in the oxidation potentials compared to ferrocene [61]. Type II (see Figure 15) derivatives show shifts twice those of pendant analogs (Type I) suggesting the cumulative electron withdrawing effect of the phosphazene operating *via* each cyclopentadienyl ring. Also the crystal structure determinations reveal that in the transannular linked complexes (Type II) the planarity of the cyclo-

Figure 14: η^6 -complexes of arylcyclotriphosphazenes

phosphazene ring is severely affected than that of type I compounds [58, 60].

2.7.2 Classical donors

Cyclophosphazenes containing exocyclic substituents with classical donor sites such as nitrogen, sulfur etc. are very limited. In complex, $\{N_3P_3(NMe_2)_4[NHCH_2CH_2NH]\}_2 \cdot NiCl_2$ an exocyclic nitrogen participation in coordination is predicted from the spectroscopic evidence [62]. However, in the complex $N_4P_4(NMe_2)_8 \cdot W(CO)_4$ (Figure 17) an endocyclic nitrogen also coordinated to the metal as confirmed by crystal structure determination [63]. Cyclophosphazenes which bear six schiff base units as substituents form hexanuclear complexes with zinc, palladium and platinum halides [64]. Macrocycles such as porphyrin [65, 66] and phthalocynin [67] linked cyclophosphazenes have been synthesized and their metallation behavior is found to be parallel to that

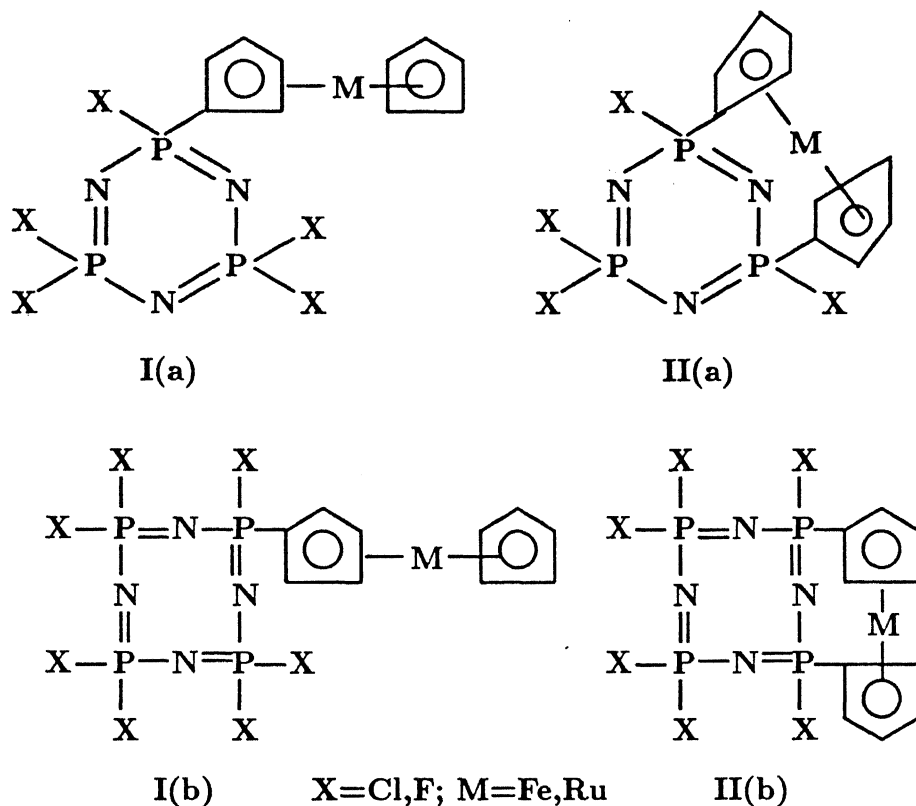


Figure 15: Types of ferrocenyl linked cyclophosphazenes

of unsubstituted macrocycles. A pendant carboranyl group of a cyclophosphazene has been found to interact with metal carbonyls [68]. Thiol functionalised cyclotriphosphazene, $\text{N}_3\text{P}_3\text{Ph}_4(\text{CH}_3)(\text{SH})$ (HL7) reacts with Ni, Pd and Pt chlorides to result in complexes $\text{M} \cdot (\text{L7})_2$ in which an exocyclic sulfur and an endocyclic nitrogen participate in coordination (Figure 17) [69]. The subject of this thesis is the coordination aspects of the pyrazolylphosphazenes which obviously falls in this category.

2.8 Concluding Remarks

It is abundantly evident from the above discussion, that cyclophosphazene based ligands are versatile in their coordination performance and lead to new variety of complexes and organometallics. Since they serve as model systems for the high poly-

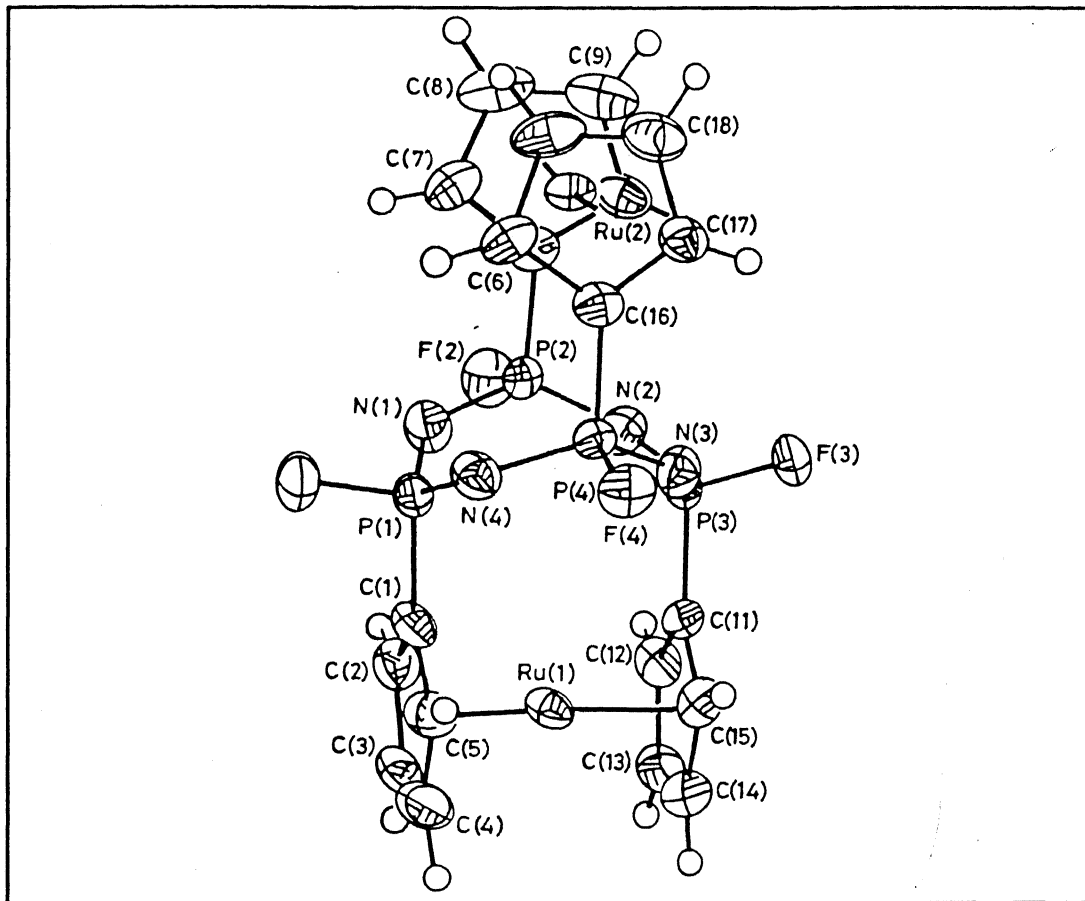


Figure 16: Crystal structure of $N_4P_4F_4[(\eta-C_5H_4)_2Ru]_2$

meric metal carriers the study on them hold promise for future industrial, catalytic and biomedical applications.

Although the facile nucleophilic substitution chemistry of cyclophosphazenes allows flexible freedom for the design of a ligand with desired donor site and geometrical constraints, large number of cyclophosphazene-transition metal derivatives were obtained mainly by using the complex- or organometallic-nucleophiles rather than starting with a genuine cyclophosphazene ligand. The reactions of complex or organometallic anions with halogenocyclophosphazenes result in a rich fare of transition metal derivatives. However, extension of these reactions to high polymers is hampered due to experimental difficulties and side reactions experienced with the small molecules. Thus, the metal loading both in model compounds and polymers

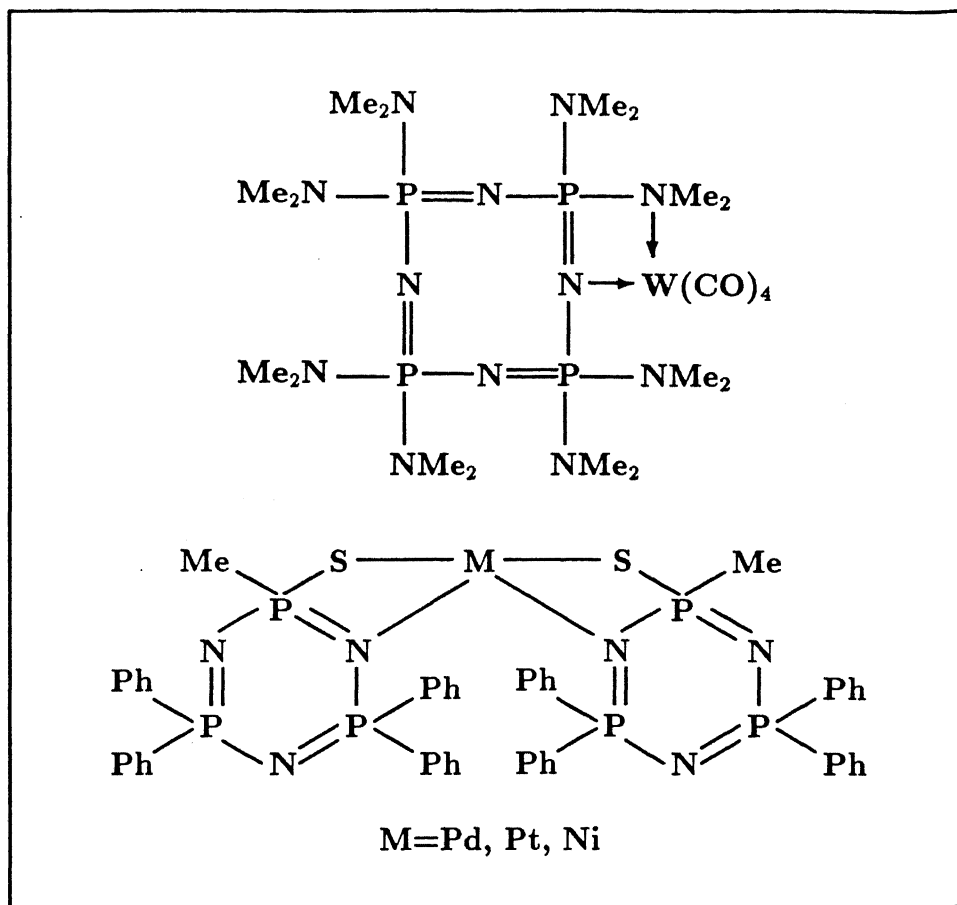


Figure 17: Examples of exocyclic group participation in coordination

could be successfully done by the former strategy, ie., linking a potential donor as side group in cyclophosphazene or polymer.

The electron-releasing tendency of the donor group or other substituents in phosphazene skeleton governs the coordination ability of skeletal nitrogen atoms. So a ligand with desired characteristics is easily accessible by controlling the nature of the substituents.

In conclusion:

- (i) High metal loading in phosphazene polymers could be easily achieved using exocyclic donor groups rather than using a mere organometallic nucleophile.
- (ii) Cyclophosphazene derived ligands containing exocyclic donor groups may exhibit interesting characteristics as that of the other known ligands such as 1,3-

diketones, polypyrazolyl borates (scorpionates), cyclopentadienes etc.

- (iii) Competition between skeletal nitrogen and exocyclic donor for metal coordination may lead to stable chelates or isomeric structures. Stereoelectronic and steric effects are likely to determine the mode of coordination to a large extent. A precise understanding of these effects can lead to the design of specific cyclophosphazene ligand systems and therefore, may aid in several applications such as synthesis of new catalysts for organic conversions or models for biological systems, besides contributing new knowledge in the area of coordination chemistry.
- (iv) The further investigation of the coordination response of cyclophosphazenes containing exocyclic donor groups remains an important and fascinating field of research deserving attention of synthetic inorganic chemists, spectroscopists and kineticists.

References

- [1] Trombe, M.C., Beaubestre, C., Sautereau, A.-M., Labarre, J.-F., Laneelle, G. and Tocanne, J.-F. *Biochem. Pharmacology*, **1984**, *33*, 2749.
- [2] Labarre, J.-F. *Top. Curr. Chem.*, **1985**, *129*, 173.
- [3] De Visser, A.C., Grolleman, C.W.J., Wolke, J.G.C., Van der Groot, H. and Timmerman, H. *J. Controlled Release*, **1986**, *4*, 133 and references therein.
- [4] Potin, Ph. and De Jaeger, R. *Eur. Polym. J.*, **1991**, *27*, 341.
- [5] Haiduc, I. *The Chemistry of Inorganic Rings*, Wiley-Interscience, London, **1970**.
- [6] Allcock, H.R. *Phosphorus-Nitrogen Compounds. Cyclic, Linear and High Polymeric Systems*, Academic Press, New York, **1972**.
- [7] Allcock, H.R. *Acc. Chem. Res.*, **1979**, *12*, 351.
- [8] Allcock, H.R. *Polymer*, **1980**, *21*, 673.

- [9] Allen, C.W. in *The Chemistry of Inorganic Homo- and Heterocycles*; Haiduc, I. and Sowerby, D.B. (Eds.), Academic Press, London, **1987**, Vol. 2, Chapter 20, p 501.
- [10] Shaw, R.A. *Pure Appl. Chem.*, **1980**, *52*, 1063.
- [11] Allen, C.W. *Chem. Rev.*, **1991**, *91*, 119.
- [12] Krishnamurthy, S.S., Sau, A.C. and Woods M. *Adv. Inorg. Chem. Radiochem.*, **1978**, *21*, 41
- [13] Shaw, R.A. *Phosphorus, Sulfur and Silicon*, **1989**, *45*, 103.
- [14] Lappert, M.F. and Srivastava, G. *J. Chem. Soc.(A)*, **1966**, 210
- [15] Moeller, T. and Kokalis, S.G. *J. Inorg. Nucl. Chem.*, **1963**, *25*, 875.
- [16] Trotter, J. and Whitlow, S.H. *J. Chem. Soc.(A)*, **1970**, 455
- [17] Allcock, H.R., Allen, R.W. and O'Brien, J.P. *J. Am. Chem. Soc.*, **1977**, *99*, 3984.
- [18] Allen, R.W., O'Brien, J.P. and Allcock, H.R. *J. Am. Chem. Soc.*, **1977**, *99*, 3987.
- [19] Harrison, W., Paddock, N.L., Trotter, J. and Wingfield, J.N. *J. Chem. Soc. Chem. Commun.*, **1972**, 23.
- [20] Harrison, W. and Trotter, J. *J. Chem. Soc. Dalton Trans.*, **1973**, 61.
- [21] Marsh, W.C., Paddock, N.L., Stewart, C.J. and Trotter, J. *J. Chem. Soc. Chem. Commun.*, **1970**, 1190.
- [22] Marsh, W.C. and Trotter, J. *J. Chem. Soc.(A)*, **1971**, 1482.
- [23] Paddock, N.L., Ranganathan, T.N., Rettig, S.J., Sharma, R. and Trotter, J. *Can. J. Chem.*, **1981**, *59*, 2429.
- [24] Gallicano, K.D., Paddock, N.L., Rettig, S.J., and Trotter, J. *Can. J. Chem.*, **1981**, *59*, 2435.
- [25] Calhoun, H.P., Paddock, N.L. and Wingfield, J.N. *Can. J. Chem.*, **1975**, *53*, 1765.

- [26] Macdonald, A.L. and Trotter, J. *Can. J. Chem.*, **1974**, *52*, 734.
- [27] Trotter, J., Whitlow, S.H. and Paddock, N.L. *J. Chem. Soc. Chem. Commun.*, **1969**, 695.
- [28] Trotter, J. and Whitlow, S.H. *J. Chem. Soc.(A)*, **1970**, 460.
- [29] Allcock, H.R., Bissell, E.C. and Shawl, E.T. *J. Am. Chem. Soc.*, **1972**, *94*, 8603.
- [30] Paddock, N.L., Ranganathan, T.N. and Wingfield, J.N. *J. Chem. Soc. Dalton Trans.*, **1973**, 1578.
- [31] Calhoun, J.P. and Trotter, J. *J. Chem. Soc. Dalton Trans.*, **1974**, 377.
- [32] Calhoun, J.P. and Trotter, J. *J. Chem. Soc. Dalton Trans.*, **1974**, 382.
- [33] Paddock, N.L. *Int. Rev. Phys. Chem.*, **1986**, *5*, 161.
- [34] Dewar, M.J.S., Lucken, E.A.C. and Whitehead, M.A. *J. Chem. Soc.*, **1960**, 2423.
- [35] Rettig, S.J. and Trotter, J. *Can. J. Chem.*, **1973**, *51*, 1295.
- [36] Allcock, H.R., Desorcie, J.L. and Riding, G.H. *Polyhedron*, **1987**, *6*, 119.
- [37] Greigger, P.P. and Allcock, H.R. *J. Am. Chem. Soc.*, **1979**, *101*, 2492.
- [38] Allcock, H.R., Greigger, P.P., Wagner, L.J. and Bernheim, M.Y. *Inorg. Chem.*, **1981**, *20*, 716.
- [39] Allcock, H.R., Wagner, L.J. and Levin, M.L. *J. Am. Chem. Soc.*, **1983**, *105*, 1321.
- [40] Suszko, P.R., Whittle, R.R. and Allcock, H.R. *J. Chem. Soc. Chem. Commun.*, **1982**, 649.
- [41] Allcock, H.R., Suszko, P.R., Wagner, L.J., Whittle, R.R. and Boso, B. *J. Am. Chem. Soc.*, **1984**, *106*, 4966.
- [42] Allcock, H.R., Suszko, P.R., Wagner, L.J., Whittle, R.R. and Boso, B. *Organometallics*, **1985**, *4*, 446.

- [43] Allcock, H.R., Riding, G.H. and Whittle, R.R. *J. Am. Chem. Soc.*, **1984**, *106*, 5561.
- [44] Nissan, R.A., Connolly, M.S., Mirabelli, M.G.L., Whittle, R.R. and Allcock, H.R. *J. Chem. Soc. Chem. Commun.*, **1983**, 822.
- [45] Allcock, H.R., Mang, M.N., Riding, G.H. and Whittle, R.R. *Organometallics*, **1986**, *5*, 2244.
- [46] Allcock, H.R., Mang, M.N., McDonnell, G.S. and Parvez, M. *Macromolecules*, **1987**, *20*, 2060.
- [47] Dash, K.C., Schmidpeter, A. and Schmidbaur, H. *Z. Naturforsch.*, **1980**, *35b*, 1286.
- [48] Schmidpeter, A., Blanck, K., Hess, H. and Riffel, H. *Angew. Chem. Int. Ed. Engl.*, **1980**, *19*, 650.
- [49] Allcock, H.R., Lavin, K.D., Tollefson, N.M. and Evans, T.L. *Organometallics*, **1983**, *2*, 267.
- [50] Allcock, H.R., Manners, I., Mang, M.N. and Parvez, M. *Inorg. Chem.*, **1990**, *29*, 522.
- [51] Allen, C.W., Malik, P., Bridges, A., Desorcie, J.L. and Pellon, B. *Phosphorus Sulfur and Silicon*, **1990**, *49/50*, 433.
- [52] Chivers, T. *Inorg. Nucl. Chem. Letts.*, **1971**, *7*, 827.
- [53] Allcock, H.R., Nissan, R.A., Harris, P.J. and Whittle, R.R. *Organometallics*, **1984**, *3*, 432.
- [54] Allcock, H.R., Dembek, A.A., Bennett, J.L., Manners, I. and Parvez, M. *Organometallics*, **1991**, *10*, 1865.
- [55] Suszko, P.R., Whittle, R.R. and Allcock, H.R. *J. Chem. Soc. Chem. Commun.*, **1982**, 960.
- [56] Allcock, H.R., Lavin, K.D., Riding, G.H. and Whittle, R.R. *Organometallics*, **1984**, *3*, 663.
- [57] Allcock, H.R., Lavin, K.D., Riding, G.H., Suszko, P.R. and Whittle, R.R. *J. Am. Chem. Soc.*, **1984**, *106*, 2337.

- [58] Allcock, H.R., Lavin, K.D., Riding, G.H., Whittle, R.R. and Parvez, M. *Organometallics*, **1986**, *5*, 1626.
- [59] Manners, I., Coggio, W.D., Mang, M.N., Parvez, M. and Allcock, H.R. *J. Am. Chem. Soc.*, **1989**, *111*, 3481.
- [60] Lavin, K.D., Riding, G.H., Parvez, M. and Allcock, H.R. *J. Chem. Soc. Chem. Commun.*, **1986**, 117.
- [61] Saraceno, R.A., Riding, G.H., Allcock, H.R. and Ewing, A.G. *J. Am. Chem. Soc.*, **1988**, *110*, 980.
- [62] Chandrasekhar, V., Krishnamurthy, S.S. and Woods, M. *Am. Chem. Soc. Symp. Ser.*, **1981**, *171*, 481.
- [63] Calhoun, H.P., Paddock, N.L. and Trotter, J. *J. Chem. Soc. Dalton Trans.*, **1973**, 2708.
- [64] Bertani, R., Facchin, G. and Gleria, M. *Inorg. Chim. Acta.*, **1989**, *165*, 73.
- [65] Allcock, H.R., Neenan, T.X. and Boso, B. *Inorg. Chem.*, **1985**, *24*, 2656.
- [66] Selvaraj, I.I., Chandrasekhar, V., Reddy, D. and Chandrashekar, T.K. *Heterocycles*, **1991**, *32*, 701.
- [67] Allcock, H.R. and Neenan, T.X. *Macromolecules*, **1986**, *19*, 1495.
- [68] Allcock, H.R., Scopelianos, A.G., Whittle, R.R. and Tollefson, N.M. *J. Am. Chem. Soc.*, **1983**, *105*, 1316.
- [69] Ahmed, F.R. *Acta. Crystallogr.*, **1986**, *32b*, 3078.

Synthesis of the Ligands and of the Coordination Compounds; Physical Methods

"The most fundamental and lasting objective of synthesis is not production of new compounds but production of properties."

—George S. Hammond in *Norris Award Lecture*, 1968.

3.1 Introduction

The design and synthesis of ligands for coordination compounds strongly depends on the accessibility of the desired functional groups. In this context recently, there is a growing interest in the synthesis of ligands containing distinct donor sites. It is believed that the coordination compounds resulting out of this multi-variant donor ligands may possess novel physical and chemical properties. We have chosen to synthesize and study the ligating properties of the pyrazolylcyclotriphosphazene ligands. They consist of both organic pyrazolyl and inorganic cyclophosphazene nitrogen donor atoms.

The pyrazolylcyclotriphosphazenes are readily synthesized by the nucleophilic substitution reaction on the halogenocyclotriphosphazene precursors with the pyrazole in the presence of a hydrogen chloride scavenger such as triethylamine [1]. The pyrazoles are readily formed through the condensation of hydrazine with either acetylacetone or 1,1,3,3-tetraethoxy propane [2]. In an attempt to introduce a spacer group between the phosphorus and pyrazolyl nitrogen (P–N), and thus increase the flexibility

of the ligand we have tried to condense N-hydroxymethyl-3,5-dimethylpyrazole with $N_3P_3Cl_6$. No products other than the hexakis(3,5-dimethyl-1-pyrazolyl)cyclotriphosphazene could be identified from the reaction mixtures. This failure is attributed to the decomposition of hydroxymethylpyrazole itself under the reaction conditions. This type of decomposition is reported earlier for N-hydroxymethylisooxazoles [3]. So we have then selected N-hydroxyethyl-3,5-dimethylpyrazole as suitable side group to study the variation in the chain length. N-hydroxyethylpyrazoles are prepared in a one step synthesis through the condensation of hydroxyethylhydrazine with 1,3-dicarbonyl derivatives [4]. The sodium salt of the hydroxyethyl-3,5-dimethylpyrazole obtained by treating sodium metal with the free alcohol reacts in a facile manner with $N_3P_3Cl_6$ to give the required ligand. The importance of these reactions will be dealt in more detail in the following chapters where the ligand complexes are discussed. In this chapter only the synthetic procedures and physical characterization techniques will be presented along with the routine data such as yield, melting point, elemental analyses, infra-red spectral frequencies, etc.

3.2 Starting Materials

Solvents were purified and dried according to standard literature procedures [5]. Most organic and inorganic materials were commercially available, of reagent quality, and used as received: Pyrazole (Aldrich), 2,2'-bipyridine (Aldrich), 1,10-phenanthroline (Aldrich), $N_3P_3Cl_6$ (Aldrich), Imidazole (Fluka), Pyridine (SDS).

3,5-Dimethylpyrazole [5], 1-(2-hydroxyethyl)-3,5-dimethylpyrazole [6], gem- $N_3P_3Ph_2Cl_4$ [7], spiro- $N_3P_3[NH(CH_2)_3NH]Cl_4$ [8] were prepared by adopting the published methods. Commercially procured hydrated copper halides were dried by heating at their dehydration temperatures on a oven for atleast 10 h and stored in a desiccator over dry $CaCl_2$.

Caution: Some compounds reported in this thesis contain perchlorate anions. Al-

though they seem to be reasonably stable to shock and heat, it should be pointed out that the use of perchlorates is hazardous because of their unpredictable explosive behavior [9] and necessitates extreme caution in their handling.

3.3 Physical and Chemical Measurements

3.3.1 Analyses and Spectroscopic measurements

Metal contents were determined complexometrically by indirect titration with $\text{Na}_2\text{H}_2\text{edta}$ and Zinc acetate after destruction of the sample with conc. HNO_3 acid [10]. C, H and N analyses were performed by the staff at microanalytical service centre, RSIC, CDRI, Lucknow or the microanalytical laboratory of the Indian Institute of Technology, Kanpur.

Infrared spectra were recorded on a Perkin Elmer 1320 spectrophotometer. Samples were prepared as potassium bromide pellets or as nujol mulls and the frequency was calibrated using polystyrene as the calibrant. Electronic spectra were obtained with a Shimadzu UV-160 spectrophotometer. Solid state electronic spectra were recorded on nujol mulls adhered to Whatman filter paper strips. The EPR spectra were obtained on a varian spectrometer at x-band frequency, and the magnetic field strength was calibrated with dpph ($g=2.0036$). The spin hamiltonian parameters were deduced from the theoretical simulation of them. For the EPR simulation a reported program was used [11]. The NMR (proton and carbon-13) spectra were obtained on a Bruker spectrometer operating at 80 or 400 MHz, and chemical shifts are reported with reference to internal tetramethyl silane. Phosphorus-31 NMR spectra were recorded on a Jeol FX 90Q spectrometer or on a Bruker spectrometer operating at 36.43 MHz and 164.5 MHz respectively. Phosphorus Chemical shifts are reported with reference to external 85% H_3PO_4 ; upfield shifts are negative. The FAB mass spectra were recorded on a JEOL SX 102/DA-6000 mass spectrometer/Data system using argon (6 kV, 10 mA) as the FAB gas. The accelerating voltage was 10 kV and

the spectra were recorded at room temperature. m-Nitrobenzyl alcohol was used as the matrix.

Solution magnetic susceptibilities of the complexes were measured at 27°C by the Evans [12] NMR method which correlates the paramagnetic shift Δf to the volume magnetic susceptibility χ_v by:

$$\chi_v = \frac{3\Delta f}{2\pi f m} + \chi_o + \frac{\chi_o (d_o - d_s)}{m} \quad (1)$$

χ_v Volume magnetic susceptibility of paramagnetic material

χ_o Volume magnetic susceptibility of solvent

f Frequency of absorption

m Mass of the paramagnetic material per ml of solvent

d_o Density of the solvent

d_s Density of the solution

The last term is generally neglected as it is very small [13]. The molar magnetic susceptibility (χ_m) is related to the experiment temperature (T) and effective magnetic moment (μ_{eff}) as below:

$$\chi_m = \chi_v \times M.Wt \quad (2)$$

$$\mu_{eff} = 2.84 \sqrt{\chi_m T} \quad (3)$$

3.3.2 Electrochemical Measurements

Cyclic voltammograms were obtained with a BAS 100A Electrochemical Analyser or with a PAR model 273 Potentiostat Galvanostat and Houston 2000 X-Y recorder. Controlled-potential coulometric tests and polarographic measurements for the heterobimetallic compounds were performed with an Amel model 551 Potentiostat with an associated coulometer (Amel model 558 integrator) in Siena, Italy. For dichloromethane solutions tetrabutylammonium perchlorate was used as a supporting electrolyte and for dimethyl formamide (DMF) and acetonitrile solutions tetraethylammonium perchlorate was used as the supporting electrolyte. The three electrode cell consisted

of a glassy-carbon working electrode, a platinum wire as a counter electrode and a reference electrode viz. saturated calomel electrode or Ag/AgCl (aq.) electrode. The solutions were thoroughly purged with dry N₂ or Ar before each experiment. Towards the end of each experiment ferrocene was added as an internal reference and the experiment repeated.

3.3.3 X-ray diffraction and Structure determinations

The data collection for the crystals were carried out on a Enraf-Nonius CAD-4 diffractometer with a monochromatic MoK α radiation ($\lambda=0.7093\text{\AA}$) in Arkansas, USA or on a Rigaku AFC6R diffractometer with MoK α radiation (graphite monochromator, $\lambda=0.71073\text{\AA}$) in Adelaide, Australia. Crystals were glued on glass fibers and transformed to a diffractometer. The programs used in the structure determinations were SHELX76 [14], SHELXS86 [15], ORTEP [16], NRC386 (PC version of NRC-VAX) [17], teXsan [18]. The data were collected at 25°C using the θ - 2θ or ω : 2θ scan technique. Three reflections were monitored every 2 h of exposure time and showed insignificant variations. The total exposure time varied from 72-96 h. Data sets were corrected for lorentz and polarization effects and an analytical absorption correction was applied [14].

Refinement of the structures were by the full-matrix least-squares procedures [14]. Non-hydrogen atoms were refined with anisotropic thermal parameters and hydrogen atoms were included in the model at their calculated positions (C-H, 0.95\AA and N-H, 0.90\AA). A weighting scheme of the form $W^{-1}=[\sigma^2(I)+PT^2]/4f^2$ was introduced and the refinement continued until convergence, final refinement details are presented in the following chapters where the complex structures are dealt. Analysis of variance showed no special features indicating that an appropriate weighting scheme had been employed. Scattering factors for copper, cobalt and nickel were from ref. 19, while those for the remaining atoms were those incorporated in SHELX76 [14]. The final

difference maps calculated at the conclusion of the refinements had no chemically significant features. Fractional atomic coordinates of the complexes for which structures have been solved are not given in this thesis, however, they are reported in the original papers (see Chapter 1 for references).

3.4 Synthesis of pyrazolylcyclotriphosphazenes

3.4.1 Hexakis(3,5-dimethyl-1-pyrazolyl)cyclotriphosphazene, $N_3P_3(Pz)_6$ (hdpctp)

A solution of $N_3P_3Cl_6$ (3.48 g, 10 mmol) in benzene (25 ml) was added dropwise to a solution of 3,5-dimethylpyrazole (5.8 g, 60 mmol) and triethylamine (6.4 g, 63 mmol) in benzene (50 ml) at 20°C with constant stirring. The reaction flask was equipped with a calcium chloride guard tube to prevent ingress of moisture. After the addition was completed (30 min) the reaction temperature was slowly raised to 80°C in an hour's time, and the reaction was allowed to proceed at this temperature for 5 h. It was cooled and filtered. The precipitate was rapidly washed with water (3×30 ml), benzene (2×10 ml) and ether (2×20 ml) and dried under vacuum. A white solid was obtained which was recrystallized from dichloromethane/hexane (1:1). Yield: 6.76 g, 96%.

Melting Point : 255-256°C(Lit.[1] m.p. 253.5-254.5°C)

IR(KBr, cm^{-1}) : 3142m, 2950s, 1574vs, 1450s, 1410s, 1371vs, 1296vs, 1220vs,br 1170vs, 1084vs, 1030m, 966vs, 902m, 828m, 802s, 756s, 636m, 611s, 510vs, 475s.

1H NMR($CDCl_3$, δ) : 2.20 (s, 18H, 3- CH_3), 2.30 (s, 18H, 5- CH_3), 5.50 (s, 6H, 4-CH).

^{13}C NMR($CDCl_3$, δ) : 12.6 (3- CH_3), 13.6 (5- CH_3), 109.7 (4-CH), 147.4 (3-C), 152.9 (5-C).

^{31}P NMR($CDCl_3$, δ) : -3.37 (s, 3P).

3.4.2 Hexakis(1-pyrazolyl)cyclotriphosphazene, $N_3P_3(pz)_6$ (hpctp)

This ligand was prepared as above, except more reaction time was required for the completion of the reaction. Yield: 80–90%.

Melting Point : 279°C(Lit.[1] m.p. 268°C (dec))

IR(KBr, cm^{-1}) : 3070m, 1521s, 1401vs, 1370vs, 1288vs, 1235vs,br, 1170vs,br, 1065vs, 1030vs, 935vs, 912m, 900m, 772s, 758vs, 628m, 615vs.

1H NMR($CDCl_3$, δ) : 6.44 (t, 6H, 4-CH), 7.91 (d, 6H, 3-CH), 8.13 (d, 6H, 5-CH).

^{13}C NMR($CDCl_3$, δ) : 108.7 (4-CH), 135.4 (3-CH), 146.7 (5-CH).

^{31}P NMR($CDCl_3$, δ) : 1.2 (s, 3P).

3.4.3 2,2-Diphenyl-4,4,6,6-tetrakis(3,5-dimethyl-1-pyrazolyl)cyclotriphosphazene, $N_3P_3Ph_2(Pz)_4$ (tdpctp)

Gem- $N_3P_3Ph_2Cl_4$ (2.16 g, 5 mmol) dissolved in benzene (60 ml) was added to a solution of 3,5-dimethylpyrazole (1.92 g, 20 mmol) and triethylamine (3.03 g, 30 mmol) at 25°C. The reaction mixture was heated under reflux for 50 h. It was cooled and triethylamine hydrochloride was filtered off. The solvent was stripped off *in vacuo* from the filtrate, leaving behind a residue which was washed with water (3×30 ml) and ether (2×20 ml) and subsequently dried *in vacuo*. The solid obtained was recrystallized from a 1:1 mixture of acetonitrile and dichloromethane. Yield: 2.7 g, 65%.

Melting Point : 219°C(Lit.[1] m.p. 217.5-219°C)

IR(KBr, cm^{-1}) : 3060m, 3000m, 2840m, 1560vs, 1457s, 1430s, 1408s, 1369s, 1295vs, 1220vs,br, 1175s, 1088vs, 960vs, 868m, 798s, 755s, 745s, 730s, 620w.

^1H NMR(CDCl_3 , δ) : 2.15 (s, 12H, 3- CH_3), 2.26 (s, 12H, 5- CH_3), 5.88 (s, 4H, 4-CH), 7.3 (m, 10H, Ph).

^{13}C NMR(CDCl_3 , δ) : 12.8 (3- CH_3), 13.7 (5- CH_3), 109.4 (4-CH), 146.7 (3-C), 152.1 (5-C), 127.7, 127.8, 128.2, 131.2, 131.4, 131.5, 135.7, 134.3 (C_6H_6).

^{31}P NMR(CDCl_3 , δ) : 20.3 (t, PPh_2), -5.4 (d, PPz_2), $^2\text{J}(\text{P-P})=25.2$ Hz.

3.4.4 2,2-Diphenyl-4,4,6,6-tetrakis(1-pyrazolyl)cyclotriphosphazene, $\text{N}_3\text{P}_3\text{Ph}_2(\text{pz})_4$ (tpctp)

This compound was obtained using a procedure analogous to tdpctp. Yield: 75%.

Melting Point : 219°C

IR(KBr, cm^{-1}) : 3060m, 1510m, 1470m, 1428s, 1392s, 1357s, 1280vs, 1220vs,br, 1165vs,br, 1118s, 1056vs, 1020vs, 990m, 928vs, 898m, 880m, 858m, 755s,br, 718s, 688s, 655m.

^1H NMR(CDCl_3 , δ) : 6.23 (t, 4H, 4-CH), 7.73 (d, 4H, 3-CH), 7.90 (d, 4H, 5-CH), 7.29-7.81 (m, 10H, C_6H_6).

^{13}C NMR(CDCl_3 , δ) : 107.8 (4-CH), 134.8 (3-CH), 145.9 (5-CH), 128.3, 128.4, 130.4, 130.5, 131.8, 133.1, 134.5, 134.7, 134.9, 145.9 (C_6H_6).

^{31}P NMR(CDCl_3 , δ) : 24.1 (t, PPh_2), -1.99 (d, Ppz_2), $^2\text{J}(\text{P-P})=30.5$ Hz.

3.4.5 2,2-Spiro-(1,3-diaminopropane)-4,4,6,6-tetrakis(3,5-dimethyl-1-pyrazolyl)cyclotriphosphazene, $\text{N}_3\text{P}_3[\text{NH}(\text{CH}_2)_3\text{NH}](\text{Pz})_4$ (stdpctp)

Stdpctp was prepared by using a similar procedure as that of tdpctp, except 2,2-spiro-(1,3-diaminopropane)-4,4,6,6-tetrachlorocyclotriphosphazene, $\text{N}_3\text{P}_3\text{Cl}_4[\text{NH}(\text{CH}_2)_3\text{NH}]$ was used instead of $\text{N}_3\text{P}_3\text{Ph}_2\text{Cl}_4$. Yield: 75-80%.

Melting Point	: 178-179°C
IR(KBr, cm ⁻¹)	: 3220m,br, 2930m, 1570s, 1460m, 1410m, 1295s, 1250s, 1205vs,br, 1140s, 1090s, 1028m, 965s, 830w, 800m, 765m.
¹ H NMR(CDCl ₃ , δ)	: 1.67 (q, 2H, -CH ₂ -), 1.97 (s, 12H, 3-CH ₃), 2.05 (s, 12H, 5-CH ₃), 3.20 (t, 4H, -NHCH ₂ -), 3.70 (s,br 2H, -NH), 5.73 (s, 4H, 4-CH).
¹³ C NMR(CDCl ₃ , δ)	: 11.8 (-CH ₂ -), 12.3 (3-CH ₃), 13.4 (5-CH ₃), 40.2 (-NHCH ₂ -), 103.38 (4-CH), 145.9 (3-C), 152.1 (5-C).
³¹ P NMR(CDCl ₃ , δ)	: 12.97 (t, Pspiro), 1.85 (d, PPz ₂), ² J(P-P)=50.7 Hz.

3.4.6 2,2-Spiro-(1,3-diaminopropane)-4,4,6,6-tetrakis(1-pyrazolyl)cyclotriphosphazene, N₃P₃[NH(CH₂)₃NH](pz)₄ (stpctp)

This new ligand was prepared as described above. Yield: 65-70%.

Melting Point	: 206-208°C
IR(KBr, cm ⁻¹)	: 3250m,br, 1510m, 1395s, 1360m, 1285s, 1235vs, 1200vs,br, 1170s, 1110m, 1055s, 1030s, 935m, 855m, 760s, 610s.
¹ H NMR(CDCl ₃ , δ)	: 1.63 (unresolved, 2H, -CH ₂), 3.16 (unresolved, 4H, -NHCH ₂), 3.36 (s,br, 2H, -NH), 6.42 (t, 4H, 4-CH), 7.75 (d, 4H, 3-CH), 8.10 (d, 4H, 5-CH).
¹³ C NMR(CDCl ₃ , δ)	: 25.6 (-CH ₂ -), 40.0 (-NHCH ₂ -), 107.4 (4-CH), 134.96 (3-CH), 145.07 (5-CH).
³¹ P NMR(CDCl ₃ , δ)	: 14.58 (t, Pspiro), -1.15 (d, Ppz ₂), ² J(P-P)=50.5 Hz.

3.4.7 Hexakis(1-(2-oxidoethyl)-3,5-dimethylpyrazolyl)cyclo-triphosphazene, $\text{N}_3\text{P}_3[\text{O}(\text{CH}_2)_2\text{Pz}]_6$ (hoedpctp)

To NaH (2.16 g, ~ 70 mmol) suspended in anhydrous tetrahydrofuran (75 ml), 1-(2-hydroxyethyl)-3,5-dimethylpyrazole (9.8 g, 70 mmol) dissolved in 50 ml tetrahydrofuran was added dropwise. The mixture was allowed to stir for further 3 h. Then, $\text{N}_3\text{P}_3\text{Cl}_6$ (3.48 g, 10 mmol) was added in small portions with vigorous stirring. After refluxing the mixture for 16 h, it was cooled and filtered. The solvent was removed under reduced pressure to leave a syrup. It was extracted with ether (3×40 ml), the ethereal extract washed with water thoroughly and dried over anhydrous Na_2SO_4 . Removal of ether under reduced pressure gave a thick syrup, which solidified on cooling to 0°C . The compound was further purified by recrystallization from hexane. Yield: 9.06 g, 93%. Alternatively the syrup was dissolved in small amount of acetone and poured into crushed ice. The resulting powdery product was filtered and air dried and finally dried over CaCl_2 in a vacuum desiccator.

Melting Point : 97°C

IR(KBr, cm^{-1}) : 3045m, 2995m, 1550m, 1460m,br, 1425m, 1382m, 1305w, 1235s,br, 1180sh, 1050s,br, 950w,br, 890w, 780m, 750sh.

^1H NMR(CDCl_3 , δ) : 2.13 (s, 36H, 3 and 5- CH_3), 4.03 (m,unresolved, 24H, $-\text{CH}_2$), 5.74 (s, 6H, 4-CH).

^{13}C NMR(CDCl_3 , δ) : 10.8 (3- CH_3), 13.3 (5- CH_3), 48.0 ($-\text{NCH}_2-$), 64.7 ($-\text{OCH}_2-$), 104.9 (4-CH), 139.8 (3-C), 147.7 (5-C).

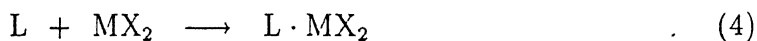
^{31}P NMR(CDCl_3 , δ) : 17.5 (s, 3P).

Elemental Analyses : Anal. calc. for $\text{C}_{42}\text{H}_{66}\text{N}_{15}\text{P}_3\text{O}_6$: C, 52.01; H, 6.86; N, 21.66. Found: C, 52.10; H, 6.82; N, 21.50.

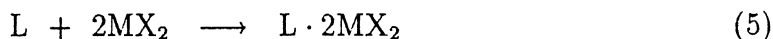
3.5 Synthesis of the Coordination compounds

3.5.1 General

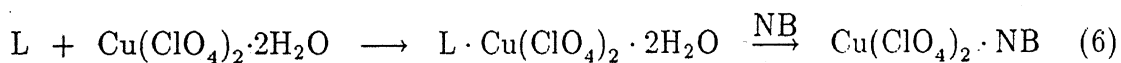
The Coordination compounds with formula $L \cdot MX_2$ [$M = \text{Cu}$ ($X = \text{Cl}, \text{Br}$), Co ($X = \text{Cl}$), Ni ($X = \text{Cl}, \text{Br}$)], where $L = \text{hdpctp}$, tdpctp , stdpctp and tpctp , were prepared by stirring the appropriate ligand (0.2 mmol) in dichloromethane (15 ml) with the anhydrous metal halide (0.2 mmol). After all the metal halide had dissolved in dichloromethane the reaction mixture was filtered and evaporated to *ca.* 2 ml. Addition of ether or hexane yielded the metal complexes generally in high yields. The complexes thus obtained were recrystallized from the 1:1 solvent mixture of dichloromethane and hexane.



For $L \cdot 2MX_2$ [$M = \text{Cu}$ ($X = \text{Cl}, \text{Br}$), Co ($X = \text{Cl}$)], where $L = \text{hdpctp}$, hpctp and hoedpctp , a similar procedure was used with two equivalents of metal halide.



With copper(II) perchlorate hexahydrate the ligands hdpctp and tdpctp give the diaquo complexes of the general formula $L \cdot \text{Cu}(\text{ClO}_4)_2 \cdot 2\text{H}_2\text{O}$. This aquo adducts undergo facile ligand displacement reactions with various monodentate and bidentate nitrogenous bases (NB) such as imidazole, pyridine, bipyridine etc. as given in Equation 6.



Typical procedures are given in the following section.

3.5.2 Illustrative procedures

hdpctp·CuCl₂: Anhydrous CuCl_2 (0.04 g, 0.3 mmol) and hdpctp (0.21 g, 0.3 mmol) were taken together in dichloromethane (30 ml) and stirred vigorously for 30 min at

room temperature. The resulting light green solution was filtered and concentrated to about 5 ml. Dry benzene (5 ml) was added and filtered. The filtrate was again concentrated and ether (10 ml) added to obtain a light green solid. Yield: 0.24 g, 96%. It was finally recrystallized by diffusion of hexane into a dichloromethane solution of the compound.

Melting Point : 207°C (dec)

Elemental Analyses : Anal. calc. for $C_{31}H_{44}N_{15}P_3Cl_4Cu$ (including one molecule of CH_2Cl_2 of crystallization): C, 40.25; H, 4.79; N, 22.71; Cu, 6.87. Found: C, 40.11; H, 4.82; N, 22.54; Cu, 6.64.

IR(CsI, cm^{-1}) : 2950m, 1573m, 1460m,br, 1440sh, 1405s, 1370m, 1310sh, 1293s, 1240s,br, 1200sh, 1170sh, 1142s, 1080m, 1042sh, 1030m, 1015m, 957m, 890m, 800m, 770m, 620m, 577vs, 520sh, 510s, 460m, 440m.

tdpctp·NiCl₂: To a solution of tdpctp (0.134 g, 0.2 mmol) in dichloromethane (25 ml) was added anhydrous NiCl₂ (0.026 g, 0.2 mmol). The suspension was stirred for 48 h. The resulting maroon solution was then filtered to remove the unreacted NiCl₂ and concentrated to about 2 ml *in vacuo*. Addition of hexane (10 ml) afforded a maroon solid identified as tdpctp·NiCl₂. Yield: 0.11 g, 69%.

Melting Point : 315°C (dec)

Elemental Analyses : Anal. calc. for $C_{32}H_{38}N_{11}P_3Cl_2Ni$: C, 48.08; H, 4.76; N, 19.28; Ni, 7.35. Found: C, 48.13; H, 4.79; N, 19.35; Ni, 7.56.

IR(KBr, cm^{-1}) : 2935w, 1565s, 1452m, 1439s, 1400s, 1369m, 1318w, 1303sh, 1290vs, 1220vs,br, 1175s, 1110s, 1080sh, 1038s, 968s, 953s, 860s, 802m, 769m, 690s, 660m, 623w.

The nickel and cobalt complexes were also obtained by reacting the phosphino precursors $M(PPh_3)_2X_2$ [$M=Ni$ ($X=Cl, Br$), Co ($X=Cl$)] with the ligands tdpctp,

stdpctp and hpctp and tpctp ($M=Co$). With hdpctp, hpctp and tpctp insoluble nickel complexes were isolated as sole products which could not be characterized in detail. An example of this alternative procedure is as follows:

tdpctp·CoCl₂: To a solution of tdpctp (0.167 g, 0.3 mmol) in dichloromethane (15 ml) was added CoCl₂(PPh₃)₂ (0.196 g, 0.3 mmol) dissolved in dissolved in dichloromethane (10 ml) dropwise with vigorous stirring. After the addition was over the reaction mixture was stirred for 1 h and filtered. The filtrate was concentrated to *ca.* 3 ml and diethyl ether (10 ml) added to yield tdpctp·CoCl₂. Yield: 0.2 g, 97%.

Melting Point : 318°C (dec)

Elemental Analyses : Anal. calc. for C₃₂H₃₈N₁₁P₃Cl₂Co: C, 48.08; H, 4.79; N, 19.27; Co, 7.37. Found: C, 48.19; H, 4.66; N, 19.35; Co, 7.47.

IR(KBr, cm⁻¹) : 2938m, 1560vs, 1450m, 1425s, 1400s, 1370m, 1315w, 1300sh, 1285vs, 1220vs,br, 1170vs,br, 1110s, 1070vs, 1030s, 973m, 960s, 900s, 880m, 860s, 845w, 800s, 765m, 750m, 745w, 732m, 720s, 695sh, 688s, 660w, 622w, 610w.

hdpctp·CuCl₂·PdCl₂·C₆H₆·H₂O: Solutions of hdpctp·CuCl₂ (0.168 g, 0.2 mmol) in benzene (10 ml) and trans-Pd(PhCN)₂Cl₂ (0.076 g, 0.2 mmol) in benzene (5 ml) were combined and stirred for 8 h in room temperature. The yellow precipitate formed was filtered off and washed with benzene and hexane twice. Crystallization from dichloromethane-benzene (1:1) afforded a yellow microcrystalline solid of hdpctp·CuCl₂·PdCl₂·C₆H₆. Yield: 0.19 g, 93%. The heterobimetallic complexes with platinum counter metal were obtained by using a similar procedure. However refluxing the reaction mixture for about 12 h was required for the completion of the reactions.

Melting Point : 209°C (dec)

Elemental Analyses : Anal. calc. for C₃₆H₅₀N₁₅P₃OCl₄CuPd: C, 38.83; H, 4.53; N, 18.87. Found: C, 38.65; H, 4.54; N, 18.78.

IR(KBr, cm⁻¹) : 3450m,br, 1570m, 1460m, 1400m, 1290m, 1220vs,br, 1140vs,br, 1100m, 1050m, 970m, 950m, 800w, 690w, 680w.

tdpctp·Cu(ClO₄)₂·bipy: The complex tdpctp·Cu(ClO₄)₂·2H₂O (0.194 g, 0.2 mmol) prepared *in situ* was treated with an equivalent amount of 2,2'-bipyridine (0.031 g, 0.2 mmol) in dichloromethane (20 ml) for 30 minutes with vigorous stirring. The resulting deep blue solution was filtered and evaporated to *ca.* 5 ml and diethyl ether (15 ml) added. A blue precipitate formed, which was washed with benzene, hexane and dried over dry CaCl₂ and finally recrystallized from dichloromethane-hexane (1:1) mixture. Yield: 0.198 g, 91%.

Yield : 91%

Melting Point : 152°C (dec)

Elemental Analyses : Anal. calc. for C₄₂H₄₆N₁₃P₃O₈Cl₂Cu: C, 46.37; H, 4.26; N, 16.74; Cu, 5.84. Found: C, 46.20; H, 4.23; N, 16.89; Cu, 5.68.

IR(KBr, cm⁻¹) : 1600m, 1570s,br, 1478m, 1467m, 1459m, 1440s, 1410m, 1310m, 1290s, 1230vs,br, 1180s, 1150sh, 1090vs,br, 1050sh, 960sh, 865w,br, 770m, 740sh, 730m, 690w,br, 625s.

The routine physical data for the remaining complexes synthesized for the present study are given below:

hdpctp·CuBr₂:

Yield : 95%

Melting Point : 168°C (dec)

Elemental Analyses : Anal. calc. for C₃₀H₄₂N₁₅P₃Br₂Cu: C, 38.79; H, 4.56; N, 22.62; Cu, 6.84. Found: C, 38.42; H, 4.25; N, 22.30; Cu, 6.50.

IR(CsI, cm^{-1}) : 2950m, 1572s, 1460s,br, 1410s, 1370m, 1292s,br, 1231vs,br, 1200vs, 1171sh, 1143s, 1080m, 1040m, 1018m, 960s, 900m, 800m, 770m, 620m, 578vs, 520sh, 505s, 470m, 440m.

hdpctp·2CuCl₂·CH₂Cl₂:

Yield : 80%

Melting Point : 164°C (dec)

Elemental Analyses : Anal. calc. for C₃₁H₄₄N₁₅P₃Cl₆Cu₂: C, 35.14; H, 4.19; N, 19.83; Cu, 11.99. Found: C, 34.87; H, 4.40; N, 19.60; Cu, 11.42.

IR(CsI, cm^{-1}) : 2950m, 1570s, 1450m,br, 1410m, 1375m, 1300m, 1240vs,br, 1190vs, 1142vs, 1110m, 1080m, 1042m, 970m, 870m, 800m, 770m, 615m, 570vs, 512vs, 450m.

hdpctp·2CuBr₂:

Yield : 90%

Melting Point : 173°C (dec)

Elemental Analyses : Anal. calc. for C₃₀H₄₂N₁₅P₃Br₄Cu₂: C, 31.27; H, 3.67; N, 18.23; Cu, 11.03. Found: C, 30.96; H, 3.42; N, 18.01; Cu, 10.83.

IR(CsI, cm^{-1}) : 2950m, 1560s, 1450m,br, 1410m, 1370m, 1340m, 1295m, 1245vs,br, 1160vs, 1140sh, 1047s, 975m, 840s, 800m, 770m, 620m, 570s, 520s.

hdpctp·Cu(ClO₄)₂·2H₂O:

Yield : 81%

Melting Point : 165°C (dec)

Elemental Analyses : Anal. calc. for $C_{30}H_{46}N_{15}P_3O_{10}Cl_2Cu$: C, 35.88; H, 4.62; N, 20.92; Cu, 6.33. Found: C, 35.64; H, 5.03; N, 20.80; Cu, 6.30.

IR(KBr, cm^{-1}) : 3450m,br, 3050m, 1555s, 1450m, 1400s, 1320w, 1290s, 1240vs,br, 1180sh, 1145s,br, 1100sh, 1080sh, 1040sh, 955s, 620s.

hdpctp·Cu(ClO₄)₂·bipy·CH₂Cl₂:

Yield : 91%

Melting Point : 132°C (dec)

Elemental Analyses : Anal. calc. for $C_{41}H_{52}N_{17}P_3O_8Cl_4Cu$: C, 40.72; H, 4.34; N, 19.69; Cu, 5.25. Found: C, 40.06; H, 4.83; N, 19.32; Cu, 5.20.

IR(KBr, cm^{-1}) : 3045m, 1590m, 1560s, 1455m, 1430s, 1300s, 1280s, 1220vs,br, 1170sh, 1080s,br, 950s, 610s.

hdpctp·CuCl₂·PtCl₂·C₆H₆:

Yield : 92%

Melting Point : 142°C (dec)

Elemental Analyses : Anal. calc. for $C_{36}H_{48}N_{15}P_3Cl_4CuPt$: C, 36.51; H, 4.09; N, 17.74. Found: C, 36.70; H, 4.15; N, 17.63.

IR(KBr, cm^{-1}) : 1555m, 1450m, 1390m, 1280m, 1215vs,br, 1140s, 1040m, 940m, 790w, 670m.

hdpctp·CuCl₂·PdBr₂·C₆H₆·H₂O:

Yield : 85%

Melting Point : 192°C (dec)

Elemental Analyses : Anal. calc. for $C_{36}H_{50}N_{15}P_3OCl_2Br_2CuPd$: C, 36.0; H, 4.2; N, 17.6. Found: C, 35.9; H, 4.2; N, 17.5.

IR(KBr, cm^{-1}) : 3450w,br, 1570m, 1460m, 1410m, 1290m, 1220vs,br, 1150s, 1050m, 985m, 977m, 960m, 810w, 690m.

hdpctp·CuCl₂·PtBr₂·1½C₆H₆:

Yield : 95%

Melting Point : 148°C (dec)

Elemental Analyses : Anal. calc. for C₃₉H₅₁N₁₅P₃OCl₂Br₂CuPt: C, 35.7; H, 3.9; N, 16.0. Found: C, 35.5; H, 3.9; N, 15.95.

IR(KBr, cm^{-1}) : 1580m, 1460m, 1410m, 1290m, 1230vs,br, 1200vs,br, 1150s, 1050m, 960m, 810w, 765m, 695m.

tdpctp·CuCl₂·CH₂Cl₂:

Yield : 95%

Melting Point : 207°C (dec)

Elemental Analyses : Anal. calc. for C₃₃H₄₀N₁₁P₃Cl₄Cu: C, 44.58; H, 4.54; N, 17.33; Cu, 7.15. Found: C, 44.49; H, 4.38; N, 17.45; Cu, 7.07.

IR(KBr, cm^{-1}) : 1560vs, 1468m, 1430m, 1405m, 1295s, 1225vs,br, 1180vs, 1140s, 1050m, 1020w, 955m, 860m, 770m, 748m, 725m, 695s.

tdpctp·CuBr₂:

Yield : 90%

Melting Point : 209°C (dec)

Elemental Analyses : Anal. calc. for C₃₂H₃₈N₁₁P₃Br₂Cu: C, 43.04; H, 4.29; N, 17.25; Cu, 7.12. Found: C, 42.95; H, 4.32; N, 17.14; Cu, 7.20.

IR(KBr, cm^{-1}) : 1565vs, 1435s, 1410s, 1295vs, 1230vs,br, 1180vs, 1125s, 1050m, 960m, 865m, 815w, 785s, 760s, 730s, 710s.

tdpctp·NiBr₂:

Yield : 75%

Melting Point : 280-285°C (dec)

Elemental Analyses : Anal. calc. for $\text{C}_{32}\text{H}_{38}\text{N}_{11}\text{P}_3\text{Br}_2\text{Ni}$: C, 43.72; H, 4.31; N, 17.35; Ni, 6.61. Found: C, 43.39; H, 4.31; N, 17.65; Ni, 6.47.

IR(KBr, cm^{-1}) : 2938m, 1569vs, 1459m, 1430s,br, 1405s, 1373m, 1320w, 1305sh, 1290vs, 1220vs,br, 1175vs,br, 1112s, 1079sh, 1040vs, 969vs, 957vs, 888w, 865m, 810m, 782m, 698s, 668m.

tdpctp·Cu(ClO₄)₂·2H₂O:

Yield : 93%

Melting Point : 208°C (dec)

Elemental Analyses : Anal. calc. for $\text{C}_{32}\text{H}_{42}\text{N}_{11}\text{P}_3\text{O}_{10}\text{Cl}_2\text{Cu}$: C, 39.67; H, 4.37; N, 15.92; Cu, 6.56. Found: C, 39.67; H, 4.40; N, 15.81; Cu, 6.45.

IR(KBr, cm^{-1}) : 3400m,br, 1562s, 1460m, 1453m, 1445m, 1430m, 1405m, 1310sh, 1300s, 1225vs,br, 1180vs, 1100vs,br, 1040s, 990w, 980w, 965m, 915w, 870m, 820w,br, 768w, 740m, 720s, 690m, 620s.

tdpctp·Cu(ClO₄)₂·2py:

Yield : 80%

Melting Point : 140°C (dec)

Elemental Analyses : Anal. calc. for $C_{42}H_{48}N_{13}P_3O_8Cl_2Cu$: C, 46.28; H, 4.44; N, 16.71; Cu, 5.83. Found: C, 46.35; H, 4.35; N, 16.93; Cu, 5.80.

IR(KBr, cm^{-1}) : 1595m, 1560s, 1440s, 1430s, 1400m, 1360m, 1310sh, 1285sh, 1230vs,br, 1175s, 1080vs,br, 1040sh, 950m, 860w,br, 732m, 720m, 690m, 618s.

tdpctp·Cu(ClO₄)₂·2ImH:

Yield : 95%

Melting Point : 213°C

Elemental Analyses : Anal. calc. for $C_{38}H_{46}N_{15}P_3O_8Cl_2Cu$: C, 42.93; H, 4.34; N, 19.67; Cu, 5.95. Found: C, 42.35; H, 4.38; N, 19.57; Cu, 6.03.

IR(KBr, cm^{-1}) : 3300m,br, 1560m, 1530m, 1450s,br, 1427s, 1400m, 1360w, 1310sh, 1283s, 1225vs,br, 1170s, 1100vs,br, 1050sh, 960sh, 950m, 860m, 800w,br, 750m, 745m, 730s, 720s, 682m, 640m, 610s.

tdpctp·Cu(ClO₄)₂·phen:

Yield : 86%

Melting Point : 168°C (dec)

Elemental Analyses : Anal. calc. for $C_{44}H_{46}N_{13}P_3O_8Cl_2Cu$: C, 47.30; H, 4.17; N, 16.37; Cu, 5.71. Found: C, 47.30; H, 4.23; N, 16.25; Cu, 5.65.

IR(KBr, cm^{-1}) : 1565s, 1510m, 1450m, 1425s, 1405m, 1305sh, 1290s, 1230vs,br, 1180s, 1150s, 1080vs,br, 1040sh, 1020sh, 951s, 865m, 840m, 800w,br, 735s, 725s, 712s, 690m, 620s.

stdpctp·CuCl₂:

Yield : 88%

Melting Point : 140°C (dec)
Elemental Analyses : Anal. calc. for $C_{23}H_{36}N_{13}P_3Cl_2Cu$: C, 38.26; H, 5.03; N, 25.22; Cu, 8.80. Found: C, 38.21; H, 5.17; N, 25.23; Cu, 8.82
IR(KBr, cm^{-1}) : 3200m,br, 1565s, 1460m, 1405m, 1295m, 1245s,br, 1180s, 1140sh, 1040m, 980w, 830w,br.

stdpctp·CuBr₂:

Yield : 83%
Melting Point : 128°C (dec)
Elemental Analyses : Anal. calc. for $C_{23}H_{36}N_{13}P_3Br_2Cu$: C, 34.07; H, 4.47; N, 22.45; Cu, 7.84. Found: C, 34.11; H, 4.35; N, 22.20; Cu, 7.92
IR(KBr, cm^{-1}) : 3225m,br, 1565s, 1460m, 1405m,br, 1320sh, 1295m,br, 1240vs,br, 1180s, 1120s, 1080sh, 1040m, 955m, 850m.

stdpctp·CoCl₂:

Yield : 75%
Melting Point : 165°C (dec)
Elemental Analyses : Anal. calc. for $C_{23}H_{36}N_{13}P_3Cl_2Co$: C, 38.51; H, 5.06; N, 25.38. Found: C, 38.40; H, 5.11; N, 25.27.
IR(KBr, cm^{-1}) : 3300m,br, 1570vs, 1460m, 1410s,br, 1380w, 1320sh, 1300s, 1245vs, 1190vs, 1160sh, 1080s,br, 1040s, 960m, 870m, 830m.

stdpctp·NiCl₂:

Yield : 80%
Melting Point : 262°C (dec)

IR(KBr, cm⁻¹) : 1505m, 1460m, 1430s, 1390s, 1350s, 1280sh, 1215vs,br, 1170sh, 1120vs, 1050vs, 1035sh, 925s, 860m, 760vs, 720s, 680s, 660m.

tpctp·CuBr₂:

Yield : 71%

Melting Point : 186°C (dec)

Elemental Analyses : Anal. calc. for C₂₄H₂₂N₁₁P₃Br₂Cu: C, 36.92; H, 2.84; N, 19.73; Cu, 8.14. Found: C, 36.85; H, 2.91; N, 19.82; Cu, 8.28

IR(KBr, cm⁻¹) : 1500m, 1460m, 1425s, 1400s,br, 1375sh, 1350m, 1280sh, 1225vs,br, 1165vs,br, 1115vs, 1050vs,br, 920m, 850m, 760vs, 720s, 680s.

tpctp·CoCl₂:

Yield : 85%

Melting Point : 144°C (dec)

Elemental Analyses : Anal. calc. for C₂₄H₂₂N₁₁P₃Cl₂Co: C, 41.94; H, 3.23; N, 22.42. Found: C, 41.85; H, 3.30; N, 22.38.

IR(KBr, cm⁻¹) : 1520m, 1445s, 1410m, 1300s, 1250vs,br, 1180vs,br, 1135s, 1060m, 1035sh, 970m, 940m, 870w, 770s,br, 740s, 700s, 675m.

tpctp·PtCl₂·CuCl₂:

Yield : 90%

Melting Point : 120°C (dec)

Elemental Analyses : Anal. calc. for C₂₄H₂₂N₁₁P₃Cl₄CuPt: C, 30.09; H, 2.31; N, 16.09; Cu, 6.63. Found: C, 30.18; H, 2.38; N, 16.01; Cu, 6.51

IR(KBr, cm⁻¹) : 1500m, 1430m, 1390m, 1280sh, 1230vs,br, 1170vs,br, 1110s, 1040s, 950m, 920m, 850m, 750vs, 710s, 670m.

[tpctp]₂·Cu(ClO₄)₂:

Yield : 58%

Melting Point : 136°C (dec)

Elemental Analyses : Anal. calc. for C₄₈H₄₄N₂₂P₆Cl₂O₈Cu: C, 41.86; H, 3.22; N, 22.37; Cu, 4.61. Found: C, 41.81; H, 3.30; N, 22.45; Cu, 4.54

IR(KBr, cm⁻¹) : 1510m, 1460w, 1430s, 1400m, 1360m, 1285sh, 1230vs,br, 1165vs,br, 1110vs,br, 1080sh, 950m, 920m, 850m, 760s, 720s, 690m, 620s.

tpctp·Cu(ClO₄)₂·2py:

Yield : 85%

Melting Point : 173°C (dec)

Elemental Analyses : Anal. calc. for C₃₄H₃₂N₁₃P₃Cl₂O₈Cu: C, 41.75; H, 3.30; N, 18.62; Cu, 6.50. Found: C, 41.81; H, 3.36; N, 18.54; Cu, 6.54

IR(KBr, cm⁻¹) : 1600m, 1480m, 1430s, 1400m, 1285sh, 1225vs,br, 1170sh, 1110vs,br, 1060sh, 930m, 860m, 755s, 720m, 690s, 620s.

tpctp·Cu(ClO₄)₂·2ImH:

Yield : 91%

Melting Point : 182°C (dec)

Elemental Analyses : Anal. calc. for C₃₀H₃₀N₁₅P₃Cl₂O₈Cu: C, 37.69; H, 3.16; N, 21.98; Cu, 6.65. Found: C, 37.78; H, 3.09; N, 21.91; Cu, 6.70

IR(KBr, cm⁻¹) : 3300m,br, 1570m, 1500w, 1480m, 1410m, 1300s, 1230vs,br, 1180vs,br, 1110vs,br, 950m, 870m, 800w, 750sh, 735s, 690m, 650m, 620s.

tpctp·Cu(ClO₄)₂·bipy:

Yield : 78%

Melting Point : 155°C (dec)

Elemental Analyses : Anal. calc. for C₃₄H₃₀N₁₃P₃Cl₂O₈Cu: C, 41.84; H, 3.10; N, 18.66; Cu, 6.51. Found: C, 41.76; H, 3.14; N, 18.61; Cu, 6.44

IR(KBr, cm⁻¹) : 1600s, 1570m, 1510m, 1440s, 1400m, 1360m, 1290vs, 1220vs,br, 1160vs,br, 1080vs,br, 930m, 900m, 860m, 760s,br, 720s, 700m, 660m, 626s.

tpctp·Cu(ClO₄)₂·phen:

Yield : 66%

Melting Point : 148°C (dec)

Elemental Analyses : Anal. calc. for C₃₆H₃₀N₁₃P₃Cl₂O₈Cu: C, 43.24; H, 3.02; N, 18.21; Cu, 6.35. Found: C, 43.06; H, 2.97; N, 18.07; Cu, 6.28

IR(KBr, cm⁻¹) : 1590w, 1520m, 1450s, 1430m, 1300vs, 1230vs,br, 1170vs,br, 1080vs,br, 920m, 830m, 760s, 720s, 690m, 620s.

hoedpctp·2CuCl₂:

Yield : 83%

Melting Point : 64°C (dec)

Elemental Analyses : Anal. calc. for C₄₂H₆₆N₁₅P₃O₆Cl₄Cu₂: C, 40.72; H, 5.37; N, 16.96; Cu, 10.26. Found: C, 40.80; H, 5.38; N, 16.82; Cu, 10.05.

IR(KBr, cm^{-1}) : 1555m, 1430m, 1400m,br, 1240s,br, 1080sh, 1040s,br, 950m, 890w, 800w,br, 745w.

hoedpctp·2CuBr₂:

Yield : 80%

Melting Point : 66°C (dec)

Elemental Analyses : Anal. calc. for $\text{C}_{42}\text{H}_{66}\text{N}_{15}\text{P}_3\text{O}_6\text{Br}_4\text{Cu}_2$: C, 35.61; H, 4.70; N, 14.83; Cu, 8.97. Found: C, 35.81; H, 4.83; N, 14.82; Cu, 8.99.

IR(KBr, cm^{-1}) : 1560m, 1470m, 1430m, 1370m,br, 1240s,br, 1080sh, 1050s,br, 960w, 895w, 800w,br, 750w.

hoedpctp·2CoCl₂:

Yield : 70%

Melting Point : 71°C (dec)

Elemental Analyses : Anal. calc. for $\text{C}_{42}\text{H}_{66}\text{N}_{15}\text{P}_3\text{O}_6\text{Cl}_4\text{Co}_2$: C, 41.02; H, 5.41; N, 17.09. Found: C, 40.98; H, 5.38; N, 17.28.

IR(KBr, cm^{-1}) : 1560m, 1470m, 1430m, 1370m,br, 1240s,br, 1085sh, 1050s,br, 960w, 895w, 800w,br, 750w.

hoedpctp·2Cu(ClO₄)₂·4H₂O:

Yield : 76%

Melting Point : 85°C (dec)

Elemental Analyses : Anal. calc. for $\text{C}_{42}\text{H}_{74}\text{N}_{15}\text{P}_3\text{O}_{26}\text{Cl}_4\text{Cu}_2$: C, 32.19; H, 4.76; N, 13.41; Cu, 8.11. Found: C, 32.30; H, 4.83; N, 13.25; Cu, 8.05.

IR(KBr, cm^{-1}) : 1560m, 1470m, 1430m, 1370m,br, 1240s,br, 1100vs,br, 1075sh, 1040s,br, 970w, 810w,br, 750w, 620s.

3.6 Concluding Remarks

In this chapter a general outline has been given about the experimental procedures to give the reader an impression of the synthetic methods and the equipments used in the elucidation of the structures. Most of the data that are routine have also been incorporated in this chapter. Other data are dealt in greater detail in the subsequent chapters of this thesis.

The ligand synthesis starting from pyrazoles and chlorocyclotriphosphazenes is straight forward and also results in a large variety of pyrazolylcyclotriphosphazene ligands. Novel substituted pyrazoles might be used to give new ligands based on this methods. Substituent control on the starting phosphazene precursors might be tuned to obtain specific functional ligands. The preparation of ligands starting from 1-(2-hydroxyethyl) pyrazoles is also relatively easy. New ligands may be obtained by using 1-(2-aminoethyl) pyrazoles. The pyrazolylcyclotriphosphazenes are quite stable in the absence of moisture and soluble in most organic and chloro solvents. However, they are insoluble in solvents such as hexane, acetonitrile, ethanol, methanol, etc.

The synthesis of the coordination compounds is straightforward. Most complexes readily crystallize from chloro/hydrocarbon solvent mixtures. Single crystals were usually obtained by patience. The compounds crystallize upon slow evaporation of the solvent in partly closed container or on vapor diffusion.

References

- [1] Gallicano, K.D. and Paddock, N.L. *Can. J. Chem.*, **1982**, *60*, 521.
- [2] Wiley, R.H. and Hexner, P.E. *Org. Synth. Coll. Vol. 4*, **1963**, 351; Jones, R.G. *J. Am. Chem. Soc.*, **1949**, *71*, 3994.
- [3] Munsey, M.S. and Natale, N.R. *Heterocycles*, **1990**, *31*, 851.
- [4] Haanstra, W.G., Driesen, W.L., Reedijk, J., Turpeinen, U. and Hämäläinen, R. *J. Chem. Soc. Dalton Trans.*, **1989**, 2309.

- [5] Furniss, B.S., Hannaford, A.J., Smith, P.W.G. and Tatchel, A.R. *Vogel's Text Book of Practical Organic Chemistry*, 5th Edition, Longmann, 1989.
- [6] Driessen, W.L., Gorter, S., Haanstra, W.G., Laarhoven, L.J.J., Reedijk, J., Goubitz, K. and Seljée, F.R. *Recl. Trav. Chim. Pays-Bas*, **1993**, *112*, 309.
- [7] Mc Bee, E.T., Okuhara, K. and Morton, C.J. *Inorg. Chem.*, **1965**, *4*, 1672.
- [8] Chandrasekhar, V., Krishnamurthy, S.S., Manohar, H., Vasudevamurthy, A.R., Shaw, R.A. and Woods, M. *J. Chem. Soc. Dalton Trans.*, **1984**, 621.
- [9] Raymond, K.N. *Chem Eng. News*, **1993**, Dec. 5, 4.
- [10] Jeffery, G.H., Bassett, J. Mendham and J. Denny, R.C. *Vogel's Text Book of Quatitative Chemical Analysis*, 5th Edition, Longmann, 1989.
- [11] Venable Jr., J.H. Ph.D Thesis, Yale University, Michigan, 1966.
- [12] Evans, D.F. *J. Chem. Soc.*, **1959**, 2003.
- [13] Bailey, R.A. *J. Chem. Educ.*, **1972**, *49*, 297.
- [14] Sheldrick, G.M. SHELX76, Program for Crystal Structure Determination, University of Cambridge, England, 1976.
- [15] Sheldrick, G.M. SHELXS86, Program for the Automatic Solution of Crystal Structure, University of Göttingen, Germany, 1986.
- [16] Johnson, C.K. ORTEP, Report ORNL-5138, Oak Ridge National Laboratory, TN, 1976.
- [17] Gabe, E.J., Le Page, Y., Charland, J-P, Lee, F.L. and White, P.S. *J. Appl. Crystallogr.*, **1989**, *22*, 383.
- [18] teXsan, Structure Analysis Package, Molecular Structure Corporation, Texas. 1992.
- [19] Ibers, J.A. and Hamilton, W.C. (Eds.) *International Tables for Crystallography*, Vol IV, Kynoch Press, Birmingham, England, 1974.

Varying the Number of Pyrazolyl Substituents in Cyclotriphosphazene Skeleton to Control the Degree of Nuclearity

".... Coordination Chemistry, the seminal, but highly augmented, legacy to science of Alfred Werner, is foundational to the understanding of the global issue of the organization of molecules in whatever sample of matter such a process may occur, be it natural or synthetic."

—Daryle H. Busch, *Chem. Rev.*, 1993, 93, 847.

4.1 Introduction

The general procedure of reacting pyrazoles with a halogenocyclotriphosphazene leads to a variety of pyrazolylcyclotriphosphazene ligands with multiple coordination sites. By varying the number of pyrazolyl substituents attached in the cyclotriphosphazene ring or changing the nature of substituents at pyrazole group, different constraints within the ligand can be studied. Also the substituents other than pyrazolyl group linked to cyclotriphosphazene skeleton may be varied and their influence can be evaluated.

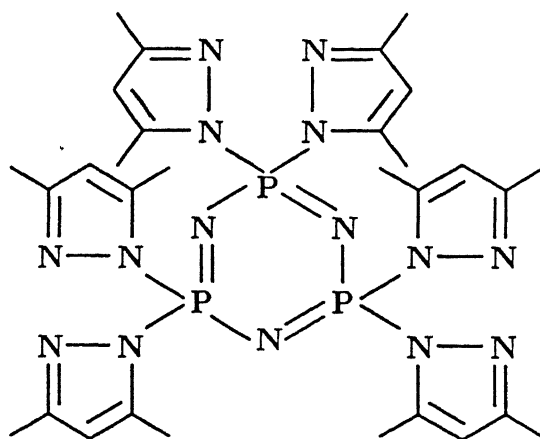
Three ligands and several of their copper, cobalt, and nickel complexes will be discussed in this chapter. At first the influence of number of exocyclic donor substituents in cyclotriphosphazene skeleton will be studied. The differences and/or the similarities between hexakis(3,5-dimethyl-1-pyrazolyl)cyclotriphosphazene (hdpctp) and

2,2-diphenyl-4,4,6,6-tetrakis(3,5-dimethyl-1-pyrazolyl)cyclotriphosphazene (tdpctp) will be examined. In tdpctp two geminal positions at cyclotriphosphazene ring are blocked by non-interacting phenyl substituents. Thus, it has two donor groups (3,5-dimethyl-1-pyrazolyl) less than that in hdpctp. The next step in this consideration is changing the non-interacting phenyl substituents in tdpctp with an amido group. A ligand 2,2-spiro(1,3-diaminopropane)-4,4,6,6-tetrakis(3,5-dimethyl-1-pyrazolyl)cyclotriphosphazene (stdpctp) has been prepared from 2,2-spiro(1,3-diaminopropane)-4,4,6,6-tetrachlorocyclotriphosphazene (stcctp) and 3,5-dimethyl pyrazole. One might expect the amido group to exert two effects: (i) It would increase the basicity of the cyclotriphosphazene skeletal nitrogens owing to their electron releasing influence and inturn may result in complexes having strong cyclophosphazene ring nitrogen-metal interactions. (ii) Alternatively, it may compete for coordination to metal along with the 3,5-dimethyl-1-pyrazolyl substituents. One may select any amido substituent or donor substituent different from pyrazole to investigate these effects. We have chosen spiro substituent 1,3-diamino propane because of its easy preparation and earlier reports on related compounds had clearly established the coordination ability of this spiro loop towards transition metals [1]. Schematic drawings of the ligands discussed in this chapter are given in Figure 1.

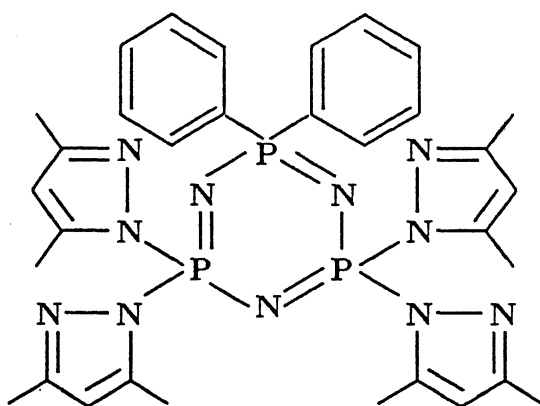
4.2 Synthesis and Characterization of the Ligands

Syntheis of pyrazolylcyclotriphosphazenes has been first reported by Paddock and co-workers[2]. They have isolated hdpctp, tdpctp (though in low yields) and other higher membered derivatives and studied their ligating properties with platinum(II) and palladium(II) halides. We have obtained the ligands hdpctp and tdpctp by using modified procedures in higher yields. Stdpctp has been prepared for the first time. The reaction schemes employed to synthesize the ligands are depicted in Figure 2.

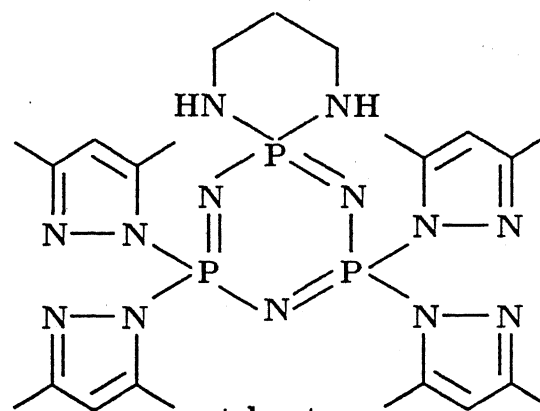
Hexachlorocyclotriphosphazene reacts with six equivalents of 3,5-dimethyl pyra-



hdpctp



tdpctp



stdpctp

Figure 1: Structures of the ligands hdpctp, tdpctp and stdpctp.

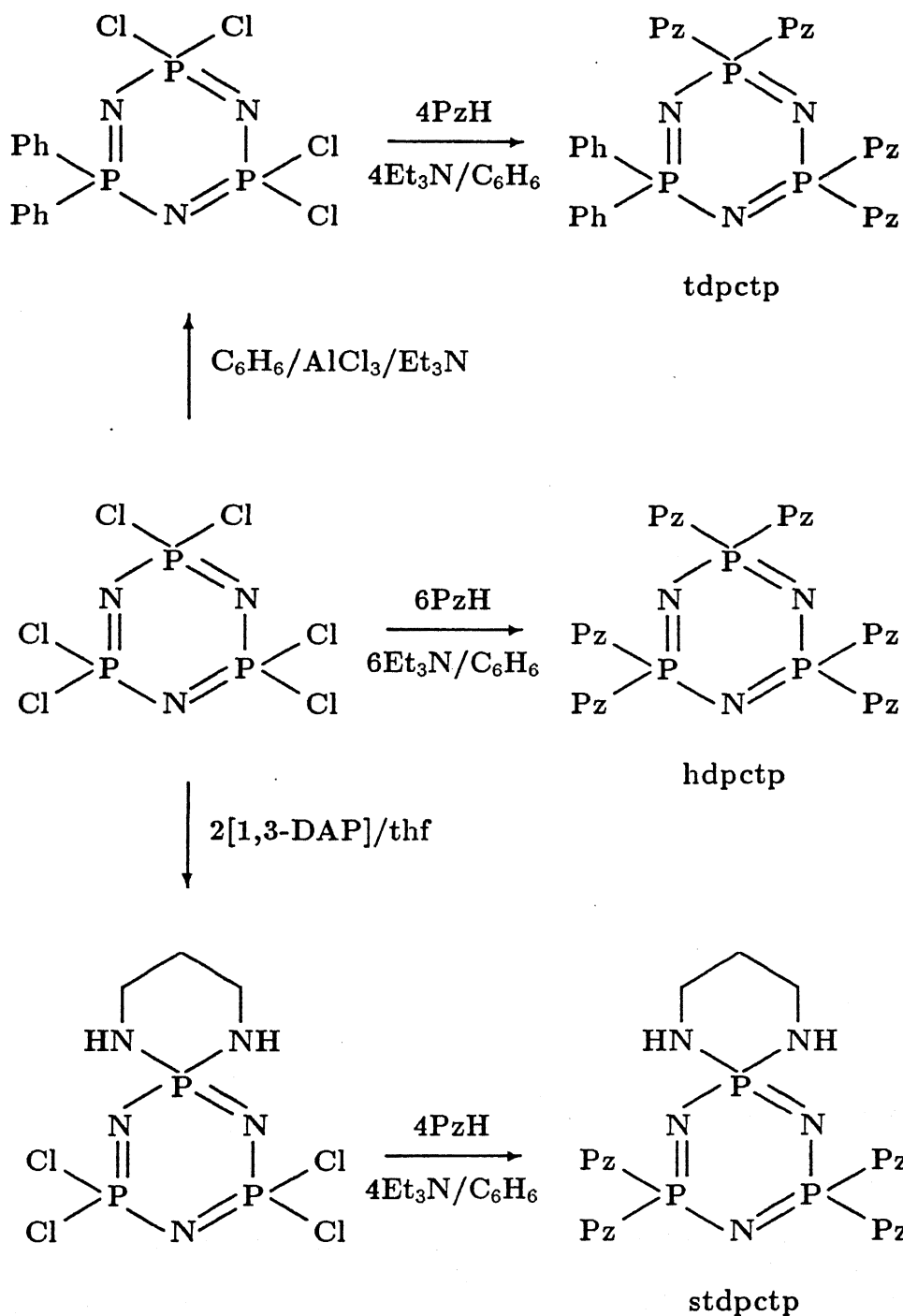


Figure 2: Synthesis of the ligands; reaction pathways.

zole in the presence of a slight excess of triethylamine in benzene to yield hexakis(3,5-dimethyl-1-pyrazolyl)cyclotriphosphazene (hdpctp). Tdpctp has been obtained by a two step method. Friedal-crafts phenylation of $N_3P_3Cl_6$ according to McBee and co-workers [3] produces the geminal 2,2-diphenyl-4,4,6,6-tetrachlorocyclotriphosphazene. This on further treatment with 3,5-dimethyl pyrazole in the presence of triethylamine as hydrogen chloride scavenger leads to the desired ligand tdpctp. Stdctp is also easily accessed by adopting available procedures in the literature. 1,3-Diamino propane when reacted with $N_3P_3Cl_6$ in tetrahydrofuran forms the spiro derivative, 2,2-spiro(1,3-diaminopropane)-4,4,6,6-tetrachlorocyclotriphosphazene (stcctp) [4]. This stcctp undergoes facile nucleophilic substitution reaction with 3,5-dimethyl pyrazole at the PCl_2 centres to generate the new ligand 2,2-spiro(1,3-diaminopropane)-4,4,6,6-tetrakis(3,5-dimethyl-1-pyrazolyl)cyclotriphosphazene (stdpctp). The ligands have been characterized by multinuclear NMR and IR spectroscopy and in case of stdpctp an x-ray diffraction analysis has also been completed but the details are not included in this thesis.

The proton NMR spectra of the ligands are dominated by the pyrazolyl protons. In 1-unsubstituted simple pyrazoles the substituent in the carbon-3 and carbon-5 are chemically equivalent. Linkage with cyclotriphosphazene phosphorus via N-1 causes them to be inequivalent, and two separate singlets are observed for the methyl substituents in carbon-3 and carbon-5 in all the ligands. The proton attached to pyrazole nucleus at carbon-4 resonates at *ca.* 5.7 ppm irrespective of the ligand. The ligands tdpctp and stdpctp show additional features due to the phenyl and 1,3-diamino propane moieties respectively. The 1H NMR spectrum of tdpctp shows a cluster of signals in the region 7.2-8.0 ppm for the phenyl groups while that of stdpctp shows a quartet at 1.67 ppm, a triplet at 3.20 ppm and a broad signal at 3.70 ppm due to the $-CH_2-$ group, the two $-NCH_2-$ groups and the two $-NH-P$ protons respectively originating from the 1,3-diamino propane spiro loop (Figure 3).

Table 1: ^{31}P NMR data for the ligands and related derivatives.^a

compound	δPPz_2	δPCL_2	$\delta\text{P}_{\text{others}}$	$^2\text{J}_{\text{P-P}}$	ref
$\text{N}_3\text{P}_3\text{Pz}_6$ (hdpctp)	-3.4	-	-	-	This work
$\text{N}_3\text{P}_3\text{Ph}_2\text{Pz}_4$ (tdpctp)	-5.4	-	20.3	25.2	This work
$\text{N}_3\text{P}_3[\text{NH}(\text{CH}_2)_3\text{NH}]\text{Pz}_4$ (stdpctp)	1.85	-	13.0	50.7	This work
$\text{N}_3\text{P}_3\text{Ph}_2\text{Cl}_4$	-	17.1	19.5	12.0	5
$\text{N}_3\text{P}_3[\text{NH}(\text{CH}_2)_3\text{NH}]\text{Cl}_4$	-	23.1	12.3	43.7	6
$\text{N}_3\text{P}_3(\text{NHBu}^t)_2\text{Cl}_4$	-	19.6	2.3	44.7	7
$\text{N}_3\text{P}_3(\text{Az})_2\text{Cl}_4$	-	21.9	34.2	30.0	8
$\text{N}_3\text{P}_3(\text{Im})_6$	-	-	2.3	-	9

^a Chemical shifts are in ppm (ref: 85% H_3PO_4) and coupling constants are in Hz

The ^{31}P NMR spectra of the ligands tdpctp and stdpctp display two resonances at -5.4 and 1.85 and at 20.3 and 13.0 as a doublet and a triplet respectively. The low frequency doublet is readily assigned to the PPz_2 groups since the values are very close to the singlet observed for hdpctp. The two bond coupling observed for the PPz_2 and P_{spiro} or PPh_2 centres in stdpctp or tdpctp are larger than that observed for PCL_2 and P_{spiro} or PPh_2 groups in the parent compounds $\text{N}_3\text{P}_3\text{Ph}_2\text{Cl}_4$ [5] and $\text{N}_3\text{P}_3[\text{NH}(\text{CH}_2)_3\text{NH}]\text{Cl}_2$ [6] respectively (Table 1). The chemical shift of a particular phosphorus atom depends on several factors such as, nature of substituent (steric and electronegativity), extent of π -bonding with the substituent, bond angles at phosphorus, etc [10]. The substituents on the adjacent phosphorus may also influence the chemical shift of a phosphorus nuclei under consideration. It is clearly evident from the Table 1 that the bulkiness of the 3,5-dimethylpyrazolyl substituent is responsible for the drastic upfield shift when compared to the other amido substituted cyclotriphosphazenes. Slight down field shift for PPz_2 group in stdpctp compared to that in hdpctp and tdpctp may be due to the electronic effect exerted by the electron rich spiro loop. The ^{13}C -NMR spectra of the ligands are consistent with the

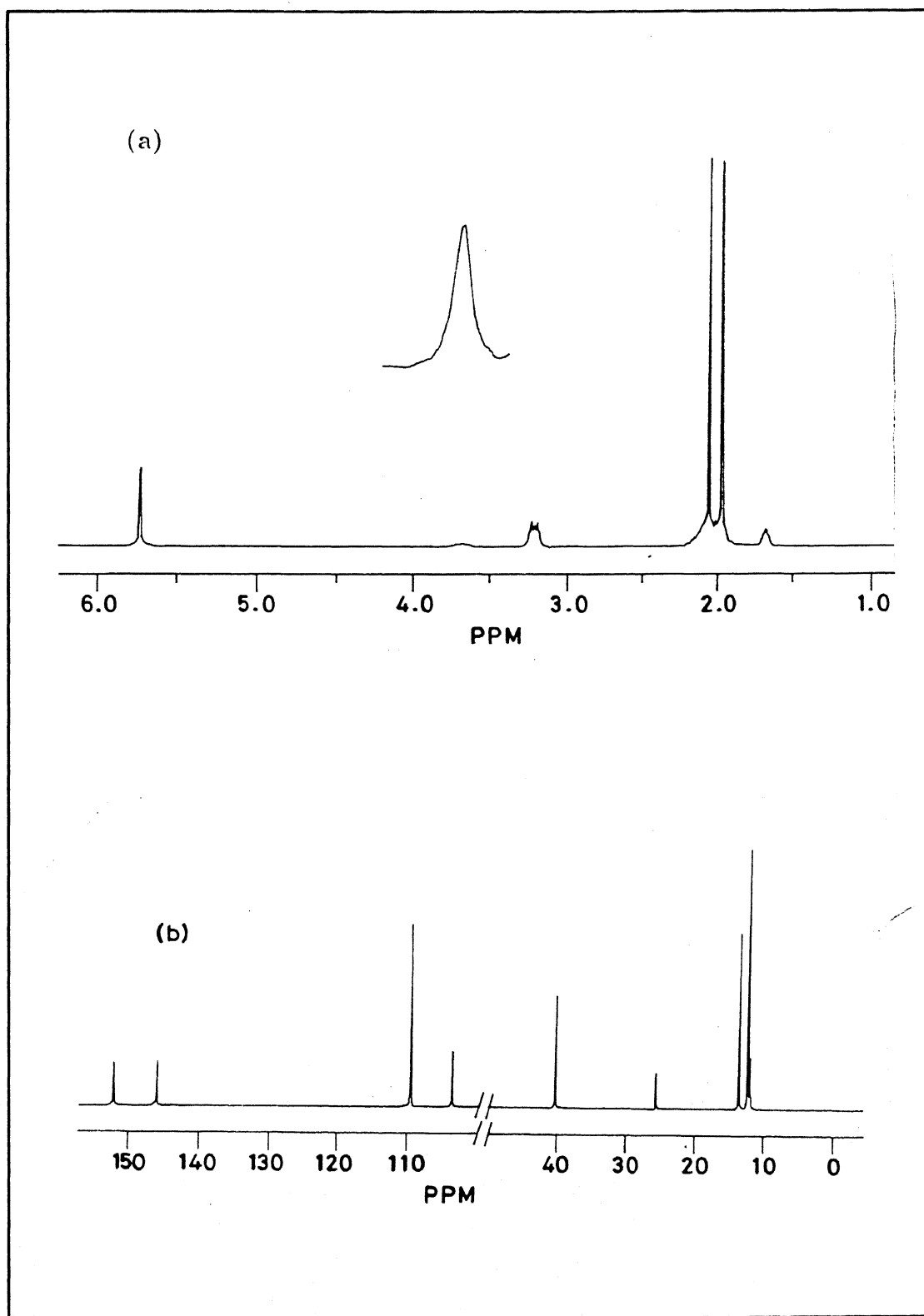


Figure 3: Proton (a) and Carbon-13 (b) NMR spectra of stdpctp

proposed structures and exhibit necessary features due to the groups present in the ligands (Figure 3b).

4.3 Coordination compounds of the ligand hexakis-(3,5-dimethylpyrazolyl)cyclotriphosphazene (hdpctp)

4.3.1 General

The ligand hdpctp is a potential multidentate ligand with three-bond bites built in between the donor atoms if the coordination is *via* nongeminal pyrazolyl substituents and cyclophosphazene skeletal nitrogen. On the other hand, the geminal coordination to metal without phosphazene ring nitrogen participation may lead to six-membered chelate complexes with bidentate ligation per metal. Either way the ligand is capable of carrying three metals [in a tris(tridentate) or tris(bidentate) fashion]. Simultaneously, the ligand environment is significantly varying in the metal *viz.*, N₃ donor in the nongeminal coordination mode and N₂ ligator in the geminal coordination pattern (cf. Chapter 1, page 2). Interestingly hdpctp yields both mononuclear (tridentate) and binuclear [bis(tridentate)] complexes. No tris(tridentate) complexes could be isolated. The mononuclear complexes behave as novel metal containing ligands and results in heterobimetallic compounds when treated with additional metal precursors. In Table 2 a summary of all coordination compounds together with their physical characteristics is given. For convenience the heterobimetallic complexes will be treated separately.

4.3.2 Mononuclear and homodinuclear complexes of hdpctp

Synthesis

The reactions of Cu(II)X₂ (X=Cl, Br) with hdpctp in dichloromethane in a 1:1 or a 1:2 molar ratio yield the mono- and dimetallated derivatives hdpctp-CuX₂ (X = Cl,

Table 2: Physical Characteristics of coordination compounds of hdpctp

compound	color	nature	μ_{eff} (BM)	Λ_m [†]
hdpctp·CuCl ₂	light green	crystalline	1.733	7.5
hdpctp·2CuCl ₂	green	crystalline	1.672	4.2
hdpctp·CuBr ₂	yellow	crystalline	1.758	4.1
hdpctp·2CuBr ₂	brown	powder	1.634	6.2
hdpctp·Cu(ClO ₄) ₂ ·2H ₂ O	light blue	crystalline*	1.820	227
hdpctp·Cu(ClO ₄) ₂ ·bipy	blue	micro-crystalline	1.980	242
hdpctp·CuCl ₂ ·PtCl ₂ [†]	green	micro-crystalline	1.840	10.0
hdpctp·CuCl ₂ ·PtBr ₂ [†]	green yellow	powder	1.810	12.8
hdpctp·CuCl ₂ ·PdCl ₂ ·H ₂ O [†]	yellow	crystalline	1.810	5.5
hdpctp·CuCl ₂ ·PdBr ₂ ·H ₂ O [†]	brown	crystalline	1.830	8.5

[†]unit: mho cm² mol⁻¹

*hygroscopic solid, takes additional water and becomes green

[†]benzene solvates, to avoid confusion they are omitted

Br) and hdpctp·2CuX₂ (X=Cl, Br). Conductivity data (Table 2) for them in acetonitrile clearly indicate that the halides are bound to copper in the coordination sphere while the magnetic moment data (Table 2) rule out any significant magnetic interaction between the metal centres in the 1:2 compounds and suggests that 1:1 compounds are monomeric in nature [11]. The reaction of copper(II) perchlorate hexahydrate with hdpctp in dichloromethane affords the mononuclear complex hdpctp·Cu(ClO₄)₂·2H₂O. It behaves as a 1:2 electrolyte in acetonitrile solution [12] (Table 2). However, in solid state the IR spectra is demonstrative of the presence of one monodentate perchlorate ion [13] (μ_3 doublet at 1100 and 1040 cm⁻¹) and an uncoordinated ionic perchlorate ion (singlets at 1080 cm⁻¹ and 620 cm⁻¹) and suggests that probably in solution acetonitrile replaces the perchlorate ion from the coordination sphere. From the pertinent references [14] it is also arrived that the water molecules are coordinating to the metal. Interestingly, this aquo complex undergoes

facile reaction with 2,2'-bipyridine to form $\text{hdpctp} \cdot \text{Cu}(\text{ClO}_4)_2 \cdot \text{bipy}$. This reaction evidently occurs via the expulsion of the aqua ligands as reflected by the disappearance of the broad absorption at $3500\text{--}3300\text{ cm}^{-1}$ in the infra-red spectra of the latter complex in contrast to the former. The IR spectra in the perchlorate region is undoubtedly indicative of ionic, non-coordinating perchlorate ions. Magnetic moments (Table 2) calculated by Evans NMR method are normal for monomeric tetragonal copper complexes with weak axial interactions [11].

The infra-red spectra of all above compounds show the presence of the ligand bands. It is known that metallation or protonation of ring nitrogen atoms in cyclophosphazene leads to a splitting of the ring $\text{P}=\text{N}$ stretching frequency, which is observed usually between 1190 and 1300 cm^{-1} . This splitting is ascribed to the unequal bond ($\text{P}=\text{N}$) bond distances within the cyclophosphazene ring [15]. On the contrary, if coordination is exclusively through exocyclic atoms the $\text{P}=\text{N}$ stretching frequency remains largely unaffected. In the free ligand hdpctp the ring $\text{P}=\text{N}$ stretching frequency is observed around 1220 cm^{-1} as a strong and broad band. In the complexes a splitting of the parent $\text{P}=\text{N}$ stretching frequency results in two bands one between $1230\text{--}1250\text{ cm}^{-1}$ and another between $1180\text{--}1200\text{ cm}^{-1}$. In all compounds, the cyclotriphosphazene skeletal nitrogen participates in coordination and the ligand hdpctp acts as a tridentate chelating or bis(chelating) ligand with two nongeminal pyrazolyl and one cyclotriphosphazene nitrogens.

Electronic spectra

The electronic spectra of the copper(II) complexes and the free ligand hdpctp are shown in Figure 4 and data compiled in Table 3. Two strong and well resolved transitions near 280 and 360 nm are seen for all of the complexes. On the basis of earlier elegant work by Schugar and co-workers [16] on $\text{Cu}(\text{II})$ -pyrazole complexes, these absorptions could be assigned as predominantly due to $\pi_2(\text{Pz}) \rightarrow \text{Cu}(\text{II})$ and

Table 3: Electronic Spectral data for mononuclear and homodinuclear complexes of
hdpctp

compound	solvent	$\lambda_{max}^{\dagger} (\epsilon_{max})$	assignment
hdpctp·CuCl ₂	CH ₂ Cl ₂	902 (0.237)	d-d
		361 (1.45), 279 (2.79)	Pz → Cu l.m.c.t.
		231 (24.00)	π - π^* intraligand
	CH ₃ CN	949 (0.245)	d-d
		458 (0.165)	d-d ?
		358 (1.24), 276 (2.79)	Pz → Cu l.m.c.t.
		225 (26.80)	π - π^* intraligand
	Nujol mull	909	d-d
		390, 300	Pz → Cu l.m.c.t.
		251	π - π^* intraligand
hdpctp·2CuCl ₂	CH ₂ Cl ₂	877 (0.472)	d-d
		364 (3.74), 277 (7.73)	Pz → Cu l.m.c.t.
		233 (39.88)	π - π^* intraligand
	CH ₃ CN	905 (0.485)	d-d
		457 (0.440)	d-d ?
		363 (3.09), 277 (5.64)	Pz → Cu l.m.c.t.
		225 (26.80)	π - π^* intraligand
	Nujol mull	876	d-d
		395, 300	Pz → Cu l.m.c.t.
		249	π - π^* intraligand
hdpctp·CuBr ₂	CH ₂ Cl ₂	902 (0.426)	d-d
		419 (1.65)	Br → Cu l.m.c.t.
		364 (1.55), 293 (2.65)	Pz → Cu l.m.c.t.
		232 (34.24)	π - π^* intraligand
	CH ₃ CN	930 (0.380)	d-d
		412 (1.32)	Br → Cu l.m.c.t.
		365 (1.26), 295 (2.10)	Pz → Cu l.m.c.t.
		223 (50.13)	π - π^* intraligand
	Nujol mull	900	d-d
		464	Br → Cu l.m.c.t.
		423, 299	Pz → Cu l.m.c.t.
		246	π - π^* intraligand

(continued)

Table 3: Continued

hdpctp·2CuBr ₂	CH ₂ Cl ₂	885 (0.730)	d-d
		427 (3.09)	Br → Cu l.m.c.t.
		361 (2.80), 291 (5.69)	Pz → Cu l.m.c.t.
		233 (41.36)	π - π^* intraligand
	CH ₃ CN	905 (0.797)	d-d
		424 (3.23)	Br → Cu l.m.c.t.
		360 (3.02), 295 (4.74)	Pz → Cu l.m.c.t.
		224 (68.50)	π - π^* intraligand
	Nujol mull	876	d-d
		465	Br → Cu l.m.c.t.
hdpctp·Cu(ClO ₄) ₂ ·2H ₂ O	CH ₃ CN	431, 299	Pz → Cu l.m.c.t.
		248	π - π^* intraligand
hdpctp·Cu(ClO ₄) ₂ ·bipy	CH ₃ CN	748 (0.098)	d-d
		311 (1.09), 260 (2.52)	Pz → Cu l.m.c.t.
hdpctp·Cu(ClO ₄) ₂ ·bipy	CH ₃ CN	225 (22.66)	π - π^* intraligand
		670 (0.06), 582 (0.07)	d-d
		308 (5.46), 267 (2.52)	bipy → Cu l.m.c.t., Pz → Cu l.m.c.t.
		225 (40.07)	π - π^* intraligand

[†] units: nm (mol⁻¹ cm⁻¹ × 10³)

$\pi_1(\text{Pz}) \rightarrow \text{Cu(II)}$ charge transfer transitions. The band at around 230 nm is attributed to the π - π^* intraligand transition with a slight contribution from $n(\text{Pz}) \rightarrow \text{Cu(II)}$ charge transfer. In the chloro derivatives the $\text{Cl} \rightarrow \text{Cu(II)}$ l.m.c.t. are probably buried in the high energy transition at *ca.* 280 nm. This is also consistent with the decreased intensity for the band at 260 nm in case of the Cu(II) perchlorate complexes. However, in the bromo analogs a new low-energy absorption at 420 nm is seen which is attributed to a $\text{Br} \rightarrow \text{Cu(II)}$ l.m.c.t. based on data available for similar bromo derivatives [17]. The bipyridine adduct hdpctp·Cu(ClO₄)₂·bipy shows increased intensity for the band at 360 nm suggesting large contribution from the bipy → Cu(II) l.m.c.t. In acetonitrile the chloro complexes hdpctp·nCuCl₂ (n=1,2) exhibit a new band at *ca.* 457 nm with low extinction coefficients (Table 3). At

present, the origin of this transition is not clear.

It is generally accepted that the presence of a single d-d absorption with a high-energy shoulder for copper(II) complexes is suggestive of a trigonal bipyramidal geometry around copper [11, 18], although the absence of such a high-energy shoulder is not necessarily indicative of alternate structures [19] while for the tetragonal complexes a low-energy shoulder is frequently located [11]. The copper(II) halide complexes of hdpctp show a single broad asymmetric metal centered transition between 870 and 950 nm. In acetonitrile, hdpctp·nCuBr₂ displays a clear high-energy shoulder at 641 nm. The spectrum remains virtually unchanged in solution and in mull transmittance (Table 3), pointing that the solid state structures are retained in the solution as well.

The d-d transition of the copper(II) perchlorate complexes is also seen as a broad and asymmetric band. The band maximum of bipyridine adduct, hdpctp·Cu(ClO₄)₂·bipy is shifted to higher energy (~70 nm) and is a overlap of two equal intense bands, reflecting the chasm in the ligand field strengths and a square pyramidal geometry [11] for copper respectively. Observation of two equal intense band is proposed as a characteristic of square pyramidal geometry [20]. The aquo complex, hdpctp·Cu(ClO₄)₂·2H₂O reveals a low energy shoulder in the d-d band demonstrative of a tetragonal geometry with weak axial interactions [11]. Theories on the intensities of the d-d transition predict that the intensity of d-d transition increases as the symmetry of the ligand field decreases [21] since the d-d transitions become allowed as electric dipole transitions. Larger intensity for the d-d transition of the aquo complex when compared with bipyridine adduct suggests a pronounced tetrahedral distortion in the former. This fact is further highlighted with a series of analogous tdpctp complexes in a latter section (see Section 4.4.2).

EPR spectroscopy

Electron paramagnetic resonance spectroscopy is a powerful tool to identify the

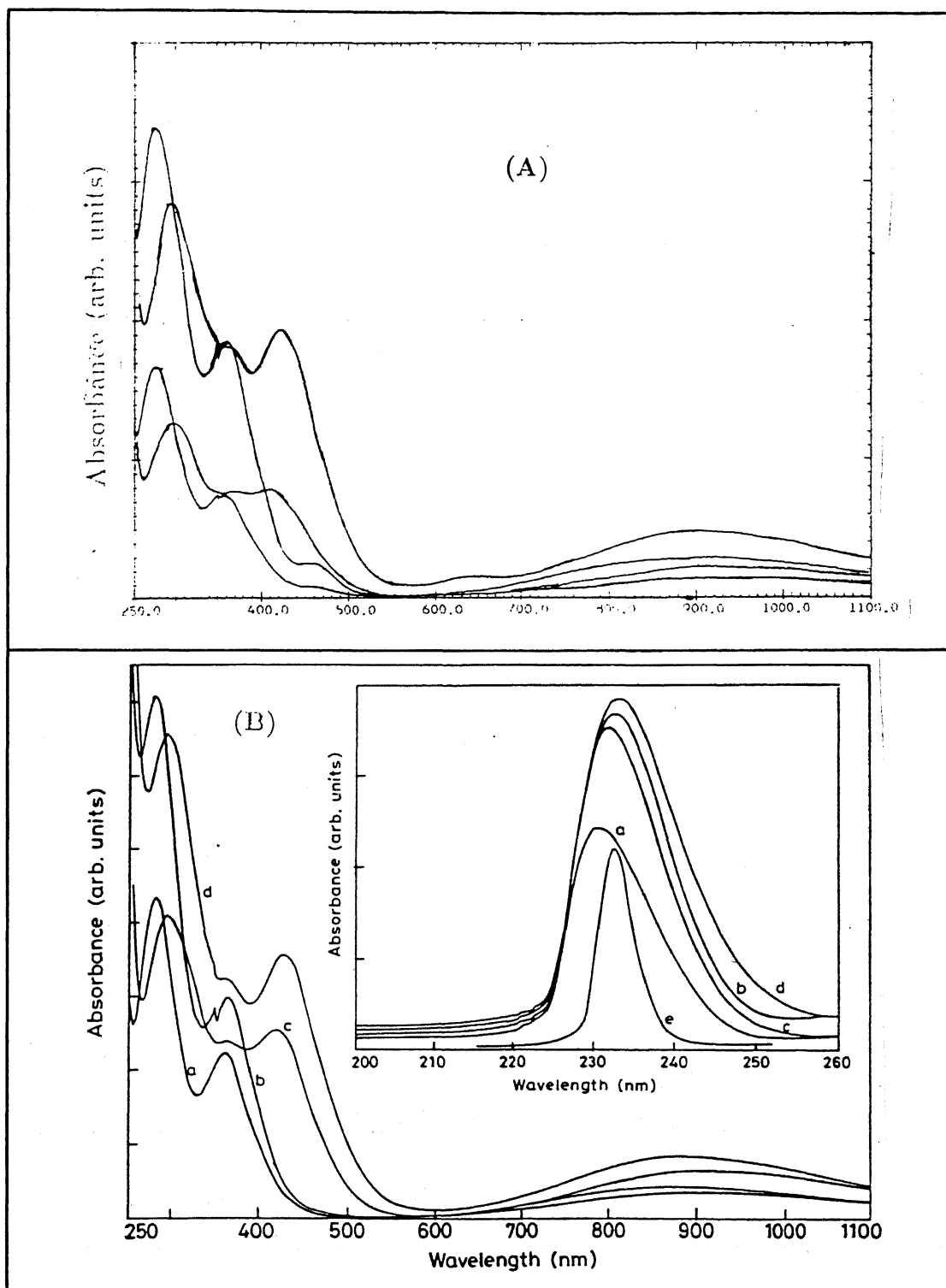


Figure 4: Electronic spectra of the complexes: (a) $\text{hdpctp}\cdot\text{CuCl}_2$ (b) $\text{hdpctp}\cdot 2\text{CuCl}_2$ (c) $\text{hdpctp}\cdot\text{CuBr}_2$ (d) $\text{hdpctp}\cdot 2\text{CuBr}_2$ and (e) hdpctp in CH_3CN (A) and CH_2Cl_2 (B)

Table 4: EPR data for mono- and homodinuclear complexes of hdpctp ^a

compound		g_1	g_2	g_3	$A_{ }$	g_{av} ^b	g_{iso}	A_{iso}	G ^c
hdpctp·CuCl ₂	d	2.046	2.119	2.255	—	2.142	—	—	4.07
hdpctp·2CuCl ₂	d	2.059	2.233	—	117	2.115	—	—	3.78
hdpctp·CuBr ₂	d	2.048	2.119	2.210	—	2.127	—	—	3.43
hdpctp·2CuCl ₂	d	2.065	2.211	—	—	2.115	—	—	3.25
hdpctp-- Cu(ClO ₄) ₂ ·2H ₂ O	d	2.072	2.351	—	131	2.169	—	—	4.88
	e	2.072	2.351	—	130	2.169	—	—	4.88
	f	2.069	2.339	—	149	2.163	2.180	71	4.91
hdpctp-- Cu(ClO ₄) ₂ ·bipy	d	2.060	2.250	—	173	2.125	—	—	4.17
	e	2.050	2.234	—	176	2.113	—	—	4.68
	f	2.042	2.232	—	173	2.138	2.137	78 ^g	5.52
	h	2.038	2.244	—	166	2.128	2.126	73 ^g	6.42

^a for axial, $g_{||}=g_2$ and $g_{\perp}=g_1$; A values are in $\times 10^{-4}$ cm⁻¹

g_{iso} and A_{iso} values are from room temperature isotropic spectra

^b from $[\frac{1}{3}(g_{||}^2+2g_{\perp}^2)]^{1/2}$ $[\frac{1}{3}(g_1^2+g_2^2+g_3^2)]^{1/2}$ for axial and rhombic spectra respectively

^c from $(g_{||}-2.0)/(g_{\perp}-2.0)$, for rhombic spectra $g_{||}=(g_2+g_3)/2$ and $g_{\perp}=g_1$

^d polycrystalline powder, room temperature

^e polycrystalline powder, liquid nitrogen temperature

^f dichloromethane solution, room and liquid nitrogen temperatures

^g a_N values and 12.6 and 13.5×10^{-4} cm⁻¹ in CH₂Cl₂ and CH₃CN respectively

^h acetonitrile solution, room and liquid nitrogen temperatures

ground state and geometry of the copper compounds. EPR spectra of regular trigonal bipyramidal copper(II) complexes are characterized by an axial pattern with $g_{\perp} > g_{||} \simeq 2.0$. Usually a hyperfine structure is seen in the $g_{||}$ region with $A_{||}$ being

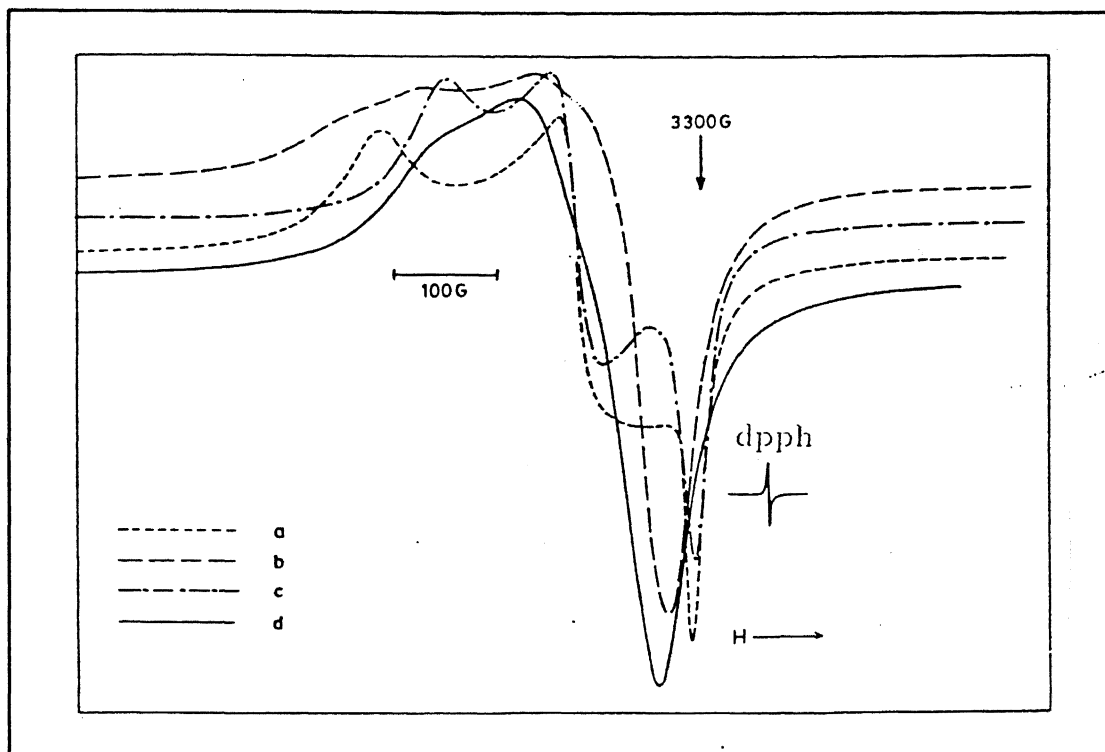


Figure 5: EPR spectra of the complexes hdpctp·nCuX₂ [X=Cl (n=1 (a) and 2 (b)), Br (n=1 (c) and 2 (d))] as powder samples

in the range $(60-100) \times 10^{-4} \text{ cm}^{-1}$ for the spin-dilute samples [22]. On the contrary the tetragonal complexes show a reverse trend of their respective g_{\parallel} and g_{\perp} values, i.e., $g_{\parallel} > g_{\perp} \simeq 2.0$ and large A_{\parallel} values usually in between $120 \times 10^{-4} \text{ cm}^{-1}$ and $200 \times 10^{-4} \text{ cm}^{-1}$.

The mononuclear copper(II) halide complexes hdpctp·CuX₂ (X=Cl and Br) show a rhombic symmetry in the EPR spectra of the powder samples (Figure 5) and the lowest principal g-values are 2.040 and 2.048 respectively (Table 4). These are closely related to the values observed for the structurally analogous compounds Cu(dmIm)₃Cl₂ [23] and Cu(terpy)X₂ (X=Cl, Br) [24, 25] where the geometry around copper has been shown to be distorted trigonal bipyramidal by single crystal x-ray studies. The dinuclear complexes show axial EPR spectra with $g_{\parallel} > g_{\perp} \simeq 2.0$ indicating a distorted trigonal bipyramidal geometry around copper with a $d_{x^2-y^2}$ ground state [11]. The A_{\parallel} value calculated from the poorly resolved hyperfine structure for

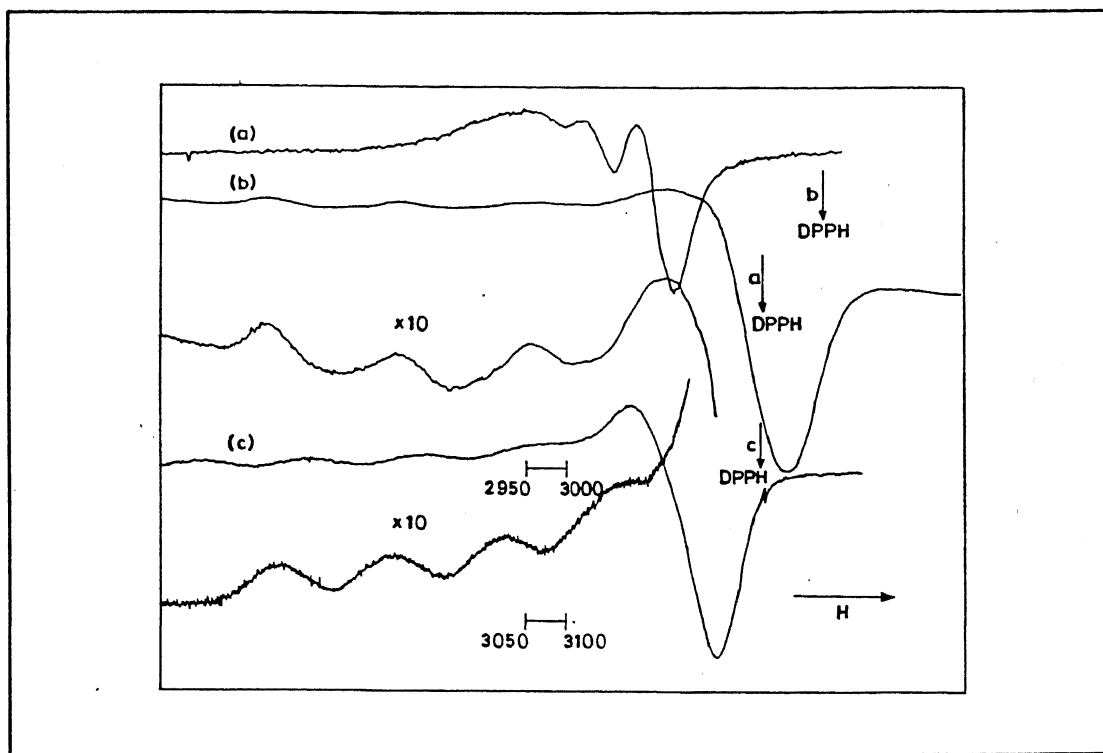


Figure 6: EPR spectra of $\text{hdpctp} \cdot \text{Cu}(\text{ClO}_4)_2 \cdot 2\text{H}_2\text{O}$ in dichloromethane solution at room temperature (a) and LNT (b) and as powder(c)

$\text{hdpctp} \cdot 2\text{CuCl}_2$ is $117 \times 10^{-4} \text{ cm}^{-1}$. It is evident from the EPR spectra of the homodinuclear complexes that both copper atoms are present in identical coordination environment with no appreciable variations in the geometries. This speculations are further in keeping with the single crystal x-ray results of the complex $\text{hdpctp} \cdot \text{CuCl}_2$ and the ligand degraded product $[\text{N}_3\text{P}_3\text{Pz}_5\text{O} \cdot 2\text{CuCl}_2]^- [\text{PzH}]^+$ (see below). The G-values of the dinuclear complexes were calculated using the equation:

$$G = \frac{g_{\parallel} - 2.0}{g_{\perp} - 2.0} \quad (1)$$

They are 3.78 and 3.25 for $\text{hdpctp} \cdot 2\text{CuCl}_2$ and $\text{hdpctp} \cdot 2\text{CuBr}_2$ respectively. G-values less than four are indicative of non-ionic compounds with strong covalent interactions [26]. For the mononuclear complexes, $\text{hdpctp} \cdot \text{CuX}_2$ taking $g_{\parallel} = (g_1 + g_2)/2$ and $g_{\perp} = g_3$ G-values were calculated, which are 4.07 and 3.43 for $\text{X} = \text{Cl}$ and Br respectively. Values of the G-parameter also reveal the absence of coupling of Cu^{2+} ions in

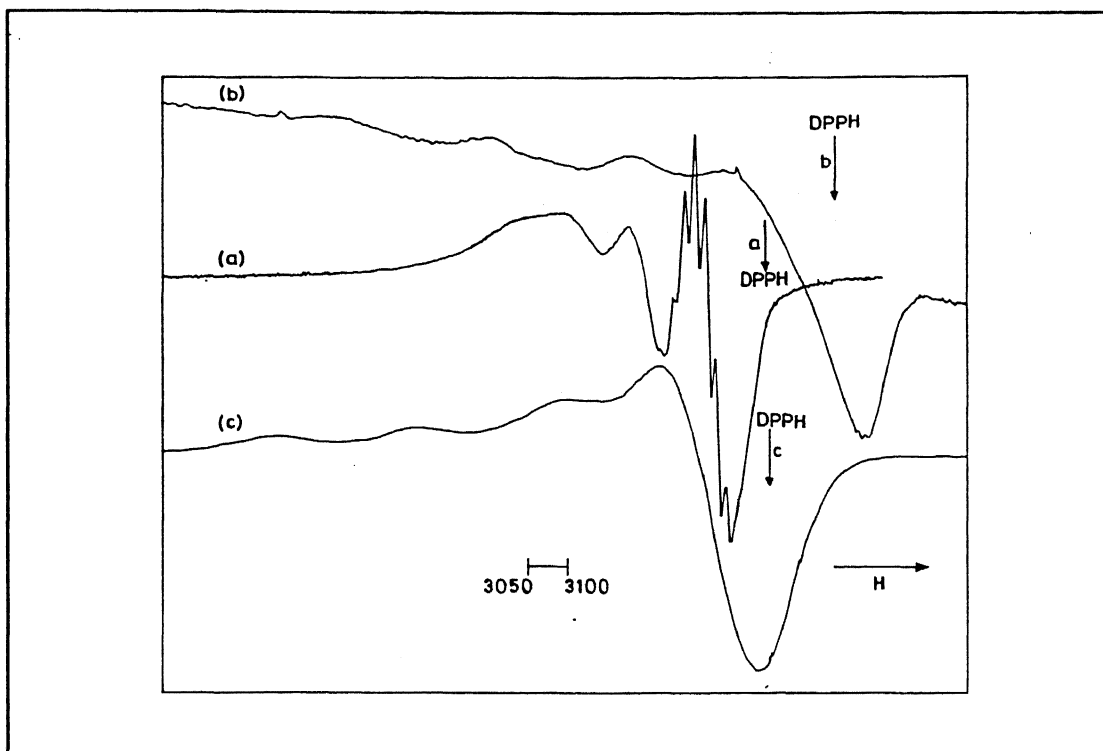


Figure 7: EPR spectra of hdpctp·Cu(ClO₄)₂·bipy in dichloromethane solution at room temperature (a) and LNT (b) and as powder (c)

the coordination polyhedra [27].

We have examined the EPR spectra of the copper(II) perchlorate derived complexes, hdpctp·Cu(ClO₄)₂·2H₂O and hdpctp·Cu(ClO₄)₂·bipy as a polycrystalline powder and as frozen dichloromethane or acetonitrile solutions (Figures 6-8). In general, the EPR spectra reveal the presence of a distorted tetragonal copper site with $d_{x^2-y^2}$ ground state in the complexes [11]. This is evident from their respective $g_{||}$ and g_{\perp} values, which in all cases show $g_{||} > g_{\perp}$ (Table 4).

An examination of the $g_{||}$ and $A_{||}$ values for the complexes hdpctp·Cu(ClO₄)₂·2H₂O indicates the high $g_{||}$ and low $A_{||}$ values when compared with hdpctp·Cu(ClO₄)₂·bipy. This is consistent with binding of less than four nitrogen atoms to the aquo complex and borders on the Peisach and Blumberg [28] plots of $A_{||}$ versus $g_{||}$ for two nitrogens and two oxygens in the equatorial plane. More over these values compare well with the analogous complex [Cu(BDGB)(H₂O)₂(ClO₄)]ClO₄ which has been proposed to

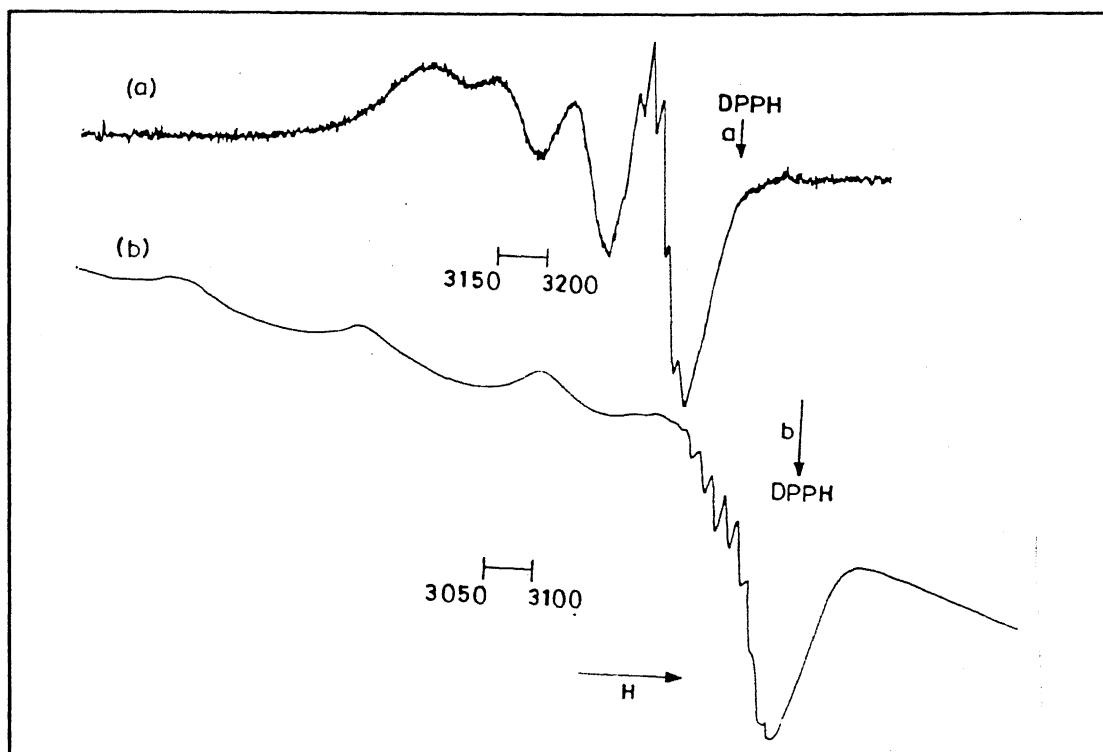


Figure 8: EPR spectra of hpdctp·Cu(ClO₄)₂·bipy in acetonitrile at room temperature (a) and LNT (b)

possess a N₂O₂ [29] chromophore. For powder sample four well resolved lines are observed while in solution less than four lines are located in the g_{\parallel} region (Figure 6) suggesting, that in solution the compound may exist in dimers resulting in a slight exchange coupling [11]. Also, in solution, the coordinated perchlorate anion comes off as is indicated by conductance measurements (Table 1) and the sixth site in all probability is occupied by a weakly bound solvent molecule in solution. However, there does not occur a change in geometric configuration in the complex as we change solvent from dichloromethane to acetonitrile. This is apparent from the g_{\parallel} and A_{\parallel} data (Table 4) in both the solvents. A slight increase in g_{\parallel} and decrease in A_{\parallel} values occur for this complex. This is indicative of the complex becoming increasingly ionic in acetonitrile. Similar effect is observed for hdpctp·Cu(ClO₄)₂·bipy as well.

The EPR spectra of hdpctp·Cu(ClO₄)₂·bipy in various solvents (Figure 7 and 8) clearly demonstrate a severe distortion of the tetragonal symmetry. They show less

than four g_{\parallel} lines and a considerable broadening of the g_{\perp} line (the g_{\perp} linewidth at half-amplitude is twice that observed in the aquo complex) (Figures 6 and 7). Such a broadening of the g_{\perp} component is indicative of lowered symmetry manifesting through a rhombic splitting [11]. Replacement of aquo ligands by electron-rich 2,2'-bipyridine lowers the g_{\parallel} values and simultaneously increases the A_{\parallel} values. The copper(II) perchlorate derived complexes thus reflect a unique compensation of subtle electronic/structural effects. From aquo to bipyridine increased covalency is the controlling effect leading to a relatively increased A_{\parallel} and lowered g_{\parallel} . Also slightly increased tetrahedral distortion in the equatorial plane is suggested for the aquo adduct from the larger $g_{\parallel}/A_{\parallel}$ quotient [30] and intensity of the d-d band. Interestingly the EPR spectra of the bipyridine adduct exhibits superhyperfine splitting due to four nitrogens strongly interacting in the equatorial plane. It is deduced that the cyclotriphosphazene nitrogen, occupying an axial site, does not interact strongly with the unpaired electron of copper(II).

Description of crystal structures

Crystal structures of a mononuclear complex, $\text{hdpctp}\cdot\text{CuCl}_2$ and a dinuclear derivative $[\text{N}_3\text{P}_3\text{Pz}_5\text{O}\cdot 2\text{CuCl}_2]^- [\text{PzH}]^+$ have been determined by x-ray diffraction studies. The crystal data are collected in Table 5.

(a) $\text{hdpctp}\cdot\text{CuCl}_2\cdot\text{CH}_2\text{Cl}_2$

An ORTEP representation of $\text{hdpctp}\cdot\text{CuCl}_2$ with atomic numbering scheme is depicted in Figure 9. The copper ion is coordinated by two nongeminal pyrazolyl pyridinic nitrogens, one cyclotriphosphazene skeletal nitrogen and two chloride ions in a compressed trigonal bipyramidal geometry, with the two nongeminal pyrazolyl nitrogen atoms along the main axis and the chloride ions and cyclotriphosphazene ring nitrogen in the equatorial plane. Relevant bond lengths and bond angles are given in Table 6. The $\text{Cu}-\text{N}_{\text{Pz}}$ distances (av. 1.981\AA) are comparable to the

Table 5: Crystal data for $\text{hdpctp} \cdot \text{CuCl}_2 \cdot \text{CH}_2\text{Cl}_2$ and $[\text{N}_3\text{P}_3\text{Pz}_5\text{O} \cdot 2\text{CuCl}_2]^- [\text{PzH}]^+ \cdot \text{CH}_3\text{CN}$

compound	$\text{hdpctp} \cdot \text{CuCl}_2 \cdot \text{CH}_2\text{Cl}_2$	$[\text{N}_3\text{P}_3\text{Pz}_5\text{O} \cdot 2\text{CuCl}_2]^- [\text{PzH}]^+ \cdot \text{CH}_3\text{CN}$
formula	$\text{C}_{31}\text{H}_{44}\text{N}_{15}\text{P}_3\text{Cl}_4\text{Cu}$	$\text{C}_{32}\text{H}_{47}\text{N}_{16}\text{P}_3\text{OCl}_4\text{Cu}_2$
f_w	925.06	1033.66
crystal color	green	green
crystal size	$0.14 \times 0.36 \times 0.50$	$0.10 \times 0.18 \times 0.36$
space group	$\text{P}2_1/\text{n}$	$\text{P}\bar{1}$
$a, \text{\AA}$	21.338(4)	11.640(3)
$b, \text{\AA}$	11.432(3)	14.497(4)
$c, \text{\AA}$	18.285(3)	14.775(3)
α, deg	—	77.62(6)
β, deg	104.37(2)	82.10(6)
γ, deg	—	74.88(6)
$V, \text{\AA}^3$	4321(2)	2342.1(21)
Cell determination		
reflections	25	25
2θ range, deg	16-17.5	14.0-16.0
$d(\text{calcd}), \text{g cm}^{-3}$	1.422	1.470
Z	4	2
linear abs. coeff., mm^{-1}	0.78	1.29
scan technique	$\omega/2\theta$	$\theta-2\theta$
scan speed, deg min^{-1}	4-16	4-16
2θ range, deg	2-47.8	2-45.9
h,k,l ranges	-24,23; 0,13; 0,20	-12,12; 0,15; 16,16
absorption range	0.76-0.70	0.69-0.89
reflections measured	6945	6785
data with $I > 3\sigma(I)$	3486	2762
$R(F^2), R_w(F^2)$	0.041, 0.049	0.070, 0.091

related compounds with copper-pyrazolyl pyridinic nitrogen interactions [31, 32]. The Cu-Cl bond lengths (of 2.2676(21) and 2.2429(19) \AA) are relatively short and the equatorial Cu- N_{CTP} distance is so long (2.360(5) \AA , cf. the Cu- N_{CTP} distance in $[\text{N}_4\text{P}_4\text{Me}_8\text{H}] [\text{CuCl}_3]$ is 2.04 \AA [33]) that a question may arise whether it can still be re-

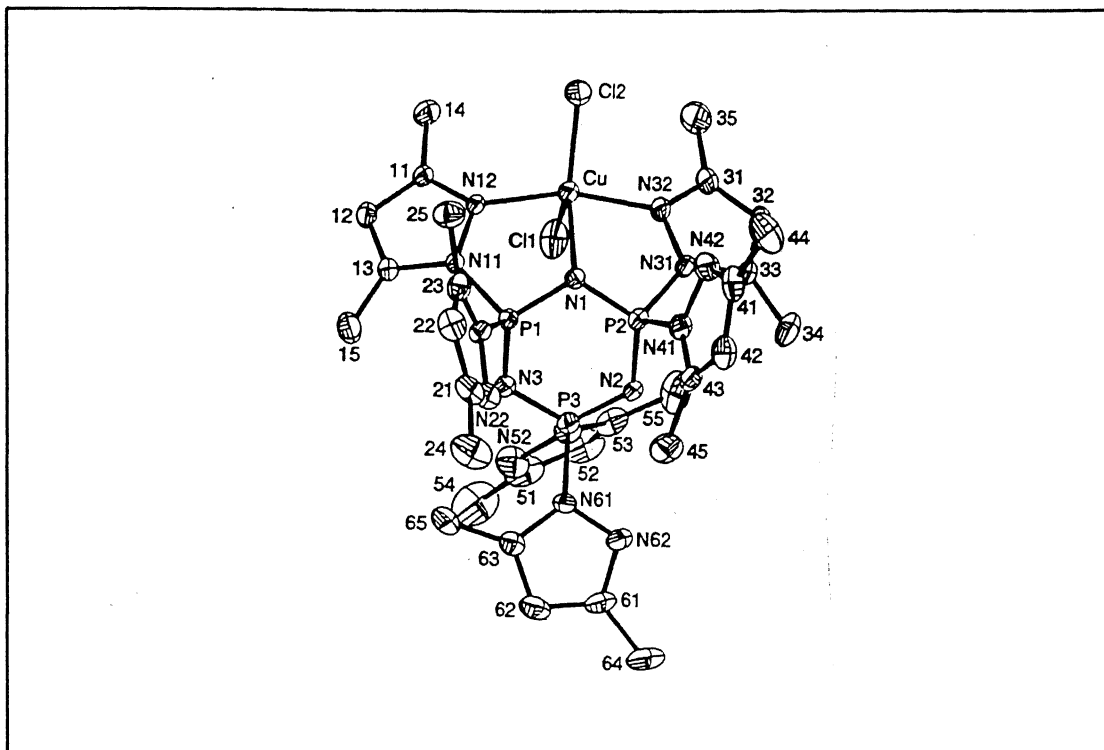


Figure 9: Perspective view of $\text{hdpctp} \cdot \text{CuCl}_2 \cdot \text{CH}_2\text{Cl}_2$

garded as a coordination bond. The Cu-N-P angles being $107.82(24)$ and $109.34(23)$ degrees nevertheless indicate that the lone pair orbital on the ring nitrogen (N_{CTP}) is directed toward the copper ion, as they are close to the expected value of 90-100 degrees. It is, therefore, concluded that the N_{CTP} is coordinating, albeit, weakly. This is reasonable as the P-N bonds flanking the coordination site are lengthened (av. $1.593(5)$ Å), when compared with the other 'normal' P-N bonds (av. $1.573(5)$ Å). Apart from being compressed, the coordination geometry has other distortions apparently originating from the steric constraints imposed by the ligand. The $\text{N}_{Pz}\text{-Cu-N}_{Pz}$ angle is $160.74(21)^\circ$. This restricted bond angle is obviously caused by the limited bite of the ligand. This constriction is also observed in other complexes (*vide infra*). The five-membered chelate ring formed by the copper ion, the cyclotriphosphazene nitrogen, the connecting phosphorus and pyrazolyl nitrogen and the pyrazolyl pyridinic nitrogen imposes a small coordination angle (Table 6).

Table 6: Selected (a) bond distances (\AA) and (b) bond angles in

(a)			
Cu-Cl(1)	2.2676(21)	P(3)-N(2)	1.575(5)
Cu-Cl(2)	2.2429(19)	P(3)-N(3)	1.578(5)
Cu-N(1)	2.360(5)		
Cu-N(12)	1.988(5)	P(1)-N(11)	1.693(5)
Cu-N(32)	1.974(5)	P(1)-N(21)	1.676(5)
P(1)-N(1)	1.596(5)	P(2)-N(31)	1.690(5)
P(1)-N(3)	1.564(5)	P(2)-N(41)	1.672(6)
P(2)-N(1)	1.589(5)	P(3)-N(51)	1.680(6)
P(2)-N(2)	1.574(5)	P(3)-N(61)	1.679(5)
(b)			
N(21)-Cu-N(32)	160.74(21)	N(1)-P(1)-N(3)	118.22(24)
Cl(1)-Cu-Cl(2)	142.28(10)	N(1)-P(2)-N(2)	117.7(3)
Cl(1)-Cu-N(1)	108.32(13)	N(2)-P(3)-N(3)	117.2(3)
Cl(2)-Cu-N(1)	109.40(13)	P(1)-N(1)-P(2)	118.4(3)
N(1)-Cu-N(12)	81.00(18)	P(2)-N(2)-P(3)	122.5(3)
N(1)-Cu-N(32)	80.68(19)	P(3)-N(3)-P(1)	121.3(3)
Cl(1)-Cu-N(12)	88.85(15)		
Cl(1)-Cu-N(32)	91.30(16)	N(11)-P(1)-N(21)	101.07(25)
Cl(2)-Cu-N(12)	96.53(14)	N(31)-P(2)-N(41)	101.4(3)
Cl(2)-Cu-N(32)	95.09(16)	N(51)-P(3)-N(61)	102.7(3)

The participation of the cyclotriphosphazene ring nitrogen in coordination to the copper ion indubitably affects the structural parameters of the inorganic heterocyclic system. The six-membered cyclophosphazene ring adopts a distorted planar conformation with the ring nitrogens N(2) (+0.130 \AA) and N(1) (-0.265 \AA) displaced away from the mean plane defined by P(1), P(2), P(3) and N(3). This distortion is probably induced by the geometrical requirements around the copper ion. Several

structural studies on cyclophosphazene have indisputably shown that either protonation or coordination of a metal to the ring nitrogen atom increases the P–N bond lengths associated with that nitrogen (see for instance: Chapter 2, Section 2.4). This feature has been interpreted as due to a nonavailability of the lone pair of electrons on the nitrogen concerned for participation in skeletal π_s -bonding thereby resulting in a decrease in the π -bond character. In the present structure the P–N bonds in the P–N(Cu)–P segment are longer (av. 1.593 Å) in comparison with other P–N bond lengths (av. 1.573 Å). These differences are much narrower, however, than those observed in many instances. Thus in $N_4P_4(NHMe)_8 \cdot PtCl_2$ where the coordination to platinum ion occurs through the antipodal ring nitrogen atoms, the P–N distances observed are 1.64 and 1.58 Å respectively [34]. Similarly in $[N_4P_4(Me)_8H][CuCl_3]$ the P–N bonds associated with the coordination site are again longer (1.635 Å) [35] than observed for $hdpcTp \cdot CuCl_2$. This clearly indicates that the interaction between the cyclotriphosphazene ring nitrogen and the copper ion is weaker as is reflected in the Cu–N(1) distance as well. Exocyclic P–N bond distances involving the coordinating pyrazolyl groups are slightly longer (av. 1.692 Å) than those linking the non-coordinating pyrazolyl groups (av. 1.667 Å). The phosphazene ring bond angles are unexceptional.

The pyrazole rings are planar with deviations less than 0.015(9) Å. The bond distances and the angles within the pyrazole ring are in the expected range.

(b) $[N_3P_3Pz_5O \cdot 2CuCl_2]^- [PzH]^+ \cdot CH_3CN$

An ORTEP drawing of the structure also showing the atomic numbering scheme is displayed in Figure 10. The structure is the first example of a cyclotriphosphazene ring functioning as a bridging ligand *via* two N_3 cores between copper atoms.

Each copper ion is coordinated by two nongeminal *cis* pyrazolyl pyridinic nitrogen atoms, one cyclotriphosphazene skeletal nitrogen atom and two chloride ions in a compressed trigonal bipyramidal geometry. Selected bond distances and angles are

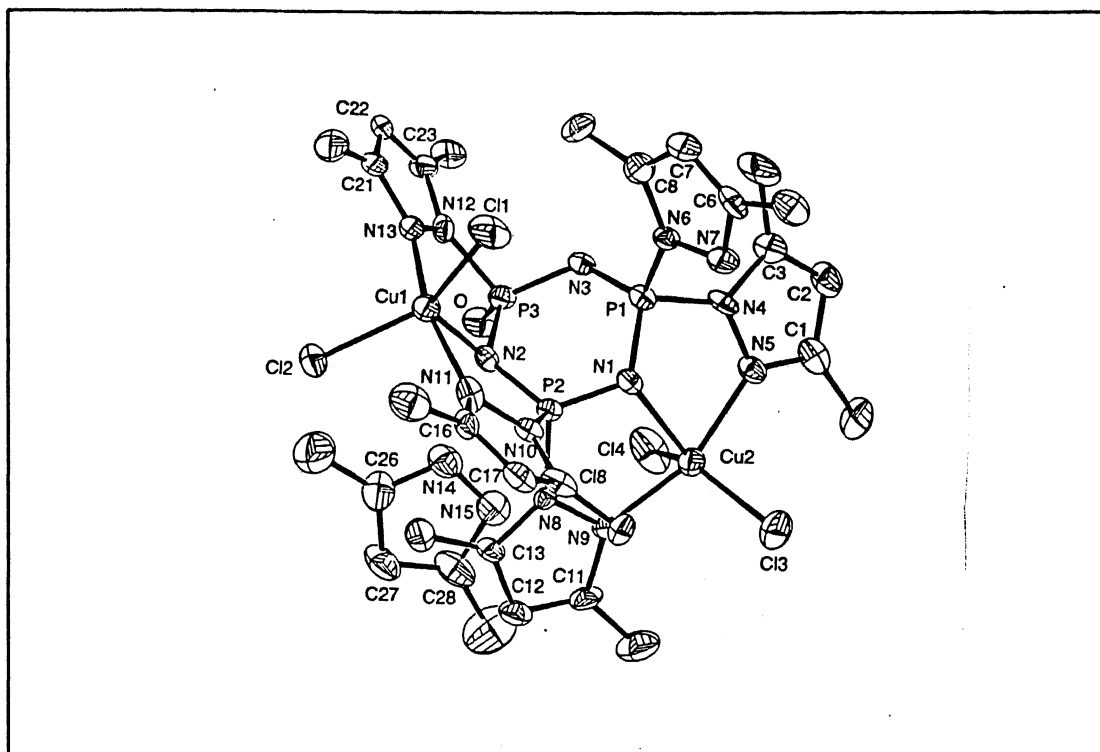
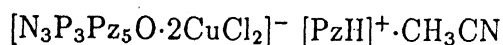


Table 7: Selected (a) bond distances (Å) and (b) bond angles (°) in

(a)			
Cu(1)–N(11)	1.978(14)	P(1)–N(1)	1.6014(12)
Cu(1)–N(13)	1.998(14)	P(1)–N(3)	1.5222(12)
Cu(1)–N(2)	2.317(12)	P(2)–N(2)	1.576(12)
Cu(1)–Cl(1)	2.266(5)	P(2)–N(2)	1.577(12)
Cu(1)–Cl(2)	2.287(5)	P(3)–N(2)	1.630(12)
		P(3)–N(3)	1.600(13)
Cu(2)–N(5)	1.982(13)		
Cu(2)–N(9)	1.969(13)	P(1)–N(4)	1.677(14)
Cu(2)–N(1)	2.366(13)	P(1)–N(6)	1.672(12)
Cu(2)–Cl(3)	2.259(5)	P(2)–N(8)	1.712(12)
Cu(2)–Cl(4)	2.296(5)	P(2)–N(10)	1.661(13)
P(3)–N(12)	1.708(13)	P(3)–O	1.505(11)
(b)			
N(11)–Cu(1)–N(13)	159.7(6)	N(5)–Cu(2)–N(9)	160.0(6)
N(2)–Cu(1)–Cl(1)	118.1(3)	N(1)–Cu(2)–Cl(3)	109.4(3)
N(2)–Cu(1)–Cl(2)	102.5(3)	N(1)–Cu(2)–Cl(4)	112.4(3)
Cl(1)–Cu(1)–Cl(2)	139.27(23)	Cl(3)–Cu(2)–Cl(4)	138.13(24)
Cl(1)–Cu(1)–N(11)	88.7(4)	Cl(3)–Cu(2)–N(5)	98.3(4)
Cl(1)–Cu(1)–N(13)	92.9(4)	Cl(3)–Cu(2)–N(9)	95.5(4)
Cl(2)–Cu(1)–N(11)	94.9(4)	Cl(4)–Cu(2)–N(5)	89.4(4)
Cl(2)–Cu(1)–N(13)	97.0(4)	Cl(4)–Cu(2)–N(9)	90.0(4)
N(2)–Cu(1)–N(11)	81.9(5)	N(1)–Cu(2)–N(5)	80.2(5)
N(2)–Cu(1)–N(13)	79.5(5)	N(1)–Cu(2)–N(9)	81.5(5)
N(1)–P(1)–N(3)	116.6(6)	N(4)–P(1)–N(6)	100.0(6)
N(1)–P(2)–N(2)	118.0(6)	N(8)–P(2)–N(10)	99.7(6)
N(2)–P(3)–N(3)	110.5(6)	N(12)–P(3)–O	105.5(6)
		P(1)–N(1)–P(2)	118.3(7)
		P(2)–N(2)–P(3)	119.9(7)
		P(1)–N(3)–P(3)	125.1(8)

less than 0.23(4) Å.

The interesting aspect of the structure is the unusual cleavage of one of the uncoordinated pyrazolyl groups from the parent ligand hdpctp. This leads to the formation of a rare oxide-containing cyclotriphosphazene along with the liberated pyrazolium cation. The negative charge on oxygen is delocalized into the phosphazene ring as is reflected in the relatively short P–O bond length (1.505 Å) comparable to those found in related systems, viz., triphenylphosphine oxide [36] (1.483(3) Å), gem-N₃P₃Ph₂(OMe)₃(OH) (1.456(1) Å) [37] and gem-N₃P₃(NEt₂)₂Cl₃(OH) (av. 1.47 Å) [38]. The expulsion of an uncoordinated pyrazolyl group is clearly a steric effect facilitated by the presence of trace amount of water.

4.3.2 Heterobimetallic compounds of hdpctp

There is a widespread research interest in the synthesis and chemistry of hetero(bi or poly)metallic compounds [39]. This activity stems from the possibility that the disparate metal centres present in the same compound could act in concert to afford novel chemical properties tunable for certain catalytic applications [40]. There are several synthetic strategies to assemble these heterobimetallic structures. Chief among these are (a) the use of heterodifunctional ligands such as diphenylphosphinocyclopentadiene anion [40], R₂P–CH₂–P=NSiMe₃ [41], pyridyl phosphines [42], etc. which contain distinct coordination sites, therefore, can selectively bind different metallic units, (b) the use of preformed metal complexes as ligands. For example, in recent years 1,1-bis(diphenylphosphino)ferrocene revealed to be a remarkable simple metal bearing ligand for preparing bi- and polymetallic compounds with varying degrees of structural complexity [43]. Keeping this in mind we have begun to explore the possibility of using the mononuclear complexes discussed in the last section as ligands for heterobimetallic hosts. In the mononuclear complexes hdpctp·CuX₂ where X=Cl, Br the copper is bound to hdpctp *via* two nongeminal cis pyrazolyl nitrogen atoms and one

cyclotriphosphazene skeletal nitrogen. This leaves several vacant coordination sites which can be utilized to interact with additional metals. The results obtained are presented here.

Synthesis

The reactions of the complexes $\text{hdpctp} \cdot \text{CuX}_2$ ($\text{X}=\text{Cl}, \text{Br}$) with $\text{M}(\text{PhCN})_2\text{Cl}_2$ ($\text{M}=\text{Pd}$ or Pt) in equimolar ratios in benzene give heterobimetallic compounds with the general formula $\text{hdpctp} \cdot \text{CuCl}_2 \cdot \text{MX}_2$ ($\text{M}=\text{Pd}, \text{Pt}$ and $\text{X}=\text{Cl}, \text{Br}$) in excellent yields as their benzene solvates. The palladium derivatives contain a water molecule as well. All the bimetallic complexes are readily soluble in common organic solvents such as dichloromethane, acetonitrile, benzene (platinum derivatives only), etc. Conductivity measurements in acetonitrile suggests that they behave as non-electrolytes, indicating that the halide ions are intact in solution as well. The interesting aspect of this reaction is the unusual and facile halide exchange between copper and the heavy metal (Pd or Pt). The evidence for the attachment of bromide to platinum or palladium rather than copper in the resulting heterobimetallic is obtained from the electronic absorption and EPR spectra and the crystal structure determination of $[\text{hdpctp} \cdot \text{CuCl}_2 \cdot \text{PdBr}_2] \cdot \text{H}_2\text{O} \cdot \text{C}_6\text{H}_6$.

The IR spectra of the compounds are analogous to that of the precursor complex $\text{hdpctp} \cdot \text{CuCl}_2$, suggesting that the cyclotriphosphazene ring nitrogen is coordinated to the metal in the heterobimetallics also. The magnetic moments measured in dichloromethane solution by using Evan NMR method are in the range 1.81-1.84 BM. Although these values are larger than the spin-only value (1.73) for $S=1/2$, they lie in the range of μ_{eff} values 1.8-2.0 generally observed for copper complexes at room temperature [11]. The larger values are attributed to a mixing-in of orbital angular momentum from excited states *via* spin-orbit coupling.

Optical Spectroscopy

The electronic spectra of the compounds were registered in dichloromethane solution.

Table 8: Electronic spectral data for the heterobimetallic complexes of hdpctp[†]

compound	$\lambda_{max}(\epsilon_{max})^{\ddagger}$	assignment
hdpctp·CuCl ₂ ·PtCl ₂	897(0.28) 350(2.45), 275(15.50) 237(29.45)	d-d Pz → Cu l.m.c.t. π - π^* intraligand
hdpctp·CuCl ₂ ·PtBr ₂	927(0.27) 350(1.96), 270(13.12) 236(29.86)	d-d Pz → Cu l.m.c.t. π - π^* intraligand
hdpctp·CuCl ₂ ·PdCl ₂	913(0.25) 358(1.93), 280(7.00) 234(30.76)	d-d Pz → Cu l.m.c.t. π - π^* intraligand
hdpctp·CuCl ₂ ·PdBr ₂	900(0.29) 358(2.51), 280sh(5.13) 233(28.84)	d-d Pz → Cu l.m.c.t. π - π^* intraligand

[†] for dichloromethane solutions, sh = shoulder

[‡] units: nm(mol⁻¹ cm⁻¹ × 10³)

Absorption maxima and tentative assignments are reported in Table 8. The high absorption maximum at *ca.* 235 nm is due to π - π^* transitions within the ligand. The Pz → Cu charge transfer bands were observed for all compounds in the range 270-370 nm. When compared with the mononuclear precursor complexes (Table 3) the heterobimetallics (Table 8) show increased intensity for the band at *ca.* 275 nm indicating that it may possess contributions from Pz → Pt or Pd charge transfer transitions. It is exciting to note that the UV-Vis spectral pattern for the heterobimetallics closely resembles that of the hdpctp·CuCl₂ rather than the bromo analogue. No band could be identified attributable to the Br → Cu l.m.c.t. (Table 8). This reveals that in the heterobimetallics derived from hdpctp·CuBr₂ the bromide ions are no longer bound to copper. This spontaneous halide exchange reaction between copper

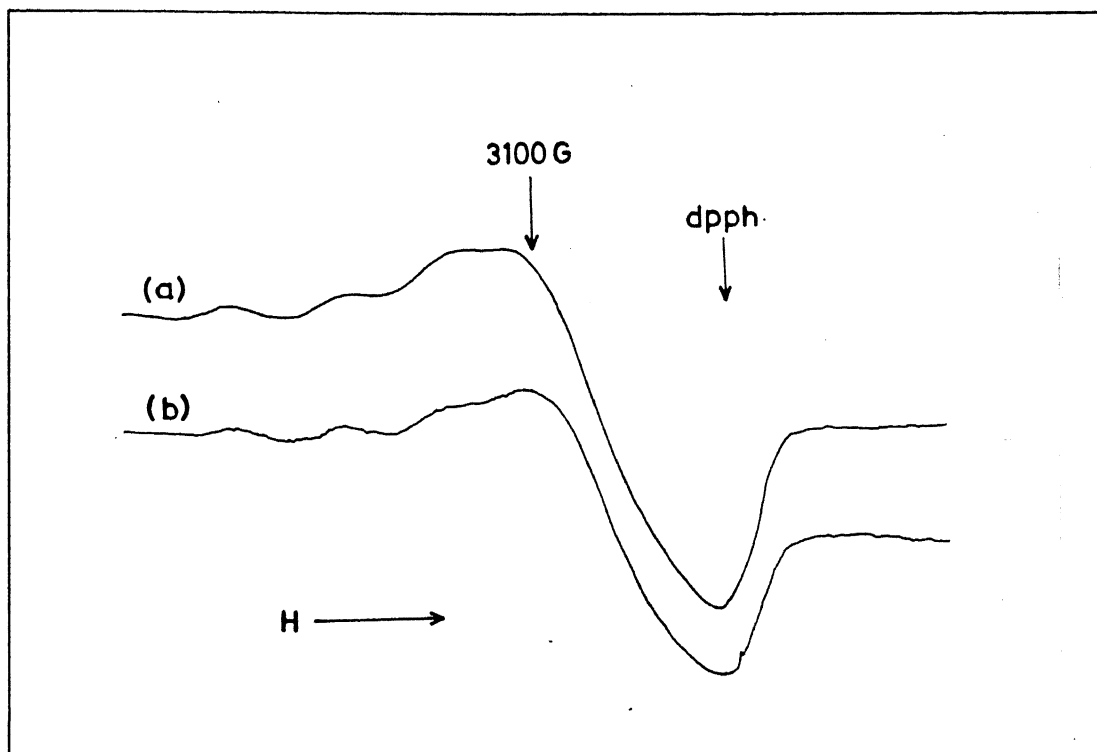


Figure 11: EPR spectra of hdpctp·CuCl₂·MCl₂ [M=Pd (a) and Pt (b)] in frozen dichloromethane solution

and palladium or platinum can be easily accounted on the basis of HSAB theory or Pearsons principle [44].

The d-d transition for the heterobimetallics is located at *ca.* 900 nm as a broad band and the intensity compares well to the starting mononuclear copper complex hdpctp·CuCl₂ (Tables 3 and 8). It appears that the ground state electronic structure of the copper chromophore is unaffected by the introduction of the additional metal.

EPR spectroscopy

The EPR spectra of the heterobimetallic compounds were recorded at x-band frequency as polycrystalline solids and dichloromethane fluid and frozen solutions. The spin hamiltonian parameters for them are presented in Table 9. At room temperature the powder samples of platinum derivatives show rhombic spectra while the palladium analogs exhibit very broad isotropic spectra with the g_{iso} values around 2.10. The observed g-parameters for the platinum complexes in solid state are reminiscent

Table 9: Spin hamiltonian parameters of Cu-Pt and Cu-Pd complexes^a.

compound		g_1	g_2	g_3	$A_{ }$	g_{av} ^b	g_{iso}	A_{iso}	G ^c
hdpcptp-CuCl ₂ ·PtCl ₂	d	2.013	2.130	2.211	-	2.138	-	-	4.35
	e	2.090	2.292	-	130	2.159	2.172	50	3.34
hdpcptp-CuCl ₂ ·PtBr ₂	d	2.018	2.125	2.255	-	2.141	-	-	3.96
	e	2.078	2.285	-	121	2.149	2.168	45	3.65
hdpcptp-CuCl ₂ ·PdCl ₂	d	-	-	-	-	-	2.140	-	-
	e	2.088	2.288	-	135	2.157	2.165	52	3.27
hdpcptp-CuCl ₂ ·PdBr ₂	d	-	-	-	-	-	2.139	-	-
	e	2.081	2.291	-	126	2.155	2.161	55	3.46

^a for axial, $g_{||}=g_2$ and $g_{\perp}=g_1$, A values are in $\times 10^{-4} \text{ cm}^{-1}$
 g_{iso} and A_{iso} values are from room temperature isotropic spectra

^b from $[\frac{1}{3}(g_{||}^2+2g_{\perp}^2)]^{1/2}$, $[\frac{1}{3}(g_1^2+g_2^2+g_3^2)]^{1/2}$ for axial and rhombic spectra respectively

^c from $(g_{||}-2.0)/(g_{\perp}-2.0)$, for rhombic spectra $g_{||}=(g_2+g_3)/2$ and $g_{\perp}=g_1$

^d polycrystalline powder, room temperature

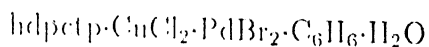
^e dichloromethane solution, room and liquid nitrogen temperatures

of the mononuclear copper(II) chloride complex, for which x-ray structure has been determined, indicating a distorted N_3Cl_2 trigonal bipyramidal environment around copper. The deviant spectra of the palladium derivatives in solid state may be attributed to the presence of a water molecule, which probably forms intermolecular hydrogen bonding and bridges copper and palladium atom of adjacent molecules *via* the halide ions. However, in frozen dichloromethane solution the spectra of all the derivatives are similar, axial with $g_{||} > g_{\perp}$ and $A_{||} \simeq 121-135 \times 10^{-4} \text{ cm}^{-1}$ suggestive of $d_{x^2-y^2}$ ground state (Figure 11). It is assumed that in solution the hydrogen bonding forces are no longer operative. Electron propagation between metal centers by the intervening hydrogen bonds are well documented in the literature [45-47]. It seems there exists no electronic transmittance between the metals through the bridging

Table 10: Crystal data for $\text{hdpctp} \cdot \text{CuCl}_2 \cdot \text{PdBr}_2 \cdot 2\text{H}_2\text{O} \cdot \text{C}_6\text{H}_6$

formula	$\text{C}_{30}\text{H}_{42}\text{N}_{15}\text{P}_3\text{Cl}_2\text{Br}_2\text{CuPd} \cdot \text{C}_6\text{H}_6 \cdot \text{H}_2\text{O}$
fw	1202.47
crystal size, mm	$0.52 \times 0.25 \times 0.28$
crystal color	brown
a, Å	10.570(2)
b, Å	28.863(4)
c, Å	16.009(5)
β , deg	98.71(1)
V, Å ³	1827(1)
cell determination	
reflections	25
2 θ angle, deg	17-20
d(calcd), gcm ⁻³	1.65
space group	P 21/c
Z	4
linear abs. coeff., mm ⁻¹	2.7
scan technique	θ -2 θ
scan speed, deg min ⁻¹	1-16
2 θ range, deg	4-14
h, k, l ranges	0, 11; 0, 30; -16, 16
exposure time, h	75
std. refl. indices	1, 4, 6; 2, 7, -5; 3, 6, 3
drift of stds, %	1.1
absorption range	0.85-1.0
refls measured	6275
unique reflections	5898
R for merge	0.02
data with $I > 1\sigma(I)$	3305
parameters refined	360
GOF	2.01
$R(F^2)$, $R_w(F^2)$	0.073, 0.12
largest Δ/σ	0.01
Final diff map, eÅ ⁻³	-1.4(2), +1.7(2)

ride ions and a cyclotriphosphazene ring nitrogen N(14) in the equatorial plane. The

Table 11: Selected interatomic distances (a) and bond angles (b) in

(a)			
Cu-Cl(1)	2.312(5)	P(1)-N(13)	1.554(15)
Cu-Cl(2)	2.319(5)	P(1)-N(15)	1.552(15)
Cu-N(6)	1.997(16)	P(2)-N(13)	1.591(16))
Cu-N(12)	2.003(16)	P(2)-N(14)	1.585(16))
Cu-N(14)	2.362(15)	P(3)-N(14)	1.586(15)
Pd-N(1)	2.073(14)	P(3)-N(15)	1.558(15)
Pd-N(7)	2.033(14)	mean distance:	
Pd-Br(1)	2.386(3))	P-N _{exo}	1.679(16)
Pd-Br(2)	2.366(3))		
Pd-P(1)	3.171(5))		

(b)			
Cl(1)-Cu-Cl(2)	143.21(21)	N(13)-P(1)-N(15)	117.7(8)
Cl(1)-Cu-N(14)	111.0(4)	N(13)-P(2)-N(14)	117.2(8)
Cl(2)-Cu-N(11)	105.7(4)	N(11)-P(3)-N(15)	114.6(8)
N(6)-Cu-N(12)	159.3(6)	P(1)-N(13)-P(2)	120.2(10)
N(6)-Cu-Cl(1)	95.2(5)	P(2)-N(11)-P(3)	120.3(9)
N(6)-Cu-Cl(2)	92.1(5)	P(1)-N(15)-P(3)	124.1(9)
N(12)-Cu-Cl(1)	96.7(5)	N(2)-P(1)-N(8)	100.8(8)
N(12)-Cu-Cl(2)	88.5(5)	N(4)-P(2)-N(5)	101.7(8)
N(14)-Cu-N(6)	80.3(6)	N(10)-P(3)-N(11)	101.1(8)
N(14)-Cu-N(12)	79.6(6)		
N(1)-Pd-N(7)	86.6(6)	Br(1)-Pd-P(1)	122.92(13)
N(1)-Pd-Br(1)	92.5(4)	Br(2)-Pd-P(1)	120.72(13)
N(7)-Pd-Br(2)	91.3(4)	P(1)-Pd-N(1)	55.5(4)
Br(1)-Pd-Br(2)	89.57(12)	P(1)-Pd-N(7)	56.0(4)
Br(1)-Pd-N(7)	178.9(4)	Br(2)-Pd-N(1)	176.1(4)

two nongeminal cis-pyrazolyl nitrogens reside at the axial positions. The geometry

around palladium is essentially square planar as would be expected based on earlier literature precedent. Two geminal pyrazolyl nitrogen atoms occupy the cis-positions with their trans positions filled by two bromide ions. Additionally there exists a weak interaction between palladium and P(1). The Pd-P(1) distance is 3.174(5) Å which is less than the sum of the Van der Waals radii of them (3.45 Å). The halide exchange between copper and palladium or platinum estimated by UV-Vis and EPR spectra is unequivocally confirmed by this structure as the bromide ions are bound to palladium. Moreover, a water molecule bridges the copper and palladium of adjacent molecules *via* halogens by hydrogen bonding, thus leading to a chain-like hydrogen bonded polymer. The relevant coordination distances, bond angles and hydrogen bond distances are given in Table 11.

Cu-N_P bond lengths are normal and agree well with the data for hdpctp-CuCl₂. The Cu-N_{C_{TP}} bond distance is longer and similar to that in hdpctp-CuCl₂. The Cu-Cl bond lengths are appreciably longer (av. 2.315(5) Å) and significantly differ from the Cu-Cl distance observed for hdpctp-CuCl₂. The average Pd-N bond length (2.053(14) Å) is typical for organic heterocyclic bases [48]. Pd-Br distances are shorter (av. 2.376(3) Å) than those found in tetrabromo palladate anions [49] and related compounds [50]. For instance, in the complex [Pd(Ino)₂Br₂] (where Ino = Inosine, a purine nucleoside) the average Pd-Br distance is 2.430(1) Å [50]. The shorter Pd-Br bond length may reflect an increased covalent character. Angles around the palladium atom vary from the idealized 90 ° by ± 3 °. The geometry is tetrahedrally distorted, with the Br(1) and N(7) atoms placed on one side and the Br(2) and N(1) atoms placed on the other side of the average coordination plane.

There exists two kinds of P-N bonds. The P-N bonds flanking the coordination site N(11) and P(2)-N(13) are longer (av. 1.587(16) Å) than the remaining P-N bonds (av. 1.555(15) Å). The six-membered P₃N₃ ring adopts a distorted planar conformation with the nitrogen atoms N(13) (0.127(16) Å) and N(14) (-0.306(16) Å) displaced

significantly out of the plane defined by P(1), P(2), P(3) and N(15). The other bond distances and angles within the cyclotriphosphazene and pyrazolyl moieties show usual variations expected upon coordination by metal and are unexceptional.

It is to be noted that this is the first example of a heterobimetallic derivative obtained by exploiting the coordination capability of a cyclotriphosphazene derived ligand. Previously heterobimetallic derivatives have been reported to form from the interaction of metal carbonyl anions with halogenocyclotriphosphazenes [51-53].

4.3.3 Redox properties of the complexes of hdpctp

There are no earlier reports of electrochemical studies on any cyclophosphazene metal complexes except certain ferrocene-substituted derivatives [54]. In view of the interest in the redox chemistry of copper complexes containing pyrazolyl or imidazolyl residues [55], we have carried out a cyclic voltammetric investigation on the present compounds. The cyclic voltammograms recorded for the complexes hdpctp·CuX₂ (X=Cl, Br) and hdpctp·2CuX₂ (X=Cl, Br) are shown in Figure 13. Table 12 summarizes the electrochemical parameters. Analysis of the cyclic voltammetric responses for mononuclear complexes hdpctp·CuX₂ (X=Cl and Br) with scan rates varying from 0.02 to 51.2 V s⁻¹ showed a simple quasi-reversible one-electron charge transfer for the Cu(II)/Cu(I) couple which is located at a relatively positive potential, 0.20 and 0.50 V respectively in dichloromethane; the anodic to cathodic peak current ratio i_{pa}/i_{pc} is constantly equal to one. The ratio between the cathodic peak current and the square root of the scan rate $i_{pc}/V^{1/2}$ is practically constant. The difference between the potential of the anodic peak and that of the cathodic peak ΔE_p gradually increases. However, the corresponding process in the dinuclear complexes hdpctp·2CuX₂ (X=Cl, Br) is indicative of a simultaneous two-electron transfer $[(Cu(II) \cdot Cu(II)) \xrightarrow{2e^-} (Cu(I)Cu(I))]$ and does not proceed by a stepwise process, $[(Cu(II) \cdot Cu(II)) \xrightarrow{e^-} (Cu(II)Cu(I)) \xrightarrow{e^-} (Cu(I)Cu(I))]$. The quasi reversibility of this

Table 12: Cyclic voltammetric data for the mononuclear and homodinuclear copper complexes of hdpctp[†]

compound	solvent	E(Cu(II)/Cu(I))	ΔE_p	E(Cu(I)/Cu(0))
hdpctp·CuCl ₂ [‡]	CH ₂ Cl ₂	+0.201	160	-1.240
hdpctp·CuBr ₂ [‡]	CH ₂ Cl ₂	+0.501	124	-1.340
	DMF	+0.435	130	-1.456
hdpctp·2CuCl ₂	CH ₂ Cl ₂	+0.495	221	-1.290
	DMF	+0.151	158	-0.760
hdpctp·2CuBr ₂	CH ₂ Cl ₂	+0.590	103	-1.280
hdpctp·Cu(ClO ₄) ₂ ·2H ₂ O	CH ₂ Cl ₂	+0.630	220	-0.580
	DMF	+0.381	120	-0.732
hdpctp·Cu(ClO ₄) ₂ ·bipy	CH ₂ Cl ₂	+0.252	150	-0.970

[†] potential values are quoted vs Ag/AgCl reference electrode and ΔE_p values for 100 mV s⁻¹ scan rate

[‡] Cu(III)/Cu(II) couples at +0.153, +1.125 and +0.727 respectively

electrode process is probably due to the stereochemical changes accompanying the Cu(II)/Cu(I) redox step from a trigonal bipyramidal to a distorted tetrahedral geometry [56]. Since the highest Cu(II)/Cu(I) potentials are in principle expected for the reversible tetrahedral Cu(II)/tetrahedral Cu(I) redox change it is likely that both the non planar geometries of the Cu(II)/Cu(I) couple and the electronic effects of the phosphazene ring act in concert to produce the notably positive location of the redox potentials of these complexes. The second cathodic step, Cu(I)-Cu(0), proceeds always in an irreversible manner, because of the extreme lability of the copper(0) complex. This is confirmed by the appearance of a strong characteristic stripping peak due to the reoxidation of electrodeposited copper metal to free copper ion during positive scan starting from high potentials. Nonplanar geometry around copper(II) ion inhibits accessibility to a planar copper(III) assembly. The redox behavior of mononuclear copper(II) halide complexes can be schematized as follows:

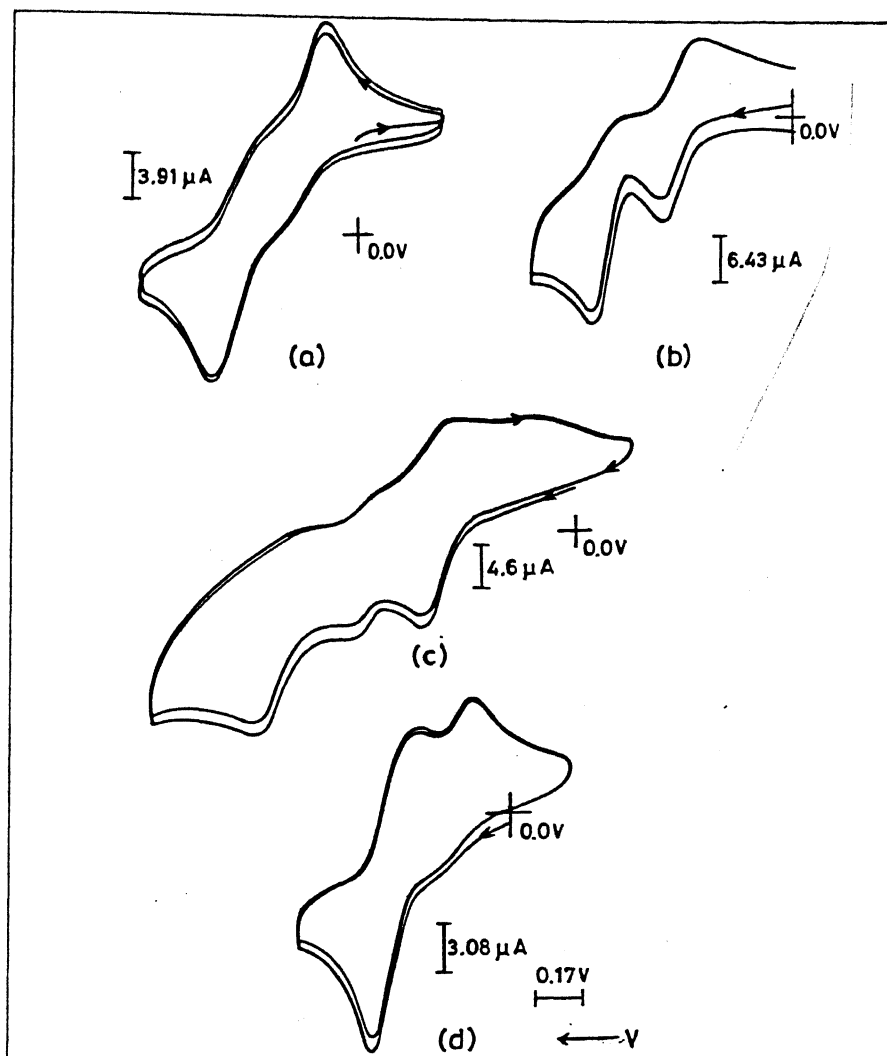
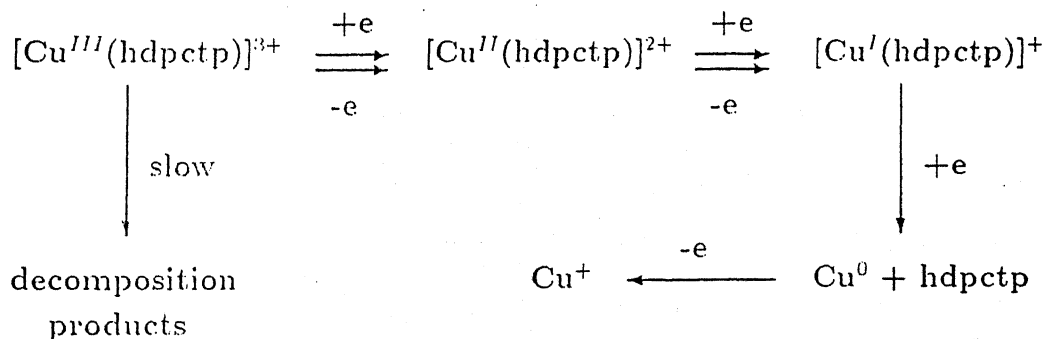
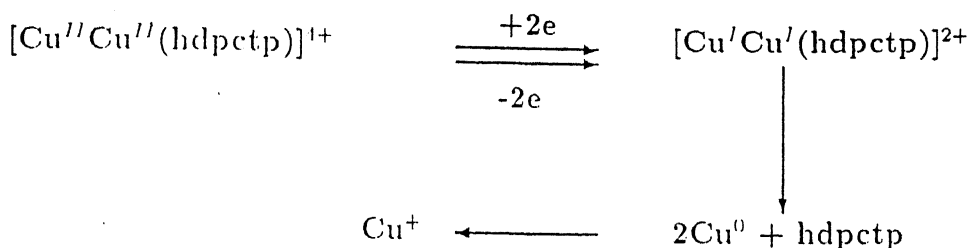


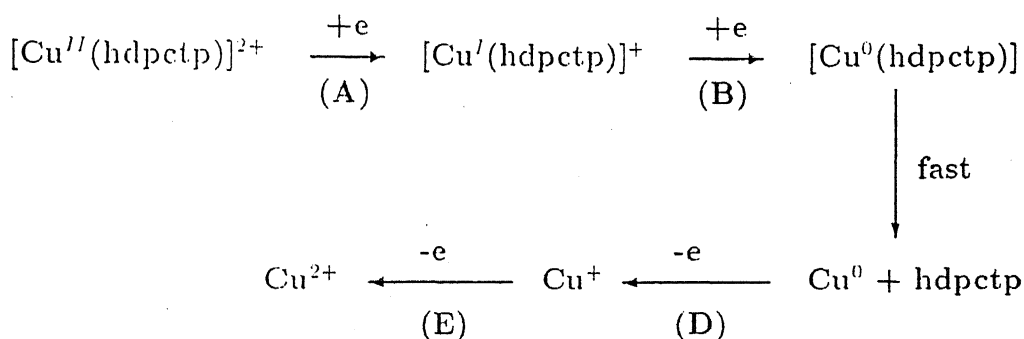
Figure 13: Cyclic voltammograms of (a) hdpctp·CuCl₂ in CH₂Cl₂ (b) and (c) hdpctp·CuBr₂ in CH₂Cl₂ and DMF respectively and (d) hdpctp·2CuCl₂ in DMF



For dinuclear complexes the valid redox equation is:



The copper halide complexes exhibit similar redox pattern in dichloromethane and dimethyl formamide solutions. However, in more reducing solvent such as acetonitrile the redox behavior is entirely different. The cyclic voltammograms recorded in acetonitrile is displayed in Figure 14 and the data provided in Table 13. They undergo irreversibly, but stepwisely the following electron-transfer sequence:



In this connection, it seems useful to point out that the two consecutive redox changes A, B shown Figure 14c which apparently look like reversible Cu(II)/Cu(I)/Cu(0) electron-transfers, because of the responses D, E in the reverse scan, indeed proved to be irreversible, in that: (i) the reoxidation peak E is lacking when the potential scan is reversed just after traversing peak A; (ii) as shown in the relevant inset, at low scan rates peak D reveals to be an anodic stripping peak.

All the heterodimetal complexes here presented display, in acetonitrile solution, irreversible reduction of the two metal(II) centres. The first cathodic process A/B (Figure 14a), which consumes two electrons per molecule in controlled potential coulometry ($E_m = -0.7$ V); in the case of platinum complexes $\text{hdpctp} \cdot \text{CuCl}_2 \cdot \text{PtX}_2$ ($\text{X} = \text{Cl}$,

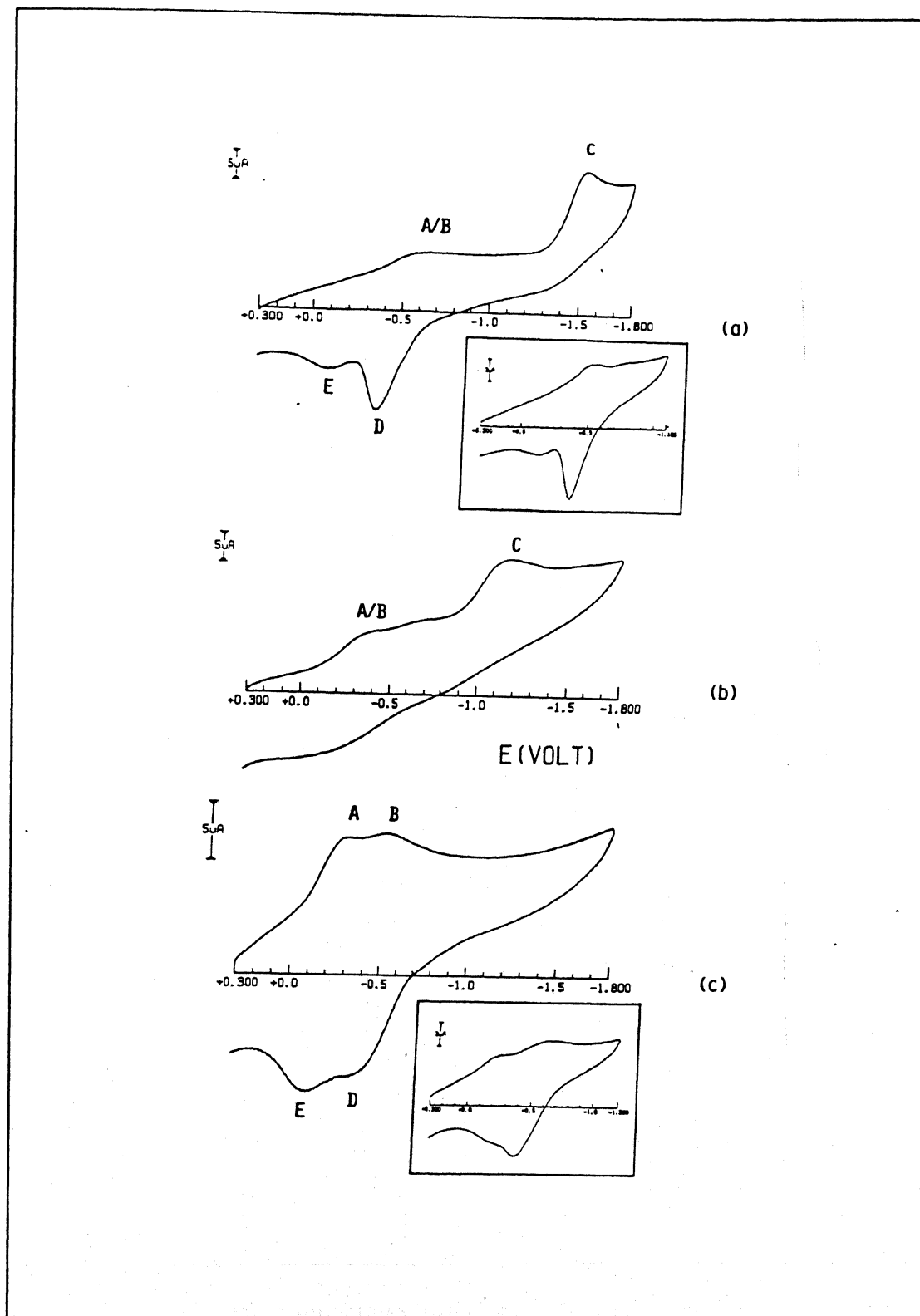


Figure 11: Cyclic voltammogram of (a) hdpctp·CuCl₂·PtCl₂, (b) hdpctp·CuCl₂·PdCl₂ (c) hdpctp·CuCl₂ in acetonitrile at 200 mV s⁻¹; inset for 50 mV s⁻¹ scan

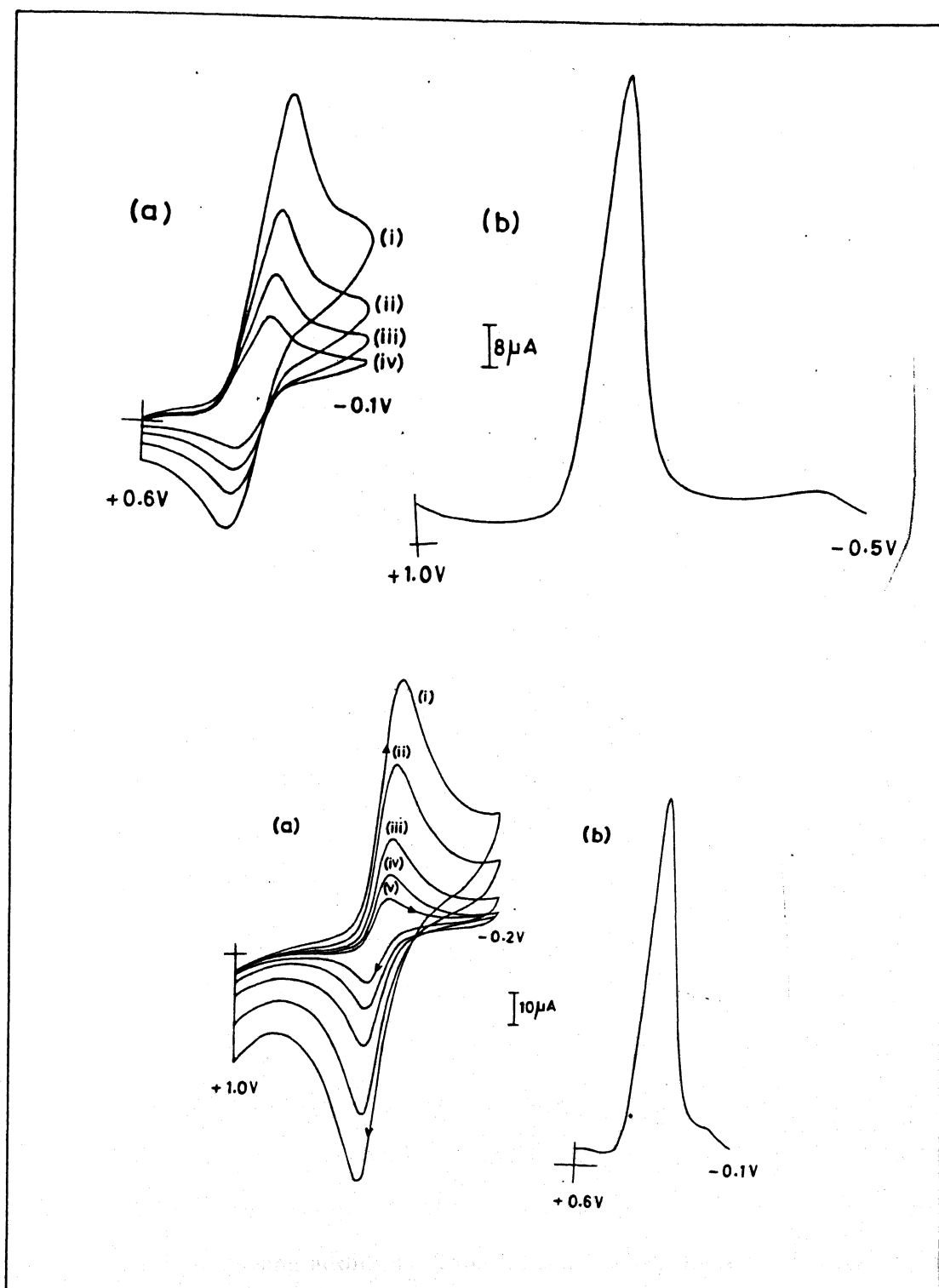


Figure 15: Cyclic voltammograms (a) and differential pulse voltammograms (b) (10 mV s^{-1}) of $\text{hdpctp} \cdot \text{Cu}(\text{ClO}_4)_2 \cdot 2\text{H}_2\text{O}$ in DMF (top) [Key: (i) 100 (ii) 50 (iii) 20 (iv) 10 (v) 5 mV s^{-1}] and $\text{hdpctp} \cdot \text{Cu}(\text{ClO}_4)_2 \cdot \text{bipy}$ in CH_2Cl_2 (bottom) [Key: (i) 500 (ii) 200 (iii) 100 (iv) 50 mV s^{-1}]

Table 13: Peak potential values (in V, vs SCE) for the reduction steps of heterobimetallic complexes in acetonitrile

compound	E_p^a *	
	Cu(II)/Cu(0)	Pt(II)/Pt(0) or Pd(II)/Pd(0)
hdpctp·CuCl ₂ ·PtCl ₂	-0.55	-1.53
hdpctp·CuCl ₂ ·PtBr ₂	-0.55	-1.50
hdpctp·CuCl ₂ ·PdCl ₂	-0.15	-1.13
hdpctp·CuCl ₂ ·PdBr ₂	-0.10	-0.96
hdpctp·CuCl ₂	-0.25 †	-0.52 ‡
hdpctp·CuBr ₂	-0.20 †	-0.45 ‡

* measured at 200 mV s⁻¹ scan rate

† Cu(II)/Cu(I) step

‡ Cu(I)/Cu(0) step

Br) the anodic stripping profile typical of many copper complexes [57]. This allows us to think the first redox process as centred on the copper fragment. The second cathodic step C (Figure 14a), which is assigned to the reduction of platinum or palladium centre, also involves the consumption of two electrons per molecule in controlled potential coulometry ($E_w = -1.6$ V). In this picture, one must conclude that the presence of the second metal centre, further increasing the stereochemical rigidity of the molecular backbone, hinders at all the redox flexibility required for the access to the geometries typical of the Cu(I) (tetrahedral) and Pt(I) (square planar) congeners, thus compelling the two metal centres to undergo simultaneous two-electron decomposing additions. Table 13 summarizes the redox potential of the heterobimetallic complexes. In spite of the irreversibility of the electron transfers, it seems that, as expected, the palladium complexation bears a markedly lower electron density than the platinum complexation does.

The copper perchlorate complexes $\text{hdpctp} \cdot \text{Cu}(\text{ClO}_4)_2 \cdot \text{L}$ ($\text{L} = 2\text{H}_2\text{O}$ or bipy) exhibit a quasi-reversible $\text{Cu(II)}/\text{Cu(I)}$ redox couple in various solvents. The data are included in Table 12. Illustrative cyclic voltammograms and differential pulse voltammograms are displayed in Figure 15. Replacement of aquo ligands by bipyridine shifts the potential to the negative side. This is attributed to the electron rich bipyridine which hinders the addition of electron to the copper.

4.4 Coordination Compounds of the Ligand 2,2-diphenyl-4,4,6,6-tetrachloro(3,5-dimethyl-1-pyrazolyl)cyclotriphosphazene (tdpctp)

4.4.1 General

The ligand tdpctp consists of two pyrazolyl groups less than that in hdpctp. Reduction of number of pyrazolyl groups should significantly affect the coordination response of tdpctp as it can now bind only one metal as a N_3 donor in its nongeminal interaction mode. However, in favorable circumstances a bis(bidentate) chelation *via* geminal N_2 is possible. If a cyclotriphosphazene nitrogen also participates in ligation along with two geminal pyrazolyl nitrogens the ligand might be viable to coordinate additional metal, with a novel N_3 fashion. It seems that this possibility is very unlikely on the basis of the prevailing structural evidences (Section 4.3), which points severe steric constraints because of methyl substituents on pyrazolyl ring.

As expected tdpctp yields selectively a variety of mononuclear coordination compounds with copper, cobalt and nickel salts. Interestingly, the nickel complexes are stable and soluble in common solvents, thus, allowing spectroscopic and other studies on them. In Table 14 a summary of all complexes together with their physical characteristics is given. The IR spectra of the metal complexes suggest the participation of pyrazolyl and cyclotriphosphazene ring nitrogens in coordination. In the complexes containing perchlorate counter cations, it is proposed on the basis of IR and

Table 14: Colors, Nature, conductivity and magnetic moment data of the complexes with the ligand tdpctp

compound	color	nature	Λ_m *	μ_{eff} (BM)
tdpctp·CuCl ₂	green	crystalline	8	1.76
tdpctp·CuBr ₂	dark yellow	crystalline	20	1.71
tdpctp·Cu(ClO ₄) ₂ ·2H ₂ O	blue	crystalline	240	1.79
tdpctp·Cu(ClO ₄) ₂ ·2py	blue	crystalline	235	1.84
tdpctp·Cu(ClO ₄) ₂ ·2ImH	blue	crystalline	250	1.82
tdpctp·Cu(ClO ₄) ₂ ·bipy	blue	crystalline	265	1.88
tdpctp·Cu(ClO ₄) ₂ ·phen	blue	crystalline	272	1.90
tdpctp·NiCl ₂	maroon	crystalline [†]	40	0.78
tdpctp·NiBr ₂	pink	crystalline	79	1.80
tdpctp·CoCl ₂	royal blue	crystalline	13	4.65

* units: mho cm² mol⁻¹

† turns green slowly on exposure to moist air over a week

conductivity data that perchlorate ions reside outside the coordination sphere. But for exception in tdpctp·Cu(ClO₄)₂·2H₂O it is inferred from IR that it contains an unidentate perchlorate ion and two water molecules. The magnetic moment values for copper complexes lie in the usual range. The magnetic moment of the cobalt complex tdpctp·CoCl₂ is 4.65 BM, indicating a high spin configuration for the trigonal bipyramidal as well as tetrahedral species present in solution (see below). The value is larger than the spin-only value (3.87) for S=3/2 and falls approximately in the middle of the μ_{eff} values observed for trigonal bipyramidal (4.26-5.03) and tetrahedral (3.98-4.82) cobalt(II) complexes [58].

4.4.2 Optical absorption spectra

The ligand tdpctp itself exhibits two bands at 235 and 267 nm. The low energy, less intense (Table 15) band at 267 nm, with vibrational fine structure, is believed to be

Table 15: Optical absorption data for tdpctp complexes

Compound	solvent	λ_{max} (ϵ_{max}) [†]	assignments
tdpctp·CuCl ₂	CH ₂ Cl ₂	931(0.21)	d-d
		359(1.24), 279sh(3.22)	Pz → Cu l.m.c.t
		259(4.59), 241(12.32)	π - π^* (intraligand)
	CH ₃ CN	961(0.27)	d-d
		460(0.18)	d-d?
		353(1.40), 285sh(3.67) 267(5.02), 224(13.78)	Pz → Cu l.m.c.t. π - π^* (intraligand)
tdpctp·CuBr ₂	CH ₂ Cl ₂	926(0.36)	d-d
		413(1.05)	Br → Cu l.m.c.t
		360(1.25), 304(2.92)	Pz → Cu l.m.c.t
		273(2.76), 240(11.85)	π - π^* (intraligand)
	CH ₃ CN	948(0.41)	d-d
		414(2.04)	Br → Cu l.m.c.t.
		365sh(1.89), 304(3.42)	Pz → Cu l.m.c.t.
		267(4.01), 223(15.14)	π - π^* (intraligand)
tdpctp·NiCl ₂	CH ₂ Cl ₂	836(0.05)	d-d
		460(0.16)	d-d
		295(1.37)	Pz → Ni l.m.c.t
		267(3.30), 235(21.67)	π - π^* (intraligand)
tdpctp·NiBr ₂	CH ₂ Cl ₂	810(0.07)	d-d
		465(0.26)	d-d
		335(1.25)	Br → Ni l.m.c.t
		274(4.28), 235(21.26)	π - π^* (intraligand)
tdpctp·CoCl ₂	CH ₂ Cl ₂	922(0.03)	d-d
		632sh(0.05), 585(0.06)	d-d
		538sh(0.06)	d-d
		265(4.50), 235(21.29)	π - π^* (intraligand)
tdpctp·Cu(ClO ₄) ₂ ·2H ₂ O	CH ₂ Cl ₂	764(0.13)	d-d
		364(1.56), 265(2.60)	Pz → Cu l.m.c.t
		236(24.00)	π - π^* (intraligand)

(continued)

Table 15: Continued ...

compound	solvent	λ_{max} (ϵ_{max})	assignment
tdpctp·Cu(ClO ₄) ₂ ·2H ₂ O	CH ₃ CN	764(0.12)	d-d
		360(1.32), 267(2.45)	Pz → Cu l.m.c.t.
		226(24.50)	π - π^* (intraligand)
tdpctp·Cu(ClO ₄) ₂ ·2py	CH ₂ Cl ₂	657(0.10), 775sh	d-d
		355(1.40), 260(2.70)	Pz → Cu l.m.c.t.
		236(22.00)	π - π^* (intraligand)
	CH ₃ CN	678(0.10), 830sh	d-d
		358(1.43), 263(2.68)	Pz → Cu l.m.c.t.
		225(21.60)	π - π^* (intraligand)
tdpctp·Cu(ClO ₄) ₂ ·2ImH	CH ₂ Cl ₂	637(0.10), 830sh	d-d
		360(1.70), 260(2.80)	Pz → Cu l.m.c.t.
		234(28.00)	π - π^* (intraligand)
	CH ₃ CN	634(0.10), 810sh	d-d
		361(1.68), 263(2.95)	Pz → Cu l.m.c.t.
		227(28.80)	π - π^* (intraligand)
tdpctp·Cu(ClO ₄) ₂ ·bipy	CH ₂ Cl ₂	688(0.08), 598(0.08)	d-d
		365(7.50)	bipy → Cu l.m.c.t.
		310sh, 260sh	Pz → Cu l.m.c.t.
		237(38.00)	π - π^* (intraligand)
	CH ₃ CN	680(0.08), 598(0.08)	d-d
		370(8.20)	bipy → Cu l.m.c.t.
		312sh, 259(3.02)	Pz → Cu l.m.c.t.
		228(38.80)	π - π^* (intraligand)
tdpctp·Cu(ClO ₄) ₂ ·phen	CH ₂ Cl ₂	685(0.06), 592(0.06)	d-d
		370(4.50)	phen → Cu l.m.c.t.
		300sh, 278sh	Pz → Cu l.m.c.t.
		236(34.00)	π - π^* (intraligand)
	CH ₃ CN	676(0.06), 580(0.06)	d-d
		372(5.45)	phen → Cu l.m.c.t.
		305sh, 280(10.22)	Pz → Cu l.m.c.t.
		226(32.40)	π - π^* (intraligand)

† sh=shoulder; units: nm (mol⁻¹ cm⁻¹)

arising from the phenyl substituents. The intensity of this band increases on complexation, sometimes the fine structure collapses, suggesting contribution from the

$Pz \rightarrow Metal$ l.m.c.t. Consistent with earlier observations another low energy band is also observed at 360 nm for the copper complexes which is assigned to $Pz \rightarrow Cu$ l.m.c.t. with confidence. The complete data are collected in Table 15, from which it is evident that the copper(II) halide complexes show very similar absorption maxima as that of analogous hdpctp complexes. While changing the solvent from dichloromethane to acetonitrile the d-d band is shifted 20-30 nm to low energy. This indicates that in acetonitrile the metal experiences weak ligand field possibly arising from the dissociation of halide ions.

The copper perchlorate complexes form an interesting class of compounds with unique trends. In the series of $tdpctp \cdot Cu(ClO_4)_2 \cdot L$, where $L = 2H_2O$, 2py, 2ImH, bipy or phen the intensity of the band at *ca.* 260 and 360 nm increases steeply as the aquo ligand is replaced by the nitrogen heterocyclic ligands. The maximum increase in intensity is noticed for the 1,10-phenanthroline adduct, indicating the additional contribution from the $N(L) \rightarrow Cu$ l.m.c.t. The complexes $tdpctp \cdot Cu(ClO_4)_2 \cdot L$ ($L = 2H_2O$, 2py, 2ImH) exhibit a rather broad absorption band with a low energy shoulder typical of tetragonal complexes [11], while the 2,2'-bipyridine and 1,10-phenanthroline adducts show two overlapping bands of comparable intensity (Figure 16). Utilizing the energy ranges covered by the d-d transitions of CuN_4-N_6 chromophores of different stereochemistries, it is reasonable to conclude that in the present case the CuN_5 chromophore containing complexes $tdpctp \cdot Cu(ClO_4)_2 \cdot L$ ($L = 2py$, 2ImH, bipy, phen) fall in the class of distorted square pyramidal, the distortion being towards a tetrahedral arrangement of equatorial ligands [59]. There is an apparent trend in the spectral properties of the compounds $tdpctp \cdot Cu(ClO_4)_2 \cdot L$ ($L = 2H_2O$, 2py, 2ImH, bipy, phen) related to the ligand field strength of the exogenous ligands. As the aquo ligands are substituted with nitrogenous bases, the absorption maximum (d-d) of the complexes shift progressively to higher energies. For instance, $tdpctp \cdot Cu(ClO_4)_2 \cdot 2H_2O$ in dichloromethane solution shows the absorption maximum centered at 764 nm while

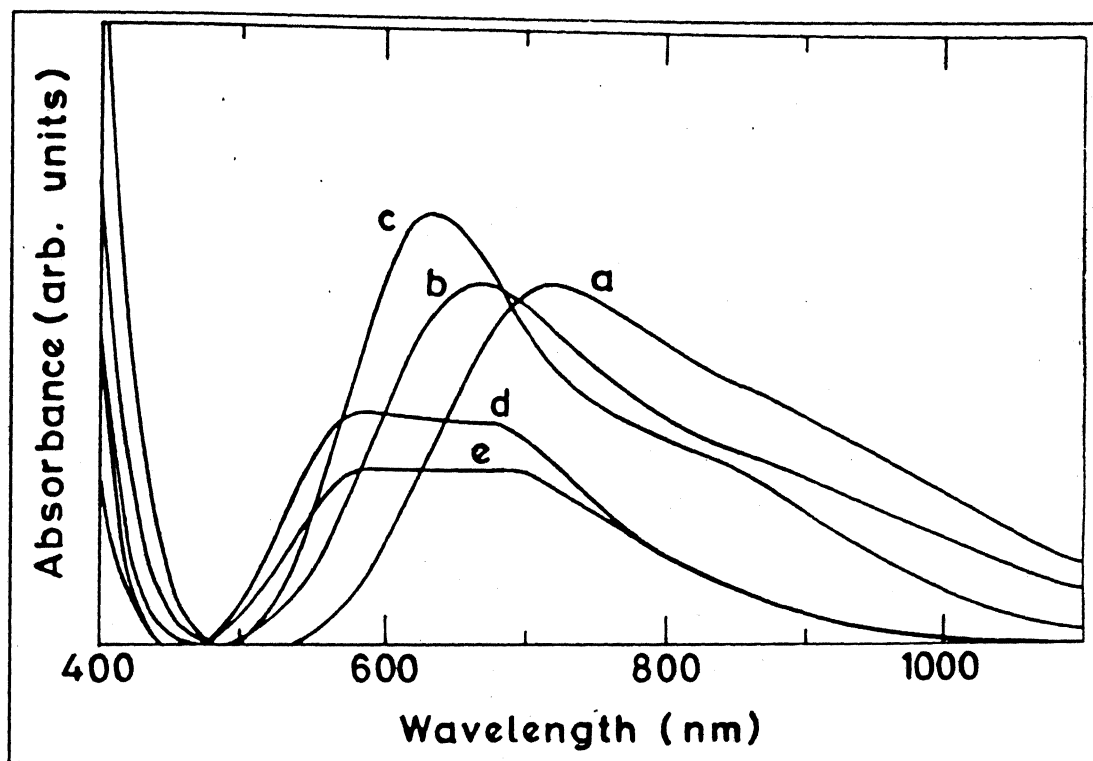


Figure 16: Ligand field spectra of the complexes $\text{tdpctp}\cdot\text{Cu}(\text{ClO}_4)_2\cdot\text{L}$ ($\text{L}=\text{2H}_2\text{O}$ (a), 2py (b), 2ImH (c), bipy (d), phen (e))

$\text{tdpctp}\cdot\text{Cu}(\text{ClO}_4)_2\cdot 2\text{ImH}$ gives a band at 637 nm with the lower energy shoulder locatable at 830 nm. The data in Table 15 suggests, therefore, that the ligand field strength of the exogenous ligands increase in the order $\text{H}_2\text{O} < \text{py} < \text{ImH} < \text{bipy} \approx \text{phen}$. Theories on the intensity of the ligand field absorption bands predict that the intensity of the d-d transition increases as the symmetry of the ligand field decreases, since the d-d transitions become allowed as electronic dipole transitions [21]. A closer inspection of Table 15 reveals that the intensities of the complexes decreases on moving from $\text{tdpctp}\cdot\text{Cu}(\text{ClO}_4)_2\cdot 2\text{H}_2\text{O}$ down to $\text{tdpctp}\cdot\text{Cu}(\text{ClO}_4)_2\cdot \text{phen}$. This is in accordance with the increased tetrahedral distortion observed by x-ray crystallographic studies on complexes $\text{tdpctp}\cdot\text{Cu}(\text{ClO}_4)_2\cdot\text{L}$ ($\text{L}=\text{2H}_2\text{O}$ and 2ImH) (*vide infra*)

The d-d spectra of the nickel and cobalt complexes are displayed in Figure 17. The nickel complexes exhibit two prominent d-d transitions in the region 400-850 nm and the band at *ca.* 460 nm shows a shoulder at the low energy side. On the basis of this

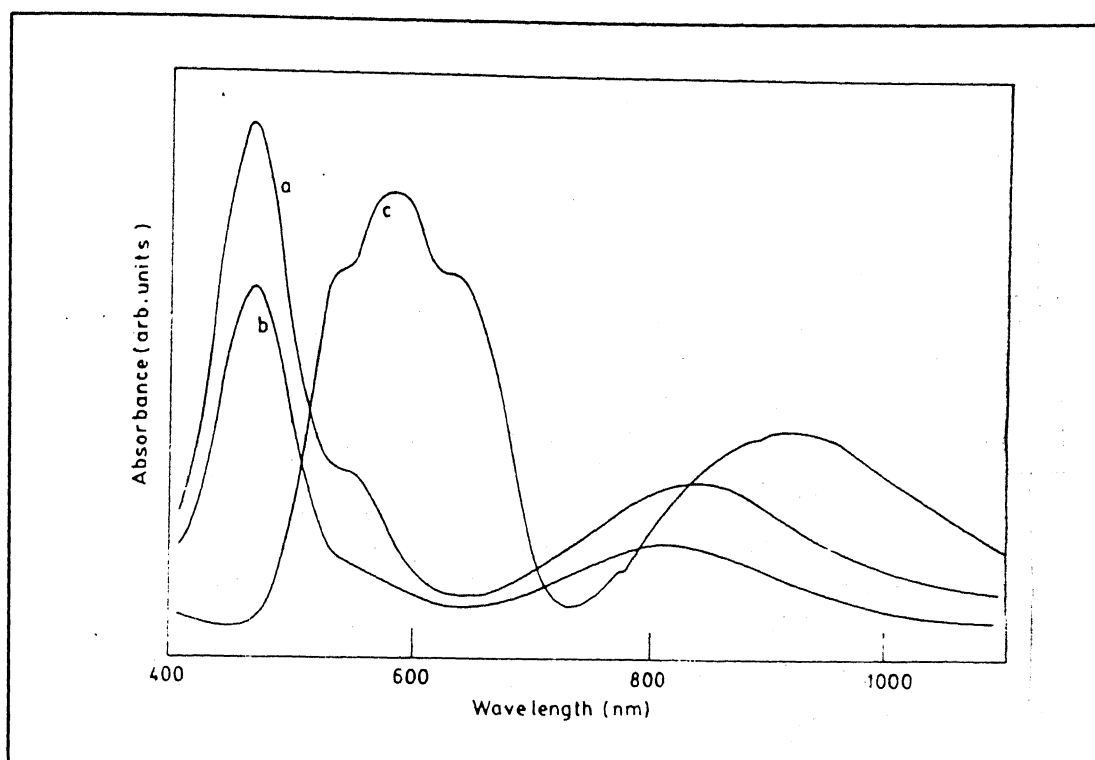
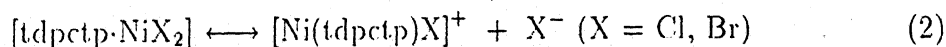


Figure 17: Electronic spectra of the complexes $\text{tdpctp} \cdot \text{MX}_2$: $\text{M}=\text{Ni}$ ($\text{X}=\text{Cl}$ (a), Br (b)) and Co ($\text{X}=\text{Cl}$ (c))

anomalous spectral pattern we propose that in solution both a diamagnetic four coordinate $[\text{Ni}(\text{tdpctp})\text{X}]^+$ ($\text{X}=\text{Cl}, \text{Br}$) and a paramagnetic five coordinate $\text{tdpctp} \cdot \text{NiX}_2$ are present. This is in agreement with the high molar conductances and low magnetic moments observed for these complexes. Since the position and intensities of the principal d-d bands are not compatible with octahedral or tetrahedral coordination for Ni(II) [60], the combined spectral, magnetic and conductance data strongly support the assignment of five coordinate structure to the paramagnetic species. Similar behavior has been reported for the complex $\text{Ni}(\text{Et}_4\text{dien})\text{Cl}_2$ [61]. The behavior of $\text{tdpctp} \cdot \text{NiX}_2$ in solution can thus be summarized by the equation:



five coordinate four coordinate

high-spin low-spin

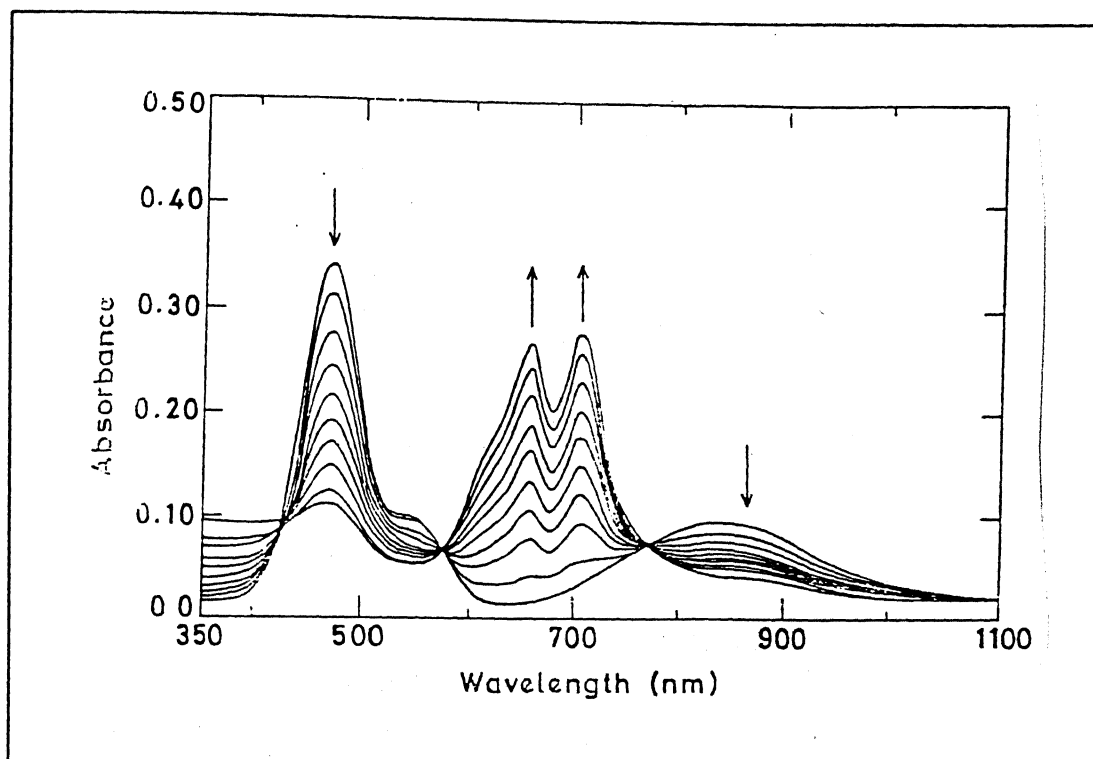


Figure 18: Absorption spectral changes on addition of Et_4NCl to tdpctp-NiCl_2 in dichloromethane solution

Consistent with Equation 1 addition of Et_4NX ($\text{X}=\text{Cl}, \text{Br}$) to dichloromethane solution of tdpctp-NiX_2 ($\text{X}=\text{Cl}, \text{Br}$) markedly decreases the intensities of the bands at *ca.* 820 and 460 nm and gives rise to new bands at *ca.* 650 and 710 nm reminiscent of five coordinate species (Figure 18).

Similarly, the electronic spectra of cobalt complex reveals that there exist an equilibrium between the five coordinate trigonal bipyramidal and four coordinate tetrahedral structures. Addition of Et_4NCl does not affect the spectra; however, addition of PPh_3 appreciably changes the band positions and intensities suggesting that the tetrahedral species may contain a neutral N_2Cl_2 donor environment rather than an ionic structure $[\text{CoN}_3\text{Cl}]^+$ in contrast to the nickel derivatives. This is also consistent with the observed low conductance value and the imaginable steric crowding at the metal centre with N_3Cl_2 donor set (five coordinate to six coordinate interchange in the presence of triphenyl phosphine is highly improbable).

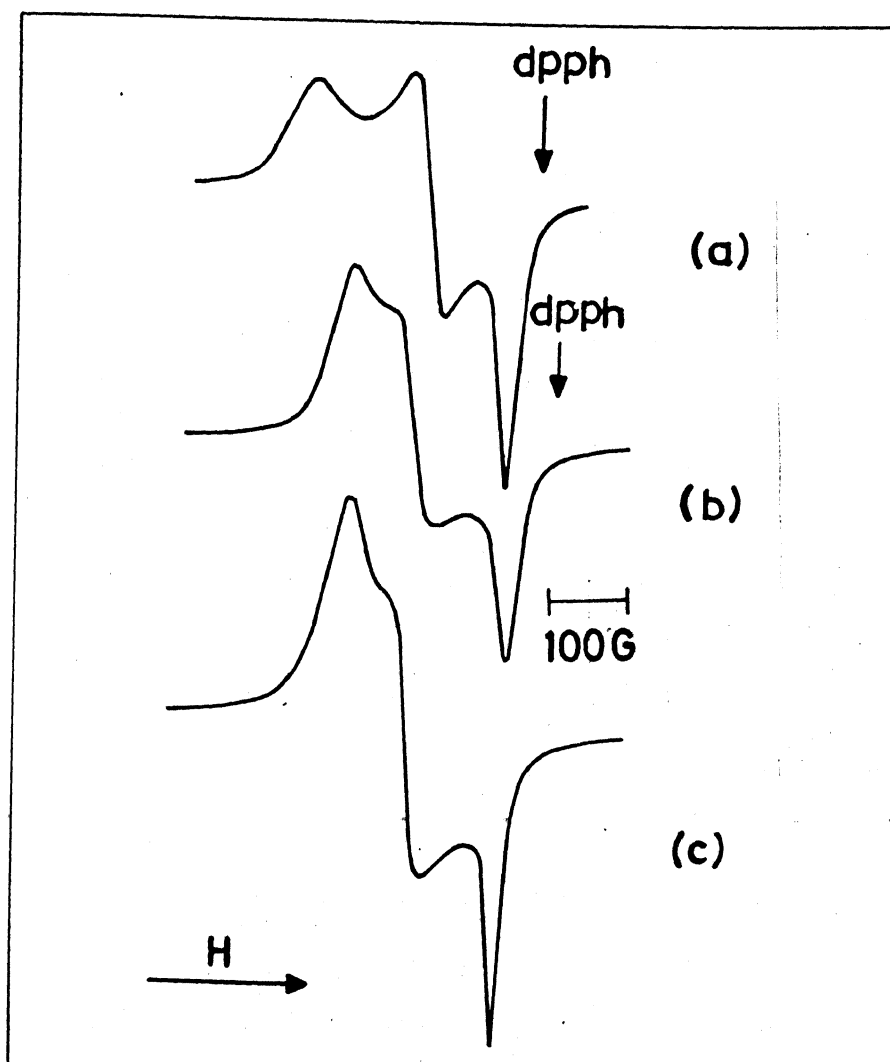


Figure 19: Polycrystalline EPR spectra of tdpctp-CuX_2 : $\text{X}=\text{Cl}$ (a) and $\text{X}=\text{Br}$ [experimental (b) and simulated (c)]

4.4.4 EPR spectroscopy

A detailed investigation on the EPR spectral properties of the copper complexes of tdpctp has been carried out. The EPR spectra of the copper(II) halide complexes tdpctp-CuX_2 ($\text{X}=\text{Cl}, \text{Br}$) exhibit a rhombic pattern in the solid state. The relevant parameters derived from the computer simulation of the spectra are given in Table 16, along with those of related complexes. The theoretical and experimental spectra are displayed in Figure 19. From these it is evident that the geometry is considerably distorted from the regular trigonal bipyramid. The large anisotropy of the two lower

Table 16: EPR parameters of the copper halide complexes of tdpctp and related ligands*

compound	g_1	g_2	g_3	g_{av}^\dagger	ref
tdpctp·CuCl ₂	2.018	2.124	2.290	2.147	This work
tdpctp·CuBr ₂	2.007	2.146	2.238	2.132	This work
terpy·CuCl ₂	2.070	2.135	2.188	2.132	24
terpy·CuBr ₂	2.032	2.126	2.239	2.134	25
terpy·CuI ₂	2.066	2.110	2.206	2.128	24
CuCl ₂ (dmIm) ₃	2.060	2.160	2.210	2.144	23

* for polycrystalline powder samples at room temperature

$$^\dagger g_{av} = [\frac{1}{3}(g_1^2 + g_2^2 + g_3^2)]^{1/2}$$

g -values (g_1 and g_2) for tdpctp·CuBr₂ compared to tdpctp·CuCl₂ would indicate a geometry rather intermediate between a square pyramid and a trigonal bipyramidal for the CuN₃Br₂ polyhedron. Similar conclusions have earlier been derived for terpy·CuBr₂ on the basis of EPR parameters [25]. However, in tdpctp·CuCl₂ the copper exists in a distorted trigonal bipyramidal geometry as identified by single crystal x-ray crystallography (*vide infra*).

The x-band EPR spectra of the powdered and solution samples of copper perchlorate complexes tdpctp·Cu(ClO₄)₂·EL (EL=2H₂O, 2py, 2ImH, bipy, phen) have been examined both at room temperature and liquid nitrogen temperatures. The spin hamiltonian parameters of them are compiled in Table 17. Representative EPR spectra are displayed in Figures 20 and 21. In general, the EPR spectra reveal the presence of a distorted tetragonal copper environment in the complexes with a $d_{x^2-y^2}$ ground state [11]. They are characterized by $g_{||} > g_{\perp}$ and $A_{||} > 120 \times 10^{-4} \text{ cm}^{-1}$. An examination of the $g_{||}$ and $A_{||}$ values for the complex tdpctp·Cu(ClO₄)₂·2H₂O indicates that it possesses the highest value of $g_{||}$ and lowest $A_{||}$ value in the series. This

Table 17: EPR spin hamiltonian parameters for tdpctp·Cu(ClO₄)₂·EL ^a

EL		g_{\parallel}	g_{\perp}	A_{\parallel}	g_{iso}	A_{iso}	g_{av} ^b	G-value	$g_{\parallel}/A_{\parallel}$ cm ⁻¹
2H ₂ O	c	2.358	2.078	131	2.171	—	2.175	4.711	181
	d	2.354	2.073	135	2.166	—	2.171	5.000	174
	e	2.305	2.069	149	2.166	56	2.151	4.512	154
	f	2.365	2.072	121	2.127	56	2.174	5.213	195
2py	c	2.267	2.078	145	2.141	—	2.143	3.482	157
	d	2.277	2.072	145	2.140	—	2.142	3.940	158
	e	2.269	2.066	154	2.153	62	2.135	4.217	147
	f	2.254	2.069	159	2.153	56	2.132	3.783	142
2ImH	c	2.260	2.053	159	2.122	—	2.124	5.070	143
	d	2.256	2.045	163	2.116	—	2.118	5.898	138
	e	2.265	2.062	145	2.151	65	2.132	4.376	157
	f	2.265	2.066	145	2.152	61	2.134	4.156	157
bipy	c	2.252	2.060	168	2.124	—	2.126	4.319	134
	d	2.245	2.055	168	2.119	—	2.121	4.579	134
	e	2.234	2.050	168	2.140	79	2.113	4.904	133
	f	2.237	2.042	170	2.139	79	2.109	5.887	132
phen	c	2.256	2.056	163	2.123	—	2.125	4.705	138
	d	2.245	2.055	168	2.116	—	2.118	4.916	134
	e	2.242	2.043	168	2.141	76	2.111	5.907	134
	f	2.238	2.049	168	2.139	75	2.114	5.035	133

^a A values have $\times 10^{-4}$ cm⁻¹ units

^b from $[1/2(g_{\parallel}^2 + g_{\perp}^2)]^{1/2}$

^c polycrystalline powder at room temperature

^d polycrystalline powder at liquid nitrogen temperature

^e dichloromethane solution at room and liquid nitrogen temperatures

^f acetonitrile solution at room and liquid nitrogen temperatures

is consistent with the binding of three nitrogen atoms and borders on Peisach and Blumberg [28] plots of A_{\parallel} versus g_{\parallel} for two nitrogens and two oxygens in the equatorial plane. This is in accordance with the x-ray results. No superhyperfine splittings from

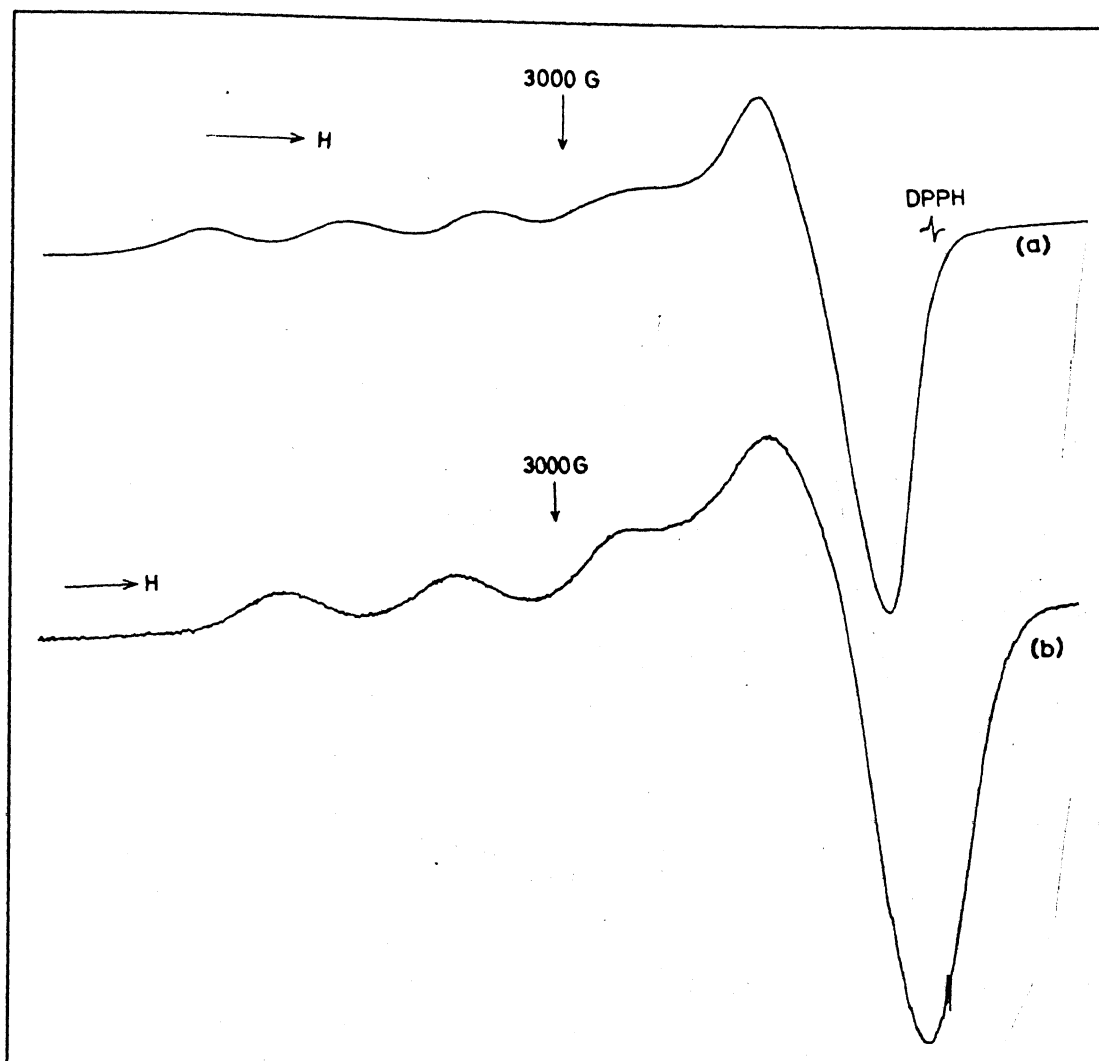


Figure 20: EPR spectra of the polycrystalline powder samples of $\text{tdpctp} \cdot \text{Cu}(\text{ClO}_4)_2 \cdot 2\text{L}$ ($\text{L} = \text{H}_2\text{O}$ (a) and ImH (b) at room temperature

the ligand are observed (Figure 20).

The EPR spectra of the ternary complexes with the nitrogenous bases show less than four parallel lines and a broadening of the g_{\perp} region (Figure 21). Such a broadening of the g_{\perp} component is interpreted as indicative of lowered symmetry [11]. The increase in the A_{\parallel} value points out that the exogeneous ligands enter the equatorial positions by displacing the water molecules. The room temperature solution EPR spectra of the complexes are isotropic with clearly visible hyperfine splitting due to copper ($I=3/2$, 4 lines). In addition, the bipyridine and phenanthroline adducts dis-

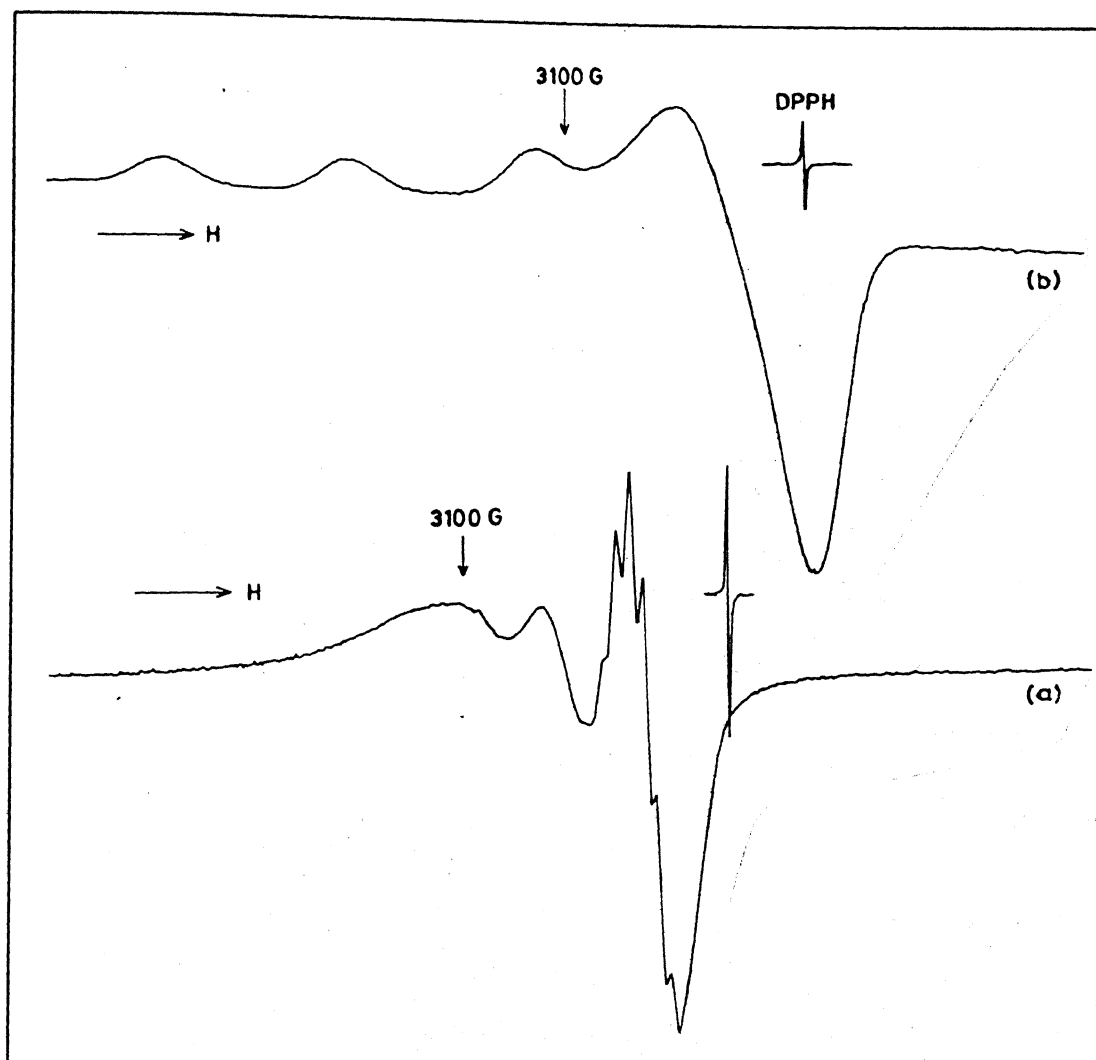


Figure 21: EPR spectra of $\text{tdpctp} \cdot \text{Cu}(\text{ClO}_4)_2 \cdot \text{phen}$ in fluid (a) and frozen (b) dichloromethane solution

play superhyperfine splitting due to five nitrogens ($I=1$, 11 lines) (Figure 21(a)). In liquid nitrogen temperature all mixed ligand complexes show axial pattern (see Figure 21(b) for example), with the g_{\parallel} and A_{\parallel} values characteristic of a square pyramidal geometry around copper.

The g_{av} values of the complexes lie with the exception of $\text{tdpctp} \cdot \text{Cu}(\text{ClO}_4)_2 \cdot 2\text{H}_2\text{O}$ in the range 2.109-2.143. Similar g -factors were found for square pyramidal N -salicylidene-glycinato or N -pyruvidene-glycinato copper(II) complexes with an additional ligand with N donors [27, 20]. The g_{av} value of compound $\text{tdpctp} \cdot \text{Cu}(\text{ClO}_4)_2 \cdot$

$2\text{H}_2\text{O}$ is typical of elongated tetragonal complexes with tetrahedral distortion [29]. The G-values for the present complexes are found to be greater than 4 (4.156-5.907) with the exception of $\text{tdpctp}\cdot\text{Cu}(\text{ClO}_4)_2\cdot 2\text{H}_2\text{O}$. High G-values indicate that the complexes are ionic in nature [11]. The smaller value for aquo adduct suggests that the presence of coupling of Cu ions in coordination polyhedra. The quotient $g_{\parallel}/A_{\parallel}$ has been considered as a convenient empirical index of tetrahedral distortion [30]. This quotient for the copper perchlorate complexes ranges from 132–188 cm. It has been pointed out earlier that for square planar structures this occurs in the range from *ca.* 105 to 135 cm. This value increases markedly on the introduction of a tetrahedral distortion to the chromophore. Thus, the severely distorted complexes $\text{Cu}[\text{GaMe}_2(\text{Me}_2\text{Pz})_2]_2$ [62] and bis(N-t-butyl pyrrole-2-carbaldiminato) copper(II) [63] have values of 244 and 210 cm respectively. The present complexes show values in the intermediate range, among them the aquo complex having a higher quotient suggestive of a comparatively larger tetrahedral distortion.

A few points deserve attention: (i) while the effective charge on the equatorial plane remains constant, exchanging a less electron rich O-atom ligand (water) to a more electron rich nitrogen atom tends to lower g_{\parallel} and increase A_{\parallel} as we move in the series $\text{tdpctp}\cdot\text{Cu}(\text{ClO}_4)_2\cdot\text{L}$ ($\text{L}=2\text{H}_2\text{O}$, 2py, 2ImH, bipy, phen). (ii) From aquo complex to nitrogenous base adducts both the increased covalency and relief in tetrahedral distortion manifests in the increased A_{\parallel} and lowered g_{\parallel} values. (iii) Finally g_{av} values suggest a weaker axial interaction for these complexes as is confirmed by the x-ray crystal structure determination of the complexes $\text{tdpctp}\cdot\text{Cu}(\text{ClO}_4)_2\cdot 2\text{H}_2\text{O}$ and $\text{tdpctp}\cdot\text{Cu}(\text{ClO}_4)_2\cdot 2\text{ImH}$, where the axial positions are being loosely bound by the cyclophosphazene ring nitrogen and a perchlorate anion.

In order to obtain a qualitative picture of the bonding nature in the complexes we have calculated the LCAO-MO coefficients for the b1g and b2g orbitals, i.e., β_1^2 and β_2^2 which express the extent of in-plane and out-of-plane π -bonding respectively and

Table 18: Computed LCAO-MO coefficients, covalency parameters and orbital reduction parameters of the complexes $\text{tdpctp-Cu}(\text{ClO}_4)_2 \cdot \text{EL}$

EL	medium	α^2	α_1^2	β_1^2	β^2	Fermi-K	k_{\parallel}	k_{\perp}
2H ₂ O	solid(r.t)	0.791	0.292	0.889	0.756	0.325	0.703	0.598
	solid(LNT)	0.798	0.284	0.871	0.700	0.320	0.695	0.559
	CH ₂ Cl ₂	0.786	0.297	0.761	0.671	0.301	0.598	0.527
	CH ₃ CN	0.769	0.316	0.991	0.762	0.323	0.763	0.586
2py	solid(r.t)	0.746	0.341	0.846	0.858	0.309	0.631	0.641
	solid(LNT)	0.739	0.349	0.823	0.912	0.310	0.608	0.696
	CH ₂ Cl ₂	0.762	0.324	0.805	0.769	0.302	0.613	0.585
	CH ₃ CN	0.732	0.357	0.855	0.829	0.298	0.626	0.607
2ImH	solid(r.t)	0.760	0.326	0.801	0.632	0.301	0.611	0.481
	solid(LNT)	0.765	0.320	0.785	0.529	0.294	0.601	0.405
	CH ₂ Cl ₂	0.730	0.359	0.853	0.775	0.309	0.623	0.566
	CH ₃ CN	0.761	0.325	0.737	0.781	0.284	0.560	0.594
bipy	solid(r.t)	0.781	0.303	0.807	0.746	0.342	0.630	0.583
	solid(LNT)	0.759	0.328	0.771	0.635	0.329	0.585	0.482
	CH ₂ Cl ₂	0.772	0.313	0.794	0.690	0.336	0.613	0.532
	CH ₃ CN	0.763	0.322	0.788	0.533	0.325	0.602	0.407
phen	solid(r.t)	0.770	0.315	0.829	0.702	0.330	0.638	0.540
	solid(LNT)	0.770	0.314	0.793	0.649	0.324	0.611	0.500
	CH ₂ Cl ₂	0.764	0.322	0.790	0.536	0.317	0.603	0.410
	CH ₃ CN	0.762	0.324	0.789	0.625	0.317	0.601	0.476

also the ligand coefficient α_{Cu}^2 in the b1g MO. They are given in Table 18. The in-plane σ -covalency parameter α_{Cu}^2 was calculated using a simplified expression [64]:

$$\alpha_{\text{Cu}}^2 = \frac{-A_{\parallel}}{P} + (g_{\parallel} - g_e) + \frac{3}{7}(g_{\perp} - g_e) + 0.04 \quad (3)$$

The α_{Cu}^2 values depend on the nature of copper-ligand bond, decreasing with increasing covalency (particularly in-plane σ -bonding) to a minimum theoretical value of 0.50. The observed values (0.730-0.798) account for the fraction of the unpaired electron density located on the copper. The unpaired electron is more localized towards

ligands in the complexes which possess extra nitrogenous base ligands.

The in-plane and out-of-plane metal π -bonding coefficients β_1^2 and β^2 respectively are obtained from the following approximate equations [65]:

$$g_{\parallel} \simeq g_e + \frac{2\alpha^2\beta_1^2\lambda_0}{E_{xy}}; \quad g_{\perp} \simeq g_e + \frac{8\alpha^2\beta^2\lambda_0}{E_{xyz}} \quad (4)$$

The uncertainty involved in the assignment of E_{xyz} transition precludes a reliable estimate of the out-of-plane π -bonding parameter β^2 . However, it is argued that the 20% error in E_{xyz} results in only a ~5% error in β^2 values. The complexes studied show $\beta_1^2 = 0.737-0.991$ indicating a covalent in-plane π -bonding. Again weaker in-plane π -bonding is proposed for the aquo complex on the basis of larger β_1^2 values. This is also supported by the comparatively larger orbital reduction factors for this complex.

4.4.5 Electrochemistry

Electrochemical behavior of the copper perchlorate complexes have been examined by cyclic voltammetric and differential pulse voltammetric studies in dichloromethane and acetonitrile solutions. The data are given in Table 19.

The aquo complex $\text{tdpctp} \cdot \text{Cu}(\text{ClO}_4)_2 \cdot 2\text{H}_2\text{O}$ shows a quasi-reversible $\text{Cu(II)}-\text{Cu(I)}$ redox couple at ca. +0.6 V (Figure 22) both in dichloromethane and acetonitrile solutions corroborating the increased tetrahedral distortion suggested by the EPR parameters as well as x-ray diffraction studies. Similarly the quasireversibility of the bipyridine and phenanthroline adducts in dichloromethane solutions indicates that there is no appreciable structural change involved prior to reduction of copper(II) complexes. However, in acetonitrile solution an irreversible $\text{Cu(II)}-\text{Cu(I)}$ redox change is observed for all the nitrogen base adducts. After the one electron reduction these complexes in acetonitrile solution probably undergo rapid decomposition. Invariably all the complexes show an irreversible one electron reduction at ca. -0.6 to -1.2 V attributable to the $\text{Cu(I)}-\text{Cu(0)}$ change. On reversing the scan all complexes exhibit a strong stripping peak characteristic of the reoxidation of the *naked* metal. The

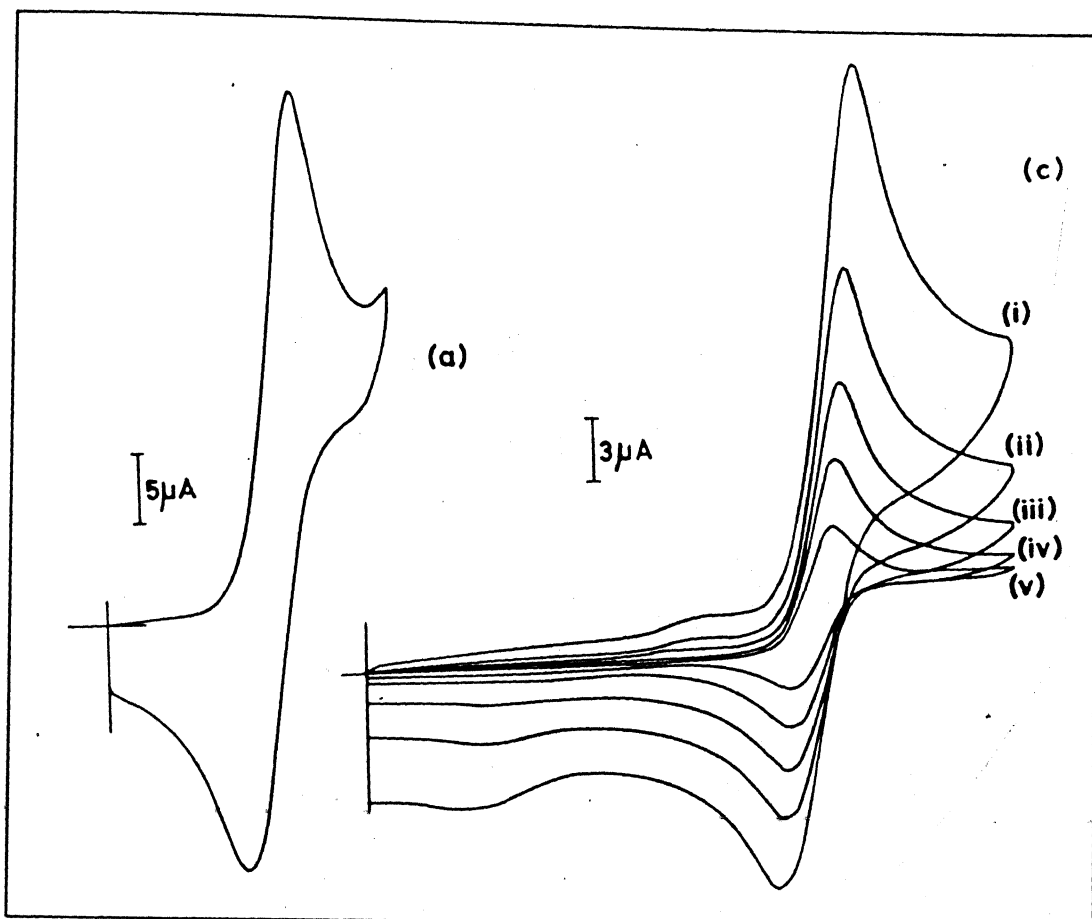
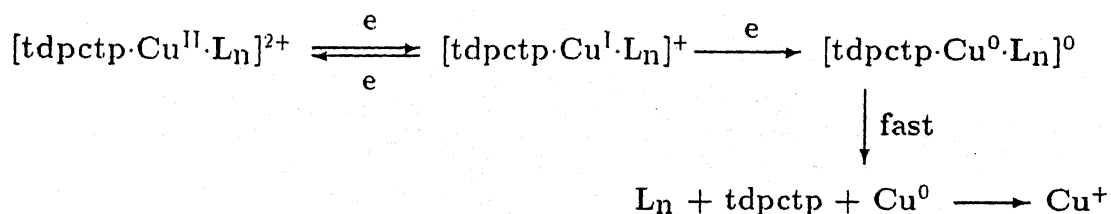


Figure 22: Cyclic voltammograms of tdpctp·Cu(ClO₄)₂·EL (EL=2H₂O [scan rate: 50 mV s⁻¹ (a) and phen (b) [scan rate: (i) 500 mV s⁻¹ (ii) 200 mV s⁻¹ (iii) 100 mV s⁻¹ (iv) 50 mV s⁻¹ (v) 20 mV s⁻¹] in dichloromethane solution

redox behavior of the complexes tdpctp·Cu(ClO₄)₂·L (L=2H₂O, bipy and phen) in dichloromethane solution may be so schematized as:



In acetonitrile solution a different mechanism may be operating with the likely expulsion of the extra ligands from the coordination sphere in an attempt to achieve a more comfortable tetrahedral geometrical arrangement to stabilize the Cu(I) species gener-

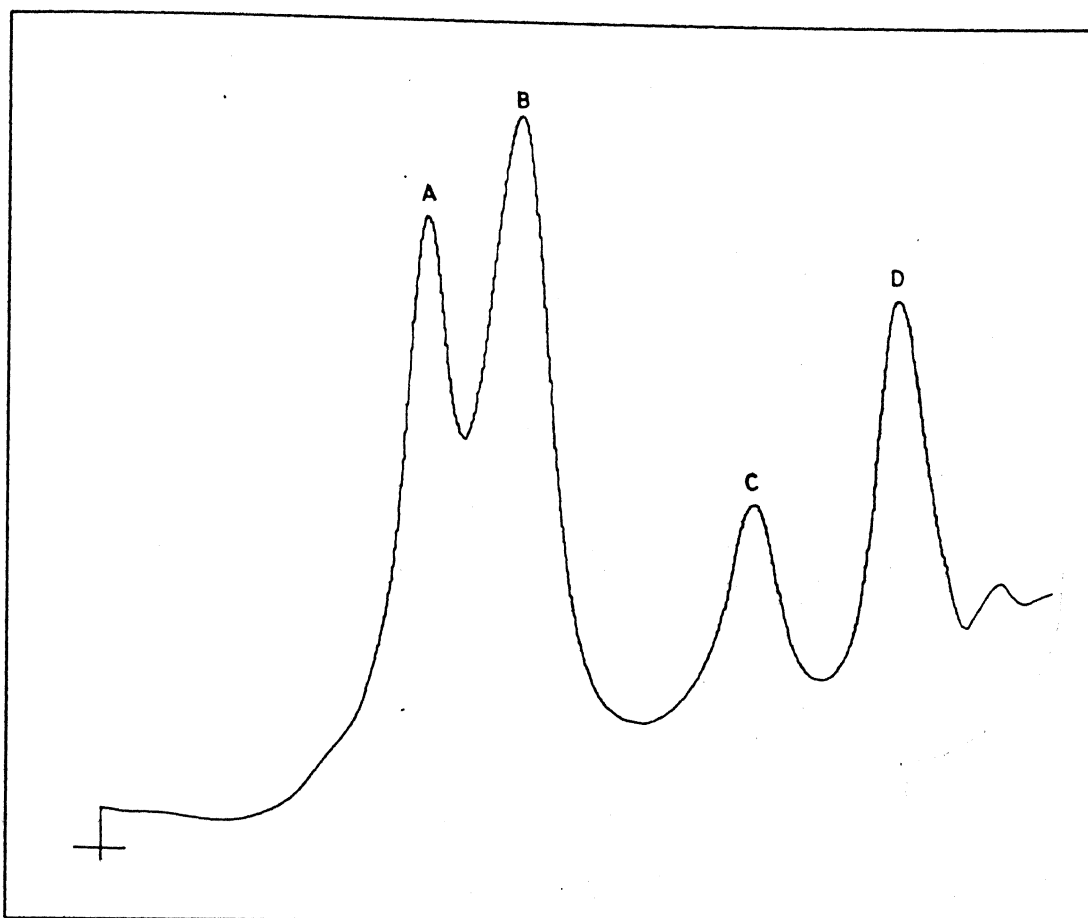
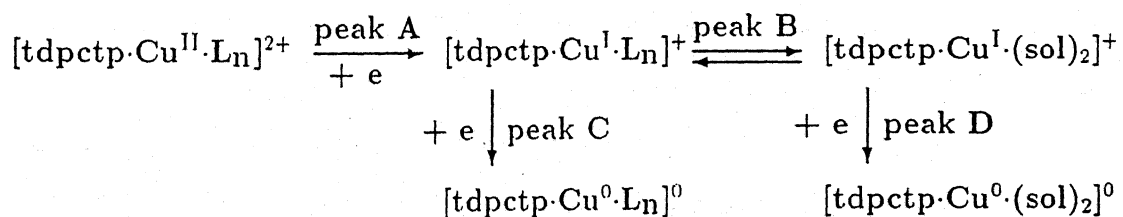


Figure 23: Differential pulse voltammogram of tdpctp·Cu(ClO₄)₂·phen in acetonitrile (scan rate: 10 mV s⁻¹)

ated. The coordinating ability of the acetonitrile may be the driving force for this kind of mechanism. The differential pulse voltammogram of complex tdpctp·Cu(ClO₄)₂·phen in acetonitrile solution is presented in Figure 23 which is compatible with the following mechanism:



It is probable that in dichloromethane the preferred geometry for the copper(I) in-

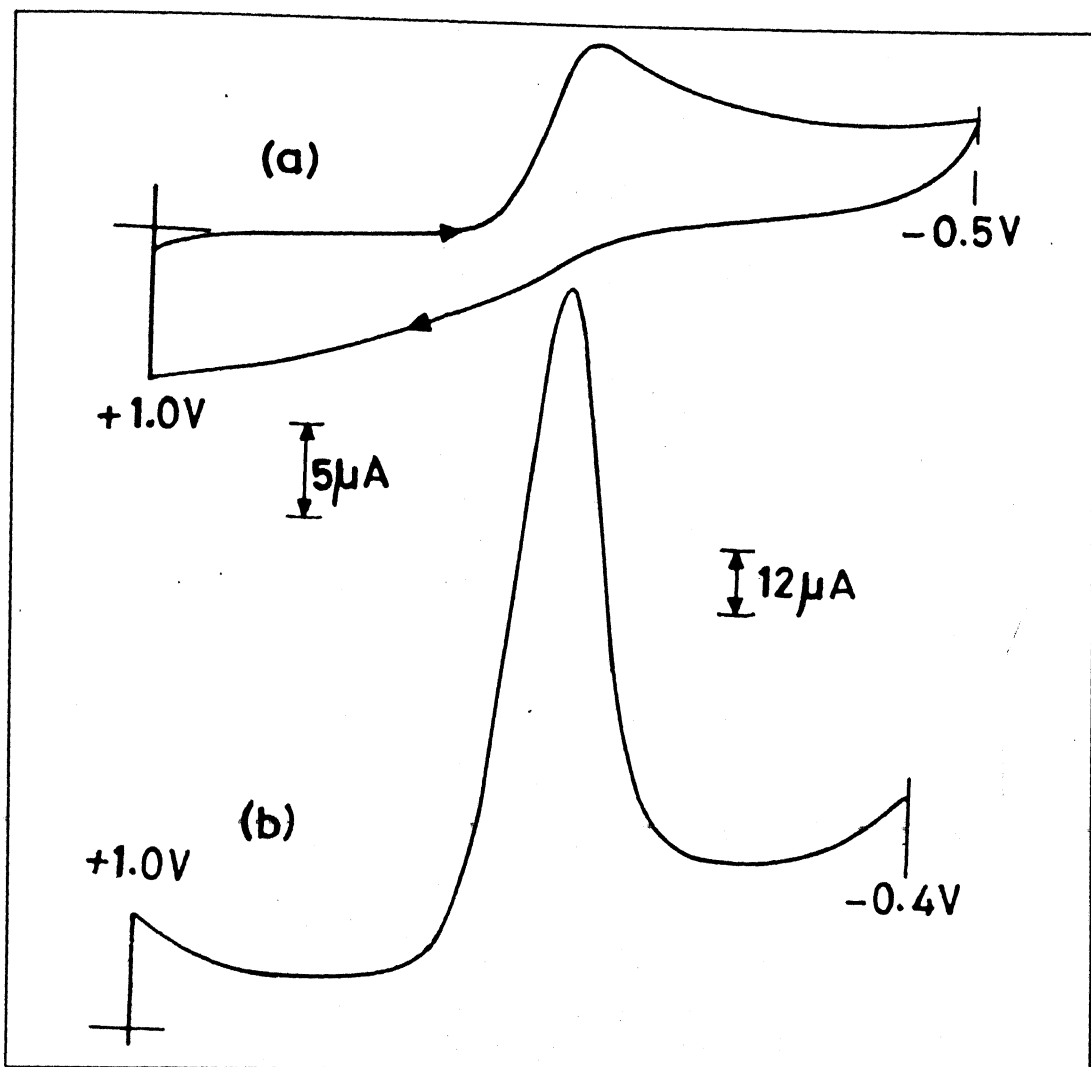


Figure 24: The cyclic (a) and differential pulse (b) voltammograms of $\text{tdpctp} \cdot \text{Cu}(\text{ClO}_4)_2 \cdot 2\text{ImH}$ in dichloromethane at scan rates 100 mV s^{-1} and 10 mV s^{-1} respectively

intermediates may be a five-coordinate distorted trigonal bipyramid. However, this conclusion awaits the structural characterization of at least one copper(I) complex. Our attempts to isolate stable copper(I) complexes using this ligand have not been successful so far.

It can be concluded that (i) the imidazole and pyridine adducts are not redox flexible owing to the observation of irreversible $\text{Cu(II)}\text{-Cu(I)}$ reduction both in dichloromethane and acetonitrile solutions (Figure 24). (ii) The high positive

Table 19: Electrochemical data for the copper perchlorate adducts

compound	solvent	Cu(II)–Cu(I) ^a		
		$E_{1/2}$ (V)	ΔE_p	$E(\text{Cu(I)}-\text{Cu(0)})$
tdpctp·Cu(ClO ₄) ₂ ·2H ₂ O	CH ₂ Cl ₂	+0.575	130	-1.24
	CH ₃ CN	+0.660	120	-0.45
tdpctp·Cu(ClO ₄) ₂ ·2py	CH ₂ Cl ₂	+0.350 ^b	c	-0.82
	CH ₃ CN	+0.450 ^b	c	-0.58
tdpctp·Cu(ClO ₄) ₂ ·2ImH	CH ₂ Cl ₂	-0.050 ^b	c	-0.50
	CH ₃ CN	+0.210 ^b	c	-0.65
tdpctp·Cu(ClO ₄) ₂ ·bipy	CH ₂ Cl ₂	+0.225	130	-0.75
	CH ₃ CN	+0.140 ^b	c	-0.55
tdpctp·Cu(ClO ₄) ₂ ·phen	CH ₂ Cl ₂	+0.215	90	-0.68
	CH ₃ CN	+0.225 ^b	c	-0.63
		-0.050 ^b	c	-1.02

^a data for 100 mV s⁻¹ scan rate

^b from differential pulse voltammograms (10 mV s⁻¹)

^c irreversible process

redox potential observed for the Cu(II)/Cu(I) redox change for the aquo complex tdpctp·Cu(ClO₄)₂·2H₂O compared with the bipyridine and phenanthroline adducts tdpctp·Cu(ClO₄)₂·L (L= bipy, phen) may be arising from the increased tetrahedral distortion in the former which would stabilize the Cu(I) congener and to the electronic effects prevalent because of the replacement of two less electron aquo ligands by electron rich bipyridine or phenanthroline ligands which hampers the addition of electrons to the metal. (iii) The conventional analysis of the Cu(II)-Cu(I) peak systems of complexes tdpctp·Cu(ClO₄)₂·L (L=2H₂O, bipy, phen) exhibited in dichloromethane solutions with scan rates varying from 0.02 V s⁻¹ to 1.0 V s⁻¹ shows that the peak-

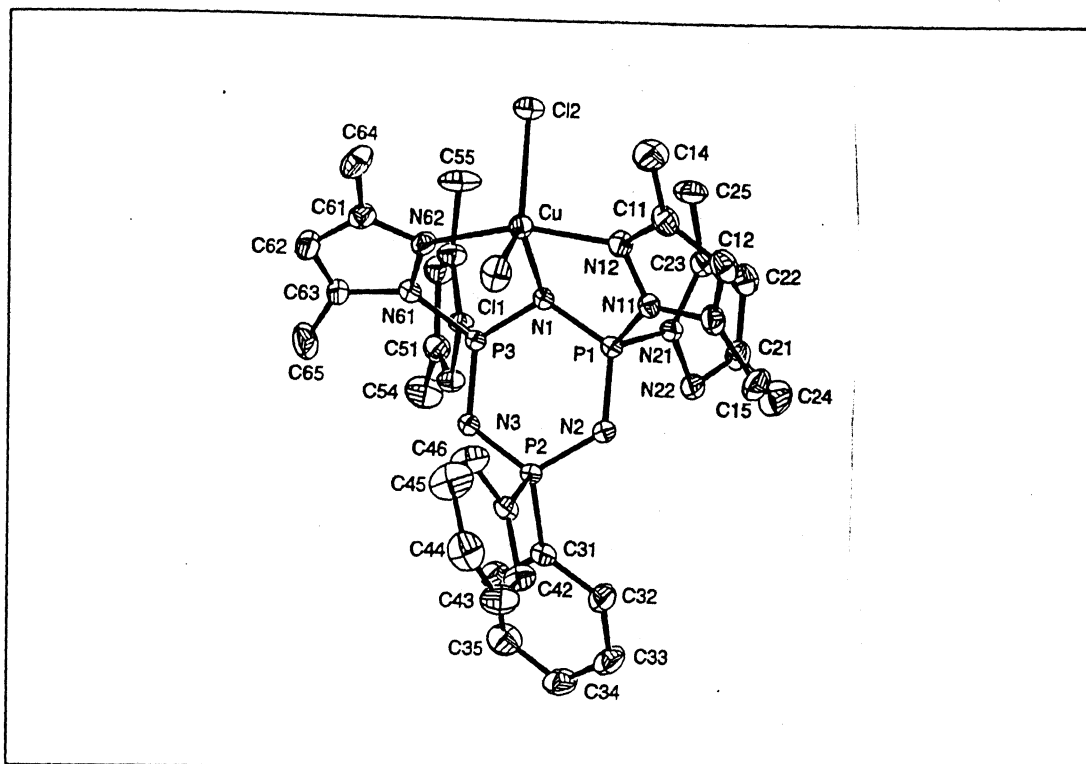


Figure 25: ORTEP plot of $\text{tdpctp} \cdot \text{CuCl}_2$

to-peak separation increases progressively from *ca.* 0.08 V to 0.28 V. This maximum departure from the constant value of 0.059 V expected for an electrochemically reversible one electron transfer denotes that a considerable geometrical reorganization accompanies the $\text{Cu(II)}\text{-Cu(I)}$ redox change [56].

4.4.6 Description of crystal structures

The single crystal structures of four complexes have been determined. The structural details are discussed below.

$\text{tdpctp} \cdot \text{CuCl}_2 \cdot \text{CH}_2\text{Cl}_2$

The ORTEP plot for the complex is displayed in Figure 25 along with the numbering scheme. Crystal data are summarized in Table 20 and the selected interatomic bond distances and angles are listed in Table 21.

In the complex the copper atom is five-coordinate and exists in a distorted tri-

Table 20: Crystal data for tdpctp·CuCl₂·CH₂Cl₂ and tdpctp·NiCl₂

compound	tdpctp·CuCl ₂ ·CH ₂ Cl ₂	tdpctp·NiCl ₂
formula	C ₃₃ H ₄₀ N ₁₁ P ₃ Cl ₄ Cu	tdpctp·NiCl ₂
fw	889.03	799.3
crystal size, mm	0.36 × 0.16 × 0.55	0.13 × 0.24 × 0.55
crystal color	green	maroon
a, Å	19.784(4)	38.190(8)
b, Å	11.666(4)	9.225(3)
c, Å	18.061(6)	21.830(4)
α, deg	91.52(3)	—
β, deg	97.24(3)	108.29(2)
γ, deg	98.26(3)	—
V, Å ³	2021.7(13)	7302 (3)
d(calcd), gcm ⁻³	1.46	1.454
space group	P-1	C2/c
Z	2	8
F(000)	913.80	3312
linear abs. coeff., mm ⁻¹	0.96	10.20
scan technique	θ-2θ	ω:2θ
2θ range, deg	4-50	1.5-27.9
refls measured	7561	9391
unique reflections	7107	8846
data used	3850 (I>6σ(I))	4414 (I>2.5σ(I))
R(F ²), R _w (F ²)	0.065, 0.080	0.045, 0.043
Final diff map, eÅ ⁻³	-0.80(3), +1.5(3)	0.34

gonal bipyramidal geometry, with a N₃Cl₂ donor set of two chloride ions and a cyclotriphosphazene skeletal nitrogen defining the equatorial plane and two nongeminal pyrazolyl groups in the axial positions (Figure 25). The Cu, Cl(1), Cl(2) and N(1) atoms have very small deviations of -0.003(10), 0.001(3), 0.0005(23) and 0.003(5) Å respectively from the least-squares plane through these atoms. This plane make an angle of 87.72(7) with the cyclotriphosphazene P₃N₃ ring plane. The Cu-N_{CTP} bond distance is longer (2.320(5) Å) and the average Cu-N_{Pz} bond length is normal (1.979(5) Å). The inequivalence in the Cu-N bond distances is consistent with that observed for hdpctp·CuCl₂. The mean Cu-Cl bond distance is 2.2731(20) Å. The main axis of

Table 21: Selected bond distances (a) and bond angles (b) in $\text{tdpctp}\cdot\text{CuCl}_2\cdot\text{CH}_2\text{Cl}_2$

(a)			
Cu-Cl(1)	2.2639(21)	P(1)-N(1)	1.601(5)
Cu-Cl(2)	2.2822(14)	P(1)-N(2)	1.561(5)
Cu-N(1)	2.320(5)	P(2)-N(2)	1.614(5)
Cu-N(12)	1.984(5)	P(2)-N(3)	1.610(5)
Cu-N(62)	1.974(5)	P(3)-N(1)	1.600(5)
mean distances		P(3)-N(3)	1.552(5)
P-N _{exo}	1.692(5)		
P-C _{exo}	1.791(6)		
(b)			
Cl(1)-Cu-Cl(2)	132.21(8)	N(1)-P(1)-N(2)	119.1(3)
Cl(1)-Cu-N(1)	123.54(14)	N(2)-P(2)-N(3)	114.9(3)
Cl(1)-Cu-N(12)	90.59(17)	N(1)-P(3)-N(3)	118.4(3)
Cl(1)-Cu-N(62)	92.19(17)	P(1)-N(1)-P(3)	117.6(3)
Cl(2)-Cu-N(1)	101.26(13)	P(1)-N(2)-P(2)	122.1(3)
Cl(2)-Cu-N(12)	97.59(17)	P(2)-N(3)-P(3)	123.1(3)
Cl(2)-Cu-N(62)	95.62(16)	N(11)-P(1)-N(21)	100.4(3)
N(1)-Cu-N(12)	80.86(19)	N(51)-P(3)-N(61)	100.2(3)
N(1)-Cu-N(62)	80.60(19)	C(31)-P(2)-C(41)	106.0(3)
N(12)-Cu-N(62)	159.39(20)		

the trigonal bipyramid constituted by N(12), Cu and N(62) is much deviated (159.39 (20) °) from the required angle 180 ° for a regular trigonal bipyramid. The Cl(1)-Cu-Cl(2) angle is increased to 132.21(8) ° which is reflected on the constriction of the bond angle Cl(2)-Cu-N(1) (101.26(13) °). These deviations result in a intermediate geometry between the square pyramid and trigonal bipyramid and accounts for the rhombic EPR spectral pattern observed for the powder sample.

The effect imparted on the cyclotriphosphazene skeletal bonding parameters due

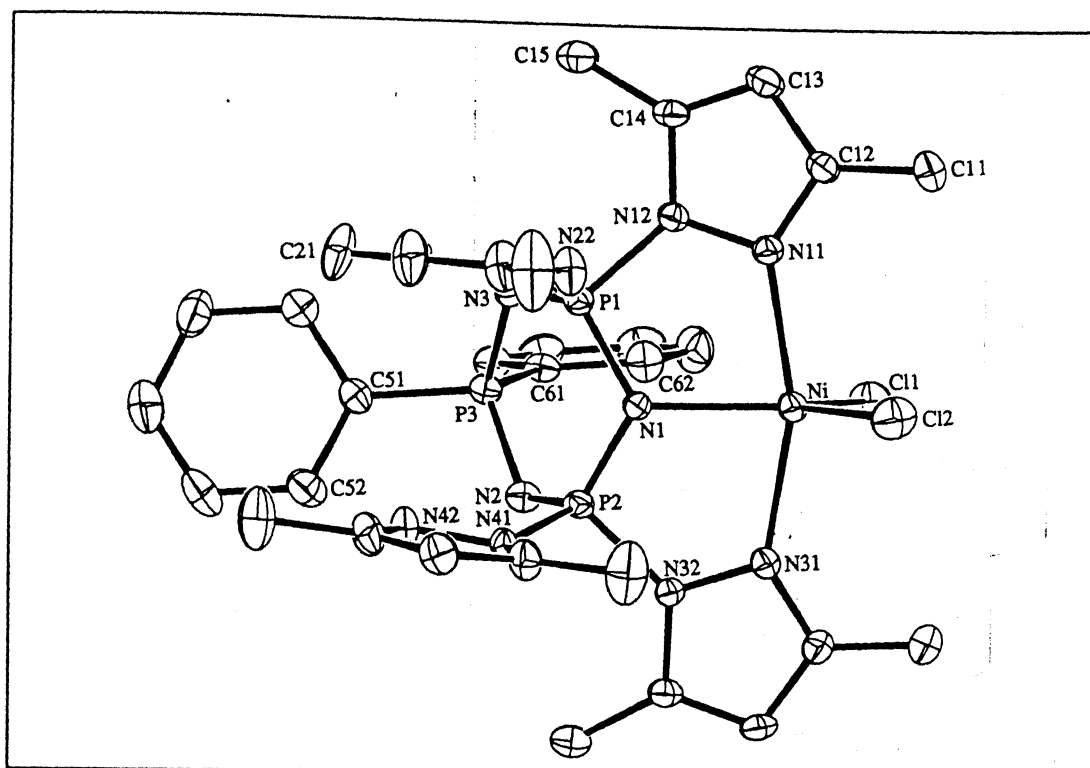


Figure 26: Perspective view of tdpctp-NiCl₂

to the ring nitrogen participation in coordination is very similar to the complexes previously described. The P-N bonds flanking N(1) are longer (1.600(5) Å) than the adjacent P-N bond lengths (1.557(5) Å). However, the depletion of skeletal π -bond is more severe in the N-P(Ph₂)-N segment owing to the presence of electron withdrawing phenyl substituents (Table 21). The cyclotriphosphazene ring adopts a distorted planar conformation. The coordinated skeletal nitrogen atom N(1) is 0.319(5) Å away from the mean plane defined by P(1), P(2), P(3), N(2) and N(3).

tdpctp-NiCl₂

The crystals of the title compound are monoclinic with space group C2/c. The unit cell dimensions and refinement parameters are collected in Table 20. The molecular structure is shown in Figure 26 and selected interatomic parameters are listed in Table 22. The lattice is comprised of essentially discrete molecules of title compound,

Table 22: Selected bond lengths (a) and bond angles (b) in tdpctp-NiCl_2

(a)			
Ni-Cl(1)	2.258(1)	P(1)-N(1)	1.590(4)
Ni-Cl(2)	2.218(2)	P(1)-N(2)	1.537(4)
Ni-N(1)	2.079(3)	P(2)-N(2)	1.591(4)
Ni-N(11)	2.080(4)	P(2)-N(3)	1.537(4)
Ni-N(31)	2.089(4)	P(3)-N(1)	1.600(4)
mean distances		P(3)-N(3)	1.611(4)
P-N _{exo}	1.670(4)		
P-C _{exo}	1.786(5)		
(b)			
Cl(1)-Ni-Cl(2)	114.77(6)	N(1)-P(1)-N(3)	117.9(2)
Cl(1)-Ni-N(1)	117.2(1)	N(1)-P(2)-N(1)	117.6(2)
Cl(1)-Ni-N(11)	92.8(1)	N(2)-P(3)-N(3)	114.8(2)
Cl(1)-Ni-N(31)	91.1(1)	P(1)-N(1)-P(2)	114.4(2)
Cl(2)-Ni-N(1)	128.0(1)	P(2)-N(2)-P(3)	120.9(2)
Cl(2)-Ni-N(11)	99.0(1)	P(1)-N(3)-P(3)	122.6(2)
Cl(2)-Ni-N(31)	97.1(1)	N(12)-P(1)-N(21)	103.2(2)
N(1)-Ni-N(11)	80.3(1)	N(32)-P(2)-N(41)	103.8(2)
N(1)-Ni-N(31)	80.5(1)	C(51)-P(3)-C(61)	108.1(2)
N(11)-Ni-N(31)	160.0(1)		

there being no significant intermolecular contacts; the closest non-hydrogen contact in the lattice occurs between the N(22) and C(35)' atoms at 3.366(7) Å (symmetry operation: $x, 1+y, z$).

The nickel atom in the complex exists in a distorted trigonal bipyramidal geometry. The equatorial plane is defined by the two chloride ions and a nitrogen donor atom derived from the cyclotriphosphazene ring; the nickel atom lies 0.0212(6) Å out of the equatorial plane in the direction of the N(11) atom. The axial positions

are occupied by two nitrogen atoms derived from two nongeminally substituted cis-pyrazolyl groups [N(11)-Ni-N(31), 160.0(1) °] and the planes through the two pyrazolyl groups involved in coordination to the nickel atom form dihedral angles of 99.7 and 78.9 ° respectively with the equatorial plane. The tdpctp ligand thus coordinates in a tridentate mode and remarkable in the structure is the equivalence of the Ni-N distances which lie in the narrow range 2.079(3) to 2.089(4) Å. These values may be compared to the range of Ni-N values of 2.01(1) to 2.05(1) found in the structure of dibromo(6,6'-dimethyl-di(2-pyridylmethyl)amine-N.N.N)nickel(II) which features a similar trigonal bipyramidal geometry defined by an N₃Br₂ donor set [66].

In the analogous copper complexes hdpctp·CuCl₂ and tdpctp·CuCl₂ the axially bound pyrazolyl nitrogen atoms formed significantly tighter Cu-N interactions compared with the equatorially bound cyclotriphosphazene nitrogen atom. Further, the Cl-Cu-Cl angle of *ca.* 142.3(1) ° in them is significantly greater than the analogous angle in tdpctp·NiCl₂ of 114.77(6) °. Clearly, the geometry about the copper in the copper complexes approaches one based on a tetragonally distorted square pyramidal geometry (with the cyclotriphosphazene skeletal nitrogen atom occupying the axial position), at least more so than that found in tdpctp·NiCl₂.

The P₃N₃ framework of the cyclotriphosphazene ligand is not planar, with the major deviations being found for the N(1) atom as shown in the torsion angles of 119.5(2) and -110.7(2) ° for Ni/N(1)/P(1)/N(3) and Ni/N(1)/P(2)/N(2) respectively.

tdpctp·Cu(ClO₄)₂·2H₂O

The title compound crystallized in the monoclinic space group P2₁/a. Crystal data and details of data collection and structure refinement are given in Table 23. The perchlorate ions are modelled as two rigid groups of ratio 0.85:0.15. Perspective view of the complex is shown in Figure 27. Selected bond lengths and bond angles are given in Table 24.

Table 23: Crystal data for $\text{tdpctp}\cdot\text{Cu}(\text{ClO}_4)_2\cdot 2\text{H}_2\text{O}$ ($\text{El} = 2\text{H}_2\text{O}$ and 1mH)

compound	$\text{tdpctp}\cdot\text{Cu}(\text{ClO}_4)_2\cdot 2\text{H}_2\text{O}$	$\text{tdpctp}\cdot\text{Cu}(\text{ClO}_4)_2\cdot 2\text{mH}$
formula	$\text{C}_{32}\text{H}_{42}\text{N}_{11}\text{P}_3\text{O}_{10}\text{Cl}_2\text{Cu}$	$\text{C}_{38}\text{H}_{46}\text{N}_{15}\text{P}_3\text{O}_8\text{Cl}_2\text{Cu}$
fw	968.11	1068.23
crystal size, mm	$0.60 \times 0.66 \times 0.70$	$0.14 \times 0.13 \times 0.56$
crystal color	blue	blue
a, Å	18.101(4)	12.121(7)
b, Å	19.927(4)	21.110(2)
c, Å	11.875(20)	19.464(5)
β , deg	90.696(15)	101.39(3)
V, Å ³	4354(15)	4882(3)
cell determination		
reflections	25	25
2 θ angle, deg	20-22	16-18.5
d(calcd), gcm ⁻³	1.18	1.45
space group	P21/a	P21/n
Z	1	4
F(000)	2000.06	2208.1
linear abs. coeff., mm ⁻¹	0.79	0.72
scan technique	θ -2 θ	θ -2 θ
scan speed, deg min ⁻¹	4-16	4-16
refls measured	5984	4827
unique reflections	5665	4544
data used	3918 ($I > 3\sigma(I)$)	2950 ($I > 2.5\sigma(I)$)
R(F ²), R _w (F ²)	0.048, 0.072	0.049, 0.067
largest Δ/σ	0.08	0.001
Final diff map, eÅ ⁻³	-0.7(7), +0.8(7)	-0.5(1), +0.6(1)

The copper ion in the complex adopts an elongated octahedral geometry with the cyclotriphosphazene skeletal nitrogen and a perchlorate anion occupying the axial positions. The basal plane is constituted by two nongeminal cis-pyrazolyl pyridinic nitrogens and two water molecules. The mean Cu-N_{Pz} bond distance 2.024(5) Å is comparable to that found in related derivatives such as $\text{hdpctp}\cdot\text{CuCl}_2$ and $\text{tdpctp}\cdot\text{CuCl}_2$. The Cu-O(3) distance (2.506(5) Å) is similar to those found for weakly coordinated axial anions or water [67]. It may be pointed out that the copper-cyclotriphosphazene ring nitrogen interaction is remarkably weak and the bond distance is even longer

Table 24: Selected bond lengths (a) and angles (b) in $\text{tdpctp}\cdot\text{Cu}(\text{ClO}_4)_2\cdot 2\text{H}_2\text{O}$

(a)			
Cu(1)-N(2)	2.383(4)	P(1)-N(1)	1.568(5)
Cu(1)-N(7)	2.037(5)	P(1)-N(2)	1.593(4)
Cu(1)-N(9)	2.010(5)	P(2)-N(2)	1.589(4)
Cu(1)-O(1)	1.961(4)	P(2)-N(3)	1.558(5)
Cu(1)-O(2)	1.990(4)	P(3)-N(1)	1.617(5)
Cu(1)-O(3)	2.506(5)	P(3)-N(1)	1.615(5)
mean distances			
P-N _{exo}		1.691(5)	
P-C _{exo}		1.789(7)	
(b)			
N(2)-Cu(1)-N(7)	78.93(16)	N(1)-P(1)-N(2)	119.44(24)
N(2)-Cu(1)-N(9)	81.31(16)	N(2)-P(2)-N(3)	119.45(24)
N(2)-Cu(1)-O(3)	177.27(16)	N(1)-P(3)-N(3)	113.9(3)
N(7)-Cu(1)-N(9)	81.31(16)	P(1)-N(1)-P(3)	118.9(3)
N(7)-Cu(1)-O(3)	101.57(17)	P(1)-N(2)-P(2)	119.4(3)
N(9)-Cu(1)-O(3)	101.30(18)	P(2)-N(3)-P(3)	119.5(3)
O(1)-Cu(1)-O(2)	90.44(17)	N(4)-P(1)-N(6)	101.04(22)
O(1)-Cu(1)-N(2)	93.46(15)	N(8)-P(3)-N(10)	100.2(22)
O(1)-Cu(1)-N(7)	88.20(18)	C(21)-P(2)-C(31)	106.3(3)
O(1)-Cu(1)-N(9)	173.68(17)	O(1)-Cu(1)-O(3)	83.89(17)
O(2)-Cu(1)-N(2)	96.75(16)	O(2)-Cu(1)-N(7)	175.38(18)
O(2)-Cu(1)-N(9)	86.76(18)	O(2)-Cu(1)-O(3)	82.67(16)

bonds flanking the phosphorus bearing the phenyl substituents as is evidenced by the longer P-N bond lengths (av. 1.616(5) Å) but is in keeping with that observed for $\text{N}_3\text{P}_3\text{Ph}_2\text{Cl}_4$ [68].

The planarity of the cyclotriphosphazene ring is affected by the skeletal nitrogen involvement in coordination to the copper. To relieve the strain produced by the

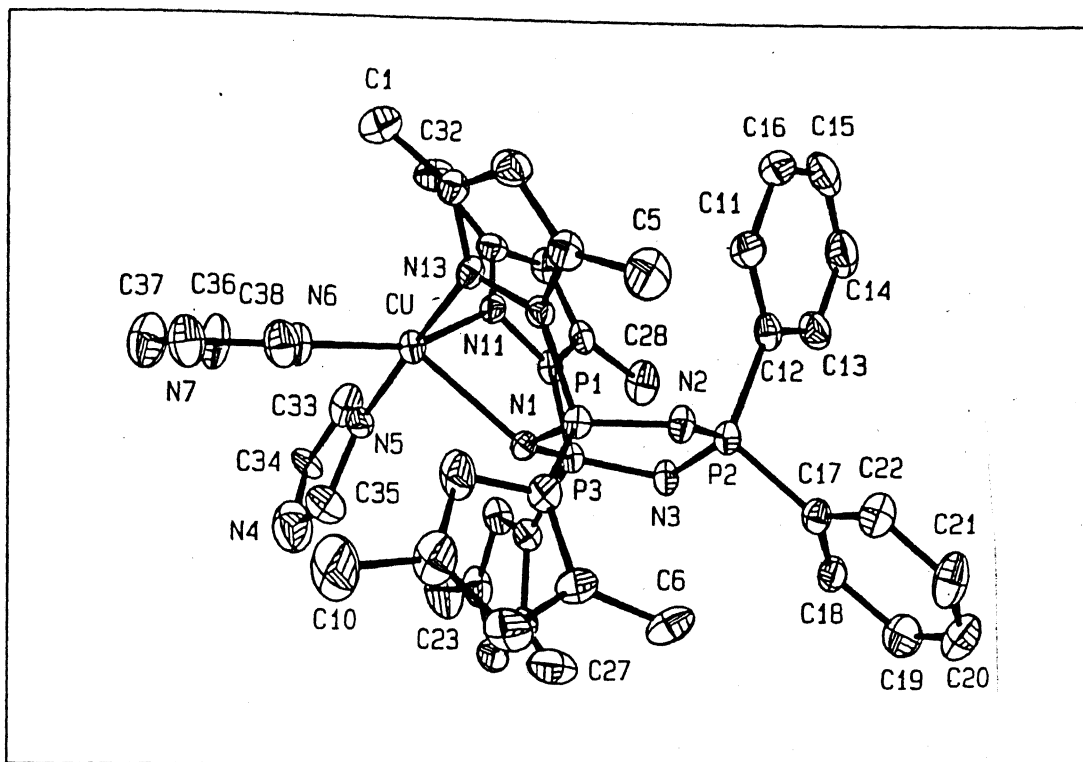


Figure 28: ORTEP plot of $\text{tdpctp} \cdot \text{Cu}(\text{ClO}_4)_2 \cdot 2\text{ImH}$

geometrical constraints, the non-interacting skeletal nitrogens are pushed away from the plane defined by the remaining atoms. Thus, the nitrogen atoms N(1) and N(3) are $-0.258(5)$ and $-0.252(5)$ Å respectively away from the plane defined by P(1), P(2), P(3) and N(2).

$\text{tdpctp} \cdot \text{Cu}(\text{ClO}_4)_2 \cdot 2\text{ImH}$

Blue crystals obtained by slow diffusion of benzene into a dichloromethane solution of $\text{tdpctp} \cdot \text{Cu}(\text{ClO}_4)_2 \cdot 2\text{ImH}$ are monoclinic. Data on intensity collection and refinement of structure are given in Table 23. The molecular structure drawn by ORTEP is displayed in Figure 28.

The geometry of the copper is best described as a distorted square pyramid with the cyclotriphosphazene ring nitrogen at the apical position and the two nongeminal cis-pyrazolyl groups and two imidazole ligands occupying the basal ones. The copper-

Table 25: Selected bond distances (a) and angles (b) in $\text{tdpctp}\cdot\text{Cu}(\text{ClO}_4)_2\cdot 2\text{ImH}$

(a)			
Cu-N(1)	2.325(6)	P(1)-N(1)	1.590(6)
Cu-N(5)	1.968(7)	P(1)-N(2)	1.569(7)
Cu-N(6)	1.981(7)	P(2)-N(2)	1.600(7)
Cu-N(11)	2.076(7)	P(2)-N(3)	1.607(7)
Cu-N(13)	2.014(7)	P(3)-N(1)	1.605(6)
mean distances		P(3)-N(3)	1.558(7)
P-N _{exo}	1.680(7)		
P-C _{exo}	1.783(9)		
(b)			
N(1)-Cu-N(5)	96.4(3)	N(1)-P(1)-N(2)	119.1(3)
N(1)-Cu-N(6)	125.2(3)	N(2)-P(2)-N(3)	114.3(3)
N(1)-Cu-N(11)	78.8(2)	N(1)-P(3)-N(3)	117.3(3)
N(1)-Cu-N(13)	80.8(2)	P(1)-N(1)-P(3)	119.2(4)
N(5)-Cu-N(6)	88.8(3)	P(1)-N(2)-P(2)	122.1(4)
N(5)-Cu-N(11)	88.3(3)	P(2)-N(3)-P(3)	120.3(4)
N(5)-Cu-N(13)	176.1(3)	N(12)-P(1)-N(14)	101.4(3)
N(6)-Cu-N(11)	156.0(3)	N(9)-P(3)-N(10)	103.2(3)
N(6)-Cu-N(13)	90.7(7)	C(12)-P(2)-C(17)	107.7(3)
N(1)-Cu-N(13)	93.7(3)		

cyclotriphosphazene skeletal nitrogen bond distance is relatively shorter (2.325(6) Å) than those found in previous ones, indicating slightly improved interaction. The mean Cu-NP_{Pz} and Cu-N_{Im} bond distances are 2.015(7) and 1.975(7) Å respectively and are consistent with those observed for analogous complexes. It is to be noted that the Cu-NP_{Pz} bond distances in the title complex are slightly longer (~0.02 Å) than those in $\text{tdpctp}\cdot\text{Cu}(\text{ClO}_4)_2\cdot 2\text{H}_2\text{O}$. The square pyramidal geometry about copper is much distorted towards trigonal bipyramidal geometry and accounts well the small

A_{\parallel} values observed for the imidazole and pyridine adducts in the EPR spectroscopy (*vide supra*). These deviations can be clearly inferred from the widened N(6)-Cu-N(1) (125.2(3) °) and constricted N(6)-Cu-N(11) (156.0(3) °) bond angles from the expected ones (90 ° and 180 ° respectively). The selected interatomic distances and bond angles are given in Table 25.

The moderately strong interaction exhibited by the cyclotriphosphazene skeletal nitrogen towards the copper ion is reflected in the phosphazene ring bond distances. The P-N length flanking the coordination site are lengthened to a slightly larger extent (1.598(6) Å) compared to that in the complex $\text{tdpctp}\cdot\text{Cu}(\text{ClO}_4)_2\cdot 2\text{H}_2\text{O}$. The P_3N_3 ring is non-planar with the atom N(3) projected 0.0305 Å from the plane defined by P(1), P(2), P(3), N(1) and N(2). The remaining P-N (exocyclic and endocyclic) bond distances and bond angles at phosphorus (endocyclic and exocyclic) and nitrogen are unexceptional.

4.5 Ligating Properties of the Ligand 2,2-Spiro(1,3-diaminopropane)-4,4,6,6-tetrakis(3,5-dimethyl-1-pyrazolyl)cyclotriphosphazene (stdpctp).

4.5.1 General

The ligand stdpctp is a potential multidentate ligand with three different donor groups. Apart from the pyrazolyl and cyclotriphosphazene nitrogen atoms, the amido nitrogens P-N(II) of the 1,3-diaminopropane spiro loop is also expected to compete for coordination to metals. The nongeminal coordinations bites involving pyrazolyl and cyclotriphosphazene nitrogens are exactly same as in the ligands hdpctp and tdpctp. However, the new N_3 core comprising a pyrazolyl nitrogen, a cyclotriphosphazene ring nitrogen and a amido nitrogen may lead to a four-membered and a five membered chelate rings. This coordination pattern is visualized in Figure 29 . As expected the

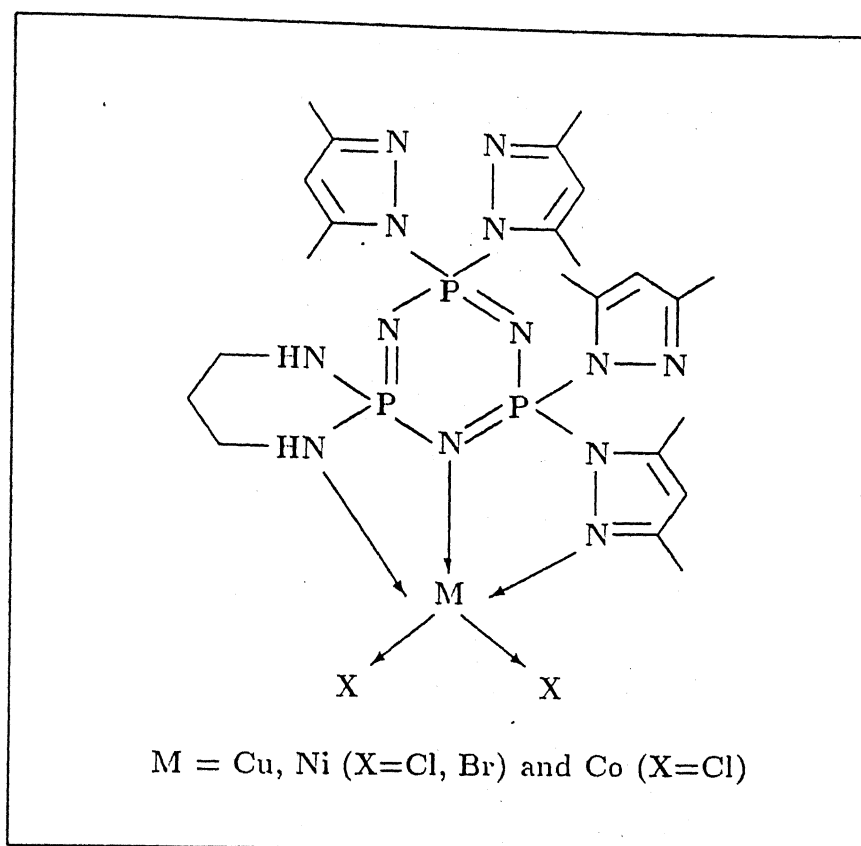


Figure 29: Coordination mode of stdpctp

ligand stdpctp prefers to interact with the transition metal *via* the latter N₃ core. It forms mononuclear complexes with copper, cobalt and nickel(II) halides.

The list of the coordination compounds and their physical characteristics are given in Table 26. Majority of the complexes decompose slowly on standing for 3-4 weeks. This suggests that probably the formation of the four-membered chelate ring (Figure 29) increases the strain in the 1,3-diaminopropane spiro loop and cleaves the P-N bond of the spiro loop to liberate an amino arm. However, at present, we do not have any corroborative evidence for this speculation. Our attempts to grow single crystals of these complexes resulted in the decomposition of complexes with the concurrent formation of very powdery and hygroscopic materials.

Table 26: Physical characteristics of stdpctp complexes

compound	color	nature	Δ_m (mho cm ² mol ⁻¹)	μ_{eff} (BM)
stdpctp·CuCl ₂	green	amorphous	12	1.74
stdpctp·CuBr ₂	yellow	amorphous	20	1.71
stdpctp·NiCl ₂	pink	amorphous	17	2.95
stdpctp·NiBr ₂	brick red	amorphous	20	3.01
stdpctp·CoCl ₂	blue	crystalline	8	4.74

4.5.2 Spectroscopic properties of the complexes

The IR spectrum of the free ligand shows a slightly broad band at 3200 cm⁻¹ attributable to the N-H stretching frequency. In the complexes it is shifted to higher energy by at least 100 cm⁻¹. This clearly suggests the coordination of amido (NH) group to the metals. The splitting of the P=N stretching band indicates cyclotriphosphazene nitrogen also participates in coordination. Similar inference has been made regarding the involvement of pyrazolyl pyridinic nitrogen in donation. The conductivity data reveal that the complexes are non-electrolytes in acetonitrile solution. The magnetic moment values of the copper, nickel and cobalt complexes are acceptable for S=1/2, 1 and 3/2 spin states respectively and indicate high spin nature of the complexes.

The electronic spectra are dominated by the π - π^* (intraligand) and l.m.c.t. bands in the region 200-450 nm. All the complexes show a ligand centred π - π^* transition at round 235 nm. The copper halide complexes stdpctp·CuX₂ (X=Cl, Br) exhibit two Pz \rightarrow Cu charge transfer bands at ca. 275 and 355 nm and a broad d-d band at ca. 880 nm. When compared with the analogous tdpctp complexes the d-d band of the stdpctp complexes are slightly blue-shifted (~20 nm) indicating strong field nature of the ligand (stdpctp). The stdpctp·CuBr₂ displays an additional band in the UV-

Table 27: Electronic spectral data for the stdpctp complexes[†]

compound	λ_{max} (ϵ_{max}) [‡]	assignment
stdpctp·CuCl ₂	885(0.22)	d-d
	360(1.72), 281(3.01)	Pz → Cu l.m.c.t
	237(13.45)	π - π^* (intraligand)
stdpctp·CuBr ₂	883(0.35)	d-d
	411(2.02)	Br → Cu l.m.c.t
	355sh, 305(2.85)	Pz → Cu l.m.c.t
	238(13.30)	π - π^* (intraligand)
stdpctp·NiCl ₂	780(0.01)	d-d
	156(0.18)	d-d
	282(1.43)	Pz → Ni l.m.c.t
	238(13.87)	π - π^* (intraligand)
stdpctp·NiBr ₂	776(0.01)	d-d
	456(0.22)	d-d
	330(1.02)	Br → Ni l.m.c.t
	274(1.68)	Pz → Ni l.m.c.t
	233(14.02)	π - π^* (intraligand)
stdpctp·CoCl ₂	902(0.01)	d-d
	631(0.14)	d-d
	260sh	Pz → Co l.m.c.t
	238(11.38)	π - π^* (intraligand)

[†] for dichloromethane solutions

[‡] units: nm (mol⁻¹ cm⁻¹)

Vis region attributable to the Br → Cu l.m.c.t. The cobalt and the nickel complexes also exhibit Pz → M l.m.c.t. band near 265 nm (Table 27). The intensity and the band positions of the d-d bands of nickel and cobalt complexes reveal a high spin N₃X₂ chromophore in comparison with analogous compounds [60, 61, 58].

The EPR spectra of the copper complexes, stdpctp·CuX₂ were recorded at x-band

frequency as polycrystalline samples. They show axial pattern with $g_{\perp} > g_{\parallel}$ demonstrative of $d_{x^2-y^2}$ ground state with compressed trigonal bipyramidal geometry [11]. No hyperfine couplings have been observed. The g_{\parallel} and g_{\perp} values for $\text{stdpctp} \cdot \text{CuX}_2$ ($\text{X} = \text{Cl, Br}$) are 2.059, 2.022 and 2.115, 2.130 respectively. On the basis of the above accumulated evidences we prefer to assign trigonal bipyramidal structures to the complexes as depicted in Figure 29. However, a final conclusion on the exact geometry of the compounds awaits crystal structure determination of atleast one compound.

4.6 Conclusions

The ligands hdpctp , tdpctp and stdpctp form penta-coordinate copper(II) compounds when treated with copper(II) halides. The ligand hdpctp forms homo- and heterodinuclear complexes also. The reduction in the number of pyrazolyl substituents in tdpctp leads to the selective formation of mononuclear complexes, while in stdpctp replacement of two pyrazolyl groups by an 1,3-diaminopropane spiro loop gives rise to competition for coordination between pyrazolyl and amido substituents. The copper perchlorate complexes of hdpctp and tdpctp are six-coordinate or five-coordinate depending upon the nature of exogenous ligands participating in coordination. While the two aquo ligands stabilize the distorted octahedral structure bulky nitrogenous bases prefer square pyramidal structure. Less variation in the coordination geometry of the copper ions observed in the complexes of these ligands is attributed to the constraints in these ligands which form two five-membered chelate rings on coordination.

References

- [1] Kirishnamurthy, S.S., Reddy, V.S., Chandrasekharan, A. and Nethaji, M. *Phosphorus, Sulfur and Silicon*, **1992**, 64, 99; Chandrasekhar, V., Krishnamurthy, S.S. and Woods, M. *A.C.S. Symp. Ser.*, **1988**, 171, 481.

- [2] Gallicano, K.D. and Paddock, N.L. *Can. J. Chem.*, **1982**, *60*, 521; Gallicano, K.D., Paddock, N.L., Rettig, S.J. and Trotter, J. *Inorg. Nucl. Chem. Letts.*, **1979**, *15*, 117.
- [3] Mc Bee, E.T., Okuhara, K. and Morton, C.J. *Inorg. Chem.*, **1965**, *4*, 1672.
- [4] Chandrasekhar, V., Krishnamurthy, S.S. Manohar, H., Vasudevamurthy, A.R., Shaw, R.A. and Woods, M. *J. Chem. Soc. Dalton Trans.*, **1984**, 621.
- [5] Keat, R., Shaw, R.A. and Woods, M. *J. Chem. Soc. Dalton Trans.*, **1976**, 1582.
- [6] Chandrasekhar, V., Krishnamurthy, S.S. Vasudevamurthy, A.R., Shaw, R.A. and Woods, M. *Inorg. Nucl. Chem. Letts.*, **1981**, *17*, 181.
- [7] Allen, C.W., Brown, D.E., Cordes, A.W. and Craig, S.C. *J. Chem. Soc. Dalton Trans.*, **1988**, 1405.
- [8] Van der Huizen, A.A., Van de Grampel, J.C., Rusch, J.W., Witting, T., Bolhuis, F. and Meetsma, A. *J. Chem. Soc. Dalton Trans.*, **1986**, 1317.
- [9] Richie, R.J., Fuller, T.J. and Allcock, H.R. *Inorg. Chem.*, **1980**, *19*, 3841.
- [10] Krishnamurthy, S.S., Sau, A.C. and Woods, M. *Adv. Inorg. Chem. Radiochem.*, **1978**, *21*, 41.
- [11] Hathaway, B.J. *Struct. Bonding (Berlin)*, **1984**, *57*, 55; Hathaway, B.J. and Billing, D.E. *Coord. Chem. Rev.*, **1970**, *5*, 143.
- [12] Geary, W.J. *Coord. Chem. Rev.*, **1971**, *7*, 81.
- [13] Nakamoto, K. *Infrared and Raman Spectra of Inorganic and Coordination Compounds*, Wiley-Interscience, New York, 1970, pp. 175.
- [14] Bouwman, E. Ph.D. thesis, Leiden University, Leiden, Netharlands; Bouwman, E., Westheide, G.E., Driessen, W.L. and Reedijk, J. *Inorg. Chim. Acta*, **1989**, *166*, 291.
- [15] Shaw, R.A. *Z. Naturforsch.*, **1976**, *31b*, 611.
- [16] Bernarducci, E., Schwindinger, W.E., Hughey IV, J.L., Krogh-Jespersen, K. and Schugar, H.J. *J. Am. Chem. Soc.*, **1981**, *103*, 1686.
- [17] Lever, A.B.P. *Inorganic Electronic Spectroscopy*, 2nd Ed., Elsevier, Amsterdam, 1984.

- [18] Thompson, L.K., Ramaswamy, B.S. and Dawe, R.D. *Can. J. Chem.*, **1966**, *5*, 41; Albertin, G., Bordignon, E. and Orio, A.A. *Inorg. Chem.*, **1975**, *14*, 1411.
- [19] Addison, A.W., Hendriks, H.M., Reedijk, J. and Thompson, L.K. *Inorg. Chem.*, **1981**, *20*, 103.
- [20] Plesch, G., Friebel, C., Švajlenová, O., Krätsmä-Šmogrovic, J. and Mlynarčík, D. *Inorg. Chim. Acta*, **1988**, *151*, 139.
- [21] Balhausen, C.J. *Introduction to Ligand Field Theory*, McGraw-Hill, New York, 1963, pp. 108, 135.
- [22] Barbucci, R. and Campbell, M.J.M. *Inorg. Chim. Acta*, **1975**, *15*, L15; Barbucci, R., Bencini, A. and Gatteschi, D. *Inorg. Chem.*, **1977**, *16*, 2117; Bencini, A., Bertini, L., Gatteschi, D. and Scozzafava, A. *Inorg. Chem.*, **1978**, *17*, 3194.
- [23] Huq, F. and Skapski, A.C. *J. Chem. Soc. (A)*, **1971**, 1927.
- [24] Henke, W., Kremer, S. and Reinen, D. *Inorg. Chem.*, **1983**, *22*, 2858.
- [25] Arritortua, M.L., Mesa, J.L., Rojo, T., Dabaerdemaeker, T., Beltrán-Porter, D., Stratemeier, H. and Reinen, D. *Inorg. Chem.*, **1988**, *27*, 2976.
- [26] Hathaway, B.J. and Stephens, F.S. *J. Chem. Soc. (A)*, **1970**, 884.
- [27] Plesch, G., Friebel, C., Švajlenová, O. and Krätsmä-Šmogrovic, J. *Polyhedron*, **1991**, *10*, 893.
- [28] Peisach, J. and Blumberg, W.E. *Arch. Biochem. Biophys.*, **1974**, *165*, 691.
- [29] Batra, G. and Mathur, P. *Inorg. Chem.*, **1992**, *31*, 1575.
- [30] Sakaguchi, U. and Addison, A.W. *J. Chem. Soc. Dalton Trans*, **1979**, 600.
- [31] Sorrell, T.N., Jameson, D.L. and O'Connor, C.J. *Inorg. Chem.*, **1984**, *23*, 190.
- [32] Sorrell, T.N., O'Connor, C.J., Anderson, O.P. and Reibenspies, J.H. *J. Am. Chem. Soc.*, **1985**, *107*, 4199.
- [33] Trotter, J. and Whitlow, S.H. *J. Chem. Soc. (A)*, **1970**, 455.
- [34] Allen, R.W., O'Brien, J.P. and Allcock, H.R. *J. Am. Chem. Soc.*, **1977**, *99*, 3987.

- [35] Trotter, J. and Whitlow, S.H. *J. Chem. Soc. (A)*, **1970**, 455.
- [36] Rutan, G. and Zabel, v. *Cryst. Struct. Commun.*, **1976**, 6, 671.
- [37] Dhathathreyan, K.S., Krishnamurthy, S.S., Vasudevamurthy, A.R., Cameron, T.S., Chan, C., Shaw, R.A. and Woods, M. *J. Chem. Soc. Chem. Commun.*, **1980**, 231.
- [38] Bullen, G.J., Dann, P.E., Evans, M.L., Hursthouse, M.B., Shaw, R.A., Wait, K. and Woods, M. and Yu, H.S. *Z. Naturforsch.*, **1976**, 31b, 995.
- [39] Pottier, Y., Matreux, A. and Petit, F. *J. Organomet. Chem.*, **1989**, 370, 333; Stephan, D.W. *Coord. Chem. Rev.*, **1989**, 95, 41; Park, S., Johnson, M.P. and Roundhill, D.M. *Organometallics*, **1989**, 8, 1700.
- [40] Bullock, R.M. and Casey, C.P. *Acc. Chem. Res.*, **1987**, 20, 167; Casey, C.P. and Nief, F. *Organometallics*, **1985**, 4, 1218.
- [41] Katti, K.V. and Cavell, R.G. *Comments Inorg. Chem.*, **1990**, 10, 53.
- [42] Organ, C.J., Cooper, M.K., Henrick, K. and McPartlin, M. *J. Chem. Soc. Dalton Trans.*, **1984**, 2377.
- [43] Miller, T.M., Kazi, J.A. and Wrighton, M.S. *Inorg. Chem.*, **1989**, 28, 2347.
- [44] Pearson, R.G., *J. Chem. Educ.*, **1987**, 64, 561; Pearson, R.G. *J. Chem. Educ.*, **1968**, 45, 581, 613.
- [45] Brondino, C.D., Casado, N.M.C., Passeggi, M.C.G. and Calco, R. *Inorg. Chem.*, **1993**, 32, 2078.
- [46] Wang, S., Trepanier, S.J., Zheng, J.-G., Pang, I. and Wagner, M.J. *Inorg. Chem.*, **1992**, 31, 2118.
- [47] Costes, J.-P., Dahan, F. and Laurent, J.-P. *Inorg. Chem.*, **1992**, 31, 284.
- [48] Pahor, N.B., Calligaris, M. and Randacio, L. *J. Chem. Soc. Dalton Trans.*, **1976**, 725; Hunter, G., McAuley, A. and Whitcombe, T.W. *Inorg. Chem.*, **1988**, 27, 2631.
- [49] Matin, D.S., Bronte, J.L., Rush, R.M. and Jacobson, R.A. *Acta Crystallogr.*, **1975**, 31b, 2538.

- [50] Quirós, M., Salas, J.M., Sánchez, M.P., Beauchamp, A.L. and Solans, X. *Inorg. Chim. Acta*, **1993**, *204*, 213.
- [51] Allcock, H.R., Suszko, P.T., Wagner, L.J., Whittle, R.R. and Boso, B. *Organometallics*, **1985**, *4*, 416.
- [52] Allcock, H.R., Wagner, L.J. and Levin, M.L. *J. Am. Chem. Soc.*, **1983**, *105*, 1321.
- [53] Allcock, H.R., Suszko, P.T., Wagner, L.J., Whittle, R.R. and Boso, B. *J. Am. Chem. Soc.*, **1984**, *106*, 4966.
- [54] Saraceno, R.A., Riding, G.H., Allcock, H.R. and Ewing, A.G. *J. Am. Chem. Soc.*, **1988**, *110*, 980.
- [55] Zanello, P. *Comments Inorg. Chem.*, **1988**, *8*, 15.
- [56] Zanello, P. In *Stereochemistry of Organometallic and Inorganic Compounds*, Ed. Bernal, L. Elsevier, Amsterdam, **1990**, vol. *4*, pp. 181.
- [57] Casella, L., Gullotti, M., Pinter, A., Pinciroli, P., Vigino, R. and Zanello, P. *J. Chem. Soc. Dalton Trans.*, **1989**, 1161; Takahashi, K., Ogawa, E., Oishi, N., Nishida, Y. and Kida, S. *Inorg. Chim. Acta*, **1982**, *66*, 97.
- [58] Banci, L., Bencini, A., Benelli, C., Gatteschi, D. and Zanchini, G. *Struct. Bonding (Berlin)*, **1982**, *52*, 37.
- [59] Hathaway, B.J. *J. Chem. Soc. Dalton Trans.*, **1972**, 1196.
- [60] Sacconi, L., Mani, F. and Benzi, A. In *Comprehensive Coordination Chemistry*, Pergamon Press, Oxford **1987**, vol. *5*, pp. 1.
- [61] Dori, Z. and Gray, H.B. *J. Am. Chem. Soc.*, **1966**, *88*, 1394.
- [62] Herning, D.G., Patmore, D.J. and Storr, A. *J. Chem. Soc. Dalton Trans.*, **1975**, 711.
- [63] Yokoi, H. and Addison, A.W. *Inorg. Chem.*, **1977**, *16*, 1341.
- [64] Kivelson, D. and Nieman, R. *J. Chem. Phys.*, **1961**, *35*, 149.
- [65] Billing, D.E., Hathaway, B.J. and Nicholls, P. *J. Chem. Soc. (A)*, **1969**, 316.
- [66] Rodgers, J. and Jacobson, R.A. *J. Chem. Soc. (A)*, **1970**, 1826.

- [67] Gazo, J., Bersuker, I.B., Garaj, J., Kabesoha, M. Kohout, J. Langfeldarva, H. Melink, M. Serator, M. and Valach, F. *Coord. Chem. Rev.*, **1976**, *19*, 253.
- [68] Mani, N.V., Ahmed, F.R. and Barnes, W.A. *Acta Crystallogr.*, **1965**, *19*, 693.

8/

Chapter 5

Substituents at the Pyrazole Ring: Electronic or Steric Influence on Coordination Behavior?

"At this stage it would be premature to attribute the differences to effects of the kind we are looking for, but it would be equally premature to give up the search."

-Henry Taube, In *Complex Ions in Solution*, 1970.

5.1 Introduction

Since the development of the Werner theory of coordination compounds chemists have accepted the concept of the preferred coordination number for a metal in a given formal oxidation state. This is understandable since the typical inorganic ligands [H^- , F^- , OH^- , H_2O , NH_3 , CO , CN^- etc.] are comparatively small allowing high coordination about a central atom to be achieved without undue intramolecular congestion. From recent more elaborate studies involving organic polydentate ligands it has become increasingly apparent that steric effects may become very important. It was shown in many instances, that the tendency of a metal to achieve a higher coordination by means of bridges could be frustrated by systematically exploiting the steric effect with judicious design of a ligand [1]. Such coordinatively unsaturated compounds may exhibit unusual chemical properties due to powerful electronic factors and find use in catalysis [2]. In the heme-protein modelling studies several model porphyrins with varying structural complexities such as picket-fence, capped, strapped

etc. have been used to prevent the irreversible formation of μ -oxo bridge [3]. By steric blocking one or both faces of the porphyrin, close approach of two porphyrin rings and therefore, μ -oxo bridge formation has been averted. Thus the studies related to the evaluation of the steric factor on the structure activity relationship among simple coordination compounds become more important.

With polypyrazolyl borate ligands a great degree of control on the environment of the chelated metal is achieved through appropriate substitution in the 3-, 4- and 5-positions of the pyrazole ring [4]. It has been shown clearly that introduction or removal of substituents on 3-position of pyrazole ring had a direct impact on accessibility of the coordinated metal to other reactants [4]. This chapter comprises the results of our studies related to the above theme.

In the preceding chapter the coordination behavior of pyrazolylcyclotriphosphazene ligands derived from 3,5-dimethylpyrazole and various cyclotriphosphazene precursors has been described. All these ligands have two methyl substituents at the three- and five-position of the pyrazole ring. To see whether these methyl groups have any influence on the ligating properties and on the geometry and characteristics of the metal complexes, two ligands hexakis(1-pyrazolyl)cyclotriphosphazene (hpctp) and 2,2-diphenyl-4,4,6,6-tetrakis(1-pyrazolyl)cyclotriphosphazene (tpctp) were prepared from pyrazole and appropriate halogenocyclotriphosphazenes. The coordination compounds of hpctp and tpctp will be described in this chapter. Figure 1 gives the line diagrams of the ligands hpctp and tpctp.

Both hpctp and tpctp were expected to form five-membered chelate rings similar to hdpctp and tdpctp. The only difference between hpctp and tpctp is the reduction of number of pyrazolyl groups attached to cyclotriphosphazene skeleton. The tpctp contains only four pyrazolyl groups while hpctp has six. The absence or presence of the peripheral methyl groups in pyrazolyl ring may influence the coordination behavior in two different ways. In the first place, the absence of methyl groups

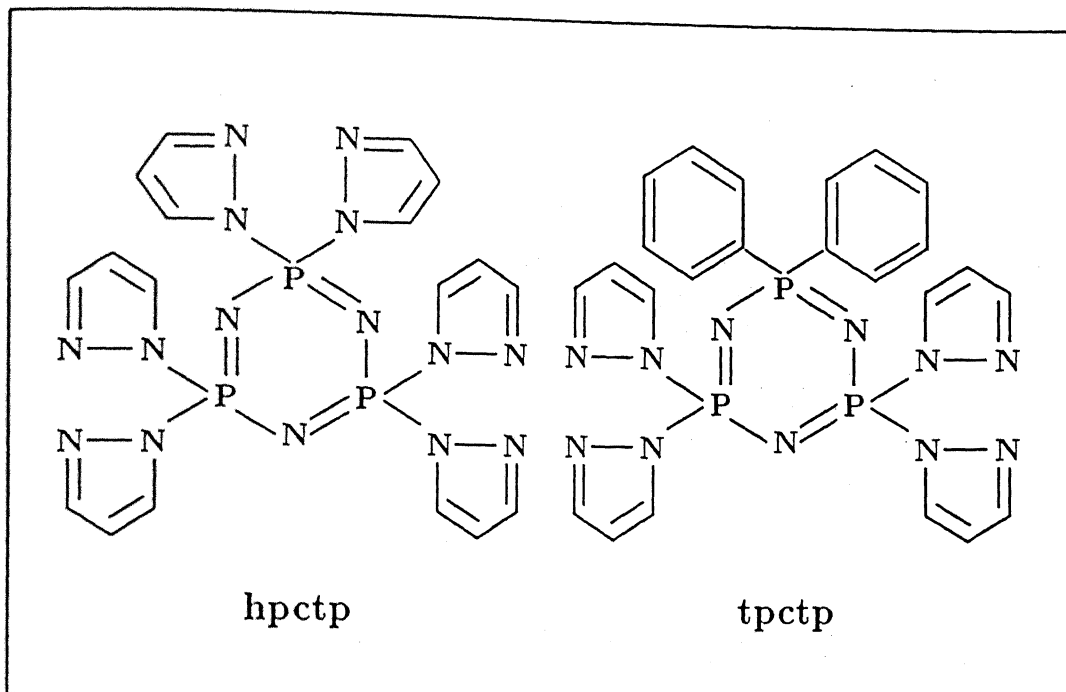


Figure 1: Pictorial representation of the ligands hpctp and tpctp

especially at the third-position of pyrazolyl ring which is very close to the coordination site (pyrazolyl pyridinic nitrogen) may relieve the steric hindrance forbidding the formation of complexes with ligand to metal ratio 2:1. Of course, there may be a secondary effect with regard to the coordination behavior resulting due to the absence of 5-CH₃ group in the the packing of the complexes in crystals. In the second place the pyrazole ring and thus the cyclotriphosphazene ring might be electronically influenced by the absence of electron donating methyl groups. The net electronic effect might be a diminished basicity of the cyclotriphosphazene skeletal nitrogens. In this context it is interesting to see how strong the cyclotriphosphazene ring nitrogen-metal interaction will be. The ligand hpctp has been prepared earlier by Paddock and co-workers [5] but no coordination compounds were reported and tpctp has been prepared by us for the first time.

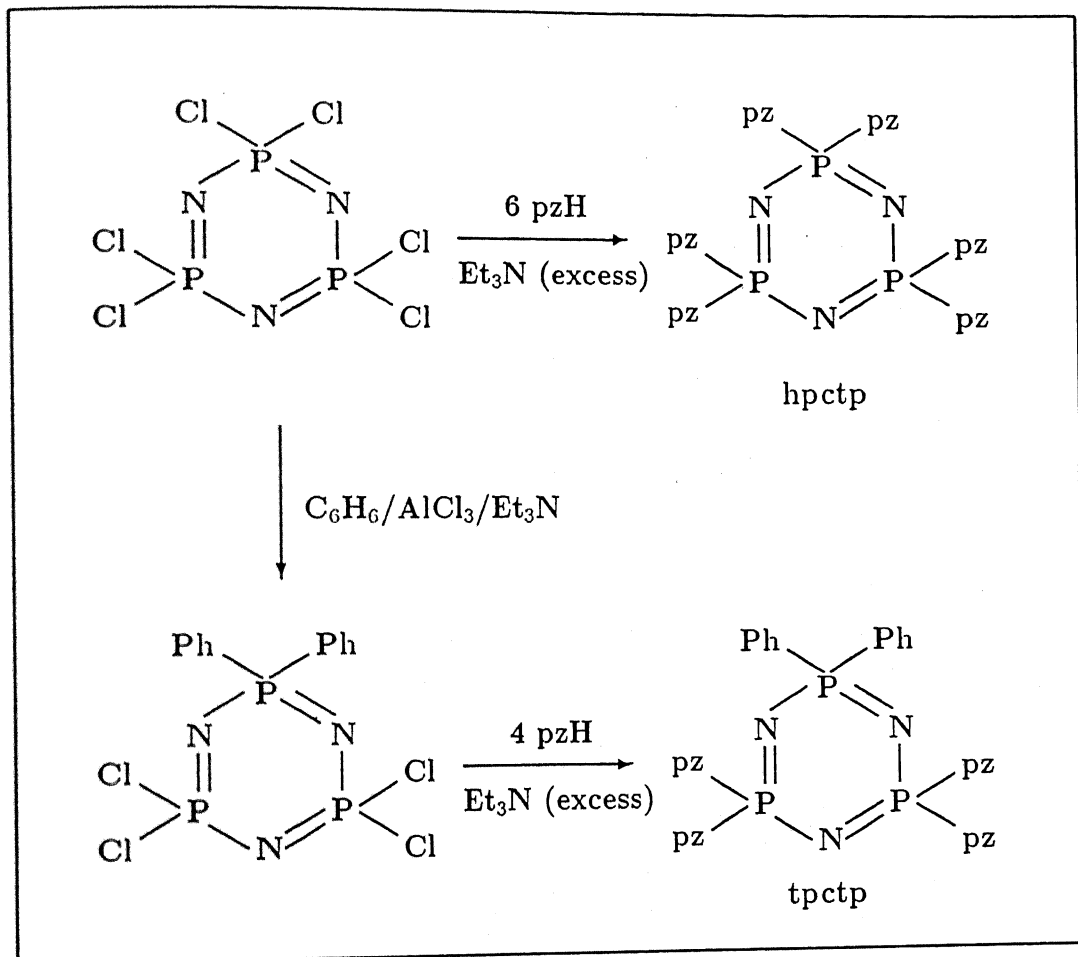


Figure 2: Reactions leading to the synthesis of the ligands **hpctp** and **tpctp**

5.2 Synthesis of the Ligands

The ligands **hpctp** and **tpctp** have been obtained by using the conventional nucleophilic substitution reactions of halogenocyclotriphosphazenes with amino compounds as schematized in Figure 2. The methodology is exactly same as that employed to prepare **hdpctp** and **tdpctp** ligands. Use of slight excess of triethylamine increased the yield of the pyrazolylcyclotriphosphazene ligands probably by facilitating the rupture of the P–Cl bond. Larger duration of reaction time is required to get appreciable yield of **tpctp** when compared to **hpctp**. The sluggish reaction of $\text{N}_3\text{P}_3\text{Ph}_2\text{Cl}_4$ with pyrazole may be attributed to the electron withdrawing phenyl substituents on the phosphorus which would enhance $p_\pi\text{--}d_\pi$ bonding interaction between the exocyclic

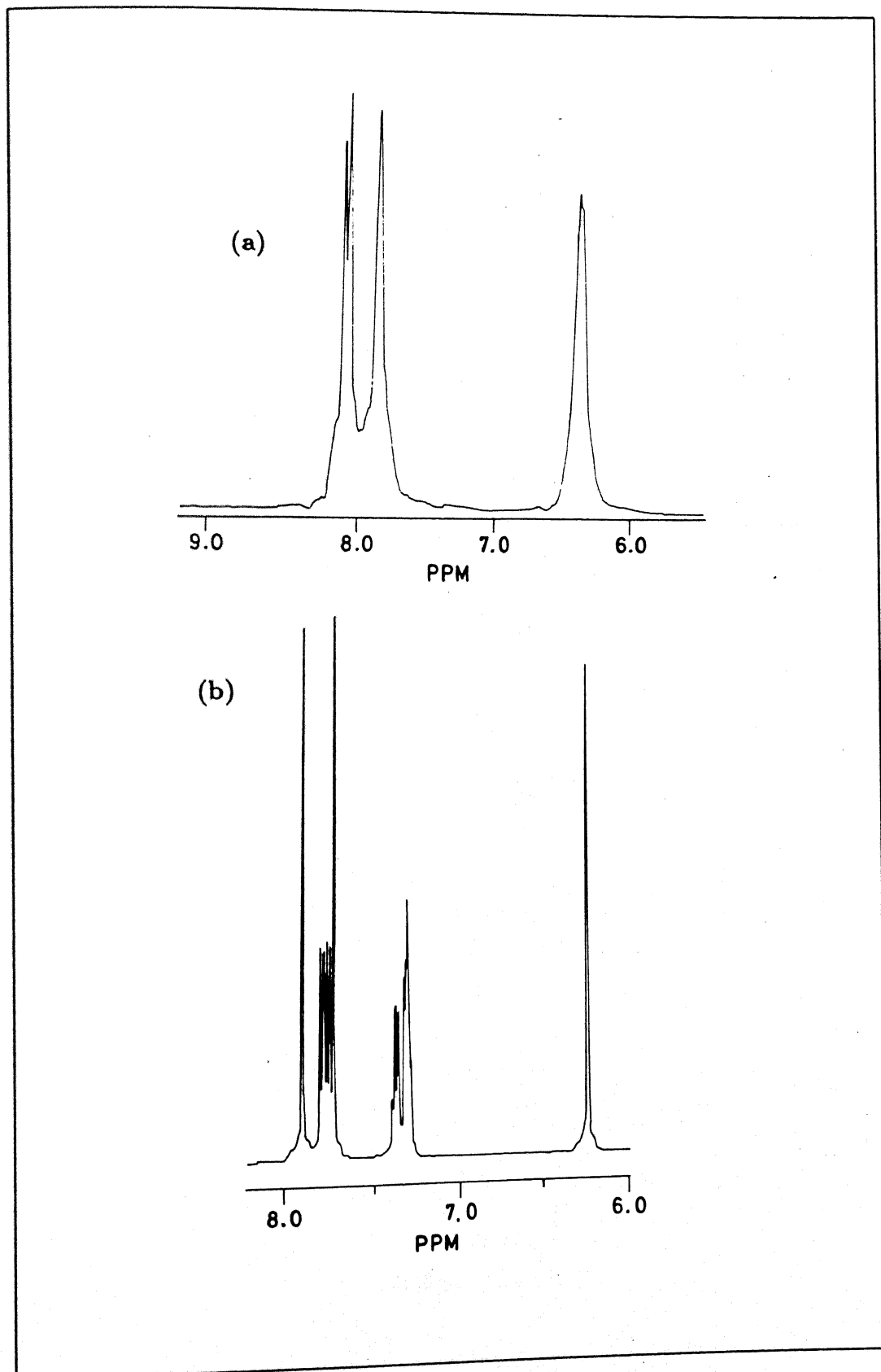


Figure 3: Proton NMR spectra of the ligands (a) hpctp and (b) tpctp

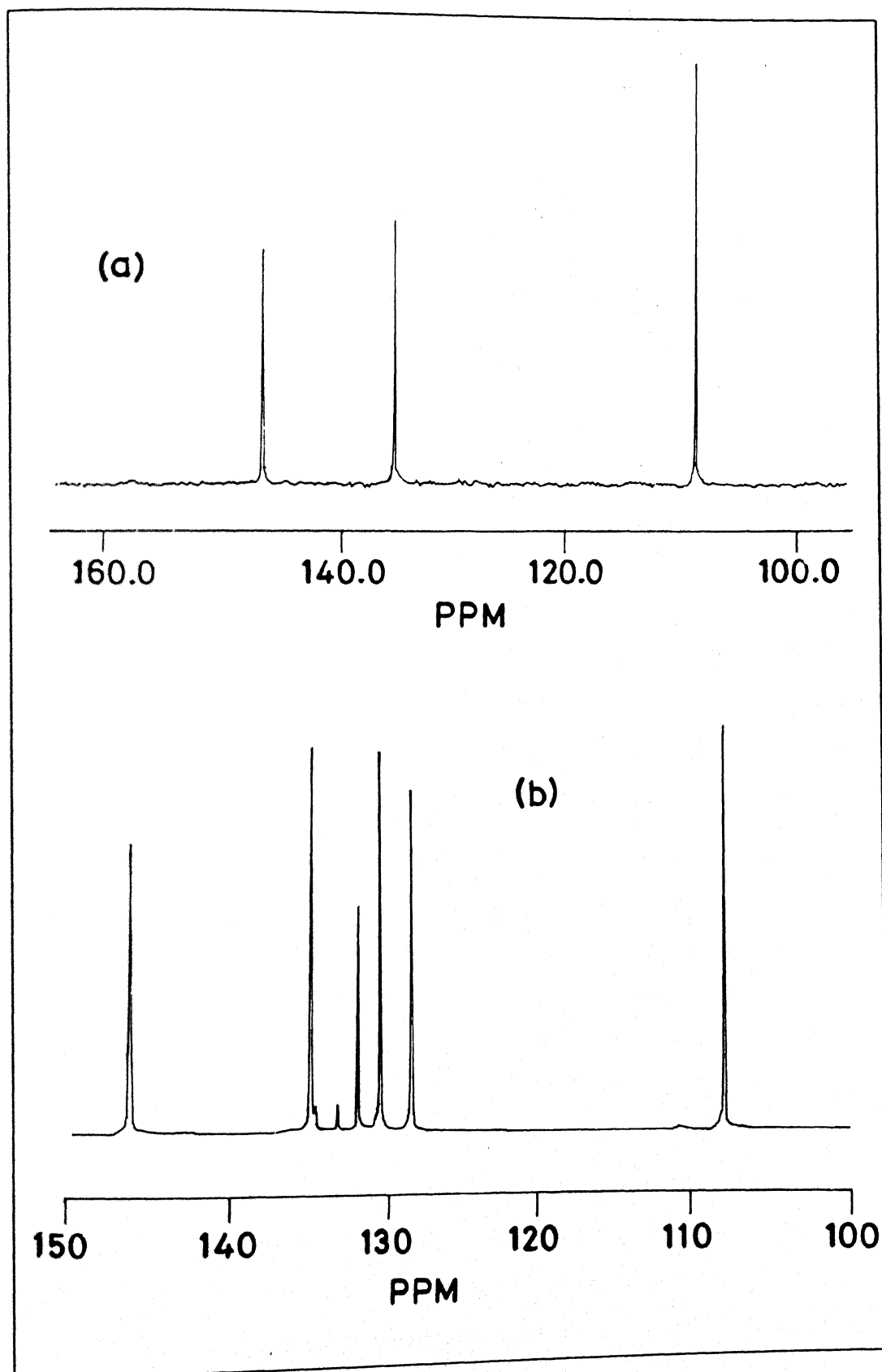


Figure 4: Carbon-13 NMR spectra of the ligands (a) hpctp and (b) tpctp

halogen and phosphorus.

In the proton NMR spectra of the ligands, the hydrogens associated with the pyrazolyl nuclei give rise to three separate signals owing to the inequivalence of hydrogen in the 3-, 4- and 5-positions. The high field triplet at 6.23 ppm is assigned to the proton in the 4-position while the two doublets at ~ 7.73 and ~ 7.90 ppm are ascribed to the 3- and 5-hydrogens respectively. The proton NMR spectra of the ligands hpctp and tpctp are displayed in Figure 3. The proton NMR spectrum of tpctp also shows peaks corresponding to the phenyl groups in the region 7.29-7.81 ppm as a multiplet.

Similarly in the carbon-13 NMR (noise decoupled) spectra of the ligands the three carbons of pyrazolyl group are well differentiated and appears at *ca.* 108, 135 and 146 ppm respectively. In tpctp additional peaks appear due to phenylic carbons in the region 120-150 ppm. The ^{13}C NMR spectra of the ligands are given in Figure 4. Final conclusive evidence for the structure of the ligands is derived from phosphorus-31 NMR spectra of them. The hpctp in which all the three phosphorus atoms are chemically equivalent show a singlet at 1.2 ppm, while the diphenyl derivative tpctp exhibits two different signals arising due to PPh_2 and Ppz_2 groups. The approximate intensity ratio of them is 1:2 consistent with the presence of two Ppz_2 moieties in the ligand tpctp.

5.3 Coordination Compounds of hpctp and tpctp

5.3.1 General

The multidentate ligands hpctp and tpctp have three-bond bites between the pyrazolyl and cyclotriphosphazene nitrogen atoms. The size of the chelate rings are exactly same as in the ligands hdpctp and tdpctp which are described in chapter 4. The ligands hpctp and tpctp are prepared from simple pyrazole, and therefore, lack the

Table 1: Colors, nature, magnetic moment and conductivity data of the complexes

compound	color	nature	$\mu_M(\text{BM})^*$	Λ_m^\dagger
hpctp·2CoCl ₂	violet blue	crystalline	5.02	12
tpctp·CoCl ₂	dark blue	crystalline	4.91	6
tpctp·CuCl ₂	bluish green	amorphous	1.78	17
tpctp·PtCl ₂ ·CuCl ₂	yellowish green	micro-crystalline	1.76	86
tpctp·CuBr ₂	yellowish brown	amorphous	1.72	18
[tpctp] ₂ ·Cu(ClO ₄) ₂	blue	amorphous	1.83	236
tpctp·Cu(ClO ₄) ₂ ·2py	blue	amorphous	1.80	242
tpctp·Cu(ClO ₄) ₂ ·2ImH	dark blue	crystalline	1.87	254
tpctp·Cu(ClO ₄) ₂ ·bipy	blue	amorphous	1.85	246
tpctp·Cu(ClO ₄) ₂ ·phen	blue	amorphous	1.80	244

* for dichloromethane solution

† for acetonitrile solution, unit: (mho cm² mol⁻¹)

methyl groups at the three- and five-positions of the pyrazole ring. The coordination behavior of these ligands is strikingly different. Except a dinuclear cobalt complex, no other coordination compound could be obtained from hpctp, which is soluble in ordinary common solvents to enable thorough characterization. The insolubility of the complexes points out their polymeric nature. However, a series of metal derivatives have been synthesized with the ligand tpctp. The complete listing of coordination compounds along with their color, nature, magnetic moment and conductivity data is given in Table 1. The ligand tpctp forms a complex with the copper(II) perchlorate hexahydrate with the metal to ligand ratio 1:2. But when this complex is allowed to react with monodentate or bidentate nitrogenous bases it breaks down to form complexes with the general formula $\text{tpctp} \cdot \text{Cu}(\text{ClO}_4)_2 \cdot n\text{NB}$, where NB is any heterocyclic nitrogen base such as pyridine, imidazole, etc.

5.3.2 Spectroscopic properties of the complexes

The infra-red spectra undubitably demonstrates that in all the complexes described in this chapter both the cyclotriphosphazene and pyrazolyl nitrogens participate in coordination. Thus a band ascribed to P=N stretching frequency is split into at least two components and the one of C=N stretching band is shifted to higher energy. In the copper(II) perchlorate derived complexes the appearance of single broad band at around 1100 cm^{-1} and a sharp singlet at 620 cm^{-1} strongly supports the presence of uncoordinated perchlorate anions [6]. This is also evident from the conductivity data for the acetonitrile solutions of them given in Table 1. From the conductivity data it is also deduced that the metal(II) halide complexes behave as non-electrolytes except the heterobimetallic derivative $\text{tpctp}\cdot\text{PtCl}_2\cdot\text{CuCl}_2$. The $\text{tpctp}\cdot\text{PtCl}_2\cdot\text{CuCl}_2$ shows appreciable conductivity owing to the decomposition of one or two metal-halogen bonds. It is difficult to identify which metal (platinum or copper) severs the tie with the chlorine from the conductivity experiment. However, later using EPR we will demonstrate that one chlorine attached to copper is replaced by acetonitrile to produce a 1:1 electrolyte [7] in appreciable quantities. The magnetic moment values are appropriate for $S=1/2$ and $3/2$ spin states for copper and cobalt complexes respectively [8, 9].

Optical absorption spectroscopy

The electronic spectral data for the complexes are presented in Table 2 with probable assignment of each band. In general all the complexes exhibit two bands attributable to the $\text{pz} \rightarrow \text{Cu}$ charge transfer at $\sim 270\text{ nm}$ and 360 nm [10]. The intensity of the higher energy band (270 nm) varies significantly according to the presence of additional ligands such as chlorine, imidazole, bipyridine, etc. suggesting other charge transfer transitions, eg. $\text{Cl} \rightarrow \text{Cu}$, $\text{phen} \rightarrow \text{Cu}$ do occur in the same wavelength. The d-d band of the copper(II) halide complexes of tpctp , is broad and extending into the

near-IR region, is characteristic of copper chromophore with $d_{x^2-y^2}$ ground state [8]. The d-d band of copper(II) perchlorate complexes is slightly shifted to higher energy and all of them show band maximum at around 650 nm and is demonstrative of distorted tetragonal geometry. For the complex $\text{tpctp}\cdot\text{Cu}(\text{ClO}_4)_2\cdot 2\text{ImH}$ distinctly a low energy shoulder at *ca.* 810 nm is also seen. This may be interpreted as copper in a square pyramidal geometry [11] with a N_5 chromophore. Striking difference between the complexes $\text{tdpctp}\cdot\text{Cu}(\text{ClO}_4)_2\cdot 2\text{H}_2\text{O}$ and $[\text{tpctp}]_2\cdot\text{Cu}(\text{ClO}_4)_2$ is that, in the latter

Table 2: Electronic Spectral data

compound	solvent	band *	assignment
$\text{hpctp}\cdot 2\text{CoCl}_2$	CH_2Cl_2	1050 (0.016)	d-d
		597 (0.140)	d-d
		560sh	d-d
		260sh	pz \rightarrow Cu l.m.c.t.
		234 (18.51)	π - π ligand
$\text{tpctp}\cdot\text{CoCl}_2$	CH_2Cl_2	1040 (0.008)	d-d
		599 (0.072)	d-d
		554sh	d-d
		266sh	pz \rightarrow Cu l.m.c.t.
		232 (13.25)	π - π ligand
$\text{tpctp}\cdot\text{CuCl}_2$	CH_2Cl_2	903 (0.192)	d-d
		360 (2.030)	pz \rightarrow Cu l.m.c.t.
		273 (6.370)	pz \rightarrow Cu l.m.c.t.
		233 (14.050)	π - π ligand
$\text{tpctp}\cdot\text{CuBr}_2$	CH_2Cl_2	877 (0.203)	d-d
		562 (0.345)	d-d
		425 (3.260)	Br \rightarrow Cu l.m.c.t.
		364 (2.820)	pz \rightarrow Cu l.m.c.t.
		276 (3.890)	pz \rightarrow Cu l.m.c.t.
		232 (13.960)	π - π ligand

(continued

Table 2: continued

compound	solvent	band *	assignment
tpctp·PtCl ₂ ·CuCl ₂	CH ₃ CN	774 (0.148)	d-d
		450sh	d-d
		360 (1.960)	pz → Cu l.m.c.t.
		262 (3.890)	pz → Cu l.m.c.t. & Cl → Cu l.m.c.t.
		224 (15.130)	π-π ligand
[tpctp]·Cu(ClO ₄) ₂	CH ₃ CN	750 (0.108)	d-d
		360 (2.120)	pz → Cu l.m.c.t.
		268 sh	pz → Cu l.m.c.t.
		223 (12.530)	π-π ligand
tpctp·Cu(ClO ₄) ₂ ·2py	CH ₂ Cl ₂	694 (0.086)	d-d
		368 (1.980)	pz → Cu l.m.c.t.
		263 (4.320)	pz → Cu l.m.c.t. & py → Cu l.m.c.t.
		234 (15.520)	π-π ligand
tpctp·Cu(ClO ₄) ₂ ·bipy	CH ₃ CN	671 (0.052)	d-d
		365sh	pz → Cu l.m.c.t.
		310 (4.370)	bipy → Cu l.m.c.t.
		260sh	pz → Cu l.m.c.t.
		225 (17.740)	π-π ligand
tpctp·Cu(ClO ₄) ₂ ·phen	CH ₃ CN	666 (0.056)	d-d
		367 (2.080)	pz → Cu l.m.c.t.
		275 (10.080)	pz → Cu l.m.c.t. & phen → Cu l.m.c.t.
		223 (14.820)	π-π ligand

* units: λ_{max} in nm and ϵ_{max} within parantheses in mol⁻¹ cm⁻¹ × 10³

compound the band maximum is blue shifted at least ~80 nm and shows no solvent dependence. This indicates the increased ligand field strength in the coordination square. The resemblance of the position of the d-d band with nitrogeneous

base adducts rather than the aquo adduct previously characterized with tdpctp supports the proposal of a N_4 basal plane in the octahedral geometry. The d-d band of the heterobimetallic compound $\text{tpctp}\cdot\text{PtCl}_2\cdot\text{CuCl}_2$ is quite different from that of $\text{tpctp}\cdot\text{CuCl}_2$. The λ_{max} value (774 nm) suggests more than three nitrogens participation in coordination probably arising from the involvement of acetonitrile apart from the two geminal pyrazolyl and one cyclotriphosphazene nitrogen nitrogens. This is reasonable while considering the preparative route and solubility of the complex. This heterobimetallic compound has been obtained by treating the platinum precursor $\text{tpctp}\cdot\text{PtCl}_2$ with CuCl_2 . When $\text{tpctp}\cdot\text{CuCl}_2$ was treated with $\text{Pt}(\text{PhCN})_2\text{Cl}_2$ it failed to produce the heterobimetallic derivative. This establishes that in $\text{tpctp}\cdot\text{CuCl}_2$ a non-geminal N_3 coordination from ligand to metal causes the unused pyrazolyl groups not suitable for coordination to a second metal. However in the square planar platinum derivative $\text{tpctp}\cdot\text{PtCl}_2$ only two geminal pyrazolyl groups participate in coordination to platinum [12] and leaves other two geminal pyrazolyl groups appropriate for second metal uptake. But the insolubility of the complex in most common organic solvents indicates halogen bridged polymeric structures in the solid state. This is also consistent with the EPR studies. The electronic spectra of the cobalt complexes $\text{hpctp}\cdot 2\text{CoCl}_2$ and $\text{tpctp}\cdot\text{CoCl}_2$ are essentially superimposable and acceptable for a high-spin trigonal bipyramidal chromophore [9]. This estimate is further confirmed by an x-ray crystal structure determination of $\text{tpctp}\cdot\text{CoCl}_2$ (*vide infra*).

Electron paramagnetic resonance spectroscopy

The EPR spin hamiltonian parameters for the copper complexes are given in Table 3. The EPR spectra of the copper halide complexes, including the heterobimetallic derivative $\text{tpctp}\cdot\text{PtCl}_2\cdot\text{CuCl}_2$ are isotropic in solid state and no useful information regarding the structure can be extracted from them. However, the heterobimetallic compound $\text{tpctp}\cdot\text{PtCl}_2\cdot\text{CuCl}_2$ displayed well resolved EPR spectra in acetonitrile

Table 3: EPR spin hamiltonian parameters for the copper complexes of tpctp

compound	medium	g_{\parallel}	g_{\perp}	A_{\parallel}	g_{iso}	A_{iso}
[tpctp] ₂ ·Cu(ClO ₄) ₂	powder	2.296	2.067	160	—	—
	CH ₃ CN	2.281	2.072	165	2.134	—
tpctp·Cu(ClO ₄) ₂ ·2ImH	powder	2.264	2.039	170	—	—
	CH ₃ CN	2.265	2.040	160	2.155	73
tpctp·Cu(ClO ₄) ₂ ·py	powder	2.267	2.067	160	—	—
	CH ₃ CN	2.272	2.056	175	2.161	68
tpctp·Cu(ClO ₄) ₂ ·bipy	powder	2.258	2.040	175	—	—
	CH ₃ CN	2.257	2.053	172	2.145	80
tpctp·Cu(ClO ₄) ₂ ·phen	powder	2.262	2.054	170	—	—
	CH ₃ CN	2.264	2.056	168	2.146	75
tpctp·CuCl ₂	powder	—	—	—	2.123	
tpctp·CuBr ₂	powder	—	—	—	2.125	
tpctp·PtCl ₂ ·CuCl ₂	powder	—	—	—	2.126	
	CH ₃ CN	2.270	2.059	148	2.132	58.3

showing necessary features that are useful in the estimation of the structures. Figure 5 shows the liquid nitrogen temperature x-band EPR spectrum of tpctp·PtCl₂·CuCl₂ in acetonitrile solution. The well resolved lineshape is indicative of a $S=1/2$ paramagnetic species in an axial symmetry ($g_{\parallel} > g_{\perp}$) with hyperfine resolution in the parallel region; a poorly but informative resolution of nine superhyperfine lines is also detectable in the perpendicular region. The overall lineshape is accounted for by magnetic coupling of the $S=1/2$ unpaired electron with the copper nucleus ($I=3/2$); the minor superhyperfine multiplet is attributable to the electron spin interaction with four nitrogen nuclei ($I=1$) (theoretical intensity of ratio = 1:5:10:14:19:14:10:5:1). The

second derivative

analysis affords a better resolution of the absorption pattern and gives the experimental values of the $A_{\perp}(N)$ superhyperfine coupling constant. The poor resolution of the spectrum in the perpendicular region and corresponding linewidth are consistent with the nonmagnetic equivalence of the four coordinating nitrogen nuclei, as confirmed by computer simulation. The computed spectrum is shown in Figure 5(b). This further supports the proposed trigonal bipyramidal arrangement of the copper environment with the three nitrogens originating from two geminal pyrazolyl groups and one acetonitrile molecule lying in the equatorial plane (higher $A_{\perp}(N)$) and the fourth one of the cyclotriphosphazene nitrogen occupying an apical position. The A_{\parallel} values suggest that the distortion may be more towards square pyramidal geometry with the weak axially interacting cyclotriphosphazene nitrogen. The parameters of the simulated spectrum are:

$$\begin{array}{ll} g_{\parallel} = 2.270 & g_{\perp} = 2.059 \\ g_{ave} = 1/3(g_{\parallel} + 2g_{\perp}) = 2.130 & \\ A_{\parallel} = 148.0 \text{ G} & A_{\perp} = 10.0 \text{ G} \\ A_{ave} = 1/3(A_{\parallel} + 2A_{\perp}) = 56.0 \text{ G} & \\ A_{\parallel} (3N) = 4.0 \text{ G} & A_{\perp} (3N) = 13.8 \text{ G} \\ A_{\parallel} (N) = 3.7 \text{ G} & A_{\perp} (N) = 12.7 \text{ G} \end{array}$$

Figure 5c shows the room temperature x-band EPR spectrum of acetonitrile solution. Both the first and the second derivative spectrum are poorly resolved and do not exhibit superhyperfine resolution. The relevant isotropic parameters ($g_{iso} = 2.132$; $A_{iso} = 58.3 \text{ G}$) well fit the liquid nitrogen temperature ones.

The EPR spectra of the copper perchlorate adducts are also axial with $g_{\parallel} > g_{\perp}$ suggestive of a d_{x-y} ground state. All the complexes exhibit very similar pattern [Figure 6] with three parallel lines and a broad line in the perpendicular region. It is surprising to note that there is no progressive decrease in the g_{\parallel} value or increase in the A_{\parallel} value on substitution by various electron rich nitrogen bases, as that

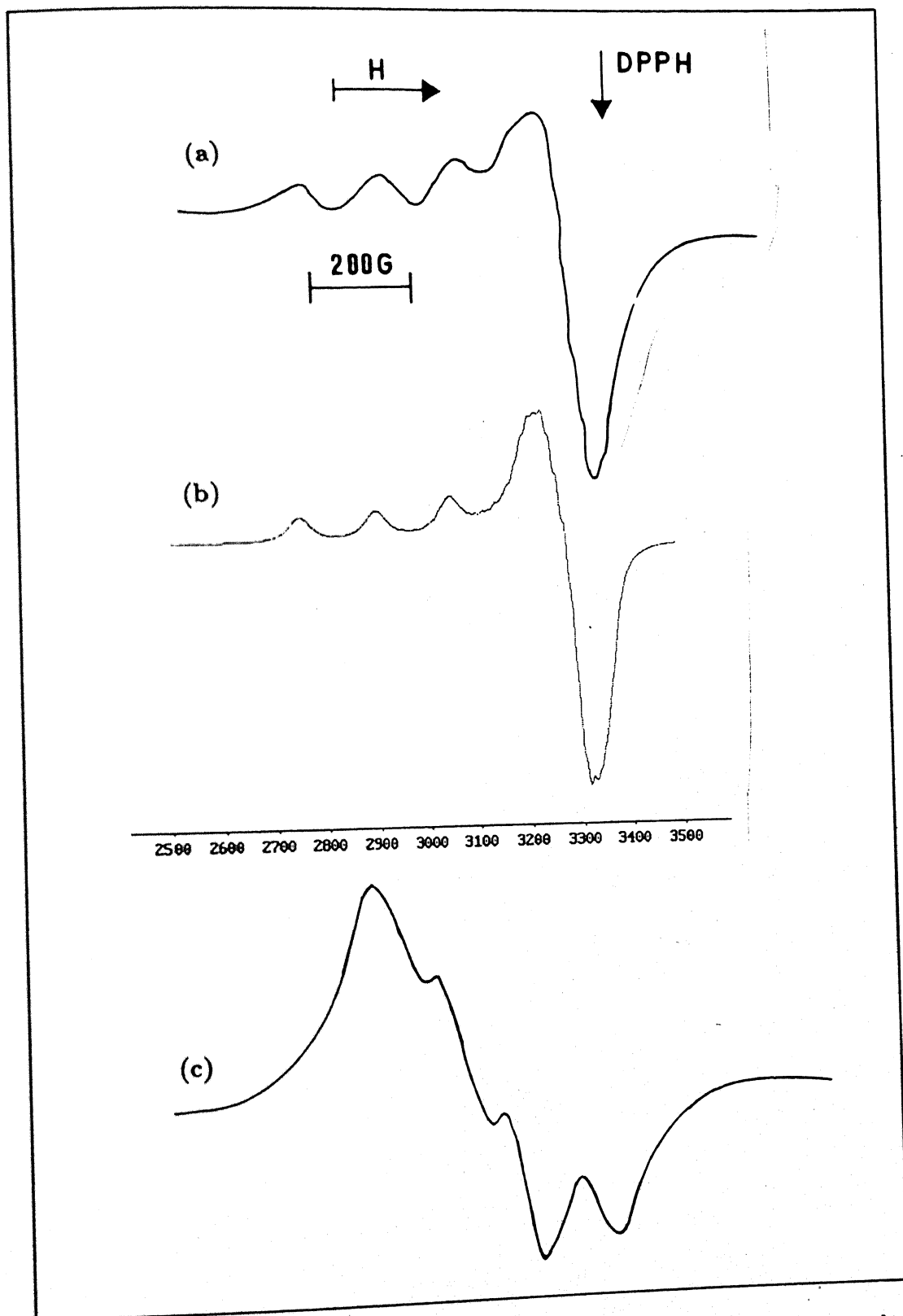


Figure 5: EPR spectra of $\text{tpctp} \cdot \text{PtCl}_2 \cdot \text{CuCl}_2$ in frozen [experimental (a), simulated (b)] and fluid (c) acetonitrile solutions

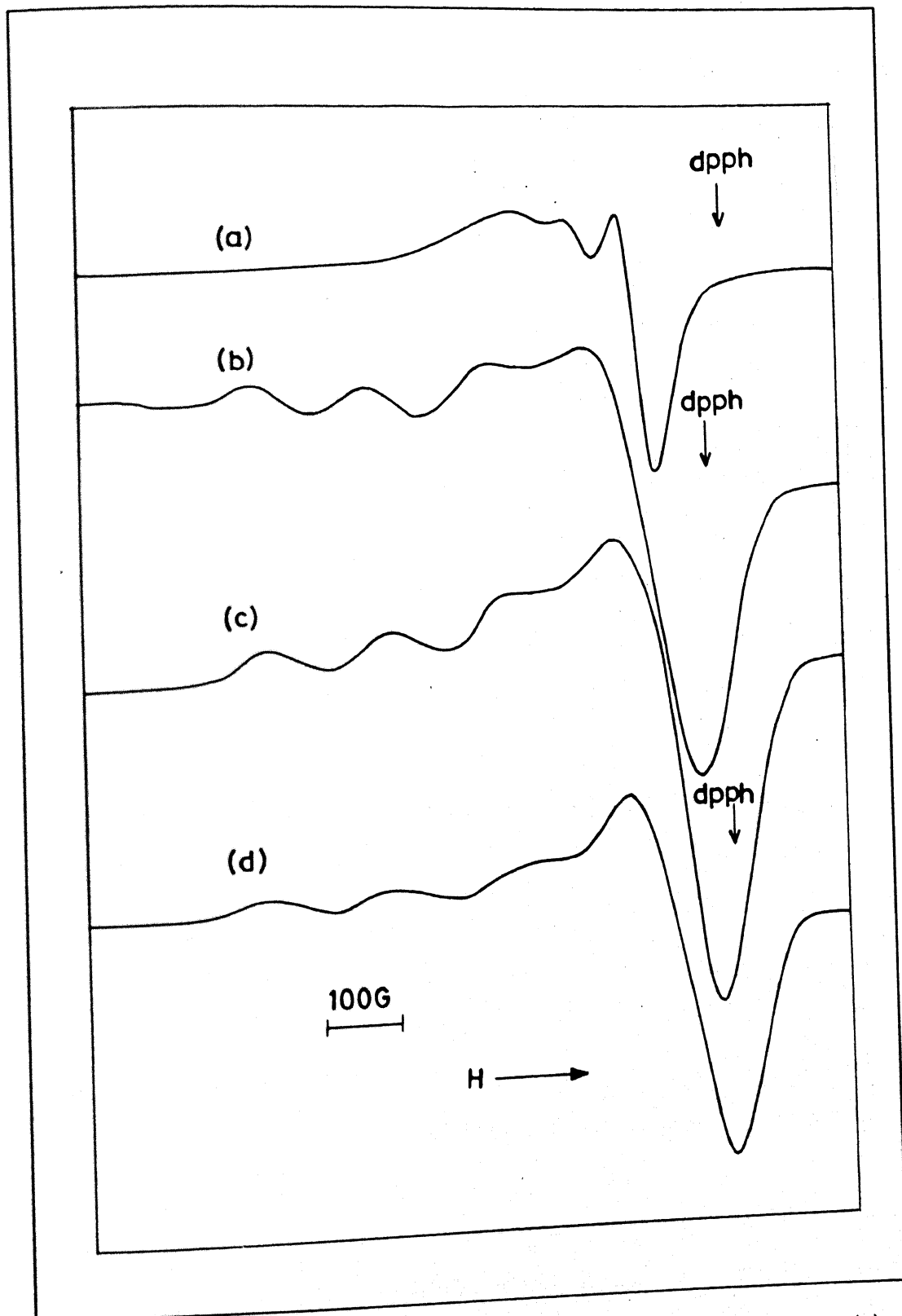


Figure 6: EPR spectra of $\text{tpctp} \cdot \text{Cu}(\text{ClO}_4)_2 \cdot 2\text{ImH}$ in acetonitrile [as fluid (a) and frozen (b) solutions] and in solid state (c) and $\text{tpctp} \cdot \text{Cu}(\text{ClO}_4)_2 \cdot \text{bipy}$ in solid state (d)

observed with tdpctp complexes. It is assumed that in tdpctp complexes the trends observed with the $g_{||}$ and $A_{||}$ values mainly arise due to the steric role played by the methyl substituents at the 3-position. Thus in the complexes $\text{tdpctp} \cdot \text{Cu}(\text{ClO}_4)_2 \cdot 2\text{NB}$ (NB=pyridine or imidazole) the 3-methyl groups of the pyrazolyl ring severely interact with the imidazole or pyridine molecules to result in considerable tetrahedral distortion and thus low $A_{||}$ values and higher $g_{||}$ values [15]. However, with bipyridine and phenanthroline adducts the rigidity of the exogenous ligands (bipyridine or phenanthroline) outweigh the steric encumbrance. Since this steric effect is no longer operative with tpctp the equatorial plane is not much distorted leading to high $A_{||}$ values irrespective of the complex. The $A_{||}$ and $g_{||}$ values match well with analogous tetragonal compounds reported in the literature [13,14] and it is suggested that these complexes possess a N_4 equatorial environment with weak axial interactions from cyclotriphosphazene nitrogens. The equatorial plane might be derived from nongeminal cis pyrazolyl groups of the ligand tpctp and two nitrogens from the exogenous bases such as imidazole, pyridine, bipyridine etc.

5.3.3 Electrochemistry of the heterodimetal complex tpctp $\text{PtCl}_2\text{CuCl}_2$

The unusual EPR spectral observations of the complex $\text{tpctp} \cdot \text{PtCl}_2 \cdot \text{CuCl}_2$ prompted us to investigate the electrochemical mechanism of it. The redox pattern exhibited by this heterodimetal complex is also very interesting. As illustrated in Figure 7, in acetonitrile solution it undergoes three subsequent cathodic steps at peaks A, B and C respectively. Controlled potential coulometric tests served to elucidate overall reduction path.

The catho-anodic peak-system A/G proved to involve a chemically reversible electron transfer, in that controlled potential electrolysis ($E_w = 0.0 \text{ V}$) consumes one electron per molecule. Concomitantly the initially EPR-active (see section 5.3.2), yellow-green solution turns colorless and EPR silent. Such final solution exhibits a cyclic

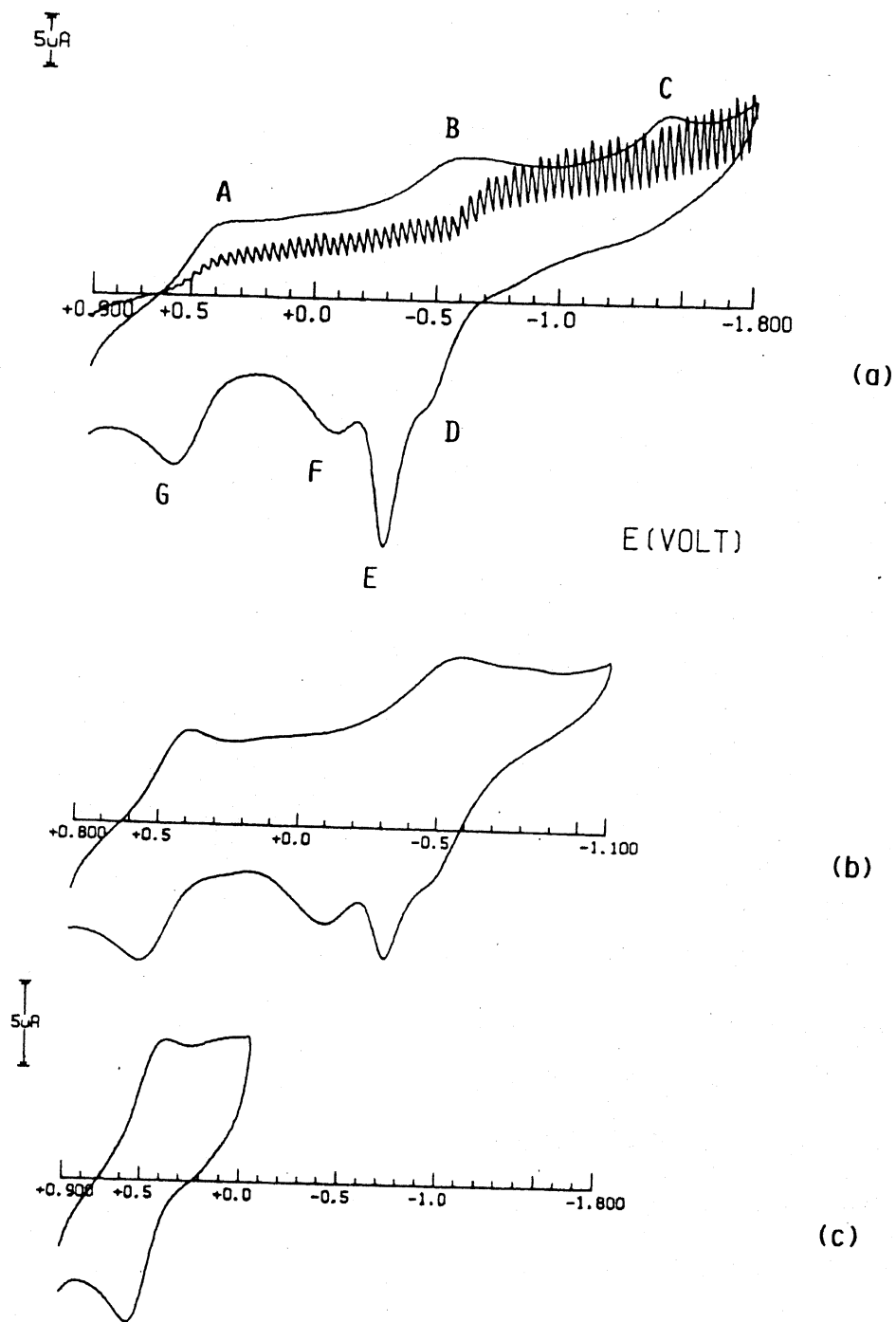
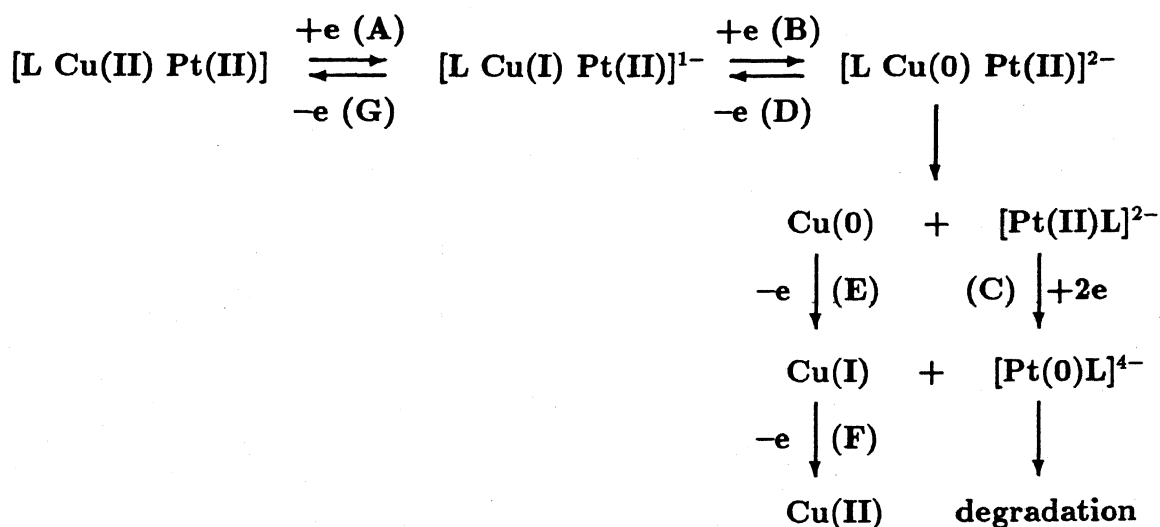


Figure 7: Cyclic voltammograms of $\text{tpctp-PtCl}_2\cdot\text{CuCl}_2$ in acetonitrile

voltammetric profile quite complementary to that illustrated in Figure 7c. Subsequent exhaustive one-electron reduction at the second cathodic step ($E_w = -1.0$ V) causes deposition of copper metal on the microelectrode surface. The resulting solution displays only the reduction process C, which we confidently assign to the reduction of the platinum(II) centre, in analogy with the results on the platinum complexes of tpctp and tdpctp. Upon reoxidation of the electrodeposited copper metal ($E_w = +0.6$ V), the solution restores the original voltammetric response shown in Figure 7. In summary, the overall redox propensity of complex tpctp·PtCl₂·CuCl₂ is so schematizable:



Finally a few points deserve comments. (i) The thermodynamically easy access to the Cu^IPt^{II}L (L=ligand) congener is quite uncommon, particularly when compared with the corresponding complex hdpctp·CuCl₂·PtCl₂, which under the same experimental conditions, undergoes the [Cu^{II}Pt^{II}L]/[Cu⁰Pt^{II}L]²⁻ reduction process through a single-stepped irreversible process ($E_p = -0.55$ V), without any stabilization of the intermediate mixed-valent species [Chapter 4]. This is likely attributable to the electronic factors arising from the substitution of two pyrazolyl groups for two electron-withdrawing phenyl groups and removal of methyl groups from 3- and 5-positions of pyrazole ring, which makes easier the addition of electrons. (ii) The analysis of the peak system A/G with scan rates varying from 0.02 Vs⁻¹ to 2 Vs⁻¹ shows

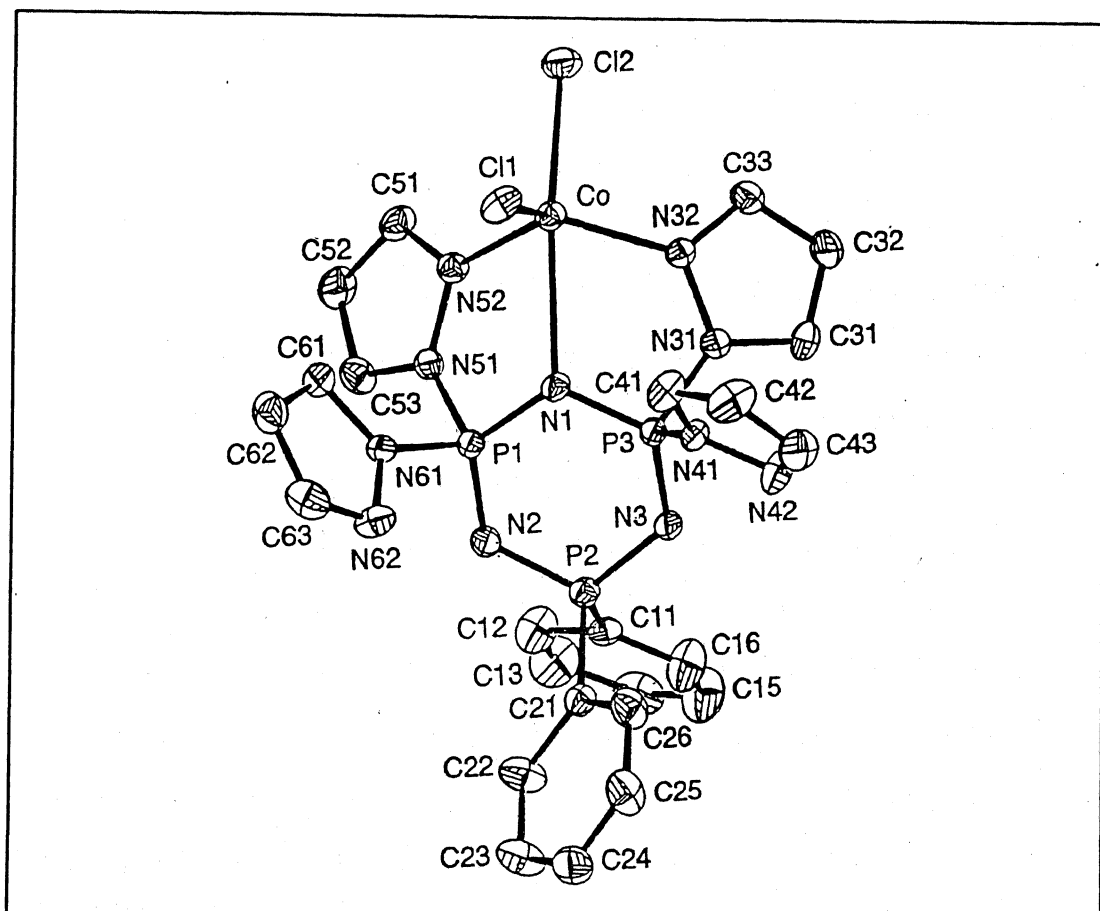


Figure 8: Perspective view of $\text{tpctp} \cdot \text{CoCl}_2 \cdot 0.5\text{CH}_2\text{Cl}_2$

that the peak-to-peak separation progressively increases from 140 mV to 315 mV. This high departure from the constant value of 59 mV expected for an electrochemically reversible one-electron transfer denotes that a considerable geometrical strain accompanies the $[\text{Cu}^{\text{II}}\text{Pt}^{\text{II}}\text{L}]/[\text{Cu}^0\text{Pt}^{\text{II}}\text{L}]^{2-}$ redox change [16].

5.3.4 Crystal structure of $\text{tpctp} \cdot \text{CoCl}_2 \cdot 0.5\text{CH}_2\text{Cl}_2$

The molecular geometry and the atom labelling scheme for the title complex is illustrated by Figure 8. The crystal data is given in Table 4.

The geometry around the cobalt is distorted trigonal bipyramidal with two nitrogen atoms from the nongeminal cis pyrazolyl groups, two chloride ions and one cyclotriphosphazene nitrogen. Interestingly the equatorial plane is constituted by two

nongeminal pyrazolyl nitrogens and one chlorine. The cobalt atom lies slightly out of the equatorial plane in the direction of the Cl(2) atom. The equatorial arrangement is in contradiction to the earlier observations with the ligands tdpctp and hdpctp. In the copper complexes of hdpctp and tdpctp the nongeminal pyrazolyl nitrogens occupied the axial positions thus leading to large N_{pz} -Cu- N_{pz} angle ($\sim 159^\circ$). In the present case the N_{pz} -Cu- N_{pz} angle is narrow and is significantly smaller ($114.03(14)^\circ$). This probably arises due to the absence of methyl groups at 3-position of pyrazolyl ring which generally prevent the formation of more tighter angle. The cyclotriphosphazene nitrogen-metal interaction is weak as is manifested in the long bond length of Co-N(1) [$2.419(3)\text{\AA}$]. This forms the longest M- N_{CTP} bond observed in the work contained in this thesis. The environment of the metal ion is significantly distorted from that of a regular trigonal bipyramid. The main axis [N(1)-Co-Cl(2)] is much deviated [$167.43(9)^\circ$] from the expected angle 180° . There is another evidence of distortion along the N(1)-Co-Cl(2) axis as the Co-Cl(2) bond is lengthened to $2.2859(15)\text{\AA}$ from $2.2709(14)\text{\AA}$ for the equatorial Co-Cl(1) bond. The occurrence of two different cobalt-nitrogen distances, namely Co- N_{pz} and Co- N_{CTP} , makes more evident this distortion. Significant deviations from idealized orthogonal geometry are found at the cobalt atom in the five-membered chelate rings CoN(1)P(1)N(51)N(52) and CoN(1)P(3)N(31)N(32), $77.30(13)^\circ$ and $75.85(13)^\circ$ for N(1)-Co-N(32) and N(1)-Co-N(52) respectively. The average Co- N_{pz} distance [$2.050(4)\text{\AA}$] is shorter than that observed for nickel complex tdpctp-NiCl₂ but greater than that of copper(II) complexes described in the earlier chapter. The selected bond angles and distances are tabulated in Table 5.

The pyrazolyl rings of the tpctp ligand are planar as expected with deviations from the mean planes not greater than 0.026\AA . However the cyclotriphosphazene ring conformation is nonplanar with the N(2) atom displaced -0.133\AA out of the plane defined by the remaining atoms, P(1), P(2), P(3), N(1) and N(3). The cyclotri-

Table 4: Crystal data for tpctp·CoCl₂·0.5CH₂Cl₂

formula	C ₂₄ H ₂₂ N ₁₁ P ₃ Cl ₂ Co·CH ₂ Cl ₂
fw	729.74
crystal size, mm	0.24 × 0.28 × 0.52
crystal color	dark blue
a, Å	11.002(3)
b, Å	11.669(3)
c, Å	12.941(2)
α, deg	92.96(2)
β, deg	94.96(2)
γ, deg	108.66(2)
V, Å ³	1563.8(6)
cell determination	
reflections	15
2θ angle, deg	18-20
d(calcd), gcm ⁻³	1.55
space group	P-1
Z	2
F(000)	739.82
linear abs. coeff., mm ⁻¹	0.993
scan technique	θ-2θ
scan speed, deg min ⁻¹	4-16
h, k, l ranges	0, 11; -12, 12; -13, 13
std. refl. indices	5, -3, 1; 4, -1, 3; -4, 1, -3
drift of stds, %	0.86
absorption range	0.782-0.833
refls measured	4319
unique reflections	4066
R for merge	0.015
data with I>3σ(I)	3038
parameters refined, GOF	383, 0.99
R(F ²), R _w (F ²)	0.036, 0.055
p, w ⁻¹ =[σ ² (I)+pI ²]/4F ²	0.05
largest Δ/σ	0.001
Final diff map, eÅ ⁻³	-0.74(6)+0.88(6)

Table 4: Selected interatomic distances in $\text{tpctp} \cdot \text{CoCl}_2 \cdot 0.5\text{CH}_2\text{Cl}_2$

<u>metal environment</u>			
Co-Cl(1)	2.2709(14)	Cl(1)-Co-Cl(2)	106.44(5)
Co-Cl(2)	2.2859(14)	Cl(1)-Co-N(1)	85.98(9)
Co-N(1)	2.419(3)	Cl(1)-Co-N(32)	113.74(11)
Co-N(32)	2.038(4)	Cl(1)-Co-N(52)	122.90(11)
Co-N(52)	2.062(4)	Cl(2)-Co-N(1)	167.43(9)
Cl(2)-Co-N(32)	98.42(11)	Cl(2)-Co-N(52)	95.57(11)
N(1)-Co-N(32)	77.30(13)	N(1)-Co-N(52)	75.85(13)
N(32)-Co-N(52)	114.03(14)		
<u>phosphazene ring</u>			
P(1)-N(1)	1.586(3)	N(1)-P(1)-N(2)	121.16(19)
P(1)-N(2)	1.548(4)	N(2)-P(2)-N(3)	115.03(19)
P(2)-N(2)	1.621(4)	N(1)-P(3)-N(3)	119.94(18)
P(2)-N(3)	1.615(4)	P(1)-N(1)-P(3)	118.64(21)
P(3)-N(1)	1.592(4)	P(1)-N(2)-P(2)	121.25(22)
P(3)-N(3)	1.551(4)	P(2)-N(3)-P(3)	122.74(23)
mean values:		N(31)-P(3)-N(41)	99.58(17)
P-N _{exo}	1.687(4)	N(51)-P(1)-N(61)	101.47(18)
P-C _{exo}	1.791(5)	C(11)-P(2)-N(21)	105.78(20)

phosphazene skeletal nitrogen participation in coordination affects the P-N bonds at the P(1)-N(1)Co-P(3) segment leading to the weakening of them as compared to the adjacent ones. The P-N bonds [P(2)-N(2) and P(2)-N(3)], associated with the phosphorus containing the phenyl groups are found to be longer [av. 1.618(4)Å] than the analogous bond in the coordination compounds derived from tdpctp ligand.

5.4 Conclusion

The ligand tpctp act as a tridentate ligand coordinating through two nongeminal pyrazolyl nitrogens and one cyclotriphosphazene nitrogen, as confirmed by the crystal structure determination of $\text{tpctp} \cdot \text{CoCl}_2 \cdot 0.5\text{CH}_2\text{Cl}_2$. In the hpctp complexes also the ligand is believed to interact with the metal *via* N_3 donor set comprising two nongeminal pyrazolyl nitrogens and one cyclotriphosphazene nitrogen. But presence of too many coordinating sites and lack of steric crowding at the metal centre of resulting complexes lead to insoluble polymeric species. The principal effect of methyl substituent at 3-position of pyrazolyl ring is two fold. (i) It prevents the formation of ligand bridged polymeric compounds. (ii) Removal of methyl groups at 3-position makes the cyclotriphosphazene nitrogen less basic by electronic influence and is manifested in the longer $\text{Co}-\text{N}_{CTP}$ bond distance. Also from electrochemical studies it is inferred that less electronegative non-methylated pyrazolyl group coordination facilitates the easy addition of electron onto the metal, thus, resulting in a redox flexible system.

Although tdpctp and tpctp are very similar except for methyl substituents at pyrazolyl ring, the complex forming behavior is rather different. Electronic influence as well as steric hindrance may play a role in the observed differences, particularly formation of complex with ligand to metal ratio 2:1 from tpctp is a clear result of the absence of steric encumbrance. Large tetrahedral distortion seen in the tetragonal complexes of the type $\text{tdpctp} \cdot \text{Cu}(\text{ClO}_4)_2 \cdot 2\text{EL}$ where EL=exogenous nitrogen bases is virtually absent in the analogous complexes of tpctp as identified by spectral methods (optical and EPR). This also possibly originates from steric effects.

The coordination geometries of the metal ion in the metal(II) halide complexes of tpctp and in the methylated analogue tdpctp are same (trigonal bipyramidal) but the arrangement of donors is significantly different. Thus in $\text{tpctp} \cdot \text{CoCl}_2 \cdot 0.5\text{CH}_2\text{Cl}_2$ the pyrazolyl nitrogens occupy equatorial positions and make smaller $\text{N}_{pz}-\text{Co}-\text{N}_{pz}$

- [15] Sakaguchi, U. and Addison, A.W. *J. Chem. Soc. Dalton Trans*, **1979**, 600.
- [16] Zanello, P. In *Stereochemistry of Organometallic and Inorganic Compounds*, Ed. Bernal, I., Elsevier, Amsterdam, 1990, vol. 4, pp. 181.

Increasing the Spacer Length Between the Pyrazolyl Group and Cyclotriphosphazene Ring to Maximize Flexibility

"Chaos is not at all a bad order because even though nothing can be found, nothing can be lost, either"

–Julian Perkal

6.1 Introduction

The rich nucleophilic substitution reaction pathways encountered with the halogeno-cyclotriphosphazenes [1-3] pave the way for numerous side groups to be incorporated in cyclotriphosphazene skeleton without much difficulty. In the last two chapters we have described the ligands containing pyrazolyl groups directly attached to the cyclotriphosphazene skeleton *via* phosphorus and their coordination compounds. There we found that the metals such as copper, cobalt and nickel accept a N_3 donor set, which is derived from two pyrazolyl groups and one cyclotriphosphazene ring nitrogen, from the ligand. Though the metal interaction with the cyclotriphosphazene ring nitrogen is weak, as reflected in the longer $Cu-N_{CTP}$ bond distances, it is pivotal in fixing the geometry of the complexes. It is felt that, by inserting an alkoxy chain between the pyrazolyl group and the cyclotriphosphazene skeletal phosphorus the flexibility of the ligand may be further enhanced.

To study the influence of enlargement of the chain between the pyrazolyl and cyclophosphazene nitrogens we have first planned to synthesize two ligands, a hypothetical hexakis(1-(oxidomethyl)-3,5-dimethyl)pyrazolylcyclotriphosphazene (homdpctp) and hexakis(1-(2-oxidoethyl)-3,5-dimethyl)pyrazolylcyclotriphosphazene (hoedpctp). The former ligand could not be synthesized from any synthetic methods starting from 1-(hydroxymethyl)-3,5-dimethylpyrazole and $\text{N}_3\text{P}_3\text{Cl}_6$ for the reasons discussed in the following section. In contrast, hoedpctp have been obtained in high yield and its ligating properties evaluated. In this chapter the copper and cobalt complexes of the ligand hoedpctp will be discussed. The schematic drawing of hoedpctp is given in Figure 1.

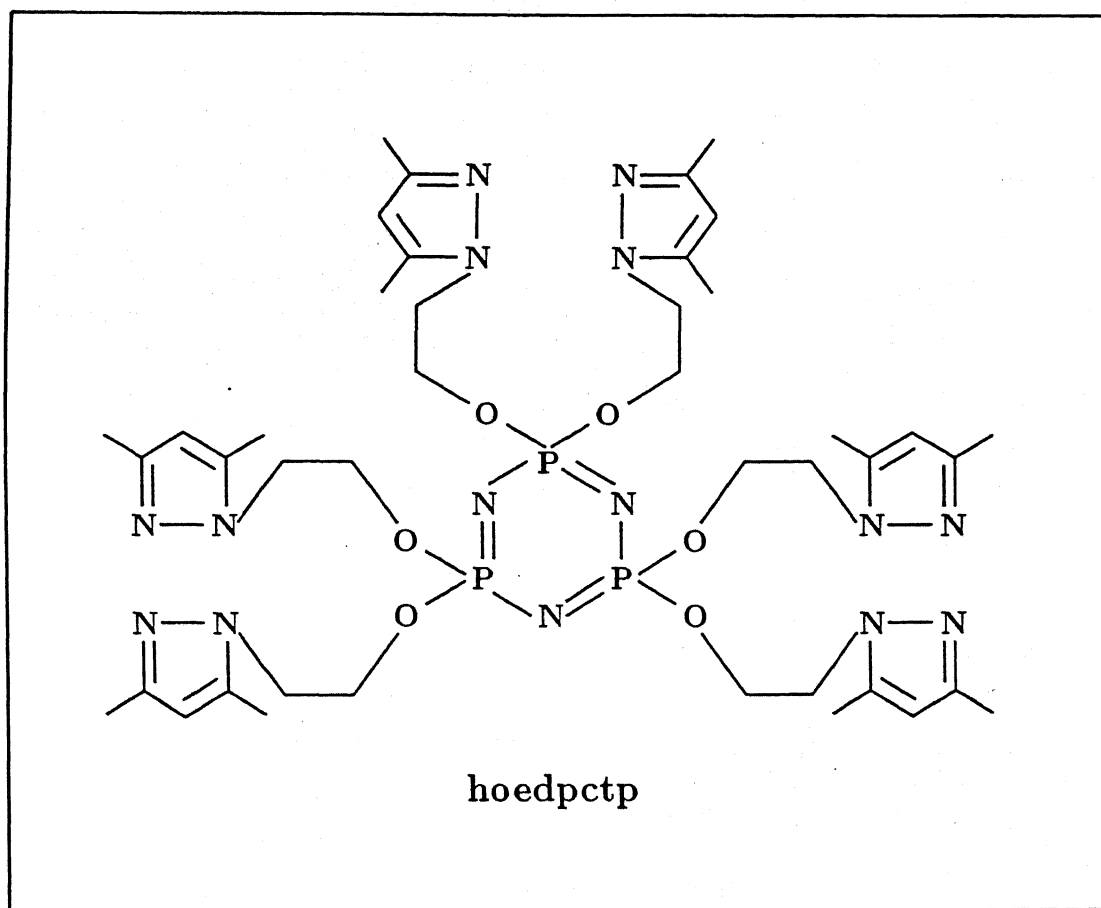


Figure 1: Line diagram of the ligand hoedpctp

6.2 Synthesis of the Ligand

At first we have tried to condense the 1-(hydroxymethyl)-3,5-dimethylpyrazole with the hexachlorocyclotriphosphazene to obtain homdpctp. Unfortunately the reactions in the presence of either triethylamine or NaH failed to proceed in the expected direction (Figure 2). Indeed, in this reactions hexakis(3,5-dimethylpyrazoly)cyclotriphosphazene, hdpctp has been isolated as a sole product. The identity of the product was established on the basis of mixed melting point with the authentic sample, ^1H and ^{31}P NMR spectra. This difficulty in the preparation of homdpctp using the above methods which mandate strong basic conditions is not surprising. The 1-(hydroxymethyl) pyrazoles are generally considered as mere hydrogen bonded adducts of pyrazoles with formaldehyde [4]. And the reactions of 1-(hydroxymethyl) pyrazoles with the divalent transition metal ions under basic conditions lead to extrusion of formaldehyde and formation of $[\text{M}(\text{Pz})_2]_n$ polymers [5,6]. With this supporting

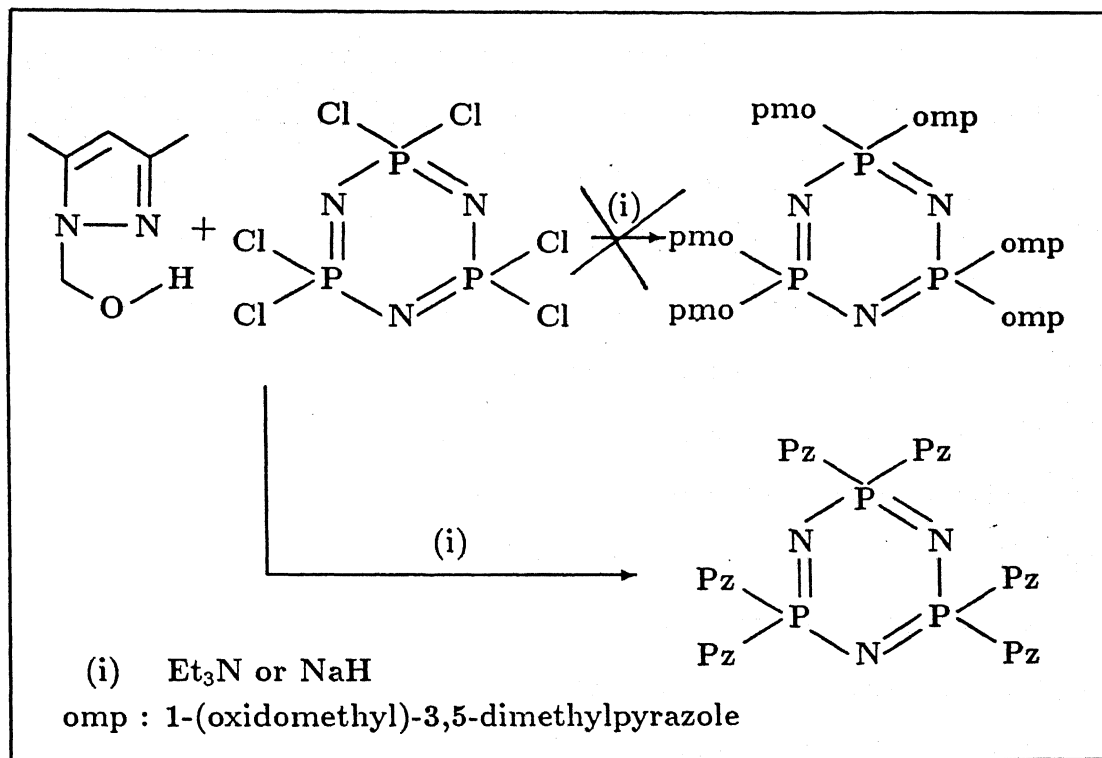
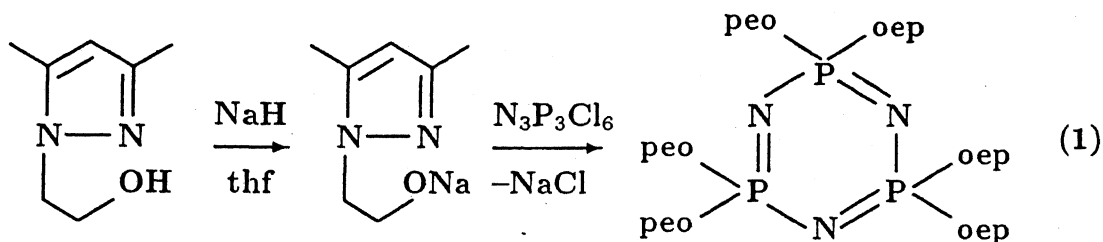


Figure 2: Reaction of 1-(hydroxymethyl)-3,5-dimethylpyrazole with $\text{N}_3\text{P}_3\text{Cl}_6$

literature evidence we strongly feel that in the present case also the same mechanism is operating and leads to the formation of hdpctp. Similar difficulties have also been experienced in the reaction of 4-(hydroxymethyl) isooxazoles with $N_3P_3Cl_6$ but for slightly different reasons [7].

The reaction of 1-(2-hydroxyethyl)-3,5-dimethylpyrazole with $N_3P_3Cl_6$ is quite smooth and yields the desired ligand hoedpctp as outlined in Equation 1.



The ligand structure was established by the combined use of multinuclear NMR, mass spectrometry and elemental analyses. In the ^{31}P NMR spectrum observation of a lone sharp singlet at 17.5 ppm is consistent with the complete substitution of chlorines. Incomplete substitution would have resulted in a AX_2 or other complicated pattern in the ^{31}P NMR [2]. The proton NMR confirms that the ethyloxy chain is intact in the product and no decomposition had occurred as that with the 1-(hydroxymethyl)-3,5-dimethylpyrazole. A multiplet corresponding to the two CH_2 groups is seen at around 4.03 ppm while the 3- and 5-methyl groups in the pyrazole resonate at 2.13 ppm as a doublet as that of the starting 1-(2-hydroxyethyl)-3,5-dimethylpyrazole [8]. The protons (4-CH) attached to the pyrazolyl nuclei is located as a singlet at 5.74 ppm. The ^{13}C and ^{31}P (inset) NMR spectra are displayed in Figure 3. The $-NCH_2$ and $-OCH_2$ carbons resonate at 48.0 and 64.7 ppm respectively. The Fast Atom Bombardment mass spectrometry indicate an molecular ion corresponding to $[hoedpctpH_2]^+$ (m/z 971, 88%). The other prominent peaks are attributed to the fragments $[N_3P_3(oep)_5OH_3]^+$ (m/z 849, 25%), $[N_3P_3(oep)_5H_2]^+$ (m/z 832, 20%),

$[\text{N}_3\text{P}_3(\text{oep})_4\text{OH}]^+$ (m/z 708, 7%) and $[\text{Hoep}]^+$ (m/z 124, 100%). All this data substantiates that the reaction of 1-(2-hydroxymethyl)-3,5-dimethylpyrazole with $\text{N}_3\text{P}_3\text{Cl}_6$ has produced the desired ligand hoedpctp.

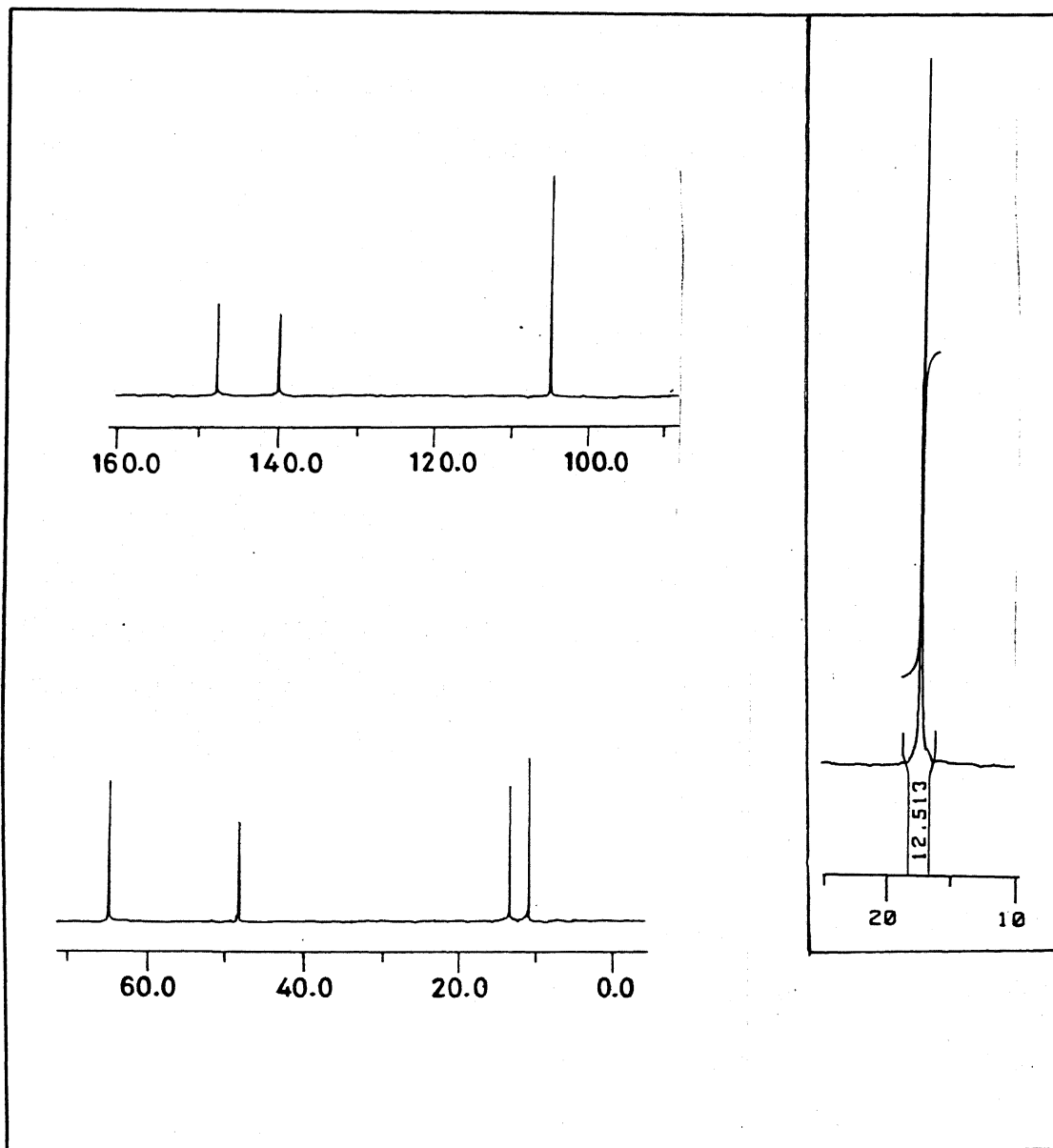


Figure 3: ^{13}C and ^{31}P (inset) NMR spectra of the ligand hoedpctp at 400 MHz

6.3 Coordination compounds of hoedpctp and their spectroscopic features

6.3.2 General

In the ligand hoedpctp the pyrazolyl groups are linked to the cyclotriphosphazene skeleton through an ethyloxy chain. It was envisaged that, as the pyrazolyl groups are separated from the cyclotriphosphazene nitrogen because of the intervening ethyloxy spacer, simultaneous coordination of both the inorganic and organic ring nitrogens to metal is unlikely. Such a nongeminal N_3 coordination would result in unstable eight-membered chelate rings. Also the geminal N_2 coordination is improbable as it involves a metallocycle consisting of twelve atoms. Alternatively hoedpctp may lead to a novel capping tridentate N_3 coordination with the three nongeminal cis-pyrazolyl groups forming the coordination sphere. Weak interactions from oxygens might stabilize these chelates.

The ligand hoedpctp forms dinuclear complexes with copper, cobalt, zinc and platinum salts. At room temperature this ligand does not form complexes with nickel salts. Similarly no mononuclear complexes could be isolated with this ligand. Harsh condition reactions have not been tried as it was feared that the resulting complex

Table 1: Color, nature, magnetic moment and EPR and conductivity data of the hoedpctp complexes.

compound	color	nature	EPR/ g_{iso}	Λ_m^a	μ_M (BM)
hoedpctp-2CuCl ₂	green	amorphous	2.134	25	1.78
hoedpctp-2CuBr ₂	brown	amorphous	2.128	48	1.81
hoedpctp-2Cu(ClO ₄) ₂ ·4H ₂ O	green	amorphous	2.164	460	1.92
hoedpctp-2CoCl ₂	blue	amorphous	—	12	4.96

^aunits (mho cm² mol⁻¹)

may decompose under high temperatures. The complexes of hoedpctp decompose when heated above 60°C. The selective formation of the dinuclear compounds exposes the flexibility of the ligand. The summary of the coordination complexes together with their color, nature, magnetic moment and conductivity and EPR data is given in Table 1.

6.3.3 IR spectroscopy

IR spectroscopy can be utilized to identify the interaction of cyclophosphazene ring nitrogen with the transition metals. The metallated or protonated cyclophosphazenes exhibit a split in the band corresponding to the P=N stretching mode. To account this it is postulated that the metal coordination or protonation to nitrogen makes the lone pair of electrons that reside on that nitrogen unavailable for skeletal π -bonding and weakens the associated P=N bonds [9]. Interestingly all the complexes of hoedpctp listed in Table 1 show a characteristic unsplit, strong and broad band at ca. 1240 cm^{-1} very identical to the one observed for the free ligand (1235 cm^{-1}). This clearly suggests that in these complexes cyclophosphazene nitrogen is not at all interacting with the metals. The band attributed to C=N stretching frequency is slightly shifted to high energy ($\sim 10\text{ cm}^{-1}$) when compared to the analogous band observed for the free ligand, indicating that the pyrazolyl pyridinic nitrogens are involved in strong interaction with the metal ions [10]. In the IR spectrum of the complex $\text{hoedpctp}\cdot 2\text{Cu}(\text{ClO}_4)_2\cdot 2\text{H}_2\text{O}$ occurrence of a broad band at 3350 cm^{-1} confirms the presence of hydrogen bonded water molecules. However, paradoxically sharp wagging mode at $1600\text{--}1650\text{ cm}^{-1}$ attributable to the coordinated water molecule is not seen. Absence of this band may not preclude the possibility of the water molecules to be present in the coordination sphere [11]. The observation of broad ν_3 doublet at 1100 cm^{-1} slightly overlapped with the P-O stretching band ($\sim 1050\text{ cm}^{-1}$) and a sharp singlet at 620 cm^{-1} points out the presence of coordinated and uncoordinated

perchlorate anions [10,12]. On this basis it is assumed that in this complex each copper is coordinated to two aquo ligands and one perchlorate anion and the other perchlorate anion resides outside the coordination sphere in the solid state. However, in acetonitrile solution the perchlorate anions are replaced by solvent molecule to result in a 1:4 electrolyte [13] consistent with the conductivity data (Table 1).

6.3.3 Optical absorption spectroscopy

The electronic spectral data in the UV-Vis region for the hoedpctp ligand complexes recorded for the dichloromethane solution are listed in Table 2 along with the tentative assignments. Figure 4 displays the representative spectra for hoedpctp·2CuCl₂, also shown in the inset is the absorption spectra for the free ligand.

It is evident from the free ligand spectrum that the high energy transition observed for the complexes belongs to the $\pi-\pi^*$ intraligand transition. The bands at ca. 270 and 360 nm are attributed to the Pz \rightarrow Cu ligand to metal charge transfer transition [14]. However, for the complex hoedpctp·2CuCl₂ the intensity of the band at 282 nm is nearly twice than that calculated for the remaining compounds. This suggests that it includes the contribution from the Cl \rightarrow Cu l.m.c.t. The addition charge transfer transition observed for the bromo analogue hoedpctp·2CuBr₂ at 420 nm is assigned to the Br \rightarrow Cu l.m.c.t. [15]. The d-d bands for the complexes hoedpctp·2CuCl₂ (X=Cl, Br) are illuminating in the sense that the band pattern and intensity resembles those of the similar complexes derived from the hdpctp and tdpctp ligands and indicate a N₃Cl₂ chromophore with the distorted trigonal bipyramidal geometry. A slight high energy shift in the band maximum of these complexes is noticed when compared to those of hdpctp and tdpctp complexes. This may be ascribed to the involvement of three pyrazolyl pyridinic nitrogens in coordination which would render a relatively strong ligand field than the one arising from two pyrazolyl and one cyclotriphosphazene skeletal nitrogens. The d-d band of the copper(ii) perchlorate hexahydrate

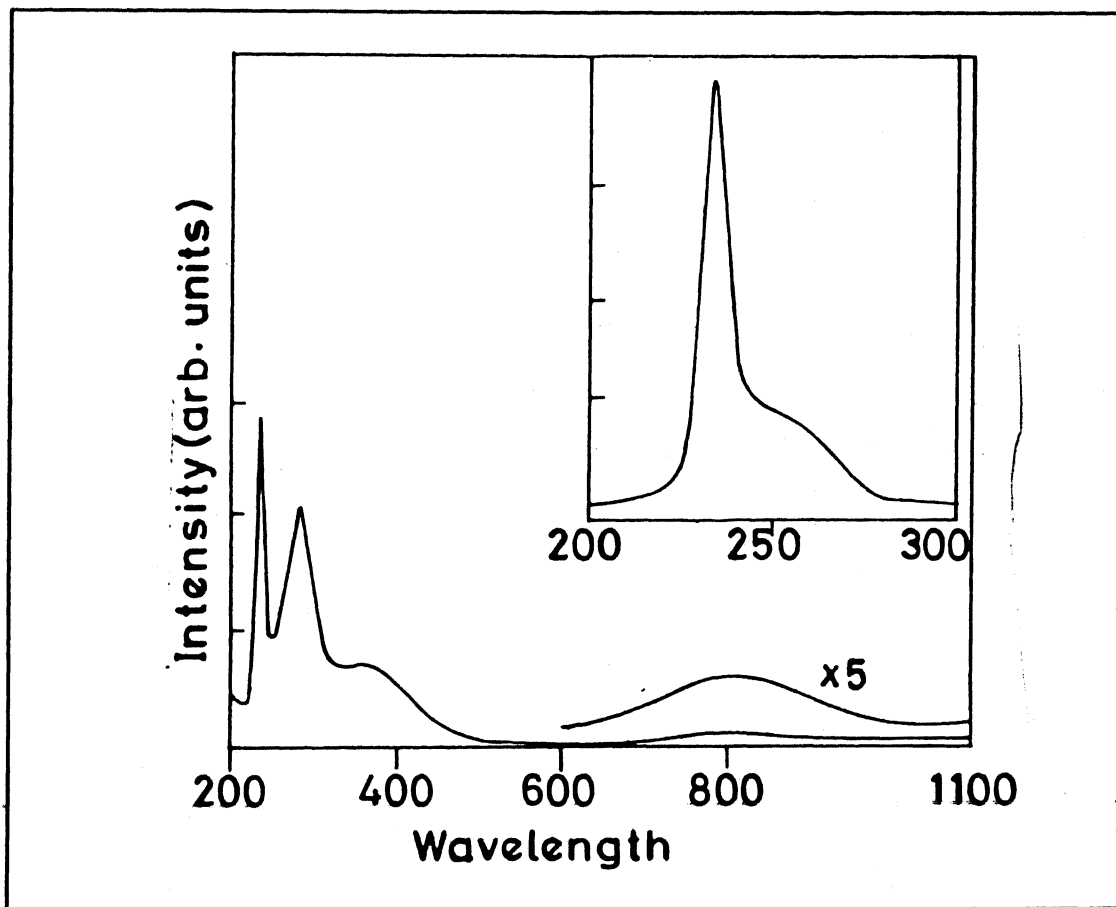


Figure 4: Optical Spectra of the complex $\text{hoedpctp} \cdot 2\text{CuCl}_2$ and hoedpctp (inset)

derived complex $\text{hoedpctp} \cdot 2\text{Cu}(\text{ClO}_4)_2 \cdot 4\text{H}_2\text{O}$ is suggestive of a distorted octahedral environment to the copper [16]. The cobalt complex, $\text{hoedpctp} \cdot 2\text{CoCl}_2$ shows two d-d bands at 583 and 645 nm with one high energy shoulder in the 645 nm band. An intense band at around 620 nm is identified as diagnostic of a high-spin Co(II) in trigonal bipyramidal geometry [17]. The observation of high energy shoulder may be interpreted as the distortion of the chromophore from the perfect trigonal bipyramidal geometry [18].

Table 2: Electronic spectral data for the metal complexes of hoedpctp

compound	λ_{max} (ϵ_{max}) ^a	assignment
hoedpctp	233(10.2)	$\pi-\pi^*$ transition
	255sh	n- π^* transition
hoedpctp·2CuCl ₂	234(10.25)	$\pi-\pi^*$ transition
	282 (6.54)	Cl \rightarrow Cu l.m.c.t.
		Pz \rightarrow Cu l.m.c.t.
	362 (2.34)	Pz \rightarrow Cu l.m.c.t.
	795 (0.24)	d-d
hoedpctp·2CuBr ₂	233(10.31)	$\pi-\pi^*$ transition
	280 (3.45)	Pz \rightarrow Cu l.m.c.t.
	365 (2.18)	Pz \rightarrow Cu l.m.c.t.
	420 (3.87)	Br \rightarrow Cu l.m.c.t.
	810 (0.24)	d-d
hoedpctp·2Cu(ClO ₄) ₂ ·4H ₂ O	236(10.30)	$\pi-\pi^*$ transition
	272 (2.85)	Pz \rightarrow Cu l.m.c.t.
	360 (2.07)	Pz \rightarrow Cu l.m.c.t.
	739 (0.14)	d-d
hoedpctp·2CoCl ₂	237(12.15)	$\pi-\pi^*$ transition
	260sh	Pz \rightarrow Cu l.m.c.t.
	583 (0.08)	d-d
	620sh	d-d
	645 (0.16)	d-d

^a units: λ_{max} in nm and ϵ_{max} in mol⁻¹ cm⁻¹ $\times 10^3$

6.3.4 Magnetic moment and EPR spectroscopy

The magnetic moments computed by adopting Evans NMR method for the dichloromethane solution and EPR parameters for the powder sample of the complexes are included in Table 1. The magnetic moment per metal for the copper and cobalt complexes of hoedpctp is consistent with the expected values for spin states with S=1/2

and 3/2 respectively [18, 19] and rules out any significant intramolecular magnetic interaction between the metal centres mediated by the bridging ligand. Probably the N_3 donation by three nongeminal cis-pyrazolyl groups keeps the metal atoms with a rather long interatomic distance. The EPR spectra of the copper complexes are isotropic and less informative. No hyperfine splitting is observed and the peaks are relatively sharp apparently arising from the weak intermolecular exchange coupling [16, 19].

To get further insight into the structure of the complexes, we have attempted to grow x-ray quality single crystals of the above compounds. Our efforts in this direction have not been fruitful. Therefore, no exact conclusions about the geometry of these complexes can be drawn in the absence of a firm x-ray evidence. However, the isomorphous IR patterns of the copper and cobalt halide complexes strongly support a proposal of similar structure for them. On the basis of the above description on the spectroscopic properties we prefer to propose that the metals solicit a N_3 donor set from the ligand hoedpctp comprising three nongeminal cis-pyrazolyl groups. Thus it is likely that two metals may reside above and below the plane passing through the cyclotriphosphazene (P_3N_3) ring of the ligand and lead to a sandwich type complexes.

6.4 Concluding remarks

Hoedpctp a potential multidentate ligand containing six 1-(2-oxidoethyl)-3,5-dimethylpyrazole arms have been shown to form dinuclear complexes with copper and cobalt salts. The complexes have been isolated as air stable solids and their spectroscopic properties have been investigated. It appears from the stoichiometry and spectroscopic evidences that the complexes derived from the metal(II) halides are pentacoordinate with the probable geometry distorted trigonal bipyramid, while the copper in the complex containing perchlorate counter anions, $\text{hoedpctp} \cdot 2\text{Cu}(\text{ClO}_4)_2 \cdot 4\text{H}_2\text{O}$ may exist in a distorted octahedral environment.

Preliminary results of the studies related to the use of hoedpctp as a separation agent for the removal of metal ions from dilute solutions indicate that hoedpctp can be used to extract copper ions selectively from a mixture of first transition metal ions. This sets a stage for future application of this system in chelation chemistry or hazardous waste clean-up, which is the central task now-a-days.

References

- [1] Allen, C.W. *Chem. Rev.*, **1991**, *91*, 133.
- [2] Krishnamurthy, S.S., Sau, A.C. and Woods, M. *Adv. Inorg. Chem. Radiochem.*, **1978**, *21*, 41.
- [3] Shaw, R.A. *Phosphorus, Sulfur, Silicon*, **1989**, *45*, 103.
- [4] Hüttel, R. and Jochum, P. *Chem. Ber.*, **1952**, *85*, 820.
- [5] Trofimenko, S. *Chem. Rev.*, **1972**, *72*, 497.
- [6] Paap, F., Bouwman, E., Driessen, W.L., de Graff, R.A.G. and Reedijk, J. *J. Chem. Soc. Dalton Trans.*, **1985**, 737.
- [7] Munsey, M.S. and Natale, N.R. *Heterocycles*, **1990**, *31*, 851.
- [8] Haanstra, W.G., Driessen, W.L., Reedijk, J., Turpeinen, U. and Hämäläinen, G. *J. Chem. Soc. Dalton Trans.*, **1989**, 2309.
- [9] Shaw, R.A. *Z. Naturforsch.*, **1976**, *31b*, 641.
- [10] Nakamoto, K. *Infrared and Raman Spectra of Inorganic and Coordination Compounds*, 4th Ed., Wiley-Interscience, New York, 1986.
- [11] Bouwman, E. Ph.D. Thesis, Leiden University, Leiden, The Netherlands.
- [12] Thompson, L.K., Ramaswamy, B.S. and Dawe, R.D. *Can. J. Chem.*, **1978**, *56*, 1311.
- [13] Geary, W.J. *Coord. Chem. Rev.*, **1971**, *7*, 81.
- [14] Bernarducci, E., Schwindinger, W.E., Hughey IV, J.L., Krogh-Jespersen, K. and Schugar, H.J. *J. Am. Chem. Soc.*, **1981**, *103*, 1686.

- [15] Lever, A.B.P. *Inorganic Electronic Spectroscopy*, 2nd Ed., Elsevier, Amsterdam, 1984.
- [16] Hathaway, B.J. *Struct. Bonding (Berlin)*, 1984, 57, 55.
- [17] Ciampolini, M. *Struct. Bonding (Berlin)*, 1969, 6, 52.
- [18] Banci, L., Bencini, A., Benelli, C., Gatteschi, D. and Zanchini, G. *Struct. Bonding (Berlin)*, 1982, 52, 37.
- [19] Hathaway, B.J. and Billing, D.E. *Coord. Chem. Rev.*, 1970, 5, 143.

Coordination Chemistry of Pyrazolylcyclotriphosphazenes: Summary and future prospects

"Science arises from the discovery of identity amidst diversity"

–William Stanley Jevons in

The Principles of Science, Chapter I, 1874.

7.1 Introduction

From the bulk of the discussion contained in the last three chapters it is abundantly evident that the pyrazolylcyclotriphosphazenes proved to be a novel class of ligands, possessing multiple donor sites, yet, selectively coordinate to the metals. The facile preparative procedures make them unique and easily accessible for studying their coordination properties. We have succeeded in evaluating the following factors:

- △ When and how both the pyrazolyl (exocyclic donor group) and cyclotriphosphazene nitrogens interact in concert with the transition metals.
- △ How many exocyclic donor groups are necessary to use the cyclotriphosphazenes as transition metal carriers for specific purposes.
- △ The competition between multi-variant donor substituents on cyclotriphosphazene skeleton for metals and their significance.
- △ Electronic and steric effects of the substituents on the exocyclic donor groups.

A brief summary of the results will be presented in this chapter.

7.2 The number and nature of exocyclic donor groups

Irrespective of the number of pyrazolyl groups present in the cyclotriphosphazene skeleton the metals such as copper, cobalt and nickel prefer to bind through two nongeminal pyrazolyl and one cyclotriphosphazene nitrogens, and the pyrazolyl groups are cis oriented. Earlier Paddock and coworkers [1] have demonstrated an involvement of two geminal pyrazolyl nitrogens in coordination to metals such as platinum and palladium. This difference mainly arises from the strong preference of platinum and palladium to achieve lower coordination (4-coordinated, square planar).

The presence of too many coordination sites complicates the coordination behavior of the hexa-substituted pyrazolylcyclotriphosphazenes (hdpctp and hpctp) particularly towards nickel. The multi-directional coordination response leads to intermolecularly bridged insoluble derivatives with nickel salts. This effect is more pronounced when the methyl substituents on the pyrazolyl rings are absent. However, with tetra-substituted pyrazolylcyclotriphosphazene (tdpctp) nickel salts result in complexes with trigonal bipyramidal structures.

The idealized geometries for copper ion, the tetragonal octahedron and the square plane, supplement a basic four-coordination: the former by semi-coordination and the latter by π -bonding. This potential for further bonding above four coordination could equally be satisfied by the formation of a five-coordinate complex. The copper(II) ion can form both trigonal bipyramidal and square based pyramidal complexes, especially the latter [2]. The former structure frequently arises where there are particular geometric factors present. The pyrazolylcyclotriphosphazenes form stable copper complexes with varying stereochemistries depending on the nature of the additional ligands or counter anions. In the copper(II) halide complexes the copper exists in a distorted trigonal bipyramidal geometry with the equatorial positions occupied by one cyclotriphosphazene nitrogen and two halide ions. The pyrazolyl nitrogens occupy ax-

ial positions. When the counter anion is perchlorate the concept of semi-coordination stabilizes the octahedral complex with two additional water molecules. However, the bulky nitrogenous bases prevent the approach of the sixth ligand through the axial site and pave way to square based pyramidal structures where the fifth position is occupied by a weakly interacting cyclotriphosphazene ring nitrogen. It is interesting to note that the hexa-substituted pyrazolylcyclotriphosphazene, hdpctp interacts with the copper salts in a stepwise fashion. Thus, it has lead to the formation of both mononuclear $[\text{hdpctp} \cdot \text{CuX}_2 \text{ (X=Cl, Br, ClO}_4)]$ and dinuclear complexes $[\text{hdpctp} \cdot 2\text{CuX}_2 \text{ (X=Cl, Br)}]$. The mononuclear complexes contained several non-interacting donor sites which set stage for the preparation of heterobimetallic compounds. When treated with platinum or palladium salts they produce bimetallics with Cu-Pt or Cu-Pd centres. The square planar geometry around platinum or palladium has been confirmed by single crystal structure determination of a representative derivative, $\text{hdpctp} \cdot \text{CuCl}_2 \cdot \text{PtCl}_2$. Unusually, in these reactions a halide exchange has also occurred.

The substituents other than the pyrazolyl groups on cyclotriphosphazene skeleton play a significant role in deciding the coordination capability of the pyrazolylcyclotriphosphazenes. The diphenyl substituted ligand tdpctp forms only the mononuclear complexes with a nongeminal N_3 coordination mode from the ligand. Eventhough two nongeminal pyrazolyl groups are still left unused in these mononuclear complexes they do not interact with a second metal, thus indicating that the intervening cyclotriphosphazene nitrogen is essential to form stable five-membered chelates.

The picture is entirely different with the 1,3-diaminopropane derived ligand, stdpctp. This ligand uses three different types of donors, viz., an amido group (P-NH), a pyrazolyl nitrogen and a cyclotriphosphazene nitrogen in complexation. The resulting complexes contain two free N_3 cores one originating from two nongeminal pyrazolyl groups and one cyclotriphosphazene nitrogen and another one derived from an amido group, a pyrazolyl nitrogen and a cyclotriphosphazene nitrogen which can

be used for the uptake of a second metal. It may be intriguing to identify out of them which (N_3 core) is preferred by the second metal during heterobimetallic formation. Unfortunately the unstable nature of the mononuclear complexes does not permit us to proceed further in this direction.

The above results, overwhelmingly, albeit qualitatively, indicate that it is mandatory to restrict the number of exocyclic donor groups if one wishes to get control over the ligating response of the cyclotriphosphazene based ligands.

7.3 Electronic versus steric effects

Despite the recent advances and clarifications of bonding theories for transition metal complexes it is still difficult to predict with any degree of certainty when a five coordinate species will form or what stereochemistry it will adopt [3]. According to Kepert [4] with most rigid tridentate ligands the structure which predominates is the one in which both monodentate ligands lie on the same side of the plane defined by the tridentate ligand. In this orientation the metal atom is positioned above the tridentate plane but below the two monodentate ligands. Also the electrostatic calculations for ML_5 compounds give evidence that a trigonal bipyramid with larger axial than equatorial M-L bond lengths is energetically slightly preferred with respect to a square pyramid in which the equatorial bonds are longer than the apical bond distance [5]. These arguments suggest that the geometry of the five coordinate Cu^{2+} polyhedra with multidentate ligands is determined equally by the bulkiness of the ligand and by electronic effects. While the steric effects may stabilize—depending upon the specific geometry and rigidity of the ligand—any square pyramidal, trigonal bipyramidal or intermediate geometry, the electronic effects always induce the expected bond length anomalies. These are a compressed trigonal bipyramidal, an elongated square pyramidal or any intermediate conformation [6].

The rigid tridentate ligands such as terpyridine [7-9] and the cyclic triamine

[9]aneN₃ [10, 11] forms square pyramidal complexes with various metal halides. In contrast, the formation of distorted trigonal bipyramidal complexes with pyrazolyl-cyclotriphosphazenes points their flexibility. In a similar complex, derived from a ligand bis(6-methyl-2-methylpyridyl)amine and nickel bromide, the nickel ion exists in a trigonal bipyramidal geometry where the Br-Ni-Br angle is exceptionally large [12] for which it has been suggested that the bulky methyl substituents in the metal-tridentate ligand plane forces the unidentate ligands (bromide ions) apart [5]. The unusual Cl-Cu-Cl bond angles observed in the copper chloride complexes of hdpctp and tdpctp can be, thus, ascribed to the presence of methyl substituents on 3-position of the pyrazolyl rings. Consistent with this hypothesis, in the cobalt complex of the non-methylated ligand tpctp the Cl-Co-Cl bond angle is narrower. The formation of complex from the ligand tpctp with the ligand to metal ratio 2:1 is another compelling evidence for the steric role of 3-methyl substituents in the pyrazolyl ring of the ligands.

In all the complexes characterized by x-ray diffraction, except the nickel derivative of tdpctp (tdpctp·NiCl₂), the metal-cyclotriphosphazene interaction is very weak and result in longer M-N_{CTP} bond lengths. The M-N_{CTP} bond is further weakened when the methyl substituents on pyrazolyl rings are removed, pointing that electron rich groups should be incorporated on cyclophosphazene to achieve tighter metal-cyclophosphazene skeletal nitrogen interactions.

Interplay of electronic effects has also been noticed in the electrochemical studies of the heterobimetallic complexes. While the hdpctp derived heterobimetallics undergo decomposing electron additions, the tpctp derived heterobimetallic tpctp·PtCl₂·CuCl₂ is redox flexible and exhibits a electrochemically reversible electron transfer involving Cu(II) and Cu(I) oxidation states.

7.4 Spacer effects

The metric factor of the spacer unit which links the exocyclic donor group and the cyclotriphosphazene skeleton is also important. When the pyrazoly groups are separated from the cyclotriphosphazene ring by oxidoethyl chain, the cyclotriphosphazene nitrogen finds it difficult to engage in coordination along with the pyrazolyl nitrogens. Similar conclusion has been derived earlier for the schiff base substituted cyclotriphosphazene ligands [13].

7.5 Concluding remarks

The cyclotriphosphazene based ligands have been demonstrated as carriers for transition metals. It is also made clear that by subtle variation of the nature of substituents on cyclotriphosphazene skeleton and on the exocyclic groups various constraints within the ligand can be studied. The facile nucleophilic substitution reaction chemistry of halogenocyclotriphosphazenes is an added advantage in these attempts. However, a few more questions have yet to be answered. Most reactions that have been accomplished with small molecule models have not yet been transformed to the polymeric systems. It will be very much interesting to see how the pyrazolyl substituted polyphosphazenes will interact with the transition metals. It is hoped that such metal bearing polymers, will find applications in various fields.

Thank you, reader: "...even the weariest river
winds somewhere safe to sea"

—Algernan Charles Swinburne *in*
The Garden of Prosperine.

References

- [1] Gallicano, K.D. and Paddock, N.L. *Can. J. Chem.*, **1982**, *60*, 521.
- [2] Hathaway, B.J. and Billing, D.E. *Coord. Chem. Rev.*, **1970**, *5*, 143.
- [3] Woods, J.S. *Prog. Inorg. Chem.*, **1972**, *16*, 227.
- [4] Kepert, D.L. *J. Chem. Soc. Dalton Trans.*, **1974**, 612.
- [5] Kepert, D.L. *Inorganic Stereochemistry*, Springer-Verlag, Berlin, 1982.
- [6] Reinen, D. and Friebel, C. *Inorg. Chem.*, **1984**, *23*, 791.
- [7] Henke, W., Kremer, S. and Reinen, D. *Inorg. Chem.*, **1983**, *22*, 2858.
- [8] Arritortua, M.I., Mesa, J.L., Rojo, T., Dabaerdemaeker, T., Beltrán-Porter, D., Stratemeier, H. and Reinen, D. *Inorg. Chem.*, **1988**, *27*, 2976.
- [9] Goldshmidt, E. and Stephenson, N.L. *Acta crystallogr.*, **1970**, *26b*, 1867.
- [10] Schwindinger, W.F., Fawcett, T.G., Lalancette R.A., Potenza, J.A. and Schugar, H.J. *Inorg. Chem.*, **1980**, *19*, 1379.
- [11] Berman, R.D., Churchill, M.R., Schaber, P.M. and Winkler, M.E., *Inorg. Chem.*, **1979**, *18*, 3122.
- [12] Rodgers, J. and Jacobson, R.A. *J. Chem. Soc. (A)*, **1970**, 1826.
- [13] Bertini, R., Facchin, G. and Gleria, M. *Inorg. Chim. Acta*, **1989**, *165*, 73.